Testing the potential of OSL dating for application to heated anthropogenic sediments (hearth and charcoal kiln remains)

GHENT UNIVERSITY

Nasrin Karimi Moayed

FACULTY OF SCIENCES

FACULTY OF SCIENCES

GHENT UNIVERSITY

Testing the potential of OSL dating for application to heated anthropogenic sediments (hearth and charcoal kiln remains)

Thesis submitted in partial fulfilment of the requirements for the degree of Doctor of Science: Geology

by Nasrin Karimi Moayed

Supervisor: Prof. Dr. Johan De Grave
Co-Supervisor: Prof. Dr. Wim De Clercq

Academic year: 2022–2023

Ghent University

Department of Geology
Faculty of Sciences
Ghent University
Campus Sterre, Building S8
Krijgslaan 281
9000 Ghent
Belgium

Please refer to this work as:
Karimi-Moayed, N., 2023. Testing the potential of OSL dating for application to heated anthropogenic sediments (hearth and charcoal kiln remains). DSc. thesis, Ghent University, Ghent, Belgium.
Digital version

Front cover:
Sonian Forest, Southeast Brussels, Belgium (picture by Nasrin K.M)

Members of examination committee:

Prof. Dr. Stephen Louwye, Ghent University (Belgium): Chair

Dr. Dimitri Vandenberghe, Ghent University (Belgium): Secretary

Prof. Dr. Kristina J. Thomsen, DTU (Denmark)

Prof. Dr. Alida Timar-Gabor, Bolyai University (Romania)

Dr. Possum Pincé, Ghent University (Belgium)

Prof. Dr. Koen Deforce, Ghent University (Belgium)

Prof. Dr. Johan De Grave, Ghent University (Belgium): Supervisor

Prof. Dr. Wim De Clercq, Ghent University (Belgium): Co-supervisor

Publications:

This dissertation is structured around the following journal articles:

Karimi-Moayed, N., Vandenberghe, D.A.G., Deforce, K., Bastiaens, J., Ghyselbrecht, E., Debeer, A.-E., De Smedt, P., De Clercq, W., De Grave, J. (2020). Bypassing the Suess-effect: Age determination of charcoal kiln remains using OSL dating. Journal of Archaeological Science, 120, 105176. https://doi.org/10.1016/j.jas.2020.105176.

Karimi-Moayed, N., Vandenberghe, D.A.G., Buylaert, J.-P., Deforce, K., Debeer, A.-E., Biernacka, P., De Smedt, P., De Clercq, W., De Grave, J. (2022). A combined OSL and ^{14}C dating study of charcoal production in the sandy environment of Zoersel forest (N Belgium). Quaternary Geochronology, 71, 101339. https://doi.org/10.1016/j.quageo.2022.101339.

Karimi-Moayed, N., Vandenberghe, D.A.G., Deforce, K., Kaptijn, E., Biernacka, P., De Clercq, W., De Grave, J. (2023). OSL dating as an alternative tool for age determination of relic charcoal kilns. February 2023, Archaeometry, 1-16. https://doi.org/10.1111/arcm.12860.

Karimi-Moayed, N., Vandenberghe, D.A.G., Verbrugge, A., Ech-Chakrouni, S., De Clercq, W., De Grave, J (2023). Using Optically stimulated luminescence as a precise historical dating tool: a case study from a 17^{th}-18^{th} century military encampment, Ninove (Belgium). Submitted to Journal of Archaeological Science.

TABLE OF CONTENTS

Acknowledgements ..... **v**

Nederlandse samenvatting ..... **vii**

English Summary ..... **xiii**

List of Figures ..... **xvii**

List of Tables ..... **xxi**

Chapter 1: Introduction and Methodology **1**

1.1 Introduction **1**

1.2 Luminescence dating **4**

1.2.1 General principles 4

1.2.2 The Equivalent Dose 6

1.2.3 The Dose rate 9

1.3 Aims and outline of the thesis **10**

PART I: Relic Charcoal Hearths **13**

Background **13**

Chapter 2: Sonian forest (Bypassing the Suess effect: age determination of charcoal kiln remains using OSL dating) **15**

2.1 Introduction **16**

2.2 Material and Methods **18**

2.2.1 Study area and setting 18

2.2.2 Kilns and Sampling 19

2.2.3 OSL dating 20

2.2.4 Radiocarbon dating 23

2.3 Results **23**

2.3.1 OSL dating 23

2.3.1.1 Luminescence characteristics and equivalent dose determination 23

2.3.1.2 OSL ages 28

2.3.2 Radiocarbon dating 29

2.4 Discussion **29**

2.4.1 Comparison between OSL and ^{14}C ages 29

2.4.2 OSL dating – potential pitfalls and possibilities 32

2.4.2.1 Sampling 32

2.4.2.2 Resetting 33
2.4.2.3 Dosimetry 35
2.4.2.4 Resolution 36
2.4.2.5 Sample throughput 37

2.5 Conclusions 37

Chapter 3: OSL dating as an alternative tool for age determination of relic charcoal kilns 39

3.1 Introduction 40

3.2 Study area and historical background 42

3.3 Material and methods 45

3.3.1 Field observations and samples 45
3.3.2 OSL dating 47
3.3.3 Anthracological analysis and radiocarbon dating 49

3.4 Experiments and results 50

3.4.1 OSL dating 50
3.4.1.1 Luminescence characteristics 50
3.4.1.2 Procedural tests 52
3.4.1.3 Equivalent doses 55
3.4.1.4 Thermal transfer and measurement of low D_e's 57
3.4.1.5 OSL ages 60
3.4.2 Anthracological analysis and radiocarbon dating 61

3.5 Discussion 61

3.5.1 Comparison between OSL and ^{14}C ages, and historical sources 61
3.5.2 Potential difficulties with ^{14}C and OSL dating 63
3.5.2.1 ^{14}C-dating 63
3.5.2.2 OSL-dating 64

3.6 Conclusions 67

Chapter 4: A combined OSL and ^{14}C dating study of charcoal production in the sandy environment of Zoersel forest (N Belgium) 69

4.1 Introduction 70

4.2 Material and Methods 71

4.2.1 Study area and sample collection 71
4.2.2 OSL dating 73
4.2.3 Radiocarbon dating 75

4.3 Experiments and results 76
4.3.1 OSL dating 76
4.3.1.1 General luminescence characteristics (8 mm aliquots) 76
4.3.1.2 Distributions of D_e in small (2 mm diameter) aliquots 77
4.3.1.3 Distributions of D_e in single grains 79
4.3.1.4 Comparison between small-aliquot and single-grain characteristics 79
4.3.1.5 OSL ages 80
4.3.2 Radiocarbon dating 81
4.4 Discussion 81
4.4.1 Comparison between OSL and ^{14}C ages 81
4.4.2 Resetting and mixing 88
4.4.3 Dosimetric aspects 90
4.5 Conclusions 92
PART II: Cooking hearths 93
Background 93
Chapter 5: Dating early-Modern and Modern hearths on a decadal to multi-annual timescale using OSL signals from heated sedimentary quartz 95
5.1 Introduction 96
5.2 Material and methods 99
5.2.1 Study area and setting 99
5.2.2 Independent age information 99
5.2.2.1 Archaeomagnetic dating 99
5.2.2.2 Historical information 101
5.2.3 OSL-dating 101
5.3 Results 103
5.3.1 Luminescence characteristics and procedural tests 103
5.3.2 Equivalent dose determination 106
5.3.3 OSL ages 107
5.4 Discussion 110
5.5 Conclusion 112
Chapter 6: Discussion and conclusion 115
6.1 Discussion 115
6.1.1 Accuracy 116
6.1.2 Precision 122

6.1.3 Possibilities and limitations 124
6.1.4 Suggestions for future research 126
6.2 Conclusions 130
Appendix A 133
A.1 Luminescence measurement facilities 133
A.2 Low-background gamma ray spectrometry 135
Appendix B 137
B.1 Kiln types 137
B.2 On mound-kiln structure and temperature regimes 139
B.3 Selection of kilns for sampling and sampling strategy 141
B.3.1 Site selection 141
B.3.2 (Ideal) sampling strategy 141
B.3.3 Reuse or multiple use of kiln sites and potential disturbances 142
Appendix C – supplementary data 145
C.1 Roasting places – Sonian Forest 145
C.2 The effect of heating on luminescence characteristics 148
C.3 Visual compilation of sampling in the Ninove Site 153
C.3.1 Feature I960 154
C.3.2 Feature I1006 155
C.3.3 Feature I210 157
References 159

Acknowledgements

Completing a Doctoral degree in my field of interest is a significant milestone, and I am deeply thankful for the unwavering support of the many individuals who have accompanied me on this journey. During the past four years, I have had the privilege of encountering remarkable individuals and experiencing unforgettable moments that have had a profound impact on both my academic and personal development. It is a great honor for me to express my heartfelt appreciation to each and every one of you.

First and foremost, I extend my sincere thanks to my supervisors, Prof. Dr. **Johan** De Grave and Prof. Dr. **Wim** De Clercq, and my heartfelt gratitude to Dr. **Dimitri** Vandenberghe for giving me the opportunity to pursue my research on luminescence dating. Your guidance, support, constructive feedback, and trust in my abilities have been invaluable throughout my research and dissertation writing.

I would also like to thank the **jury members** (Prof. Dr. **Koen** Deforce, Prof. Dr. **Kristina** Thomsen, Prof. Dr. **Alida** Gabor and Dr. **Possum** Pincé) for their insightful feedback, which helped improving the quality of my dissertation. In addition, this endeavour would not have been possible without the UGent Special Research Fund (BOF-IOP project 01IO3318), which funded my research.

I am deeply grateful to my esteemed colleagues and co-authors, **Arne** Verbrugge, **Eva** Kaptijn, **Jan** Bastiaens, **Jan-Pieter** Buylaert, **Koen** Deforce, **Philippe** De Smedt, **Souad** Ech-Chakrouni, and **Elke** Ghyselbrecht for their unwavering support, exceptional cooperation, and invaluable contributions throughout the journey of my PhD thesis.

I express my gratitude to Prof. Dr. **Morteza** Fattahi, who supervised my MSc, as well as Prof. Dr. **Andrew** Murray, Dr. **Reza** Sohbati and **all the members of the luminescence laboratory at Risø DTU** (Denmark) for providing me with a solid background in theoretical and practical aspects of luminescence dating, which laid the groundwork for my current research. A special thanks to Dr. **Jan-Pieter** Buylaert (DTU, Denmark) for doing the single-grain measurements and for valuable insights into my research paper.

I would like to thank **Patrick** Huvenne, **Wim** Pauwels, and the Agency for Nature and Forests (Flemish Government) for their permissions and assistance with sampling in the Sonian and Zoersel Forests. I am also grateful for the support provided by the **MSc students Geology**, UGent, of the Classes 2016-2017 and 2018-2019 during the

fieldwork. Special thanks go to the volunteers who helped identify charcoal kilns on LiDAR images and assisted me during my fieldwork in the Veluwe.

I would also like to thank the technicians, **Ann-Eline** Debeer and **Veerle** Vandenhende for their support.

I just wanted to take a moment to give a big, heartfelt thanks to **Johan** and **Dimitri** for treating me like a member of their own family and always being there to offer support and help. I would also love to extend my gratitude to **Emiel** and **Arno** Vandenberghe, as well as **Maren** De Grave, for being so kind and making my time in Belgium all the sweeter.

I would like to express my sincere gratitude to **Krista** and **Linda** Frickelo for their maternal affection and support during my stay in Belgium. Their kindness made it easier for me to cope with being away from my own family.

I appreciate the time spent with my colleagues, including **Ana** Carolina Liberal Fonseca, **Ann-Eline** Debeer, **Paulina** Biernacka, **Possum** Pincé, **Fernanda** Zago da Cruz, **Cristiana** Esteves, **Joana** Rosin, **Wenbo** Su, **Zhiyuan** He, **Dongxu** Cai, **Gerben** Van Ranst, **Simon** Nachtergaele, **Shana** De Clercq, and **Patsy** Billemon who made each day enjoyable.

I would like to extend my sincere thanks to my friends in Denmark **Elaine** Sellwood, **Rosio** Bernal, **Raju** Kumar, and **Emran** Khan who supported me to embark on this four-year journey. Special thanks to my dear friend **Nina** Ataee for her unwavering spiritual support and invaluable feedback throughout my academic endeavors. Her insights were crucial in my thesis, papers, and conferences.

I would also like to thank my friends in Belgium, **Elnaz** Nabavi, **Fatemeh** Loni, **Nasrin** Esmailian, **Pendar** Azimi, **Arash** Ghazi, **Behzad** Parvizi, **Mahdi** Mahmoudinia, **Parviz** Yazdani and **Sepehr** Madani Kashani (my sincere gratitude to him) for their warm and memorable moments during my PhD life.

I extend my gratitude to all the members of the Department of Geology, especially **Marion** Braekeleire, **Wim** Lievens, **Kurt** Blom, and **Marc** De Batist, for their assistance and support during my academic journey.

Last but not least, I am indebted to my lovely and wonderful husband, Mahmoud '**Mory**' Khalili, and **my family**, who provided me with unconditional love and encouragement during my PhD journey.

Nasrin (Gent, Spring 2023)

Nederlandse samenvatting

Optisch gestimuleerde luminescentiedatering (*OSL-datering*) van sedimentair kwarts wordt momenteel veelvuldig gebruikt in een brede waaier van disciplines in het Quartair onderzoek. De methode heeft als voordelen dat ze gebruikt maakt van de belangrijkste minerale bestanddelen van sedimenten (zoals kwarts en veldspaat), een breed tijdsvenster bestrijkt (10^0-10^5 jaar in het geval van kwarts) en direct een ouderdom in kalenderjaren oplevert zonder nood aan kalibratie. Het tijdstip dat wordt gedateerd, is de laatste blootstelling van de mineralen aan licht (bijv. tijdens erosie en transport) of warmte (bijv. tijdens verhitting door de mens). Op dit ogenblik wordt OSL-datering van kwarts voornamelijk ingezet om het tijdstip te bepalen waarop onverhitte sedimenten werden afgezet. De methode vindt echter haar oorsprong in archeologische toepassingen en het dateren van verhitte sedimentaire materialen (zoals keramiek) in het bijzonder.

Dit proefschrift onderzoekt het potentieel van OSL-signalen van kwarts om sedimenten te dateren die door de mens werden verhit en geassocieerd zijn met twee specifieke archeologische sporen in de ondergrond (*houtskoolmeilers* en *kookhaardjes*). Het onderzoek richt zich in het bijzonder op mogelijkheden om die restanten te dateren die niet meer dan een paar honderd jaar oud zijn. De restanten van dergelijke relatief recente houtskoolmeilers, en haardjes in het algemeen, kunnen op een aanzienlijke en toenemende wetenschappelijke belangstelling rekenen. Het is echter algemeen geweten dat ze erg moeilijk in de tijd te plaatsen zijn met een voldoende hoge accuratesse en/of precisie. Radiokoolstofdatering (^{14}C-datering), bijvoorbeeld, wordt algemeen toegepast, maar is niet in staat om sporen die recenter zijn dan ~1650 CE (*Common Era*, of *onze jaartelling*) van elkaar in de tijd te onderscheiden. Het dateren met behulp van archeomagnetisme heeft een groot potentieel, maar vereist goed bewaarde, onverweerde in-situ/georiënteerde fragmenten, relatief hoge verhittingstemperaturen, en een geschikte standaardcurve van het archeomagnetisch veld ter kalibratie. Deze specifieke vereisten ontbreken echter heel vaak, of zijn betwistbaar, althans voor de types van sporen die in dit proefschrift worden onderzocht.

Het eerste deel van dit proefschrift spitst zich toe op de OSL-datering van de overblijfselen van houtskoolmeilers, zoals die bewaard zijn in twee verschillende types van sediment: een lemig (Zoniënbos, België) en een zandig (Zoerselbos, België en de

Veluwe, Nederland). Het merendeel van de restanten van houtskoolmeilers die in Europa werden gevonden, dateren van de 17de tot 19de eeuw CE. ^{14}C-datering laat niet toe om ze meer precies in de tijd te begrenzen. De nadruk van dit luik van het onderzoek lag dan ook op het testen van de accuratesse en precisie die met OSL-datering van kwarts kan worden gehaald in deze context.

Voor elk van de onderzochte sporen en stalen werden eerst en vooral de karakteristieken van het kwarts-OSL-signaal gedocumenteerd, en dit in termen van de uiteenlopende procedurele tests die algemeen worden gebruikt om de geschiktheid van het zogenaamde *single-aliquot regeneratieve dosis (SAR) protocol* te evalueren. Dit is een meetprotocol dat gebruik maakt van één enkel sub-staaltje (*single-aliquot*) en geregenereerde OSL-signalen om de equivalente dosis (D_e) te bepalen. De resultaten tonen aan dat - voor alle stalen en aliquots – de meetprocedure reproduceerbaar is, en in staat is om accuraat gekende laboratoriumdosissen te bepalen. Dit protocol werd bijgevolg gebruikt om de D_e te bepalen in zowel grote aliquots (die bestaan uit duizenden kwartkorreltjes) en kleine aliquots (die bestaan uit 100-200 korrels). Voor een aantal stalen werden ook individuele kwartskorrels uit de zandfractie (*single grains*) geanalyseerd. Het stralingsdosistempo werd berekend uit de radionuclideconcentraties die werden bekomen met behulp van lage-achtergond Ge-gammaspectrometrie, en de best mogelijke inschattingen van de verschillende parameters die vereist zijn om tot een OSL-datering te komen (zoals het tijdsgemiddelde vochtgehalte, de begravingsdiepte, enz.). Dit wil zeggen dat een gekende en wijdverspreide OSL-methodologie werd gebruikt. De accuratesse van de bekomen OSL-dateringen werd geëvalueerd door ze te vergelijken met onafhankelijke ouderdomsinformatie (^{14}C-dateringen en historische bronnen). De precisie werd geëvalueerd door ze te vergelijken met die van de ^{14}C-methode.

Bij het onderzoek in het Zoniënbos (Centraal-België; een lemige ondergrond) werden de restanten van zeven houtskoolmeilers, net als ook het onderliggend sediment, onderzocht (14 stalen in totaal). De meilers werden onafhankelijk in de tijd geplaatst door ^{14}C-datering van zorgvuldig geselecteerde en geïdentificeerde houtskoolfragmenten. De ^{14}C-resultaten tonen aan dat vijf van de onderzochte meilers ouder zijn dan 1650 CE, en twee meer recent. De bekomen OSL-dateringen zijn volledig in overeenstemming met de ^{14}C-dateringen, waaruit werd besloten dat de OSL-methode accuraat is. De precisie van de OSL-methode is vergelijkbaar met die van ^{14}C

voor relicten die ouder zijn dan 1650 CE, maar kan significant beter zijn voor de meer recente (post -1650 CE) sporen. Indien de OSL-klok volledig op nul werd gesteld, zou OSL-datering het bovendien mogelijk moeten maken om vergelijkbare restanten van elkaar te onderscheiden met een tijdsresolutie van 2-4%. Dit onderzoek illustreerde ook hoe het initiële en lineaire gedeelte van de groeicurve kan worden benut om relatief snel grote datasets te genereren zonder dat dit de accuratesse of de precisie compromitteert.

Deze oefening werd vervolgens uitgebreid naar de restanten van houtskoolmeilers bewaard in een zandige ondergrond. In de Veluwe (Centraal-Nederland) werden vijf houtskoolmeilers samen met het onderliggend sediment onderzocht (18 stalen in totaal). Hierbij werd gebruik gemaakt van dezelfde methodologie als voor de meilers in het Zoniënbos. Voor vier van de vijf onderzochte sporen zijn de OSL-ouderdommen in volledige overeenstemming met de onafhankelijke ouderdomsinformatie (^{14}C-dateringen en geschreven bronnen). Ook hier werd vastgesteld dat de precisie van OSL-datering aanzienlijk beter kan zijn dan die van ^{14}C voor restanten uit de voorbije paar eeuwen, en dat de methode potentieel heeft om relatieve ouderdomsrelaties vast te leggen met een resolutie van een tiental tot enkele jaren. Voor één van de onderzochte meilers leveren zowel OSL als ^{14}C-datering ouderdommen op die consistent zijn met de – weliswaar weinig precieze - historische ouderdomsinformatie, maar waarbij de ^{14}C-datering echter significant ouder is. De oorzaak voor deze discrepantie is nog niet begrepen. Vanuit een OSL-methodologisch perspectief, waarin ook de spreiding in D_e in de stalen werd onderzocht, is er op dit ogenblik echter geen enkele reden waarom de OSL-ouderdom voor deze specifieke meiler minder accuraat zou zijn dan deze die werden bekomen voor de andere meilers. Met dezelfde aanpak werden ook de restanten van elf houtskoolmeilers en het onderliggend sediment (32 stalen in totaal) uit het Zoerselbos (Noord-België) onderzocht. In schril contrast tot de twee eerdere studies, zijn de OSL-ouderdommen doorgaans significant ouder dan de ^{14}C-ouderdommen. Voor een aantal stalen werd dit verwacht op basis van de spreiding die werd geobserveerd in de distributies van D_e in kleine aliquots. Voor vier van de onderzochte relicten (acht stalen) werden ook OSL-ouderdommen bekomen door het analyseren van individuele kwartskorrels. Deze resultaten zijn ofwel consistent met de ^{14}C-ouderdommen, of overschatten deze in dezelfde mate als de dateringen met behulp van kleine aliquots. Een potentiële en gedeeltelijke verklaring voor deze discrepantie is dat

verhitting weliswaar een homogeen proces is, maar in het verleden mogelijks ontoereikend was (in temperatuur en/of duur) om de OSL-klok volledig op nul te stellen. De aard van de houtskoolproductie in Zoerselbos verschilt echter van die in andere regio's in Europa, zodat niet kan worden uitgesloten dat ook andere factoren een rol spelen, zoals bijvoorbeeld variaties in het stralingsdosistempo doorheen de tijd en/of de gebeurtenis die met ^{14}C-analyse van een welbepaald houtskoolfragment wordt gedateerd. Los hiervan werd de hypothese vooropgesteld dat distributies van OSL-intensiteit kunnen informeren over de verhittingsgeschiedenis die individuele kwartskorrels hebben ervaren. Deze hypothese dient evenwel nog verder te worden onderzocht.

In het tweede deel van dit proefschrift werd dezelfde OSL-methodologie gebruikt om de restanten van (kook)haardjes in de tijd te plaatsen. Deze haardjes zijn geassocieerd met post-middeleeuwse militaire kampementen in Ninove (Centraal-Oost België). Op deze locatie werden talrijke van dergelijke sporen gevonden die op basis van doorgaans indirecte gegevens worden toeschreven aan kampementen uit 1692 CE en/of 1693 CE, en 1745 CE. Er werd niet verwacht dat ^{14}C-datering zou toelaten om sporen uit de 17de en het midden van de 18de eeuw CE van elkaar te onderscheiden. Drie haardjes (zes stalen) werden onderzocht met de OSL-methode. Aangezien de resultaten niet significant van elkaar verschilden, kon besloten worden dat deze drie haardjes even oud zijn. Dit resulteerde in een gemiddelde OSL-ouderdom van 1748 ± 59 CE (met ongeveer ~ 95% waarschijnlijkheid), wat nagenoeg volledig samenvalt met een ouderdom van 1745 CE die op basis van archeologische vervolgonderzoek aan deze sporen werd toegeschreven. De OSL-resultaten bekomen voor de haardjes in Ninove illustreren hoe de methode andere dateringstechnieken zoals archaeomagnetisme kan informeren, en tonen bovenal de mogelijkheid aan om vergelijkbare sporen van elkaar in de tijd te onderscheiden met een relatieve resolutie van 1-3% met ~ 95 % waarschijnlijkheid. Voor sporen uit de voorbije paar honderd jaar komt dit op een tiental jaar (of minder). Een dergelijke tijdsresolutie is ongeëvenaard in vergelijking met andere radiometrische technieken.

Het algemene besluit van dit onderzoek is dat SAR-OSL-datering van kwarts een krachtige techniek is om de restanten van houtskoolmeilers en kookhaarden, en haarden

in het algemeen, in de tijd te plaatsen, ongeacht of deze nu ouder of jonger zijn dan 1650 CE. Aangezien ^{14}C-datering goed ingebed is in het archeologische en jong-Quartair onderzoek, is het eerder onwaarschijnlijk dat OSL-datering in de toekomst ook daadwerkelijk zal worden ingezet om routinematig sporen te dateren die ouder zijn dan 1650 CE. Dit is eerder onterecht aangezien de methode niet materiaal-specifiek is, doorgaans de gebeurtenis van interesse direct dateert en dus niet berust op associatie, niet afhankelijk is van andere ouderdomsinformatie voor kalibratie, en in staat is om vergelijkbare sporen van elkaar te onderscheiden met een relatieve tijdsresolutie van 2-3%. De voordelen van de OSL-methode, ten opzichte van de mogelijkheden geboden door andere technieken zoals ^{14}C en archeomagnetisme, zijn vooral duidelijk en significant voor archeologische sporen uit de voorbije paar honderd jaar. Niettemin werden ook een aantal problemen vastgesteld, waarvan de oorzaken nog niet gekend zijn, en die dus verder moeten worden onderzocht. Voor toekomstig onderzoek wordt een strategie aanbevolen waarin verschillende dateringsmethoden worden ingezet en meerdere stalen van eenzelfde spoor met de OSL-methode worden onderzocht, en dit in een hechte samenwerking tussen alle betrokken onderzoekers.

English Summary

Optically stimulated luminescence (OSL) dating of sedimentary quartz and feldspar is now widely used in a range of Quaternary research topics. It is advantageous as it uses the main mineral constituents of the sediments (e.g. quartz and feldspar), covers a wide age range (typically 10^0 - 10^5 years in case of quartz), and provides numerical age information (in calendar years), without the need for calibration through independent age information. The event being dated is the last exposure of the minerals to light (e.g. during erosion and transport) or heat (e.g. during anthropogenic firing or natural heating events). At present, quartz-based OSL dating is mainly used for establishing deposition chronologies for unheated sediments. Nevertheless, the origins of luminescence dating lie in the application in archaeological context, and the dating of heated sedimentary materials (such as ceramics) in particular.

This dissertation investigates the potential of quartz-based OSL signals for dating anthropogenically heated sediments associated with two particular features – *relic charcoal kilns* and *cooking hearths* – over the particular timespan of the last few centuries. Both types of features are receiving increasing interest by the scientific community but are notoriously difficult to date with sufficient accuracy and/or precision. Radiocarbon (^{14}C) dating is commonly applied, for instance, but essentially provides no meaningful time-resolution from around 1650 CE onwards. Archaeomagnetic dating has great potential but requires well-preserved, unweathered in-situ/oriented fragments, relatively high firing temperatures, and an appropriate standard calibration curve of the archaeomagnetic field; very often these conditions are lacking or contentious, at least for the types of features investigated here.

The first part of this dissertation focusses on the optical dating of *relic charcoal kilns* as preserved in two different lithological substrates, a loamy one (Sonian Forest, Belgium) and a sandy one (Zoersel Forest, Belgium and the Veluwe, The Netherlands). The majority of the relic charcoal kilns found in Europe date to between the 17th and the 19th century CE, but cannot be constrained in time more precisely using ^{14}C dating. The emphasis of the research was on the testing of the accuracy and precision that can be attained using OSL dating.

For each of the investigated features and samples, the quartz OSL characteristics are documented in terms of the various procedural tests that are commonly used to assess the appropriateness of the single-aliquot regenerative-dose (SAR) protocol. The results suggest that, in all cases, the measurement procedure is reproducible and is able to accurately measure known laboratory doses. The SAR protocol was therefore used to determine equivalent doses in both large aliquots (composed of thousands of grains) and small aliquots (composed of 100-200 grains); for a few samples, single grains were analysed as well. The dose rate was derived from radionuclide analysis using high-resolution gamma-ray spectrometry, and our best possible estimates of the various parameters involved in the calculations (such as time-averaged moisture content, burial depth and others). As such, a more or less widely adopted mainstream OSL-dating methodology was deployed. The accuracy of the resulting OSL-dates is evaluated through comparison with independent age control (^{14}C and archaeomagnetic dating and historical sources); precision is evaluated in comparison to that of ^{14}C-dating.

The study at Sonian forest (Central Belgium; loamy substrate) used a set of 14 samples collected from seven relic charcoal kilns and underlying parent material. The kilns were independently dated using ^{14}C of carefully selected charcoal fragments; the results show that five of the investigated kilns pre-date 1650 CE, while the other two are more recent. The OSL ages are entirely consistent with the ^{14}C-ages, indicating that the approach is accurate. The precision of OSL dating is comparable to that of ^{14}C-dating for pre-1650 CE features, and can be significantly better for post-1650 CE ones. Moreover, in case of complete resetting, it is suggested that OSL-dating might allow distinguishing between comparable features with a relative time-resolution of 2-4%. Finally, it is illustrated that the linear part of the dose response curve can be exploited to obtain large datasets, without compromising accuracy or precision of the results.

The exercise was extended to relic charcoal kilns preserved in sandy substrates. In the Veluwe (Central Netherlands), seven samples from five relic charcoal kilns and 11 complementary samples from the underlying sandy substrate were investigated. The research adopted the same approach as for the kilns in Sonian Forest. For four of the five investigated kilns, OSL ages are consistent with independent age information (^{14}C-dating and written sources). Also here, it is observed that the precision can be significantly higher than that of ^{14}C-dating for post-1650 CE features, with potential for establishing relative age relationships on decadal to even multi-annual timescales. For one of the kilns, both ^{14}C and OSL dating yield ages that are consistent with (poorly

constrained) historical age information, but with the ^{14}C date being significantly older. The cause for this discrepancy remains to be understood; at least from a methodological perspective (including examinations of the distributions of equivalent dose), there is at present no evidence for the OSL-date for this particular feature to be less accurate than those obtained for the other kilns. The same exercise was performed in Zoersel Forest (Northern Belgium), where a suite of 32 samples from 11 relic charcoal kilns were investigated. In contrast to the two aforementioned studies, the OSL dates overestimate the ^{14}C-dates for most of the features. For some of the samples, this could be anticipated based on the spread observed in the distribution of equivalent dose in small aliquots of quartz. For four of the investigated features (8 samples), OSL ages were also obtained using single grains of quartz, which are either consistent or overestimate the ^{14}C-dates to the same extent as the ages obtained using small aliquots. A potential and partial explanation for this discrepancy is that heating is a homogenous process, but may not have been sufficiently stringent to fully reset the quartz-OSL signal. The character of charcoal production at Zoersel Forest differs from that in other regions in Europe, however, implying that other factors (related to e.g. dose rate variations through time and/or independent age determination) might be partially responsible as well. Apart from this, it is hypothesized that distributions of signal brightness might give information about heating regimes experienced by the grains; this remains to be explored.

The second part of this dissertation examines the same optical dating methodology for application to *relic (cooking) hearths* associated with early-Modern (late 15th – late 18th CE) and Modern (late 18th – present) military encampments in Ninove (Central-East Belgium). A vast amount of such traces were discovered at this site and are allocated to 1692 CE and/or 1693 CE, and 1745 CE, essentially on the basis of more or less circumstantial evidence. As for the relic charcoal hearths, ^{14}C-dating was not expected to help distinguishing between features from the end of the 17th and those from the mid-18th century CE. Optical ages were obtained for six samples from three relic hearths – the ages do not differ significantly, indicating that the sampled features are coeval. The average optical age of 1748 ± 59 CE (~ 95 % probability) practically coincides with insights subsequently gained from archaeological research (1745 CE). The results illustrate how OSL dating cannot only provide information for archaeomagnetic dating, but reinforces the potential for distinguishing – relatively - between comparable

features from this period of time at a decadal time scale with 95% confidence. The time-resolution that can be achieved is thus unrivalled compared to that of other radiometric techniques.

The overall conclusion of this study is that quartz-based SAR-OSL dating is a powerful tool for dating relic (charcoal) hearths, regardless of whether they pre- or postdate 1650 CE. Given that ^{14}C-dating is well embedded in archeological and young-Quaternary research, it is unlikely that OSL-dating will be readily considered for dating pre-1650 CE features. This is unfortunate given that the method is not material specific, directly targets the event of interest (no association), does not rely on independent age information for calibration purposes, and offers a potential relative time-resolution of 2-4%. For post-1650 CE features, OSL dating offers the most obvious and significant advantages over other radiometric techniques such as ^{14}C-dating. Some issues remain, however. OSL analyses of multiple samples from a single feature, as part of a multiple-method-dating strategy and in close collaboration with all researchers involved, is recommended.

List of Figures

Figure 1.1: Age range and relative importance of Quaternary dating methods.....1

Figure 1.2: Radiocarbon calibration curve for the past few hundred years.....3

Figure 1.3: Principle of OSL dating.....5

Figure 1.4: A SAR dose response curve for equivalent dose (D_e) determination. 8

Figure 2.1: Location maps of the studied charcoal kilns remains in Sonian Forest. ...19

Figure 2.2: Photographs of the profile pits in two relic charcoal kilns in the Sonian Forest.....20

Figure 2.3: Representative quartz OSL decay and SAR growth curve for a burnt sample 25

Figure 2.4: Representative quartz OSL decay and SAR growth curve for an unburnt sample 25

Figure 2.5: Dependence of D_e, recycling ratio and recuperation on preheat temperature 27

Figure 2.6: Dependence of dose recovery ratio, recycling ratio and recuperation on preheat temperature.....27

Figure 2.7: Summary of dose recovery data 28

Figure 2.8: Distributions of D_e in small aliquots of two burnt samples.....30

Figure 2.9: Distributions of D_e in small aliquots of two unburnt samples.....30

Figure 2.10: Comparison between OSL and calibrated ^{14}C-ages 31

Figure 3.1: Location maps of the studied charcoal kiln remains in the Veluwe.....43

Figure 3.2: Photographs of the profile pits in three relic charcoal kilns in the Veluwe 46

Figure 3.3: Representative quartz OSL decay and SAR growth curve for a burnt sample 51

Figure 3.4: Summary of recuperation, recycling and OSL IR depletion data for samples collected from dark charcoal-rich layers.....52

Figure 3.5: Summary of recuperation, recycling, and OSL IR depletion data for samples from sediments underlying the dark charcoal-rich layers.....53

Figure 3.6: Dependence of D_e, recycling and recuperation on preheat temperature ...54

Figure 3.7: Dependence of dose recovery ration recycling and recuperation on preheat temperature 55

Figure 3.8: Summary of dose recovery data 56

Figure 3.9: Distributions of D_e in small aliquots of samples collected from dark charcoal-rich layers and underlying sediments 57

Figure 3.10: Distributions of D_e in small aliquots of samples collected from dark charcoal-rich layers and underlying sediments (Fig. 3.10 continued) 59

Figure 3.11: Distributions of measured dose following optical and thermal resetting 60

Figure 3.12: Distributions of recovered dose following optical and thermal resetting 62

Figure 3.13: Comparison between OSL ages, ^{14}C ages and historical evidence 66

Figure 4.1: Location map and illustrative photographs of charcoal kiln remains in Zoersel Forest 72

Figure 4.2: Representative OSL decay and SAR growth curve for a burnt sample 76

Figure 4.3: Summary of dose recovery data for samples collected from dark charcoal-rich layers 78

Figure 4.4: Summary of dose recovery data for samples collected from sediments underlying the dark charcoal-rich layers 78

Figure 4.5: Distributions of D_e in small aliquots and single grains of quartz from samples collected from dark charcoal-rich layers 82

Figure 4.6: Distributions of D_e in small aliquots for all samples 84

Figure 4.7: Distribution of signal intensity distribution from single grains of heated quartz 89

Figure 4.8: Comparison between OSL and calibrated ^{14}C-ages 91

Figure 5.1: Location maps of the investigated cooking hearths in Ninove 97

Figure 5.2: Illustrative pictures of large excavated structures 98

Figure 5.3: The main Quaternary sedimentation areas in Belgium 100

Figure 5.4: Photographs of sample collection 100

Figure 5.5: Representative quartz OSL decay and SAR growth curve 104

Figure 5.6: Dependence of D_e, dose recovery ratio, recycling ratio and recuperation on preheat temperature 105

Figure 5.7: Summary of dose recovery data 105

Figure 5.8: Distributions of D_e in small aliquots of quartz 107

Figure 5.9: Distributions of D_e in small aliquots of quartz (Fig. 5.8 continued) 108

Figure 5.10: Comparison between OSL ages, archaeomagnetic ages and historical information 111

Figure 6.1: Summary of age comparison for all samples investigated in this study 117

Figure 6.2: Effect of water content on an OSL 120

Figure 6.3: Effect of organic matter on an OSL age. 121

Figure 6.4: Detailed uncertainty budget for two samples 122

Figure 6.5: Contribution of cosmic radiation to the total dose rate and effect on an OSL age, as a function of depth 123

List of Tables

Table 1.1: Generalized single-aliquot regenerative-dose (SAR) protocol.....7

Table 2.1: Summary of analytical data and calculated OSL ages for the samples from the Sonian Forest.....21

Table 2.2: Summary of results from ^{14}C-dating at Sonian Forest.....29

Table 3.1: Summary of analytical data and calculated OSL ages for the samples from the Veluwe 48

Table 3.2: SAR measurement sequence and conditions used for determining the D_e in samples from the Veluwe.....50

Table 3.3: Summary of results from ^{14}C-dating at the Veluwe 63

Table 3.4: Results from anthracological analysis. 64

Table 4.1: Summary of analytical data and calculated OSL ages for the samples from Zoersel Forest.....74

Table 4.2: Summary of ^{14}C-dating at Zoersel Forest.....88

Table 5.1: Summary of analytical data and calculated OSL ages for the samples from Ninove.....109

Chapter 1: Introduction and Methodology

1.1 Introduction

At present, luminescence dating is the second most widely used Quaternary radiometric dating method, following radiocarbon dating (Duller, 2011; Figure 1.1). The method determines when minerals such as quartz and feldspar were last exposed to sunlight or heat, over an age range from several hundreds of thousands of years, to (tens of) years. Over the past 20 years it has revolutionized a range of disciplines in Quaternary research, essentially covering topics in earth and archaeological sciences.

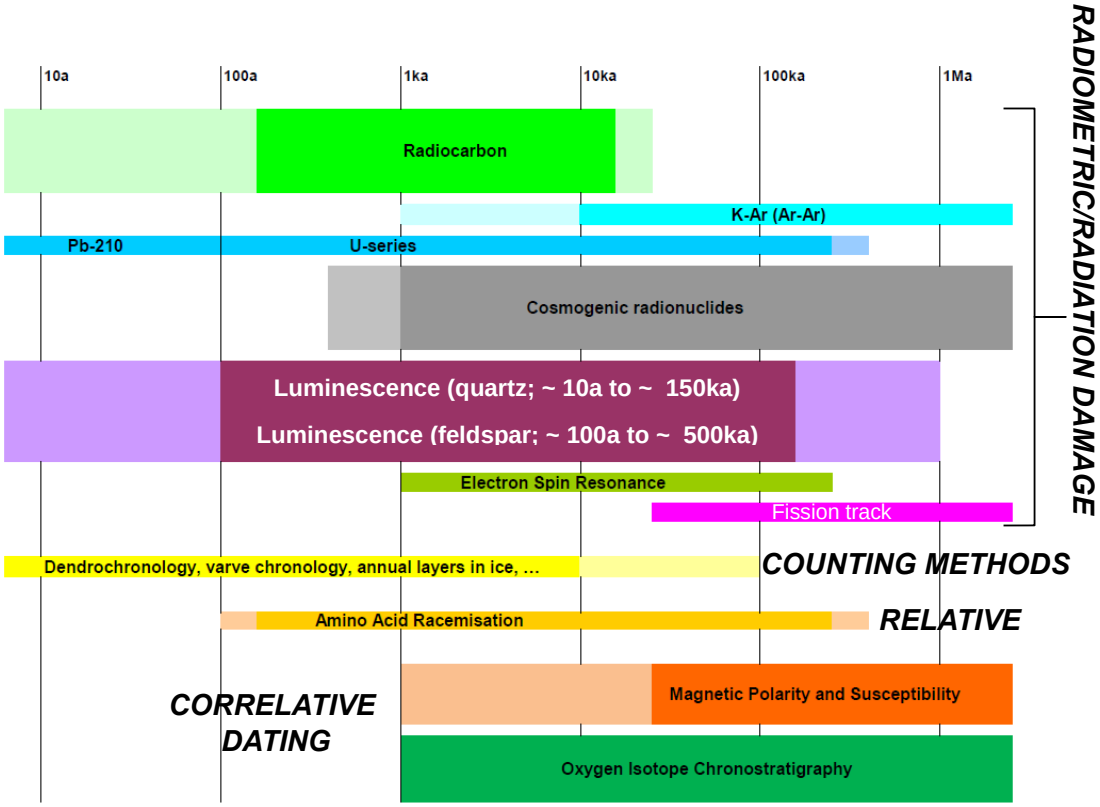

Figure 1.1: Age range and use of Quaternary dating methods (modified after Aitken, 1998 and Murray and Buylaert, 2017). Note the logarithmic time-axis. The length of the bars indicates the time range over which each method is applicable; lighter shades illustrate where the methods are pushed towards their limits. The width of the bars is a proxy for relative importance, as derived from applied published studies.

Luminescence dating encompasses various techniques, depending on whether the signals are stimulated by heat (thermoluminescence - TL), or light (optically stimulated luminescence – OSL; infrared stimulated luminescence – IRSL). OSL dating of unheated quartz and IRSL dating of unheated K-feldspar are currently the mainstream applications. These aim at establishing sediment deposition chronologies to help

improve our understanding of, e.g., palaeo-environment and climate, dynamics of geomorphological processes, geological hazards, patterns of human occupation and migration, and man-environment interactions (Murray and Olley, 2002; Duller, 2004; Lian and Richards, 2006; Wintle 2008; Tsukamoto et al., 2009; Rhodes, 2011; Bateman, 2019). In terms of number of publications, these applications dominate those involving the dating of heated materials (e.g. ceramics, bricks, burnt flints,…). Luminescence dating, however, finds its origin in answering dating questions pertaining to heated materials (for overviews, see Aitken, 1985; Wagner, 1998).

Early work on anthropogenically heated materials concerned the use of thermoluminescence signals (Aitken et al., 1964; Aitken, 1985; McKeever, 1985; Aitken, 1990). Applications for dating, however, were hampered by poor precision and hence the focus shifted towards authenticity testing (Aitken et al., 1972; Zimmerman et al., 1974) for which it is still widely used (Stoneham, 1991; Leung et al., 2005; Guidorzi et al., 2021). Use of signals stimulated by light, which are also reset by heat, in combination with single-aliquot protocols (see §1.2.2) for measuring accumulated dose, offered improved precision (e.g. Liritzis et al, 1994; 1997; Mejdahl and Bøtter-Jensen, 1994; 1997; Murray and Mejdahl, 1999; Murray and Wintle, 2000). Such approaches have been applied to ceramics (or pottery), bricks, burnt sediments and stones, as well as slags. Relevant studies in addition to those mentioned in the above include Hong et al. (2000), Gautier (2001), Takano et al. (2003), Lamothe (2004), Benea et al. (2007), Bailiff, (2007), Thomas et al. (2008), Liritzis et al. (2016), Zander et al. (2019), Sun et al. (2021), Khamsiri et al. (2022a,b) and Wang et al. (2022a,b). For the sake of completeness, it is added that some studies have explored the use of luminescence properties to distinguish between burnt and unburnt soil samples and to improve our understanding of the impacts of wildfires on the sediments (e.g. Rengers et al., 2017; Zhang et al., 2022). The potential of luminescence methodologies to directly date juvenile volcanic minerals and xenoliths has also been investigated (Bösken and Schmidt (2020). These investigations all concern naturally heated materials, and fall beyond the scope of this dissertation.

The above overview illustrates that OSL/IRSL dating of heated materials has been mainly performed to help in addressing geoarchaeological, archaeological and historical research questions. Within these contexts, radiocarbon (^{14}C) dating has been applied far more widely (Taylor, 2014; Taylor and Bar-Yosef, 2014; Bayliss, 2009).

This approach, however, covers a limited age range (Figure 1.1), and requires that suitable organic material is present which can be associated with some degree of confidence to the event of interest, and that the measured ages are calibrated. Especially for providing age constrains on materials and events from the last few centuries, ^{14}C is problematic because of plateaus in the calibration curve (De Vries and Suess-effects). These plateaus are caused by variations in sunspot activities, and the dilution of atmospheric $^{14}CO_2$ by fossil fuel derived CO_2 which does not contain ^{14}C (Stuiver, 1961; Tans et al., 1979); this is illustrated in Figure 1.2.

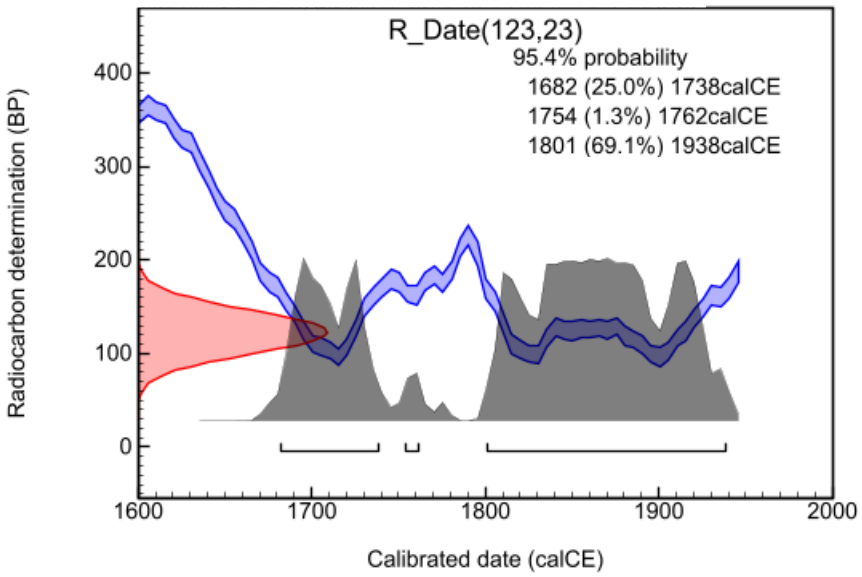

Figure 1.2: Illustrative example of calibrating a conventional ^{14}C age of 123 ± 23 BP (sample LE19-M1; see Chapter 3) using OxCal v4.4.4 (Bronk Ramsey, 2009) and the IntCal20 calibration curve (Reimer et al., 2020).

In addition to the limitations posed by the calibration process, there are several inherent challenges and issues associated with dating charcoal using the radiocarbon method. One of these factors is the "old wood effect," which refers to the age discrepancy between the inner and outer tree rings used in charcoal production. This inconsistency can lead to potential errors of hundreds of years in radiocarbon dating results, unless the samples come from short-lived tree species or twigs. (Kim et al., 2019; Deforce et al., 2021). Another challenge is the time gap between the death of the plant and the production of charcoal. This gap introduces uncertainty in establishing the precise age of the charcoal, as there may be a delay between when the plant died and when it was actually used for charcoal production (Gavin, 2001). Additionally, the presence of intrusive charcoal further complicates the radiocarbon dating of charcoal fragments.

Intrusive charcoal refers to charcoal that has been introduced into a sedimentary context at a later time, either naturally or through human activities.

Luminescence dating does not require calibration and it has been shown to be applicable to heated features from the last few centuries with an overall relative uncertainty of 6-10 % (at the 1 sigma or 68.3 % probability confidence interval; see e.g. Bailiff, 2007, for bricks). From a critical review of the available literature (see above), however, this potential has remained largely untapped. Indeed, the available studies on the subject are limited in both the number of publications, and the types and age of heated features investigated. Most studies have focused on bricks and pottery, with only a few examining heated sediments (e.g. Sun et al., 2012; Armitage and King, 2013; Yu et al., 2016), and rarely (or not) concerned the past few centuries. Providing a contribution to try and fill this gap is at the heart of this dissertation (see §1.3).

1.2 Luminescence dating

1.2.1 General principles

Luminescence dating is based on the radioactivity in the natural environment, storage of the energy delivered by this radiation in the crystalline structure of minerals such as quartz and feldspar, and the release of stored energy as a result of exposure to heat or light.

Natural radioactivity is omnipresent. Of interest in luminescence dating are the long-lived radionuclides ^{238}U, ^{235}U, ^{232}Th and their active radiogenic daughters, ^{40}K and ^{87}Rb, as well as cosmic radiation. Upon exposure to this radiation, minerals such as quartz and feldspars function as dosimeters, in that they are able to store the amount of radiation energy, which increases as a function of time. The energy stored can be released when the minerals are heated, or when they are exposed to light. This occurs e.g. during erosion and transport of sediments, or when they are fired; these processes can effectively reset the "clock" to zero. Once the zeroing agent is removed, energy storage, due to continued exposure to natural radiation, resumes, for example when the sediment is buried after deposition and is again shielded from sunlight, until a sample is collected and analyzed in the laboratory. This analysis involves the same agents (heat or light) to release the stored energy, which is accompanied by the emission of light known as “luminescence”. This luminescence signal is detected, and its intensity is proportional to the time that has elapsed between the two zeroing events. If the signal

is released by exposure to heat, the resulting luminescence is called thermoluminescence (TL); in case of exposure to light, it is generally called optically stimulated luminescence (OSL).

As such, the event being dated in luminescence dating is the last exposure to light or heat of the analyzed material (Figure 1.3). The age is obtained from the following equation:

$$Luminescence\ Age\ (a) = \frac{Absorbed\ dose\ (Gy)}{Ionizing\ radiation\ (Gy\ a^{-1})} \qquad (1.1)$$

implying that two parameters need to be experimentally determined. The absorbed dose is the total amount of radiation energy stored in the mineral since the last resetting event and is derived from luminescence measurements (§1.2.2). The dose rate is the rate at which this dose (of natural radiation) has accumulated by the mineral under investigation and can be derived from radionuclide concentration analyses (§1.2.3). The following two subsections briefly summarize some of the essentials on equivalent dose and dose rate determination that are directly relevant to this work. Comprehensive reviews of principles and methods, as well as applications, are available in literature (e.g. Aitken, 1998; Duller, 2008a; Bateman, 2019; Murray et al., 2021).

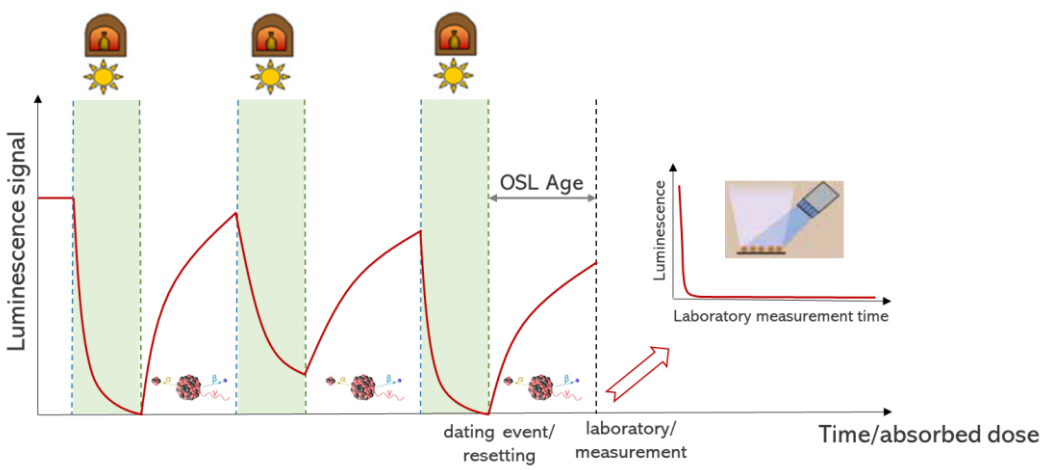

Figure 1.3: Scheme illustrating loss and build-up of luminescence signal and the event that is dated. The solid red lines in the green highlighted are periods where the luminescence signal is reset by light (during erosion or transport) or heating (e.g. anthropogenic firing during the production of pottery, bricks or charcoal). Once the resetting agent is removed the signal starts to build up as a results of exposure to natural radioactivity (alpha, beta, and gamma ionizing radiation, as well as cosmic rays). Multiple cycles of resetting and build-up are possible, until a sample is collected and the acquired luminescence signal measured in the laboratory.

1.2.2 The Equivalent Dose

The equivalent dose (D_e) refers to the dose measured in the laboratory, which is assumed to be equivalent to the absorbed dose, i.e. the total amount of energy that a mineral has absorbed since its last resetting event. The unit of ionizing radiation dose in the International System of Units (SI) is *gray* (symbol: Gy), defined as the absorption of one joule of radiation energy per kilogram of matter. The D_e is determined as the artificial dose that is required and generated in the laboratory to induce a luminescence signal in the material under investigation that is equal to that acquired in nature.

Over the past six decades or so, multiple methods have been proposed for determining the equivalent dose (for those that use the OSL signal from quartz, see e.g. Vandenberghe, 2004). At present, the single-aliquot regenerative-dose (SAR) protocol is probably the most widely used one (Murray and Wintle, 2000, 2003; Murray et al., 2021).

The SAR protocol was developed for use with OSL signals from quartz, which is also the approach that was implemented in this work. Essentially, the SAR protocol consists of measuring the natural and regenerated luminescence signals from one and the same single sub-sample or aliquot, which can consist of multiple grains or even a single sand-sized grain. The natural signal is the one that the sample has acquired since the last resetting event, while the regenerated signals are those that are subsequently induced by exposing the aliquot to different artificial radiation doses in the laboratory. Repeated use of this single aliquot, however, can induce sensitivity changes, i.e. a change upon re-use of the luminescence signal emitted per unit of dose administered. The unique feature of the SAR-protocol is that it seeks to correct for these changes, by measuring the luminescence response to a constant test dose, following each main measurement. By tracking this change in sensitivity, its changes can – at least in principle – be corrected for. This main principle is illustrated in Table 1.1 and Figure 1.4.

The SAR-protocol has two tests for assessing its performance and these can be built into any measurement routine, such as the measurement of the dose response curve as illustrated in Figure 1.4. The first test aims at assessing whether sensitivity-changes occurring throughout the measurement cycles are adequately corrected for. This is done by repeating the measurement of the response to a previously administered regenerative dose. Once corrected for sensitivity-change, both responses should ideally be the same, i.e. their ratio should be equal to unity (open circle in Figure 1.4).

Table 1.1: Generalized single-aliquot regenerative-dose (SAR) protocol (Murray and Wintle, 2003). During the thermal pretreatment (steps 2 and 5), it is possible to record the TL signal. Optical stimulation time (steps 3, 6 and 7) depends on the intensity and the wavelength of the light source.

No.	Treatment	Observed
1	Give dose (D_i)	
2	Preheat (160-300 °C for 10 s)	(TL)
3	Optically stimulate for 40 s at 125 °C	L_N, L_i
4	Given test dose (D_t)	
5	Heat to 160 °C (to <preheat in step 2)	(TL)
6	Optically stimulate for 40 s at 125 °C	T_N, T_i
7	Optically stimulate for 40 s at >preheat	
8	Return to 1	

This ratio is called the “Recycling Ratio". Murray and Wintle (2000) suggested values between 0.90 and 1.10 as an acceptable range, although, more recently, Murray et al. (2021) have shown that rejection of aliquots based on poor recycling may not be justified.

The second test determines the degree of charge carry-over from one cycle to another by measuring the response to a zero regenerative dose. Ideally, this should give zero signal although, in practice, a finite above-background signal is measured. This “recuperated” signal should be small compared to the sensitivity-corrected natural OSL signal and Murray and Wintle (2000) suggested it should remain below 5% (open square in Figure 1.4). It remains to be established, however, to what extent recuperation above 5% affects the accuracy of D_e-estimates (Murray et al., 2021).

While recycling and recuperation can be useful indicators of the performance of a particular SAR protocol to a specific sample/aliquot, they do not allow testing whether the response to the test-dose that is measured after the natural signal also accurately reflects the sensitivity by which this natural signal was acquired. The best laboratory-based approach that is currently available to investigate this, consists of giving the sample a known laboratory dose subsequent to optical resetting but prior to any heating. The sample is then analysed using the SAR-protocol that one had selected for measuring D_e. If the SAR protocol performs properly and as expected, the measured dose should be equal to the known, given dose, i.e. the ratio should be (close to) unity. This test is known as the dose recovery test, and the ratio of the measured to the given

dose as the dose recovery ratio. The dose recovery test is the most complete test for assessing the performance of a particular SAR protocol for any given sample. It should be noted, however, that it cannot be applied to the same aliquots as used for D_e-determination and does not establish whether this chosen SAR protocol will also determine natural doses (D_e's) with the same level of accuracy and precision.

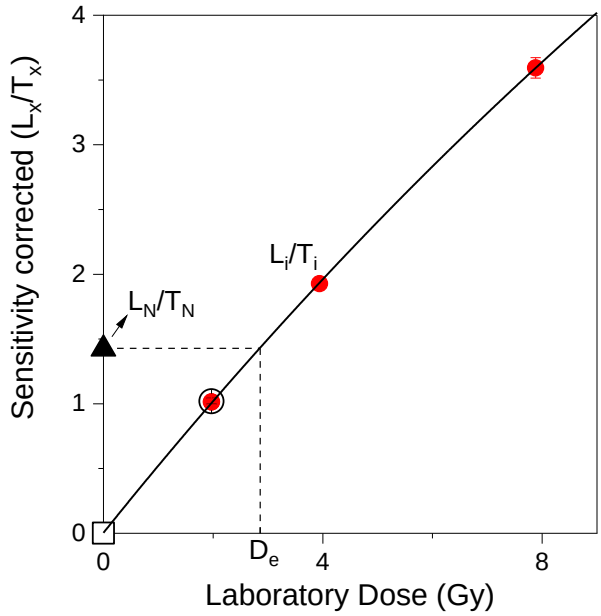

Figure 1.4: A SAR dose response curve for equivalent dose (D_e) determination. Following the measurement of the natural signal (L_N), various regenerative doses are administered and the luminescence responses measured (L_i). The luminescence response to a fixed test dose (T_N & T_i) is measured immediately after that of L_N and L_i, respectively. Correction can be made for changes in sensitivity by dividing the luminescence signal (L_i) by the response to the fixed dose (T_i), resulting in a sensitivity corrected dose response curve. The D_e is determined by interpolating the corrected natural OSL signal (L_N/T_N; solid triangle) on the corrected dose response curve. The open square represents the response to a zero dose, the open circle is a repeat measurement of the second lowest (and first administered) regenerative dose. The data shown are for an aliquot of quartz extracted from sample GLL-194314 (see Chapter 4).

The three aforementioned tests are routinely performed. Additional SAR procedural tests can consist of examining the dependence of D_e, measured dose and/or thermally transferred dose on specific SAR-measurement parameters such as preheat, cut heat or size of the test dose (see e.g. the review by Murray et al., 2021 for some examples). The SAR protocol has the particular advantage that all measurements required for determining the D_e can be made on a single aliquot. A single aliquot can be composed of thousands, hundreds, tens or even a single grain. The more grains a single aliquot contains, the larger the degree by which grain-to-grain variations in luminescence properties and D_e are averaged out (e.g. Duller, 2008a). If the number of grains on an

aliquot is sufficiently reduced (ideally to a single grain), the distribution of D_e within a sample can be examined, which enables identifying incomplete resetting and/or post-depositional disturbances. (e.g. Wallinga, 2002a,b; Thomsen et al., 2005; 2007; Bateman et al., 2007a; Duller, 2008a,b).

1.2.3 The Dose rate

Of equal importance in determining a luminescence age is the dose rate (Eq. 1.1) experienced by the sample over the period that is to be dated. It refers to the dose from naturally occurring ionizing radiation that is absorbed by the sample per unit of time (unit: Gy per unit of time, e.g. Gy/a).

This radiation consists of alpha (α) particles, beta (β) particles and (γ) gamma rays emitted through the decay of the ^{238}U, ^{235}U and ^{232}Th decay series, and of ^{40}K and ^{87}Rb; cosmic rays contribute to the dose rate as well. The different types of radiation interact with matter in a different manner resulting in different penetration ranges (for α, β and γ-radiation several 10^{-2} mm, 10^{0} mm and 10^{2} mm, respectively). In addition, not all types of radiation are equally efficient in inducing luminescence. Compared to β and γ-radiation, for instance, α-radiation, will induce significantly less luminescence per unit absorbed dose (Aitken, 1985, 1998). While these properties complicate both sampling and evaluation of the dose rate, they can also be put to advantage. In the coarse-grain technique, e.g., sediment grains from the sand-sized fraction (63-250 μm) are used. During sample preparation, an outer layer of about~ 10 μm is etched away from the grain rims, which is generally accepted to reduce the contribution from α-particles to a negligible level (for summaries and discussion, see Aitken, 1985 and Vandenberghe, 2004). A variety of analytical techniques is available to determine the dose rate (i.e. radionuclide concentration), including neutron activation analysis, inductively coupled plasma mass spectrometry, alpha-counting, beta-counting, and gamma-ray spectrometry. All of these methods essentially rely on concentration determinations (in mg/kg or Bq/kg) which are then converted to amount of energy absorbed per unit of mass and time (Gy/a) using tabulated nuclear data (e.g. Adamiec and Aitken, 1998; Guérin et al., 2011; Cresswell et al., 2018). In the case of the coarse-grain technique, which is used in this work, calculated dose rates need additional corrections for the effects of etching and attenuation, as well as water (and perhaps also organic) content in the sediment or material under investigation (Aitken, 1985; Lian et al., 1995). The contribution of cosmic rays to the dose rate depends on latitude, altitude,

and burial depth. It is usually not determined directly but calculated from expressions available in the literature (e.g. Prescott and Hutton, 1994).

In contrast to the large body of literature that is available on luminescence measurement protocols and luminescence behavioral studies, the dose rate appears to have received significantly less attention over the past few decades. The most comprehensive review available is probably that by Aitken (1985), followed by the overviews presented by Wagner (1998), Hossain (2003) and Vandenberghe (2004). Updates of nuclear data and associated conversion factors are made available at regular time intervals (see above). In recent years, several programs have been made accessible to facilitate dose rate calculations (Durcan et al., 2015; Martin et al., 2018; Liang and Forman, 2019). In addition, new computational developments for simulating the transit of particles through matter have been implemented to improve quantification of dose rate effects (Guérin et al., 2011; Murray et al., 2012; Cunnigham et al., 2018; Riedesel and Autzen, 2020).

A short description on the instrumental facilities and procedures for equivalent dose and dose rate determination as implemented at the Ghent Luminescence Laboratory, is provided in Appendix A.

1.3 Aims and outline of the thesis

The overall aim of this dissertation is to investigate the potential of quartz-based OSL dating for application to two specific types of anthropogenically heated features, with a particular emphasis on those dating from the last few centuries. As such, it seeks to assess whether the approach can allow obtaining meaningful chronometric information over that time range where ^{14}C-dating is highly limited. The specific studied features are relic charcoal kilns or hearths and remains of early-Modern and Modern cooking hearths. The case studies were particularly chosen in the framework of providing a chronometric context to specific archaeological research questions. This is explained in greater detail in the background preceding each of the two main parts of this dissertation, together with the specific challenges that each of these features poses in terms of chronometry and luminescence dating in particular.

Part I concerns luminescence chronometric research on relic charcoal kilns and comprises 3 chapters. Chapter 2 investigates whether quartz-based OSL dating can yield accurate age information for loamy sediments that were heated during charcoal

production in the Sonian Forest (Central Belgium) and, if so, to what level of precision. It uses a set of samples from seven kilns, of which six pre-date and one postdates 1650 CE on the basis of independent ^{14}C-dating of charcoal. It also seeks to develop a work-flow, and identify potential difficulties and pitfalls of OSL dating applied to these materials. Chapters 3 and 4 extend the aforementioned exercise to relic charcoal kilns in sandy environments. Here, samples from relic charcoal kilns in the Veluwe (Central Netherlands) and Zoersel Forest (Central Belgium) are investigated and results are compared with independent age information (^{14}C-dating and historical sources). In addition to standard OSL analyses using large and small multiple-grain analyses, that of single sand-sized grains of quartz is explored as well.

Part II consists of Chapter 5 which, building on insights gained in Part I, extends the investigations to remains of early-Modern and Modern cooking hearths. These hearths were recently discovered during a large-scaled archaeological excavations at Ninove (East-Flanders, Belgium) and are associated with one or more military encampments built sometime between the end of the 17th to the mid-18th century CE.

The concluding Chapter 6 seeks to combine all experimental evidence and insights gained to address the main, overall research question: can quartz-based optically stimulated OSL-dating yield both accurate and precise age information for these particular features, and those from post-1650 CE in particular? Possibilities and limitations are outlined, together with possible directions for future luminescence-based research of relatively recent anthropogenically heated materials in general.

PART I: Relic Charcoal Hearths

Background

Before the extensive use of fossil coal from the 19th century CE onwards, charcoal was an important source of fuel. Compared to wood, it has a higher caloritic value, and it is a lot lighter. As such, it could be used for a range of purposes, including ones that require high temperatures (such as iron melting and glass production), and it could be transported over longer distances where needed. Charcoal was produced in many forested regions in Europe (Nelle, 2003; Ludemann, 2010; Carrari et al., 2017; Paradis-Grenouillet and Dufraisse, 2018; Schneider et al., 2020) and North America (Hart et al., 2008; Potter et al., 2013). The numerous remains of former charcoal production sites (*relic charcoal kilns* or *hearths*) testify to the importance of this activity (e.g. Ludemann, 2003; 2010; Nelle, 2003; Deforce et al., 2013; 2021b). These remains are increasingly studied by researchers from a wide range of disciplines, such as historical geography, archaeology, paleoecology, geomorphology, climate change, carbon sequestration, for various purposes.

Charcoal production had a significant impact on the extent and composition of former forests. Anthracological analysis and dating of suitable charcoal fragments recovered from the relic hearths can provide information about wooden taxa prevailing in a forest at a particular time, on shifts in woodland composition, and on the extent of former primeval forests (Ludemann, 2003; 2010; Nell, 2003, Deforce et al., 2013; 2021a,b). Subsequently, this can provide information about human occupation and settlement dynamics (Groenewoudt and Spek, 2016; Deforce et al., 2020). Heat generated during charcoal production alters the properties of the soil in the layers closest to the surface, preventing continuous tree growth and development as well as tree regeneration, which has implications for forest management practices (Carrari et al., 2016a; Mastrolonardo et al., 2018). Remains of charcoal kilns are also examined to investigate the impact of biochar on carbon sequestration, soil properties, vegetation composition, biodiversity, and growth rate for comparative purposes. The role of biochar in the carbon cycle and soil fertility is a topic of ongoing debate (Hardy et al., 2017a). The charring of botanical materials results in their preservation in soil for an extended period of time due to their high stability, leading to a significant amount of carbon remaining in the soil and reducing the impact of greenhouse gases on the atmosphere. The stability of biochar can be studied by dating charcoal remains of relic kilns (Hardy et al., 2017a; Hirsch et

al., 2017, 2018; Mastrolonardo et al., 2018). Furthermore, the remains of charcoal kilns likely play a significant role in the alterations of terrain topography, soils, soil microbial communities, vegetation, and their associated water, carbon, and nutrient cycles (Hirsch et al., 2017; Deforce et al., 2021a; Raab et al., 2022).

Charcoal production technology changed through time from pit kilns to above-ground mound-kilns at around 1200-1300 CE, as the latter allow producing significantly larger volumes of charcoal (Deforce et al., 2021a, b). In the Low Countries, this has been related to changes in iron production technology (Deforce et al., 2021a). Not all relic charcoal hearths can be related to iron production, however, adding to the complexity of understanding drivers for charcoal production (Deforce et al., 2013). The relics of the more recent, above-ground mound-kilns have been studied more extensively. That is because they represent (small) elevations in the landscape, which can be detected through remote sensing technologies (Lambers et al., 2019; Deforce et al., 2021a) and subsequently verified through field-prospection (Koops, 2021). These early-Modern to Modern charcoal kilns are the most challenging from a chronometric point of view (for the reasons outlined in Chapter 1). Radiocarbon dating is commonly applied as charcoal is abundant in the hearths where it was produced. Several studies have illustrated the limitations of the approach for dating relic charcoal hearths post-dating 1650 CE (e.g. Reimer et al., 2013; Deforce et al., 2013, 2021a) due to plateaus in the calibration curve (De Vries and Suess-effect; see section 1.1). This implies that the age and chronological order of charcoal burning events during the last few centuries is in fact unknown, significantly hampering the interpretation of the majority of the relic charcoal hearths that is being studied.

The following three chapters investigate whether quartz-based OSL dating of sediments that were heated during charcoal production can be an accurate and more precise alternative to ^{14}C.

Appendix B provides more background information on kiln types structure, and operation; it also briefly details the rationale for the site and kiln selection, as well as the sampling strategy adopted in this work.

Chapter 2: Sonian forest (Bypassing the Suess effect: age determination of charcoal kiln remains using OSL dating)

Nasrin Karimi Moayed, Dimitri Vandenberghe, Koen Deforce, Jan Bastiaens, Elke Ghyselbrecht, Ann-Eline Debeer, Philippe De Smedt, Wim De Clercq, Johan De Grave

This chapter is slightly modified from the published version in the Journal of Archaeological Science. The modifications concern formatting, inclusion of the supplementary material in the main text, and minor suggestions made by the examination commission.

Author contributions

Nasrin Karimi Moayed: Field investigation, Sampling, Sample processing, Data analysis, Methodology, Data curation, Writing.
Dimitri Vandenberghe: Field investigation, Sampling, Methodology, Writing, review and editing.
Koen Deforce: Field investigation, Sampling, Methodology, Writing, review and editing. *Jan Bastiaens:* Field investigation.
Elke Ghyselbrecht: Sampling.
Ann-Elaine Debeer: Sample processing.
Phillipe De Smedt: Field investigation.
Wim De Clercq: Supervision, Funding acquisition.
Johan De Grave: Supervision, Field investigation, Sampling, Writing, review and editing, Funding acquisition.

Abstract

Ancient forests all over Europe often preserve remains of (pre)historic charcoal production (kilns), informing on past forest composition and anthropogenic woodland exploitation. So far, the chronology of these features has been entirely derived from ^{14}C-dating of associated charcoal. Though generally successful, ^{14}C-dating cannot provide more precise age information for post-1650 CE features, while most of the archaeological remains of charcoal kilns date to this period. Here, we investigate the potential of quartz-based optically stimulated luminescence (OSL) dating of sediments that were heated during charcoal production as a more precise alternative tool for age determination of these kilns.

Using a set of 14 samples collected from both relict charcoal kilns and the underlying parent material, we first document the quartz OSL characteristics in terms of the procedural tests commonly used to assess the appropriateness of the single-aliquot

regenerative-dose (SAR) protocol. The results suggest that the measurement procedure allows determining equivalent doses both accurately and precisely. We then demonstrate how the linear part of the dose-response curve can be exploited to examine completeness of resetting and/or post-depositional disturbance without compromising instrument time, precision and laboratory accuracy. Optical ages derived from these distributions are consistent with the available independent (^{14}C) age information for the charcoal kilns. We conclude that OSL can provide more precise and viable alternative to ^{14}C and will be especially useful to constrain post-1650 CE features in time. Our results also suggest that the approach may allow establishing relative chronologies with a time resolution of 2-4 %.

Keywords: Charcoal production, OSL dating, Radiocarbon dating, Middle ages, Modern age, Sonian forest

2.1 Introduction

Remains of former charcoal production sites (charcoal kilns) can be found in many forested areas in Europe (Nelle, 2003; Ludemann, 2010; Carrari et al., 2017; Paradis-Grenouillet and Dufraisse, 2018; Schneider et al., 2020) and North America (Hart et al., 2008; Potter et al., 2013). Two major types of charcoal kilns have been described, i.e. pit kilns, which generally date from the Iron Age till 1200 CE, where charcoal has been produced in small rectangular or circular pits (e.g. Groenewoudt, 2007; Deforce et al., 2021b; Drailly and Deforce, 2019), and mound kilns, dating between 1300 CE and the 20th century CE, where large, above-ground dome-shaped stacks of wood have been carbonized (e.g. Ludemann, 2003; 2010; Nelle, 2003). Archaeological remains of these charcoal kilns are frequently used in palaeoecological studies, as they are an important source of information on former forest composition and past human woodland exploitation and fuel production (e.g. Ludemann, 2003; 2010; Nelle, 2003; Deforce et al., 2013; 2021b). More recently, charcoal kiln remains are also studied to identify the role of biochar in relation to soil properties (e.g. Hardy et al., 2016; 2017a; Hirsch et al., 2017; 2018), carbon sequestration (e.g. Hardy et al., 2017b; Hirsch et al., 2017; Mastrolonardo et al., 2018) and composition, biodiversity and growth rate of the vegetation. All these studies require a chronological framework for the original kilns, which is generally established using radiocarbon (^{14}C) dating (Carrari et al., 2016a, b; Buras et al., 2020). In exceptional cases, dendrochronology can be applied when

charcoal fragments from specific taxa containing a large number of growth rings can be recovered (e.g. Raab et al., 2015), or when radiocarbon dating and dendrochronology of old trees growing on top of the kiln sites can be combined (e.g. Deforce et al., 2013). The majority of the charcoal kilns found in Europe (e.g. Ludemann, 2010; Raab et al., 2015; Carrari et al., 2017) and the Americas (Raab et al., 2017; Patzlaff et al., 2018) are mound kilns dating between the seventeenth and nineteenth century CE. Age determination of post-1650 CE archaeological features using radiocarbon dating is problematic because of plateaus in the calibration curve (De Vries and Suess-effects), caused by variations in sunspot activities and the dilution of atmospheric $^{14}CO_2$ by fossil fuel derived CO_2 which does not contain ^{14}C (Stuiver, 1961; Tans et al., 1979). This is a major constraint for studies using former charcoal production sites and an alternative dating method would therefore be of great value.

At present, luminescence dating is widely used for establishing sediment deposition chronologies by determining when the constituent mineral grains (such as quartz and feldspar) were last exposed to sunlight (e.g. Duller, 2004, 2008b; Rhodes, 2011). Sufficient exposure to heat, however, also resets the luminescence 'clock' allowing application to a range of fired materials such as pottery, bricks, hearths and burnt sediments (e.g. Aitken, 1985; Wagner, 1998; Benea et al., 2007; Armitage and King, 2013). Based on field hearth experiments (Yu et al., 2016) and measurements of magnetic susceptibility and soil organic matter (Hirsch et al. (2018) it has been suggested that the heat generated during charcoal production should be sufficient to reset the optically stimulated luminescence (OSL) signal from quartz in sandy sediments underlying the kilns up to depths of about 5 cm.

In this paper, we report on an exploratory investigation into the potential of quartz-OSL signals for dating heated sediments associated with archaeological remains of charcoal kilns. Our approach is empirical in that we test the applicability of OSL dating procedures that are widely adopted by luminescence geochronologists around the world. To that respect, the underlying rationale is straightforward: as reliable chronometric information is required for a vast amount of charcoal kilns, it is desirable to have a dating tool that is also workable in practice (i.e. readily accessible instrumentation, a cost and time-effective workflow for laboratory analysis, etc.). We document our experimental design and the general quartz-OSL characteristics for samples collected from both pre and post-1650 CE features. For each of these features,

we then evaluate both the accuracy and the precision of the resulting OSL ages through comparison with independent ^{14}C ages. The entire dataset is then used to discuss sampling strategies, dose rate issues, resetting and precision.

2.2 Material and Methods

2.2.1 Study area and setting

The charcoal kilns examined in this study are all remains of mound kilns located in the Sonian forest (Central Belgium; Figure 2.1a, b), one of the few areas in North and Central Belgium where such relics are known to be well-preserved. The Sonian forest mainly consists of beech and oak trees (Vandekerkhove et al., 2018) and is one of the largest beech forests in the Benelux region (Belgium, the Netherlands and Luxemburg). It covers an area of 43.83 km^2, of which 2.69 km^2 have been recognized as part of the UNESCO World Heritage site "Ancient and primeval beech forests of the Carpathians and other regions of Europe" (Kirchmeier and Kovarovics, 2016). The Sonian forest is believed to be a remnant of the *Silva Carbonaria* or *Carbonaria Silva* (charcoal forest), a vast forest that covered the larger part of central Belgium up to at least the end of the Early Medieval period (Vander Linden, 1923; Tack et al., 1993). The *Silva Carbonaria* is mentioned in several historic documents and its name indicates that it was an important area for charcoal production (Duvivier, 1861; Vander Linden, 1923; Schmidt-Wiegand, 1981). Except for some small parts, the Sonian forest is one of the few forested areas in Belgium that has never been cleared for agriculture and has known a continuous woodland cover since the early Holocene period (Tack et al., 1993; Langohr, 2009). It has been used for both iron and charcoal production during the early medieval period (475-1000 CE), as indicated by the presence of numerous remains of low furnaces, accumulations of iron slags, and charcoal (pit)kilns dating to this period (Metalidis et al., 2008; Deforce et al., 2021b). While iron smelting activities in the forest ceased at the end of the early medieval period, charcoal production continued until the 20th century CE (Van der Ben et al., 1997).

The Quaternary cover in the study area is essentially composed of continental, homogeneous aeolian deposits (loess), consisting of 5-15% clay, 80% silt and 3-20% fine to very fine sand (Van Ranst, 1981; Van Ranst et al., 1982); the mineralogical composition (following post-depositional decalcification) is dominated by quartz (up to 80%; Louis, 1969).

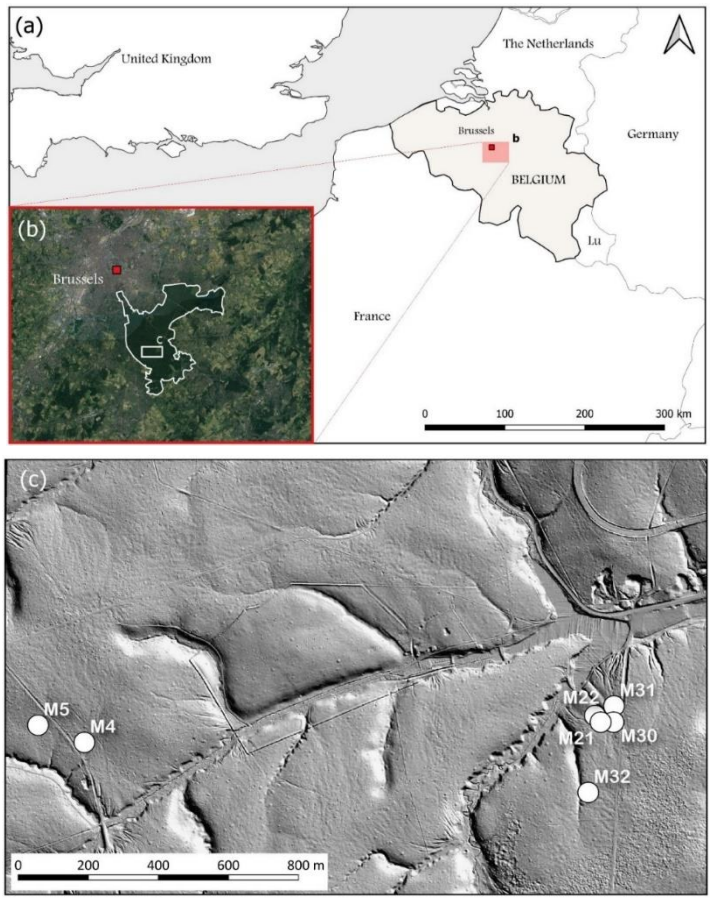

Figure 2.1: (a) Location of the Sonian Forest, southeast of Brussels, in Belgium. (b) The area delineated in white shows the limit of the remaining forest. (c) Hillshade map of the sampling site area within Sonian Forest; the sampled charcoal kiln remains are shown by white circles.

2.2.2 Kilns and Sampling

Samples from sediments associated with seven charcoal kilns were collected for OSL dating. The location of the sites is indicated in Figure 2.1c.

Small sampling pits of about 50 cm wide and 70-80 cm deep were dug. In general, the stratigraphic sequences consist of a vegetation and litter layer overlying a dark (black/grey or brownish) layer of ~30-40 cm thick, which is rich in charcoal and rooted through. In some of the exposed sections, this is followed by a lighter, greyish to yellow layer, which can be more than 25 cm thick and contains some charcoal and rootlets. The deepest unit that was observed is a homogeneous yellow silt, representing the typical mid-Weichselian loess cover in this region. Examples of the examined profiles are shown in Figure 2.2. The samples for OSL-analysis were collected by hammering stainless steel cylinders with a diameter of 5 cm into fresh exposures of hand-made pits.

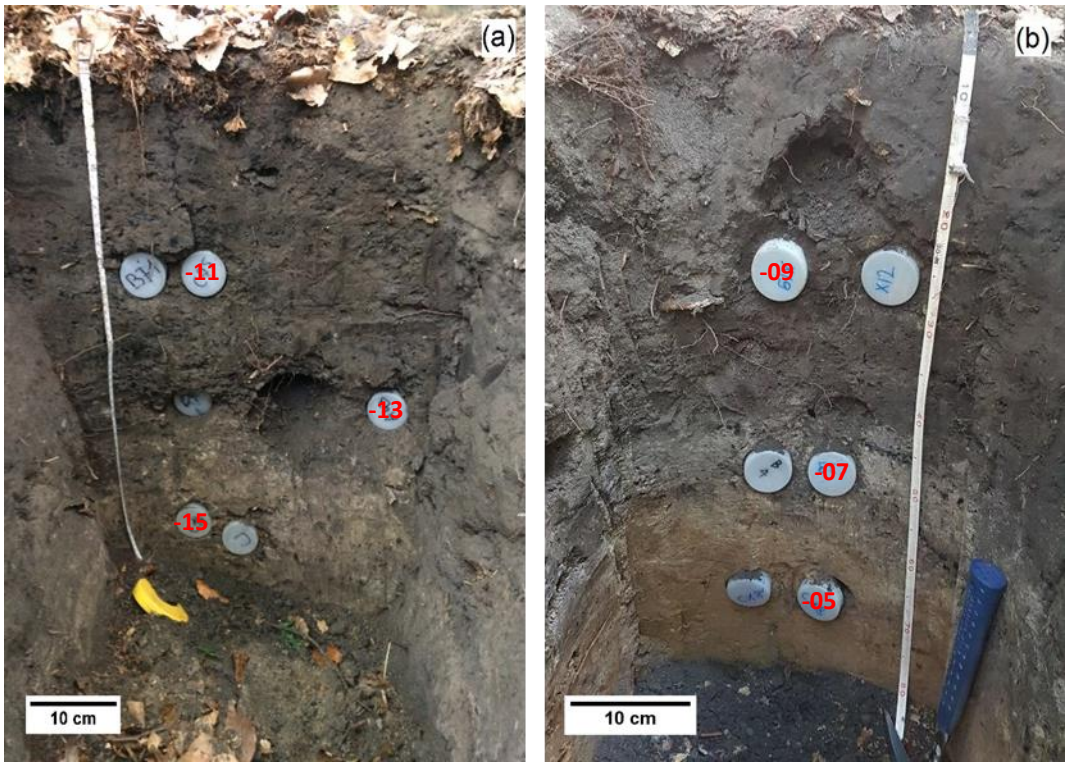

Figure 2.2: Photographs of the profiles observed during sampling of features M32 (a) and M31 (b).

The cylinders were dug out, during which the surrounding sediment was collected for radiometric analyses. The stratigraphic position of the samples is indicated in Table 2.1, with "D" referring to the dark layer containing charcoal and "L" to underlying layers lighter in color; as such these denotations refer to color only. Additional undisturbed sediment samples were taken for evaluation of the time-averaged moisture content. From the central part of each charcoal kiln, bulk sediment samples (c. 10 l.) were taken from the charcoal rich layer for radiocarbon dating and (future) anthracological analysis.

2.2.3 OSL dating

The samples for luminescence analyses were prepared in line with widely adopted protocols for extracting quartz grains of the 63-90 or 63-250 µm fraction (HCl, H_2O_2, wet and dry sieving, HF). The purity of the quartz extracts was tested by measuring their sensitivity to stimulation with infrared light (OSL IR depletion ratio; Duller, 2003). The sensitivity to infrared stimulation was defined as significant if this ratio deviated more than 10% from unity; none of the samples or aliquots had to be rejected on this basis. For measurement, the quartz grains were fixed on the inner 8 mm (large

Table 2.1: Specific radionuclide activities used for dose rate evaluation, estimates of past moisture content (F*W), calculated dose rates, D_e's and relative standard deviations (RSD), optical ages and random (σ_r), systematic (σ_s) and total uncertainties (σ_{tot}). The total dose rate includes the contribution from internal radioactivity and cosmic radiation. The number of aliquots used for D_e-determination is given in italics between parentheses in subscript. The uncertainties mentioned with the dosimetry and D_e data are random; except for the Cal CE ages given in the last column, all uncertainties represent 1 sigma. The samples were ranked according to their stratigraphic position in each feature, with D and L referring to the darker and lighter layers, respectively, in which the samples were taken (see text for details).

Feature	*Layer*	*GLL-code*	*Depth*	*^{234}Th*	*^{226}Ra*	*^{210}Pb*	*^{232}Th*	*^{40}K*	*F*W*	*Total dose rate*	*D_e*		*Age*	*σ_r*	*σ_{sys}*	*σ_{tot}*	
			(cm)	*(Bq kg^{-1})*	*(Bq kg^{-1})*	*(Bq kg^{-1})*	*(Bq kg^{-1})*	*(Bq kg^{-1})*	*(%)*	*(Gy ka^{-1})*	*(Gy)*	*RSD (%)*	*(ka)*	*(%)*	*(%)*	*(%)*	*Age CE (± 2σ)*
M21	D	160808	30	26 ± 2	37.7 ± 0.4	42 ± 2	32.9 ± 0.3	411 ± 4	31 ± 5	2.20 ± 0.03	0.99 ± 0.01 $_{(69)}$	10	0.45 ± 0.05	1.7	11.25	11.38	1561 ± 103
M22	D	160812	25	31 ± 3	33.7 ± 0.7	28 ± 2	31.2 ± 0.3	399 ± 4	22 ± 3	2.15 ± 0.03	1.52 ± 0.03 $_{(67)}$	14	0.71 ± 0.06	2.14	8.84	9.09	1306 ± 129
	L	160810	40	28 ± 1	35.6 ± 0.4	28 ± 1	34.5 ± 0.3	456 ± 5	17 ± 3	2.40 ± 0.02	7.5 ± 0.3 $_{(71)}$	32	3.10 ± 0.30	3.99	7.84	8.8	1084 ± 600
M4	D	160814	20	22 ± 2	33.3 ± 1.7	48 ± 2	32.0 ± 0.3	405 ± 4	24 ± 4	2.35 ± 0.03	0.48 ± 0.01 $_{(68)}$	14	0.21 ± 0.02	2.12	9.28	9.52	1810 ± 57
	L	160816	30	31 ± 2	36.9 ± 1.1	35 ± 2	36.1 ± 0.4	453 ± 5	11 ± 2	2.63 ± 0.04	1.52 ± 0.07 $_{(71)}$	38	0.58 ± 0.05	4.75	6.69	8.21	1439 ± 95
M5	D	160820	15	33 ± 3	35.3 ± 0.7	31 ± 3	32.9 ± 0.7	417 ± 5	26 ± 4	2.18 ± 0.04	1.22 ± 0.01 $_{(67)}$	7	0.56 ± 0.06	2.17	10.01	10.24	1455 ± 115
	L	160818	30	36 ± 2	38.7 ± 0.4	31 ± 3	35.3 ± 0.4	471 ± 5	12 ± 2	2.63 ± 0.04	3.72 ± 0.14 $_{(71)}$	30	1.40 ± 0.10	4.09	6.87	8	600 ± 226
M30	D	184301	25	33 ± 1	33.2 ± 0.7	35 ± 2	31.6 ± 0.6	405 ± 4	43 ± 6	1.93 ± 0.02	0.82 ± 0.02 $_{(66)}$	16	0.43 ± 0.06	2.74	14.38	14.64	1592 ± 125
	L	184303	48	37 ± 2	35.3 ± 0.4	37 ± 3	35.3 ± 0.4	441 ± 4	28 ± 4	2.29 ± 0.03	1.73 ± 0.05 $_{(71)}$	25	0.75 ± 0.08	3.22	10.51	10.99	1263 ± 166
M31	D	184309	25	36 ± 2	33.3 ± 1.0	40 ± 4	33.2 ± 0.3	411 ± 4	47 ± 7	1.96 ± 0.04	0.70 ± 0.02 $_{(69)}$	22	0.36 ± 0.06	3.4	15.54	15.9	1661 ± 114
	L	184307	48	37 ± 3	36.1 ± 1.1	33 ± 3	35.7 ± 0.4	438 ± 4	28 ± 4	2.25 ± 0.03	1.04 ± 0.05 $_{(64)}$	35	0.46 ± 0.05	5.03	10.57	11.71	1555 ± 155
	L	184305	65	38 ± 2	36.7 ± 0.4	32 ± 2	37.7 ± 0.4	480 ± 5	24 ± 4	2.42 ± 0.03	1.86 ± 0.08 $_{(66)}$	35	0.77 ± 0.08	4.47	9.69	10.68	1249 ± 164
M32	D	184311	20	31 ± 2	34.2 ± 0.7	32 ± 3	32.4 ± 0.3	408 ± 4	41 ± 6	1.94 ± 0.03	0.75 ± 0.03 $_{(65)}$	35	0.39 ± 0.06	4.31	13.75	14.41	1632 ± 111
	L	184313	35	32 ± 2	34.6 ± 0.3	38 ± 3	32.6 ± 0.3	420 ± 4	44 ± 7	1.97 ± 0.03	0.82 ± 0.03 $_{(63)}$	28	0.42 ± 0.06	4	14.94	15.47	1601 ± 129
	L	184315	55	35 ± 2	37.0 ± 0.7	37 ± 2	35.7 ± 0.4	444 ± 4	29 ± 4	2.27 ± 0.03	1.50 ± 0.05 $_{(63)}$	29	0.66 ± 0.08	3.56	10.95	11.52	1356 ± 153

aliquots) or 2 mm (small aliquots) of stainless steel discs with a thickness of 0.5 mm and a diameter of 9.7 mm, using an aerosol of silicone oil as adhesive. The luminescence measurements were made using automated Risø TL/OSL readers equipped with blue (λ_{max} = 470 nm) and infrared (λ_{max} = 850 or 870 nm) light emitting diodes. All luminescence emissions were detected through a 7.5 mm thick Hoya U-340 UV filter. Details on the measurement apparatus can be found in Bøtter-Jensen et al. (2003a) and Lapp et al. (2015). The equivalent dose (D_e) was determined using the single-aliquot regenerative-dose (SAR) protocol (Murray and Wintle, 2000; 2003). Unless mentioned otherwise, a preheat of 10 s to 220 °C and a cut heat to 160 °C were adopted. Stimulation with the blue diodes was for 38.5 s at 125 °C.

All calculations used the initial part 0.31 s of the decay curve, minus a background evaluated from the following 0.77 s of stimulation. Each measurement of the response to the test dose was followed by a stimulation with the blue diodes for 38.5 s at 280 °C to minimize recuperation (Murray and Wintle, 2003).

The sediment that was collected for dose rate determination was dried at 110 °C (until constant weight), pulverized and homogenized. A subsample of this material was then cast in wax to prevent radon loss and to provide a well-defined and reproducible counting geometry (Murray et al., 1987; De Corte et al., 2006). The samples were then stored for at least one month before being measured on top of a low-level extended energy-range HPGe gamma-ray spectrometer. The specific radionuclide activities were converted to dose rates using the data tabulated by Adamiec and Aitken, (1998). A factor of 0.9 (± 5% relative uncertainty) was adopted to correct the external beta dose rates for the effects of attenuation and etching (Mejdahl, 1979). The external beta and gamma dose rates were corrected for the effect of moisture following the procedure outlined in Aitken, (1985). The water content in fully saturated samples was measured in the laboratory and we assumed that, during burial, the average water content was half of these values (± 15% relative uncertainty); this corresponds approximately to the mid-value of variations in moisture content as observed over one year (March 2003 CE–March 2004 CE) by De Vos, (2005). An internal dose rate in quartz grains of 0.013 ± 0.003 Gy ka^{-1} was adopted (Vandenberghe et al., 2008). The contribution of cosmic radiation was calculated following Prescott and Hutton (1994).

2.2.4 Radiocarbon dating

Bulk samples (c. 10 l each) were collected from the charcoal rich layer of the kilns and were wet sieved on a 0.5 mm mesh to recover charcoal fragments. The sieved residues were air-dried and a minimum of 100 charcoal fragments was randomly selected from this residue for taxonomic identification. Each charcoal fragment was broken along a transverse, tangential and radial plane. Wood anatomical characteristics on these surfaces were studied using a reflected light microscope with dark field illumination (50x - 500x). Identifications are based on wood anatomy atlases and identification keys (Schweingruber, 1990; Schoch et al., 2004) and the reference collection of artificially charred wood samples of the Flanders Heritage Agency. From the identified charcoal fragments, samples with the lowest potential age at the time of charring were selected, i.e. twigs or taxa with a low maximal expected age, to avoid a potential old wood-effect.

Charcoal samples for radiocarbon dating were combusted to CO_2 and transformed into graphite, after which the radiocarbon concentrations were measured in a MICADAS AMS-machine at the Royal Institute for Cultural Heritage, Brussels (Belgium) (Boudin et al., 2015). Results were calibrated with OxCal 4.3 (Bronk-Ramsey, 2009) using the Intcal13 calibration curve (Reimer et al., 2013).

2.3 Results

2.3.1 OSL dating

2.3.1.1 Luminescence characteristics and equivalent dose determination

Figure 2.3a shows typical OSL decay curves for an aliquot of quartz grains extracted from one of the samples collected in the dark charcoal-rich layer (sample GLL-184311). The signals are bright and decay rapidly with stimulation time, as one would expect for a quartz OSL-signal that is dominated by the fast component (e.g. Jain et al., 2003). A representative dose response curve is shown in Figure 2.3b; it is well represented by a single saturating exponential function (solid black line).

The inset to Figure 2.3b illustrates where the sensitivity corrected natural OSL signal intersects the dose response curve. In this region of interest, the signal grows linearly with dose. Figure 2.3b also illustrates the good behavior of the samples in the SAR protocol, with the dose response curve passing through the origin (indicating that recuperation is negligible; open square) and the ability to re-measure the response to a

regenerative dose (indicating that sensitivity changes occurring throughout the measurement cycle are accurately corrected for; the solid and open circle overlying each other). These finds were exploited to facilitate further analyses of these "young" samples (see further), in that we shortened the SAR sequence to include measurements of the natural and one regenerative dose point (0.5-2.0 Gy) only; this was followed by a measurement of the response to a zero dose and the same regenerative dose (to assess recuperation and recycling, respectively). An IRSL measurement at 60 °C preceded that of the recycled OSL signal to screen for the presence of feldspar. The size of the test dose was chosen to be same as that of the regenerative dose. Figure 2.4 shows the same data for one of the samples collected in a lighter-colored layer (GLL-184305); the only difference is that, here, the natural OSL signal may also intersect with the non-linear region of the dose response curve. Of particular concern when dating young samples (or low D_e's) is the thermal pre-treatment or preheat.

In OSL terminology – and exposure to light being the resetting agent – *basic or thermal transfer* (Aitken, 1998; Wintle and Murray, 2006) refers to the transfer of relic charge in thermally relatively stable traps that are less (or not) sensitive to light, to thermally more stable light-sensitive traps, resulting in an overestimation of the D_e. In this work, heating is supposed to be the main resetting agent. One would thus expect the phenomenon to be of no concern as long as firing in the past was able to reach the temperature required to reset, even partially, the quartz OSL signal; this signal is thought to originate with the thermoluminescence (TL) signal commonly referred to the quartz 325 °C TL peak (Spooner et al., 1988; Spooner, 1994; Wintle and Murray, 1997; Murray and Wintle, 1999). When using OSL signals, the importance of thermal transfer, and hence an indication of completeness of resetting, can be examined by assessing the effect of the preheat temperature on estimates of D_e.

The dependence of D_e on preheat was investigated using sample GLL-184301. Three large (8 mm diameter) aliquots were measured at each of seven preheat temperatures in the range of 160 °C–280 °C, and the "shortened" SAR protocol as outlined in the above. The results are summarized in Figure 2.5. The D_e is independent of preheat temperature up to at least 260 °C. Across this temperature range, recycling ratios are consistent with1.0 ± 0.1 and recuperation remains below 0.2% of the corrected natural OSL signal; the correction for sensitivity changes performs less at the highest preheat temperature

of 280 °C. For this sample, we also investigated the dependence of measured dose on preheat using a dose recovery test (Murray and Wintle, 2003).

In this test, large (8 mm diameter) natural aliquots were first bleached for two times 250 s using the blue diodes at room temperature, with a 10 ks pause in between the two bleaching treatments. They were then given a dose chosen to approximate the natural dose and measured using the SAR protocol. The results are shown in Figure 2.6.

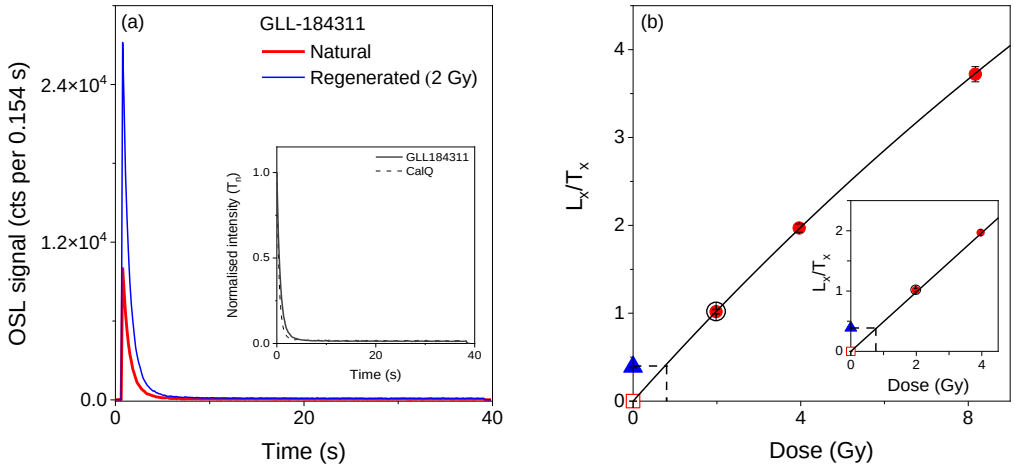

Figure 2.3: (a) Representative OSL decay curves for an aliquot of sample GLL-184311. The natural and regenerated signals are shown as the red and blue lines, respectively. The inset compares the regenerated OSL decay curve (normalized to intensity in the first 0.15 s of stimulation) from the sample with that from calibration quartz (GLL-CalQ). (b) SAR growth curve for an aliquot of this sample. Recycling and recuperation points are represented by the open circle and square, respectively. The black solid line represents a single saturating exponential function fitted to the regenerated data. The natural signal (solid triangle) intersects with the linear region of the dose response curve (inset).

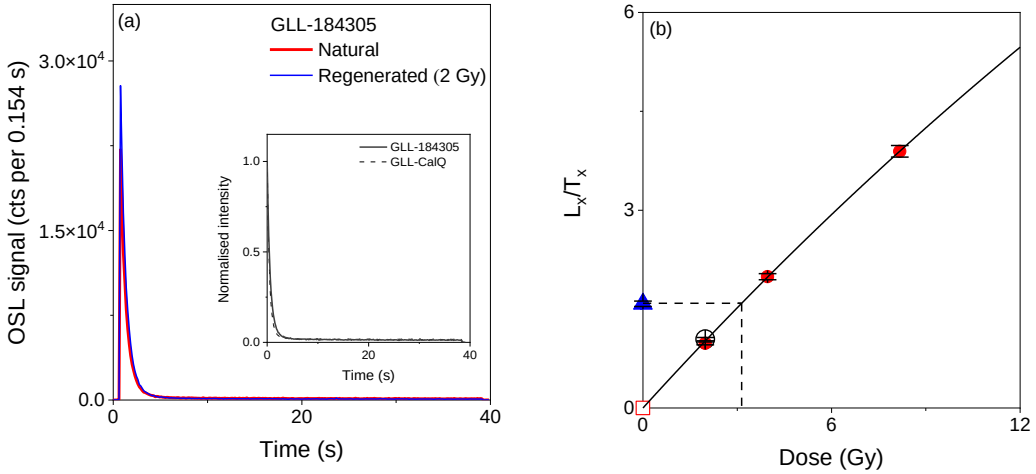

Figure 2.4: Same as in Figure 2.3, for an aliquot of sample GLL-184305.

The ability to recover a known dose seems independent of preheat across the entire temperature range, and within analytical uncertainties (standard error on the mean), the dose recovery ratios to not differ more than 5% from unity. The overall average (i.e. over all 21 aliquots; ± 1 standard error) measured to given dose ratio is 1.02 ± 0.01. Recycling ratios are consistent with 1.0 ± 0.1, and recuperation remains below ~ 0.5% of the corrected natural signal. The lack of sensitivity of D_e and measured known dose to preheat temperature indicates that thermal transfer is not significant for these samples. The combined dataset suggests that the SAR protocol in combination with any preheat up to at least 260 °C is suitable. For all further analysis, we adopted a preheat of 10 s at 220 °C, which was chosen as the approximate middle of the plateau region.

We evaluated the overall performance of the SAR protocol (using the 220 °C preheat) by applying the dose recovery test to our entire suite of samples. In between 3 to 72 small (2 mm diameter) aliquots were used for each sample. The average dose recovery ratios per sample are shown in Figure 2.7a, while Figure 2.7b summarizes the entire dataset (n = 125) as a histogram. Within 1 standard error, individual ratios do not differ by more than 5% from unity. The values are normally distributed around an overall average recovered to give dose ratio (± 1 standard error) of 0.991 ± 0.013, with an RSD of 15%. These results, in combination with the aforementioned finds, demonstrate that the SAR protocol should be suitable for measuring the D_e's in our samples.

For all samples, 72 replicate measurements of D_e were made using small aliquots. Occasionally (less than 4% of measurements), an aliquot did not emit a net natural test dose signal ("T_n") higher than three times the standard deviation of the background signal, and was hence excluded. Representative results for two samples collected from dark charcoal-rich layers (GLL-184301 and GLL-160808) are shown as histograms in Figure 2.8. As histograms are, in contrast to e.g. radial plots (Galbraith, 1988), conceptually easier to understand but do not allow for differences in precision by which each value is measured, a graph of D_e versus uncertainty is shown above each histogram.

For all samples, the dataset mainly consists of values that appear to belong to a single dose population and a few aliquots that yielded significantly higher D_e's. We adopted a simple procedure for data analysis, in which values that differed by more than 3 SD's from the average were iteratively rejected (less than 6.5% of measurements).

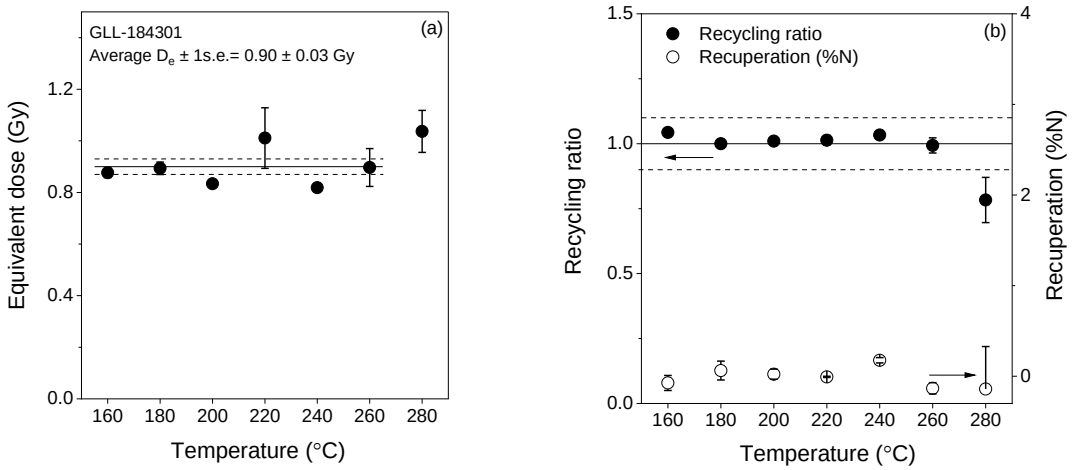

Figure 2.5: (a) Dependence of equivalent dose on preheat temperature for sample GLL-184301. Each datapoint represents the average (± 1 standard error; 1 s.e.) of 3 measurements. The solid and dashed lines indicate the average ± 1 s.e. over the 160 °C – 260 °C temperature region. (b) Corresponding data for the recycling ratio (solid circles; left Y-axis) and recuperation (open circles; right Y-axis).

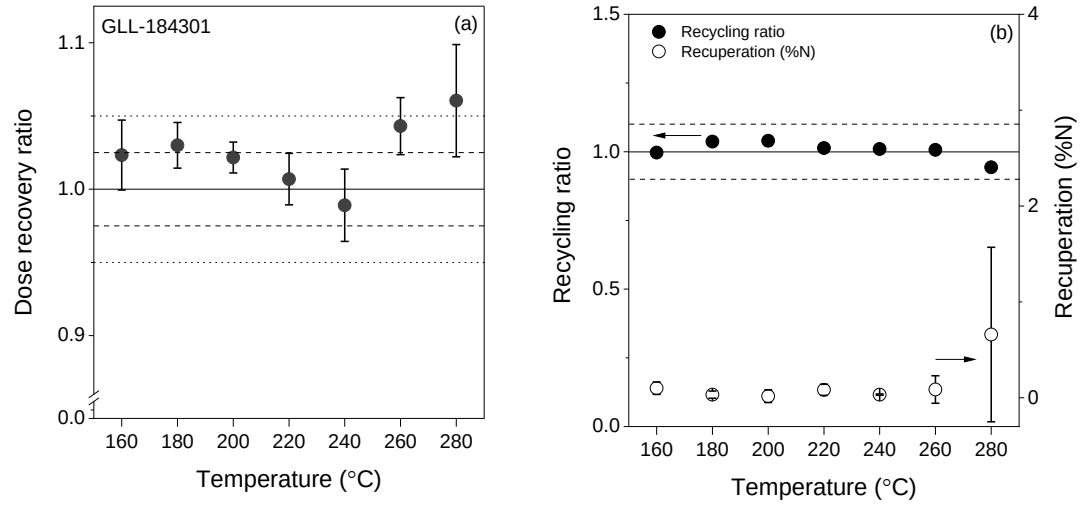

Figure 2.6: (a) Dose recovery data (ratios of measured to given dose) as a function of preheat temperature for sample GLL-184301. Each datapoint represents the average (± 1 standard error; 1 s.e.) of 3 measurements. The solid, dashed and dotted lines are eyeguides, bracketing a 2.5% and 5% deviation of the ratio from unity. (b) Corresponding data for recycling and recuperation.

The resulting distributions are characterized by RSD's in the range of 7-35%; we interpret these to reflect a single event and the mean D_e was used for age calculation (see further). The results for two samples collected from underlying layers lighter in color (GLL-160816 and GLL-160818) are shown in Figure 2.9, and the data were processed in the same manner. The resulting D_e values are spread over a (significantly) wider range, with RSD's between 28-38%. This may reflect an inherent characteristic of the material, whether or not in combination with post-depositional mixing and incomplete resetting.

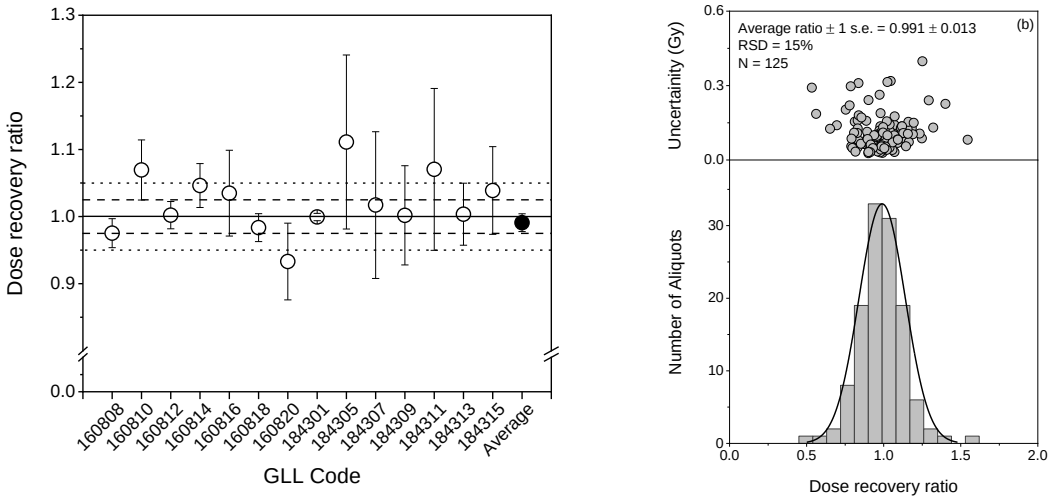

Figure 2.7: Summary of dose recovery data shown as averages per sample (a) and combined for all aliquots and samples in a histogram (b).

2.3.1.2 OSL ages

The analytical data and OSL ages are summarized in Table 2.1. Uncertainties on the OSL ages were calculated as summarized in Aitken, (1985), with systematic sources of uncertainty as in Vandenberghe (2004) and Vandenberghe et al. (2004). The total uncertainties associated with the ages range from ~ 8% to ~ 16%; systematic sources of uncertainty are the main contributor, which as a result, mainly reflect uncertainty associated with our estimates of past water content. Random uncertainties are associated with the measurement of D_e and radionuclide activities only and are in between ~ 2 and 5%. Except for feature M32, the measurements for the samples collected from the uppermost darker layers are more precise (σ_r = ~ 2-3%) than those for samples taken from underlying layers (σ_r = ~ 4-5%). This basically reflects the differences in the spread in D_e's in these samples (Figures 2.8 and 2.9).

The optical ages for the samples collected in the dark layers range from 0.21 ± 0.02 ka to 0.71 ± 0.06 ka. For features where multiple samples were collected, the ages are consistent with their stratigraphic position. The OSL dates refer, at least in principle, to the time that has elapsed between the zeroing event in the past and the time of sampling (2016 or 2018, indicated by the first two digits in the GLL-code). To facilitate comparison with ^{14}C-dating (see further), which is more commonly used in this type of research, the OSL ages were recalculated to Ages CE and expressed within 95.4% probability (2 sigma).

2.3.2 Radiocarbon dating

The results from ^{14}C dating are summarized in Table 2.2. The oldest feature is M5 with an age in between ~ 1300–1400 cal CE. The youngest features M4 and M30 postdate 1650 CE and their wide age probability distributions illustrate the difficulties of ^{14}C dating in this period of time, due to De Vries and Suess-effects.

Table 2.2: Summary of ^{14}C dates.

Feature	***Sample ID***	***Sample***	***Lab code***	***uncal BP (±1σ)***	***cal CE (± 2σ)***
M4	*Fagus sylvatica*	*twig*	RICH-22066	49 ±30	1694 (21.6%) 1728
					1812 (73.8%) 1919
M5	*Carpinus betulus*	*twig*	RICH-22067	591 ±31	1299 (68.2) 1370
					1380 (27.2%) 1413
M21	*Salix/Populus*	*twig*	RICH-24066	330 ±28	1480 (95.4%) 1643
M22	*Betula* sp.	*stem/large branch*	RICH-24065	486 ±30	1406 (95.4%) 1451
M30	*Salix/Populus*	*twig*	RICH-27329	160 ±25	1665 (16.3%) 1700
					1721 (39.5%) 1786
					1792 (10.8%) 1819
					1832 (9.6%) 1880
					1915 (19.2%) …
M31	*Salix/Populus*	*stem/large branch*	RICH-27330	372 ±24	1449 (60.8%) 1524
					1559 (1.0%) 1563
					1571 (33.5%) 1631
M32	*Fagus sylvatica*	*twig*	RICH-27331	373 ±25	1448 (60.7%) 1524
					1559 (1.3%) 1564
					1569 (33.4%) 1631

2.4 Discussion

2.4.1 Comparison between OSL and ^{14}C ages

Figure 2.10 compares the ^{14}C ages derived from charcoal fragments and the OSL ages obtained from samples from the uppermost dark layers. Both datasets are expressed on the same scale (Age CE) and cover 95.4% probability (or the two-sigma confidence interval). For this comparison, the total uncertainties on the OSL ages should be considered (σ_{tot} in Table 2.1; grey error bars in Figure 2.10).

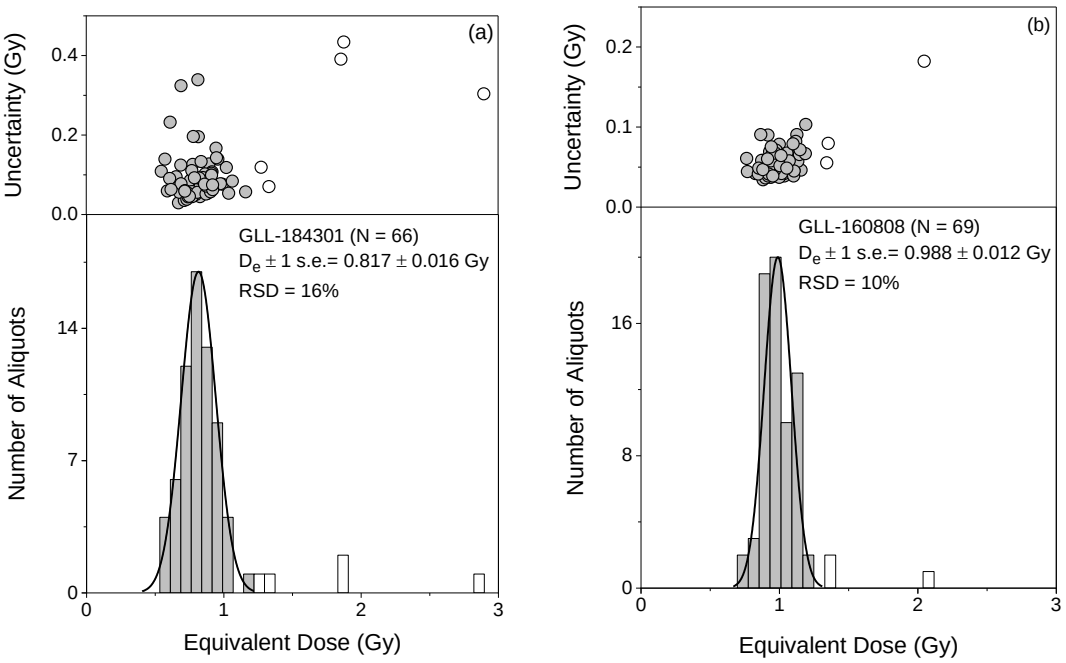

Figure 2.8: Results from measurements of equivalent dose (D_e) in small (2 mm diameter) aliquots for samples GLL-184301 (a) and GLL-160808 (b) that were collected in dark layers. A plot of D_e versus uncertainty is shown above each histogram; the median from this distribution was used for binning the data. The open symbols refer to aliquots that were rejected for D_e calculation (see text for details).

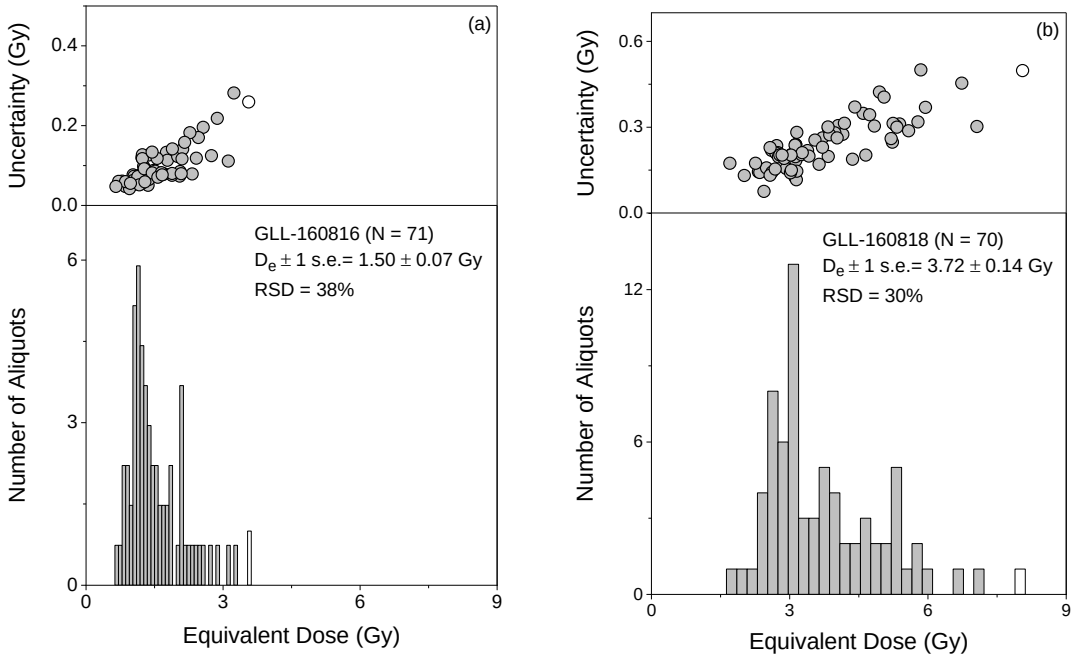

Figure 2.9: Same as in Figure 2.8 for samples GLL-160816 (a) and GLL-160818 (b), which were collected from sediments underlying the dark charcoal-rich layer.

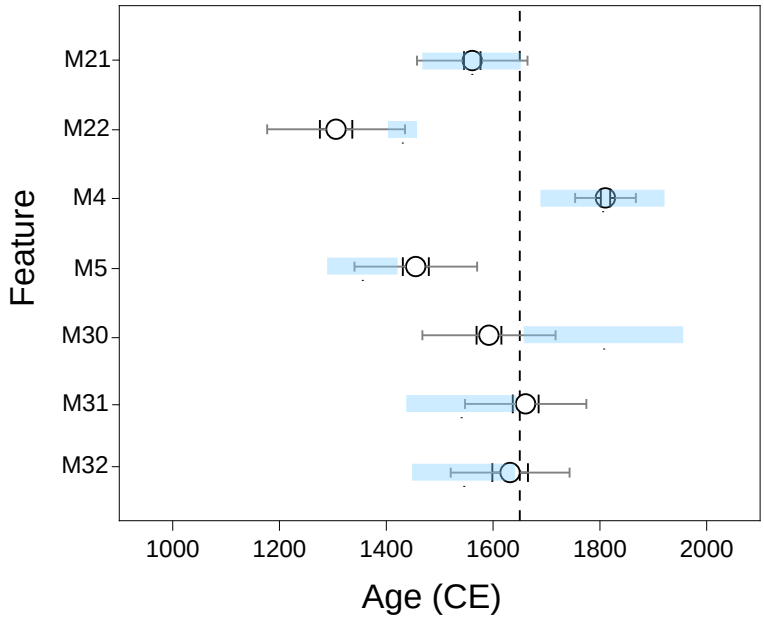

Figure 2.10: Comparison between OSL and calibrated ^{14}C-ages. The OSL data are represented by open circles; the associated random and total uncertainties are given by the black and grey error bars, respectively. The calibrated ^{14}C ages are represented as age ranges by the blue highlighted boxes. All ages are expressed as ages Common Era (CE) and cover 95.45 % probability.

Within these uncertainties, both datasets are entirely consistent. There is no evidence for systematic over- or underestimation of the OSL ages. One cause for OSL-age overestimation, and of particular concern for sediments associated with this type of features, is incomplete resetting owing to insufficient exposure to heat in the past. At least for the samples investigated in this study, our finds experimentally confirm those by Hirsch et al. (2018). These authors examined the properties of soils at two relict charcoal hearths in Germany and suggested that a sandy layer underlying a charcoal hearth may have experienced sufficient heating up to a depth of least ~ 2 cm to allow OSL-dating. While the charcoal hearths that we investigated have silty substrates (loess) that may transfer heat in a different manner, the good agreement between OSL and ^{14}C indicates that the heating was sufficiently stringent for complete resetting of the OSL clock.

It is interesting to note that for six out of the seven features we investigated, the uncertainties associated with the OSL ages are comparable or more precise than those associated with the calibrated ^{14}C ages. The latter especially holds for the two post-1650 CE features, which is not unexpected given the limitations of ^{14}C-dating in this window. As such, the whole of our dataset strongly suggests that OSL dating is a viable

complementary or alternative chronometric tool for determining the age of these features.

2.4.2 OSL dating – potential pitfalls and possibilities

2.4.2.1 Sampling

The question remains as to which stratigraphic layers one could preferentially sample for an optimal result. At the very onset of our study, we envisaged sediments immediately underlying the charcoal hearths (the former topsoil or A-horizon), as these 1) would have experienced the most stringent heat regime when the kiln was burning, 2) yield sufficient material for dating, and 3) are better protected from surficial processes. In practice, we found it impossible to distinguish between the lowermost part of the charcoal kiln itself and the dark upper layer of the buried soil (A-horizon), confirming earlier observations by Mees (1989); see also Gebhardt (2007). Samples for OSL dating were therefore taken in the lowermost "darker" layers, either near their base or somewhat higher (Figure 2.2). Alternatively, a sample could also be taken from the middle of a charcoal-rich layer as long as it is expected to yield a sufficient amount of datable clastic material. Our study focused on sand-sized quartz, but sand-sized K-feldspar, silt-sized quartz and silt-sized undifferentiated mixtures of minerals may qualify as well. It should be noted that we used sampling tubes with a diameter of 5 cm, in line with our laboratory protocol and is consistent with the hypothesis that a temperature of at least 210-220 °C, reached to a depth of 5 cm, is sufficient to reduce the luminescence signal in sandy sediments to reset (§2.4.2.2). The consistency between the OSL and ^{14}C ages (Figure 2.10) indicates that this vertical resolution of sampling covered a single event. Our dataset (Table 2.1; Figures 2.8-2.9) also suggests that it can be an added value to collect multiple samples in a well-defined vertical stratigraphical pane. OSL investigations of sediments underlying the dark, charcoal-rich layer may not be of direct interest and/or yield ages that are of little or no significance in itself; they help, however, in assessing the reliability of the date for the event of interest through stratigraphic consistency, comparison of luminescence characteristics and distribution of doses. The latter can help assessing the degree of resetting and/or post-depositional disturbances (see also below) especially as such processes cannot always be macroscopically discerned in the field.

2.4.2.2 Resetting

The prerequisite for OSL dating is that the clock in a sample was adequately reset at some point in the past - this either by heat, light or a combination of both – and that the sample subsequently remained shielded from this resetting agent until measurement. With respect to heating as the resetting agent, we have (apart from the dark layers being rich in charcoal) little or no macroscopic information informing on possible temperature regimes in the layers that were targeted for OSL-dating. At this stage, no proxies such as mineralogical transformations or soil organic matter (SOM) were examined. Hirsch et al. (2018) mention that temperatures within a charcoal hearth during the charring process generally range from 350 °C to 600 °C. For sandy soils underlying the remains of kilns, they derived that soil mineralogy in an approximately 2 cm thick contact zone was affected by temperatures of ~ 400 °C and that combustion of SOM, which requires a temperature of at least 210 – 220 °C, reached up to a depth of ~ 5 cm.

The quartz OSL-signal preferably used for dating (the so-called fast-component) originates with the thermoluminescence (TL) signal commonly referred to as the 325 °C TL peak; heating to 400 °C thus resets this signal. Prolonged exposure to lower temperatures, however, may be equally effective; this is e.g. used in isothermal decay methods for determining signal stability (e.g. Aitken, 1985; Durcan, 2018) and dating (e.g. Jain et al., 2005; Buylaert et al., 2006; Vandenberghe et al., 2009a).

Charring of wood in traditional kilns may require up to 20 days (Hirsch et al., 2018; Lepoivre and Septembre, 1941) and may thus generate a sufficiently stringent heating regime to fully remove the OSL/325 °C TL signal. This is relevant given that temperatures not only vary vertically, i.e. as a function of depth in the substrate below the hearth, but also laterally, i.e. across the structure. When working in small profile pits (e.g. to minimize disturbance and/or owing to practical limitations imposed by obstructing tree roots, as were both the case here), it is not always possible to sample those regions that are expected to have locally reached the highest temperatures. In contrast to light exposure during sediment transport, heating is a homogeneous process, but the heat is transferred as a function of depth into the soil (e.g. Aldeias et al., 2016). The implication of such a thermal gradient is that sediments can be homogeneously incompletely reset, and progressively so with increasing distance from the heat source. The observed increase of the OSL ages as a function of depth (Table 2.1) may very well reflect such a process. While the stratigraphic consistency is reassuring in itself, the

results for the samples underlying the dark charcoal-rich layer should therefore be considered with caution and may be of no significance in terms of determining when a discrete event (such as charcoal production or sediment deposition) actually happened. While the construction of kilns involves sediments, we do not think that exposure to light ("bleaching") is an important resetting process for the investigated features. If bleaching occurred during build-up, operation and/or harvesting, and was adequate, this is not a problem and should yield the same age information as when a sample was heated. In fact, the resetting agent (heat and/or light) does not matter, as long as the clock was reset.

The above holds in a closed system where the samples were not exposed to heat or light after the charring event. Given their location, context and stratigraphy, the sampled charcoal kilns can be confidently interpreted as representing single events that were not affected by subsequent anthropogenic activities. None of the kiln sites showed multiple layers of charcoal indicating repeated use of the site for charcoal production, as has been observed in mountainous areas where charcoal production is done on artificial terraces (e.g. Knapp et al., 2015).

Pedo-/bioturbation is a concern, however, and may have a significant effect on luminescence ages (Bateman et al., 2003; 2007b; Vandenberghe et al., 2009b). On top of the remains of the charcoal kilns is a litter layer from which an initial soil develops, and the deposits are often rooted through, especially by trees. The D_e distributions (Figure 2.8) in combination with the good agreement between the OSL and ^{14}C ages (Figure 2.10) strongly indicate that post-depositional mixing (associated incomplete resetting or not) is not an issue for the dark layers in which we are interested, which is in line with earlier finds (Mees, 1989; Gebhardt, 2007; Langohr, 2009). This cannot be excluded, however, for samples in underlying layers (Figure 2.9). These "L" -layers consist of sediments that were originally transported and deposited by wind (loess) and are stratigraphically located below undisturbed remains of charcoal hearths. Previous studies have demonstrated that the spread in D_e in undisturbed windblown deposits is significantly larger than in heated materials, which is not related to analytical or instrumental uncertainties (see e.g. Vandenberghe et al., 2003; 2009b). While the observed spread may thus be sample intrinsic, the OSL ages for these "L layers" cannot be reconciled with undisturbed preservation of loess that was deposited during the

Weichselian (Table 2.1). This points at one or more processes following loess deposition but prior to kiln harvesting, which remain to be identified.

2.4.2.3 Dosimetry

As a rule of thumb, a change in water content of 1% changes the OSL age by about 1% (when sand-sized quartz is used, as is the case here). We have based our estimates of past water contents on gravimetric/volumetric measurements of samples that were collected specifically for this purpose in combination with finds reported by De Vos (2005) (see §2.2.2). The latter reports on 5000 measurements of soil moisture contents over a period of one year in the same area, but focusing on the present topsoil and archaeologically sterile substrate. Moisture contents can vary significantly over a period of one year, with values generally in between 15 vol% and 50 vol% in the topsoil (0–10 cm) and in between 20 vol% and 40 vol% in underlying (20–30 cm) substrate, and higher values peaking during periods with pronounced rainfall (De Vos, 2005). In luminescence dating, it is the time-averaged moisture content that is of importance. We adopted a value of half the water content at saturation, which corresponds approximately to the moisture content at the time of sampling and is about the mid-value of the aforementioned yearly variations. We associated a relative uncertainty of 15% (1 sigma) with this value to allow for possible variations over longer times. Given that, over the period to be dated, climatological conditions have been stable in the study region, our estimates of past water content should not be a major source of inaccuracy.

The samples of main interest come from organic-rich layers. Organic matter may influence (1) the accuracy by which specific radionuclides activities are determined and (2) the effective dose rate experienced by the samples. Samples rich in organic matter differ significantly in composition from the calibrants used in gamma-ray spectrometry, which may introduce significant inaccuracies in quantification using low-energetic gamma-rays (e.g. 46.5 keV for ^{210}Pb and 63.3 keV for ^{234}Th; De Corte et al., 2004). In addition, organic matter absorbs radiation and hence reduces the dose rate; this is similar to the effect of moisture, but the attenuation factors for organic matter and water differ (e.g. Lian et al., 1995). At this stage, we made no measurements of organic matter content so any possible effect cannot be quantified; a more comprehensive study on this issue is underway.

While there may be room to improve the dosimetric data, the consistency between the OSL and ^{14}C dates (Figure 2.10) indicates that no significant systematic errors were introduced and that possible sources of uncertainty were adequately accounted for.

2.4.2.4 Resolution

As indicated earlier, the uncertainties associated with the OSL and ^{14}C ages are more or less comparable for most of the pre-1650 CE features and can be (significantly) more precise for the post-1650 CE ones (Tables 2.1 and 2.2; Figure 2.10). This illustrates the time-resolution that can be achieved using OSL for establishing a numerical chronological framework. We evaluate the accuracy of OSL dating using the pre-1650 CE features as, for these, reliable independent age information could be obtained using ^{14}C dating. This comparison, visualized in Figure 2.10, confirms the applicability of the method, adding confidence to its stand-alone use. For pre-1650 CE features, OSL dating is a viable complementary or alternative to ^{14}C. In this time window, however, we do not consider it particularly advantageous, especially as ^{14}C is already well embedded for dating former charcoal production sites and precisions are comparable. If solid prior knowledge on the pre-1650 CE age is available, and although there is always merit in combining methods, it thus seems likely that ^{14}C-dating will remain the technique of choice. If this knowledge is not available, or if the features are expected to post-date 1650 CE, we strongly recommend that samples for OSL dating are collected. It is especially for post-1650 CE features that OSL dating offers significant advantages, as illustrated here most clearly by the results obtained for feature M4. In this case, the OSL-age is about twice as precise as the ^{14}C-age (Tables 2.1 and 2.2).

As the darker layers that were dated are similar and all analytical data were acquired using the same methodology and instrumental facilities, it is reasonable to expect that at least some sources of systematic uncertainty (incorporated in σ_{sys} in Table 2.1) are shared between the samples. To a first approximation, uncertainties associated with calibration of the instrumental facilities, and with the conversion and attenuation factors, e.g., can be considered to contribute with the same value to the total uncertainty on a luminescence age (σ_{tot}) for each sample. Hence, these components can be omitted when comparing the luminescence ages amongst each other. This opens up the possibility for distinguishing, in a relative manner, between features and phases with a significantly higher precision, rather than establishing an actual time for past charcoal charring. If we consider the random uncertainties (i.e. the uncertainties associated with

the measurement of D_e and specific radionuclide activities, only) as the minimum limit for precision, the implication is that different charcoal production events can be recognized to within 2-4% (1 σ_r; Table 2.1). While reality is probably more complex, as some sources of systematic uncertainty are unlikely to be equally shared (e.g. moisture content), the approach has significant potential for constructing "floating" chronologies for similar sites at a given location with an unprecedented precision.

2.4.2.5 Sample throughput

Obtaining an OSL date is time-consuming, requiring substantial input from analysts and instrument time. As such, it is desirable to optimize the methodological design and workflow (which may also help reducing associated expenses). It is well-known that the sensitivity-corrected quartz-OSL dose-response curve at low doses is (close to) linear (Bøtter-Jensen et al., 2003b; Wintle and Murray, 2006; see also e.g. Figure 2.3). Once procedural tests (e.g. recycling, recuperation, dose recovery; see earlier) confirm that a given SAR-procedure should be applicable to a suite of samples, there should thus be no a priori impediment in limiting the measurements to that of the natural signal and the response to a single regenerative dose chosen to be larger than the natural dose, but still in the linear region of the dose response curve. While previously alluded on (Madsen and Murray, 2009) and may be practiced in some luminescence laboratories (e.g. Chamberlain et al., 2017), this seems to have been underexploited in the literature. Here we experimentally demonstrate that it is indeed feasible to obtain a large amount of data for small (2 mm diameter) aliquots (required for assessing the distribution of D_e in a sample; Figure 2.8), without compromising precision or the need for additional instrument time.

2.5 Conclusions

Our study investigated the potential of a mainstream OSL-dating methodology for application to heated sediments associated with past charcoal production in a forested area on a silty (loess) subsurface. We conclude that the approach is viable, as indicated by the agreement between the OSL and ^{14}C dates. We find no evidence for systematic age over- or underestimation. The precision is comparable to ^{14}C and can be more precise for post-1650 CE features, and we highlight the potential of OSL dating to distinguish between similar events at an unprecedented time-resolution. We demonstrate that it is effectively possible to exploit the linear part of the dose-response

curve for obtaining sufficiently large datasets, without compromising precision or accuracy. This may help increasing sample throughput, at least for as far as OSL measurements are concerned. In general, we conclude that the results obtained in this study may provide an incentive towards innovative OSL-based chronometric research of similar remnants as encountered elsewhere in the world.

Chapter 3: OSL dating as an alternative tool for age determination of relic charcoal kilns

Nasrin Karimi Moayed, Dimitri Vandenberghe, Koen Deforce, Eva Kaptijn, Paulina Biernacka, Wim De Clercq, Johan De Grave

This chapter is a modified from the published version in the journal Archaeometry. The modifications concern formatting, inclusion of the supplementary material in the main text, and minor suggestions made by the examination commission; relevant contextual information that had to be removed from the accepted manuscript on account of word-count limitations, have been reincorporated.

Author contributions

Nasrin Karimi Moayed: Field investigation, Sampling, Sample processing, Data analysis, Methodology, Data curation, Writing.
Dimitri Vandenberghe: Field investigation, Sampling, Methodology, Writing, review and editing.
Koen Deforce: Field investigation, Sampling, Methodology, Writing, review and editing.
Eva Kaptijn: Field investigation, Sampling, Writing, review and editing.
Paulina Biernacka: Sampling.
Wim De Clercq: Supervision, Funding acquisition.
Johan De Grave: Supervision, Field investigation, Writing, review and editing, Funding acquisition.

Abstract

Chronometric studies of the remains of past charcoal production have been largely based on ^{14}C dating of associated charcoal. Owing to intrinsic limitations, however, this method does not provide a sufficiently precise time-resolution for features that post-date 1650 CE. This effectively hampers a range of environmental studies that draw from these archives. Here, we investigate the potential of optically stimulated luminescence (OSL) dating of heated sandy sediments as an alternative and complementary tool for age determination of charcoal kiln remains.

Our study uses 7 samples collected from five relic charcoal kilns, and 11 complementary samples from the underlying sandy substrate. Through a range of procedural tests we first demonstrate that the single-aliquot regenerative-dose (SAR) procedure in combination with OSL signals from quartz allows determining equivalent doses both accurately and precisely. For four of the five investigated kilns, the resulting

OSL ages are entirely consistent with independent age information provided by ^{14}C-dating and written sources. Especially for post-1650 CE features, the precision can be significantly higher than that of ^{14}C dating and we highlight the potential of OSL dating for distinguishing, relatively, between charcoal production phases with an unprecedented time-resolution. We conclude that the approach is a most promising alternative to ^{14}C. The observation that, for one of the kilns, the OSL and ^{14}C ages differ significantly, illustrates the added value of using both methods in conjunction.

Keywords: Charcoal kilns, OSL dating, Radiocarbon dating, Modern ages, woodlands.

3.1 Introduction

Charcoal was widely used as fuel in a range of industrial and domestic applications before the extensive exploitation of coal from the nineteenth century CE onwards (Gale 2003; Deforce et al., 2021a). Charcoal production was therefore a common and important economic activity in many forested areas throughout Europe (Nelle, 2003; Ludemann, 2010; Carrari et al., 2017; Paradis-Grenouillet and Dufraisse, 2018; Schneider et al., 2020) and North America (Hart et al., 2008; Potter et al., 2013). This industry had a significant physical and chemical impact on the natural environment, by affecting the composition, deterioration or even destruction of woodlands, the composition of soils, and the evolution of the surficial landscape.

The remains of charcoal production sites (charcoal kilns) can be studied to give information about former forest composition, evolution and exploitation (e.g. Ludemann, 2003, 2010; Nelle, 2003; Deforce et al., 2013, 2021b), and to detect formerly wooded areas (Foard, 2001). This, in turn, can provide insights into past settlement dynamics (Groenewoudt and Spek, 2016; Deforce et al., 2021a) and associated subsistence and market economies (Raab et al., 2015; Rutkiewicz et al., 2017; Olesen, 2019). While interesting from a historical perspective, it is increasingly recognized that these activities continued to affect ecosystems on the longer term and that an understanding of the archives significantly aids in the design of present-day and future management and conservation strategies (e.g. Foster et al., 2003; Willis and Birks, 2006). Recently, relics of charcoal production have also received interest in relation to carbon sequestration (e.g. Hardy et al., 2017b; Hirsch et al., 2017; Mastrolonardo et al., 2018), soil properties (e.g., Hardy et al., 2016, 2017a; Hirsch et

al., 2017, 2018; Schneider et al., 2022), and composition, biodiversity, and growth rate of vegetation (Carrari et al., 2016a, b; Buras et al., 2020). In some areas, deforestation to produce the vast amounts of charcoal required for iron and glass melting have been associated with large-scale sand-drifting; in this case, the charcoal-rich horizons underlying the wind-blown sediments have been used to establish this causal relation and constrain the temporal-framework, with relevance to spatial planning, environmental management, and heritage in its broadest sense (e.g. Dulias, 2018).

All the aforementioned areas of research aim at tapping the information contained in the remains of past charcoal production in one way or the other, requiring a robust chronological framework. This is most commonly and logically accomplished through radiocarbon (^{14}C) dating of charcoal, which is abundant in the archaeological remains of charcoal kilns. This approach, however, is limited to features older than about 1650 CE, as the ^{14}C-calibration curve for the past few hundreds of years is affected by strong wiggles caused by variations in sunspot activities, followed by a broad plateau, and finally a sharp drop, caused by the dilution of atmospheric $^{14}CO_2$ levels due to the massive burning of fossil fuels (Stuiver 1961; Tans et al., 1979; Deforce et al., 2021a). The vast majority of charcoal kilns in Europe date from this post-1650 CE period, resulting from a rapidly growing demand for charcoal as fuel for the iron industry during the early days industrialisation, when coal was not yet commonly used (Hardy and Dufey, 2012; Raab et al., 2015). An alternative and – above all – complimentary method to ^{14}C-dating, would thus be of extreme value to studies of post-1650 CE charcoal production.

A number of studies demonstrated the applicability of optically stimulated luminescence (OSL) dating to geological materials heated in hearths (e.g. Moska et al., 2010; Rhodes et al., 2010; Armitage and King, 2013). Recently, Karimi-Moayed et al. (2020) demonstrated the potential of OSL dating of sediments heated during past charcoal production. That study, which focused on kiln remains in a forested area on a silty (loamy or loessic) subsurface in Central Belgium, reported on a good agreement between ^{14}C and OSL dates for pre-1650 CE features; for post-1650 CE features, it highlighted the possibility for obtaining OSL ages with a higher precision, and thus for ranking events with an increased time-resolution. The work by Karimi-Moayed et al. (2020), although independently performed in a different lithological setting, confirmed the suggestion by Hirsch et al. (2018) that heating should have been sufficiently

stringent to fully reset the quartz OSL-signal in sandy sediments underlying charcoal kilns up to depths of about 5 cm.

The present study follows the approach taken by Karimi-Moayed et al. (2020) but examines the potential of quartz-based OSL dating of remains of charcoal kilns in a sandy substrate. The underlying rationale is that, in this particular sedimentary context, heat transfer and maximum temperatures reached may differ from those in the setting previously investigated (loess), with possible implications as to the applicability of OSL dating. In addition, all the features investigated here are thought to be relatively recent (post-1650 CE, based on historical sources). As such, this paper explicitly examines that period of time over which OSL dating could be most advantageous.

3.2 Study area and historical background

The charcoal kilns that are the subject of this study are situated in the Veluwe area (Central Netherlands; Figure 3.1a). The name "Veluwe" is often explained as deriving from "Vale Ouwe" – a still popular denotion for this region – meaning fallow/bare region or wasteland and reflects intensive clearance of the original forests, from which they were unable to recover on their own. Although most of this landscape has now been re-stabilized by a natural or planted vegetation cover, it still is the largest area of dynamic sand drifting in NW Europe (Koster, 2009).

The term "drift sand" has a specific meaning in that it typically refers to sand moving as a result of anthropogenic pressure on the natural landscape. Activities such as deforestation and agriculture are generally thought to have triggered reactivation of the sands (Pierik et al., 2018), eventually resulting in loss of arable lands and even settlements (e.g. Derese et al., 2010). Deforestation and increased drift sand activity has sometimes been connected to the large-scale early medieval iron production and coupled charcoal production that took place on the Veluwe. Between c. 700 and 900 CE, the Veluwe was the iron production centre of northwestern Europe (Joosten, 2004). A recent study into driftsands, however, has shown that large-scale deforestation only started after the 10th century CE and continued up to the 19th century CE (Pierik et al., 2018). Although new excavations are broadening the time range of Veluvian iron production (Zuyderwyk, 2020), there is no direct link between the early medieval iron industry and large-scale drift sand activity. Nevertheless, both metallurgy and charcoal burning were important activities in the region at some time in the past, as testified by

their numerous remains (Groenewoudt, 2007; Verschoof-van der Vaart et al., 2020). Charcoal burning is, however, not restricted to iron production and there is ample evidence that the practice continued when iron production shifted to other areas. Within the scope of the Heritage Quest project, volunteer scientists have investigated LiDAR maps of the Veluwe and identified ca. 700 potential charcoal kilns (Verschoof-van der Vaart et al., 2020). These kilns are all of the large, above ground type that is in German referred to as the Platzmeiler. While the kilns discussed here are the first dated examples of this type on the Veluwe, research from other regions shows that these likely post-date the smaller pit kilns often related to the iron production (Deforce et al., 2021a). The large number of charcoal kilns shows that, while charcoal burning for the iron industry cannot be directly related to the heightened drift sand activity, the kilns are part of the increasing impact of human activity on the landscape, which resulted in increased drift sand activity.

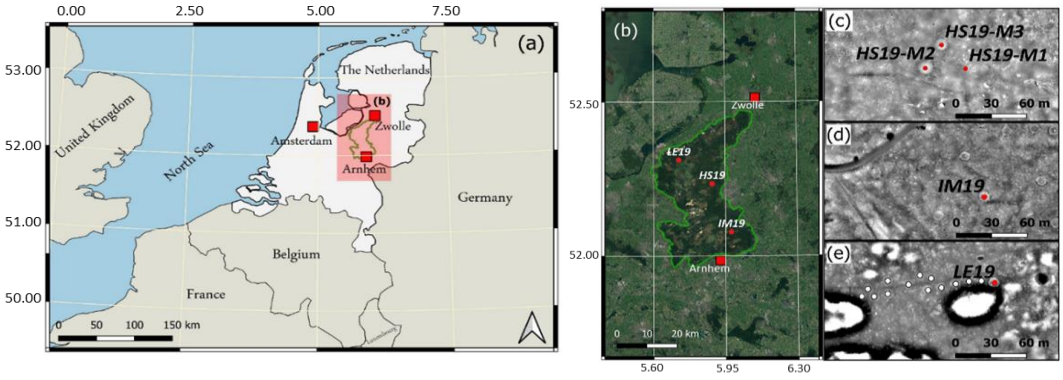

Figure 3.1: (a) Location of the Veluwe area (central Netherlands). (b) The area delineated in green shows the limit of the remaining Veluwe forest. (c,d,e) LiDAR maps of the Veluwe sampling sites; the sampled charcoal kiln remains are shown by red solid circles. The white solid circles in (e) illustrate the cluster of kilns oriented along a forest track.

While the Veluwe is currently the most heavily forested area in the Netherlands, large parts of the Veluwe were thus open heathland or drift sand areas until reforestation started by large landowners and later the state from c. 1800/1850 CE onwards. In the frame of this study, a total of five charcoal kilns at three different localities in the Veluwe were studied (Figure 3.1b): three in Hoog Soeren forest (HS19; Figure 3.1c), one in the Imbosch (IM19; Figure 3.1d) and one in Leuvenum forest (LE19; Figure 3.1e). Leuvenum forest and the Imbosch were part of this open heathland until the 19th century, whereas Hoog Soeren forest has been documented as a forested area over several centuries. A charter from 814 CE mentions a “Silva Suornum”, which has been

explained as either ‘forest that is situated up-high’, ‘southern forest’, or ‘forest of the swines’, and is supposed to refer to the area currently known as Hoog Soeren forest (Buis, 1985). This is taken as evidence that it must have represented a more or less important forest for quite some time. A map from around 1524 explicitly indicates ‘Hoech Zuere bosch’ (Van’t Hoff, 1964). As was the case for many other forests in the area at that time, (usually nearby) communities had the right of use through a system of “shareholders”. This implied, amongst other things, a share in timber yield, the right to herd a certain amount of pigs in the forest, and some say in the woodland management and exploitation itself (Buis, 1985). The first records documenting these rights at Hoog Soeren date back to 1482 CE (De Rijk, 2011). There are no detailed records on size and character of the forest before c. 1750. However, between 1687 and 1755, owners of a share in this forest were given part of the profit in money, oak or beech (De Rijk, 2011). It is estimated that in 1766 the forest consisted of c. 400 ha deciduous forest and 500 ha of oak coppice (De Rijk, 2011). Around 1832 CE, the forest consisted of coppice and standards. Financial records show that beech and oak standards, beside oak coppice, dominated the forest economy. In the 19th century, small amounts of pine appear in the records beside beech and oak standards and oak coppice (De Rijk, 2011). Heathlands bordered the forest, which at the end of the 19th century and early 20th century CE were forested with mainly Scots pine. By buying shares, the entire Hoog Soeren forest became property of the Dutch royal family between 1684 and 1766 CE. It still is royal property at present, implying that access is strictly regulated. Boosten et al. (2010) and De Rijk (2011), e.g., provide detailed information on the history of Hoogen Soeren forest. In short, the historical sources clearly indicate that the sampling locations for our study were already forested in at least the late 15th to early 16th century CE.

At Imbosch, a land register from 1832 CE shows that the sampling location was taxed as heathland, while the archive of the landowner records that the terrain across the road to the east was planted with pine in 1764. From 1850 CE onwards, maps show a forested area at the sampling location, as do more recent ones (e.g. First Dutch forest inventory; 1938-1942 CE). While dating based on maps is imprecise, they indicate forest or forestation from somewhere in the mid-19th century CE onwards.

The situation for Leuvenumse forest is similar to that of the Imbosch. A topographic map from 1815 CE shows a landscape of heath and drift sands, while from 1832 CE

onwards, the area was forested. Koops (2021) provides a map with years of germination of different species of trees showing a dominance of (Scots pine), which also dates furthest back in time (i.e. 1850 CE); other species, such as Japanese larch, northern red oak, common beech or spruce, were introduced from around the 1930's CE onwards.

The aforementioned sources do not provide explicit evidence for the woods being exploited for charcoal production. One exception is an interview with a charcoal burner published by a local newspaper (Schilder's Nieuwsblad, 24 October 1991), and reconstructs the history of charcoal burning at Leuvenumse forest. It is said to have started at around 1850 CE, when two German charcoal burners who were active in the nearby province of Overrijssel moved to Leuvenumse forest upon request of the owner. Although this account cannot be verified, oral tradition relates that the practice of charcoal burning was taken over by Gerrit Schuurkamp (1828-1911), who has been documented. With Gerrit Schuurkamp a family tradition started continuing over five generations with ample records of charcoal burning for the last three generations of Schuurkamps. Charcoal burning continued until the 1960's CE. The kiln sampled in this study is part of a cluster that is oriented along a forest track (see Figure 3.1e; white solid circles). This track first appears on a map from 1900 CE, making this a probable starting date for charcoal burning at this particular location.

3.3 Material and methods

3.3.1 Field observations and samples

The sample locations at sites HS19 and IM19 are both located on sandy deposits of the push moraine from the Saale glaciation. In these deposits podzolisation has occurred with its typical horizons. At location LE19, drift sand has covered the original deposits. In each kiln, a shallow pit of about 50 × 50 × 50 cm was manually dug.

At site HS19 (kilns M1, M2 and M3), the stratigraphic sequences are very similar (Figures 3.2a-c). The top layer consists of organic material and humous soil ((I) in Figure 3.2a-c) of ~ 5-10 cm thickness. This layer overlies a dark charcoal-rich sandy layer of ~10 cm thick ((II) in Figure 3.2a-c), followed by a dark brown layer of loamy sand (the B horizon; (III) in Figure 3.2a-c) with the same thickness. The base is made up of light orange/brown sand (the parent material or C horizon; (IV) in Figures 3.2a-c).

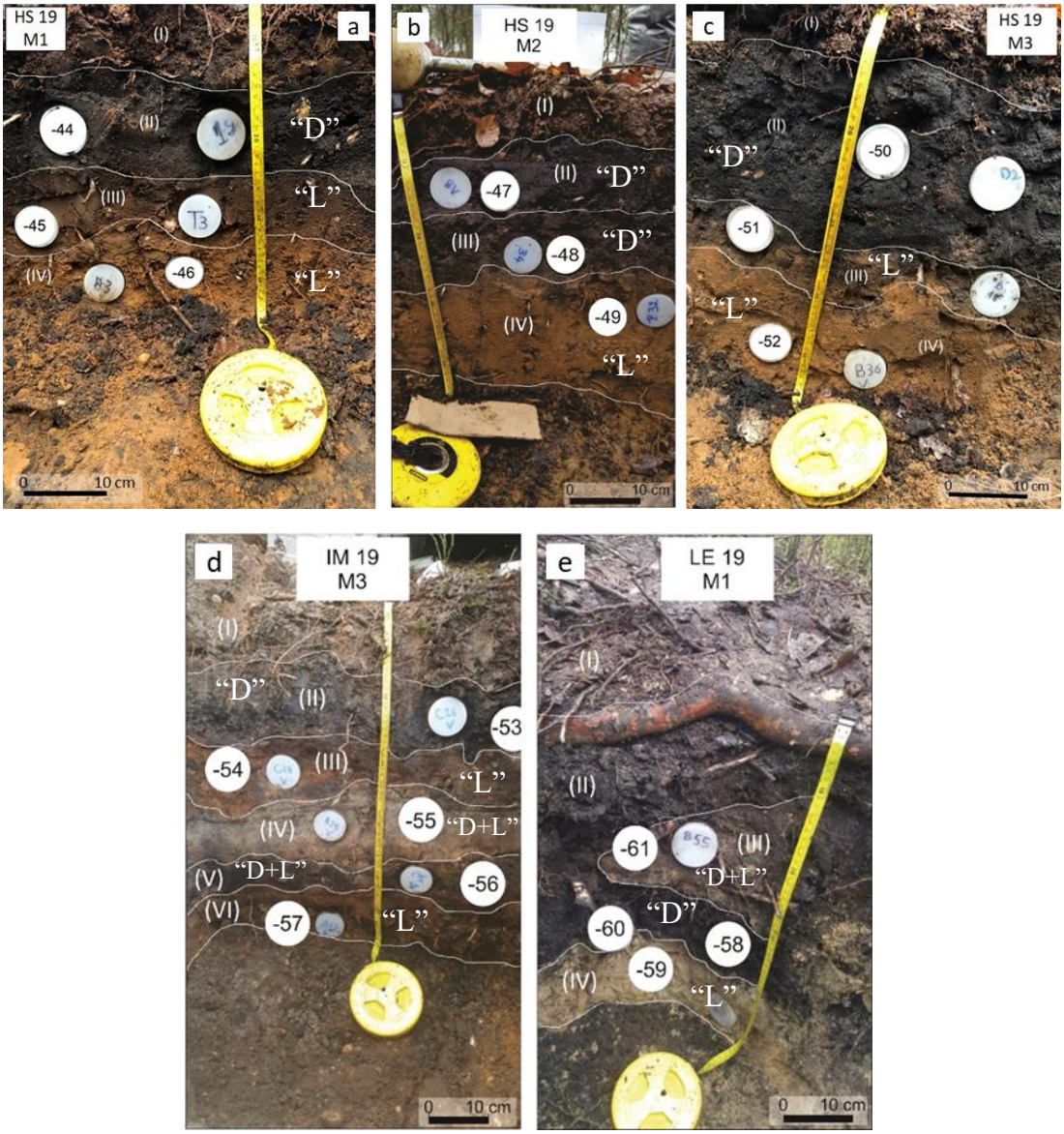

Figure 3.2: Photographs of the profiles observed during sampling of features HS19-M1 (a), HS19-M2 (b), HS19-M3 (c), IM19-M3 (d) and LE19-M1 (e). Bulk samples for ^{14}C and anthracological analysis were collected from layer II.

At site IM19 (kiln M3; Figure 3.2d), the exposed sequence comprises a layer of ~ 10 cm thick consisting of organic material and sand with a high humous content ((I) in Figure 3.2d). This overlies a ~ 5-10 cm dark sandy layer ((II) in Figure 3.2d), which is rich in charcoal. A heterogeneous orange/brown layer of loamy sand of ~ 5-10 cm thick ((III) in Figure 3.2d) separates this charcoal-rich layer from a lighter grayish sandy layer ((IV) in Figure 3.2d) of ~ 10-20 cm thickness. Traces of the upper dark charcoal layer can also be seen in parts of this orange/brownish layer. The grey layer (IV) is interpreted as the evulsion or E horizon typical of the podzol soils that cover most of the Veluwe. Below layer IV, there is a 5 cm thick B horizon consisting of dark brown loamy sand

(V). The base of the pit is formed by a mottled orange sandy layer of at least 15 cm thick (the B/C horizon; (VI) in Figure 3.2d). Both layers V and VI consist of coarse loamy sand with a small amount of gravel.

At site LE19 (kiln M1; Figure 3.2e), a top layer of ~ 5 cm thick ((I) in Figure 3.2e) consisting of partly decomposed leaves and very humous sandy soil (A horizon) overlies a dark charcoal-rich sandy layer ((II) in Figure 3.2e) of ~ 30 cm thickness. It is likely that a tree root caused the patches of lighter brownish sands observed in one side of profile ((III) in Figure 3.2e). At the bottom of the profile, lighter yellowish sand is observed in which no soil formation has taken place (C horizon; (IV) in Figure 3.2e).

All layers in all the sequences are rooted through to a certain degree. Samples for OSL dating were collected by hammering stainless-steel tubes (5 cm diameter and 15 cm long) into the fresh exposures. While the tubes were dug out, the surrounding sediment from the same layer was collected for radiometric analyses. In addition, undisturbed samples were taken to evaluate moisture content; these samples were collected using Kopecky rings, adjacent to the OSL samples. For each kiln, every layer was sampled (as illustrated in Figure 3.2).

The stratigraphic position of the samples is indicated in Table 3.1, where the layers with a darker, lighter and mottled color are denoted as “D”, “L” and “D+L”, respectively. From each kiln, bulk sediment samples (about 10 l) were taken from the uppermost charcoal rich layer (layer II) for radiocarbon dating and anthracological analysis.

3.3.2 OSL dating

Quartz-rich extracts (125-180 µm) were separated from the inner material of the OSL-tubes (i.e. the portion not exposed to light during the sampling) following conventional procedures (sieving, HCl, H_2O_2 and HF, but without density or magnetic separations). For luminescence measurements, the grains were spread out on the inner 8 mm (large aliquots; to investigate the basic characteristics) or 2 mm (small aliquots; for determining equivalent doses) of stainless-steel discs with a thickness of 0.5 mm and a diameter of 9.7 mm, using silicon spray as adhesive. All the measurements were carried out using an automated Risø TL/OSL reader with an automated Detection And Stimulation Head (DASH) equipped with blue (λ_{max} = 470 nm) and infrared (λ_{max} = 850 nm) light emitting diodes; all signals were detected through 7.5 mm Hoya U-340 UV filter. For details on the luminescence measurement equipment, see Bøtter-Jensen et al. (2003, 2010) and Lapp et al. (2015). The single-aliquot regenerative-dose (SAR)

Table 3.1: Specific radionuclide activities, estimates of past moisture content (F*W), calculated total dose rates, D_e's, OSL ages and random (σ_r), systematic (σ_s) and total uncertainties (σ_{tot}), and the OSL ages expressed as ages CE (± 2 σ total uncertainties). The total dose rate includes the contribution from internal radioactivity and cosmic radiation. The number of aliquots used for D_e-determination is given in italics between parentheses in subscript. The uncertainties mentioned with the dosimetry and D_e data are random; except for the ages CE (last column), all uncertainties represent 1 sigma. The samples were ranked according to their stratigraphic position in each feature, with "D", "L" and "D+L" referring to the darker, lighter and the brownish/black mottled layers from which they were collected, respectively. Indicated in bold are the results for the samples collected from the "D"-layers.

Pit	*Depth* (cm)	*Material*	*Lab code*	^{234}Th (Bq kg^{-1})	^{226}Ra (Bq kg^{-1})	^{210}Pb (Bq kg^{-1})	^{232}Th (Bq kg^{-1})	^{40}K (Bq kg^{-1})	*F*W*	*Total dose rate* (Gy ka^{-1})	D_e (Gy)	*Age* (ka) (± 1σ)	σ_r (%)	σ_{sys} (%)	σ_{tot} (%)	*Age* (CE) (± 2σ)
HS19-M1	**20**	**D**	**194344**	**10 ± 1**	**12.5 ± 0.5**	**14 ± 2**	**13.03 ± 0.20**	**210 ± 4**	**0.16 ± 0.02**	**1.25 ± 0.02**	**0.54 ± 0.02$_{(45)}$**	**0.44 ± 0.04**	**4.3**	**7.35**	**8.51**	**1580 ± 75**
HS19-M1	29	L	194345	12 ± 1	13.8 ± 0.4	11 ± 1	14.30 ± 0.20	220 ± 2	0.16 ± 0.02	1.26 ± 0.02	1.48 ± 0.19$_{(10)}$	1.21 ± 0.18	12.7	7.37	14.69	806 ± 356
HS19-M1	40	L	194346	12 ± 1	13.9 ± 0.4	11 ± 1	14.88 ± 0.16	226 ± 2	0.13 ± 0.02	1.30 ± 0.01	3.71 ± 0.58$_{(11)}$	2.93 ± 0.50	15.7	6.76	17.09	-908 ± 1001
HS19-M2	**14**	**D**	**194347**	**11 ± 2**	**14 ± 1**	**15 ± 1**	**13.47 ± 0.20**	**219 ± 3**	**0.14 ± 0.02**	**1.29 ± 0.02**	**0.52 ± 0.01$_{(46)}$**	**0.40 ± 0.03**	**2.48**	**6.94**	**7.37**	**1623 ± 58**
HS19-M2	**23**	**D**	**194348**	**13 ± 1**	**14.5 ± 0.4**	**14 ± 1**	**15.02 ± 0.22**	**243 ± 2**	**0.16 ± 0.02**	**1.33 ± 0.02**	**0.61 ± 0.01$_{(44)}$**	**0.46 ± 0.04**	**2.16**	**7.37**	**7.68**	**1562 ± 70**
HS19-M2	34	L	194349	13 ± 1	15.9 ± 0.5	10 ± 1	16.5 ± 0.2	264 ± 2	0.15 ± 0.02	1.36 ± 0.02	1.47 ± 0.13$_{(11)}$	1.07 ± 0.12	8.9	7.21	11.45	946 ± 246
HS19-M3	**20**	**D**	**194350**	**8 ± 1**	**14 ± 1**	**35 ± 2**	**12.6 ± 0.2**	**241 ± 2**	**0.23 ± 0.03**	**1.50 ± 0.02**	**0.27 ± 0.01$_{(45)}$**	**0.18 ± 0.02**	**3.8**	**8.79**	**9.57**	**1842 ± 34**
HS19-M3	33	L	194351	11 ± 1	14.3 ± 0.3	12 ± 1	14.1 ± 0.2	295 ± 2	0.19 ± 0.03	1.38 ± 0.02	0.67 ± 0.04$_{(11)}$	0.48 ± 0.05	5.88	7.9	9.85	1542 ± 94
HS19-M3	50	L	194352	9 ± 1	14.6 ± 0.4	11 ± 1	15.24 ± 0.21	326 ± 3	0.13 ± 0.02	1.51 ± 0.02	4.87 ± 0.69$_{(11)}$	3.19 ± 0.50	14.17	6.87	15.75	-1172 ± 1005
IM19-M3	**23**	**D**	**194353**	**6 ± 1**	**7.7 ± 0.3**	**18 ± 2**	**8.04 ± 0.16**	**139 ± 3**	**0.47 ± 0.07**	**0.82 ± 0.02**	**0.23 ± 0.01$_{(38)}$**	**0.28 ± 0.04**	**6.27**	**13.06**	**14.5**	**1738 ± 81**
IM19-M3	32	L	194354	12 ± 1	11.4 ± 0.5	12.1 ± 1.2	12.4 ± 0.2	165 ± 2	0.18 ± 0.03	1.03 ± 0.02	6.06 ± 0.68$_{(43)}$	5.75 ± 0.79	11.4	7.64	13.72	-3727 ± 1577
IM19-M3	39	D+L	194355	6 ± 1	9 ± 1	8.1 ± 1.2	8.13 ± 0.20	162 ± 2	0.09 ± 0.01	0.95 ± 0.02	0.41 ± 0.02$_{(40)}$	0.43 ± 0.04	5.7	6.23	8.44	1585 ± 73
IM19-M3	44	D+L	194356	16 ± 2	14.9 ± 0.5	12 ± 1	16.86 ± 0.24	146 ± 4	0.29 ± 0.04	0.96 ± 0.02	6.70 ± 0.35$_{(10)}$	6.79 ± 0.76	5.4	9.87	11.25	-4772 ± 1529
IM19-M3	64	L	194357	14 ± 1	15.9 ± 0.4	14 ± 2	17.69 ± 0.32	215 ± 3	0.13 ± 0.02	1.30 ± 0.03	95.7 ± 13.0$_{(12)}$	73.97 ± 11.12	13.7	6.69	15.24	-70948 ± 22246
LE19-M1	22	D+L	194361	7 ± 1	8.95 ± 0.26	13 ± 1	7.70 ± 0.15	179 ± 2	0.19 ± 0.03	1.00 ± 0.02	0.141 ± 0.002$_{(47)}$	0.14 ± 0.01	1.89	7.86	8.09	1877 ± 23
LE19-M1	**33**	**D**	**194358**	**6 ± 1**	**6.44 ± 0.26**	**16 ± 1**	**5.71 ± 0.13**	**141 ± 2**	**0.70 ± 0.11**	**0.68 ± 0.01**	**0.1223 ± 0.0003$_{(45)}$**	**0.17 ± 0.03**	**1.43**	**17.13**	**17.2**	**1846 ± 60**
LE19-M1	**33**	**D**	**194360**	**6 ± 1**	**5.98 ± 0.26**	**12 ± 1**	**5.66 ± 0.13**	**167 ± 2**	**0.70 ± 0.11**	**0.74 ± 0.01**	**0.117 ± 0.002$_{(45)}$**	**0.16 ± 0.03**	**2.35**	**17.34**	**17.5**	**1858 ± 57**
LE19-M1	48	L	194359	8 ± 2	10.37 ± 0.38	7 ± 1	8.80 ± 0.19	221 ± 2	0.10 ± 0.01	1.09 ± 0.02	4.37 ± 0.61$_{(47)}$	3.92 ± 0.60	13.97	6.38	15.36	-1898± 1203

protocol (Murray and Wintle, 2000; 2003) was used for determining the equivalent dose (D_e) (Table 3.2).

Unless stated otherwise, a preheat for 10 s at 200 °C and a cut heat to 160 °C were adopted. Stimulation with the blue diodes was for 38.5 s at 125 °C; the initial 0.31 s of the decay curve minus a background evaluated from the following 0.77 s of stimulation was used in the calculations (Cunningham and Wallinga, 2010). Each measurement of the response to the test dose (2 Gy) was followed by a stimulation for 38.5 s with the blue diodes at 280 °C to minimize recuperation (Murray and Wintle 2003). At the end of a measurement of each aliquot, the sensitivity to stimulation with infrared light was measured (OSL IR depletion ratio; Duller, 2003), to check for the presence of feldspar. The sediment collected for dose rate determination was dried at 110 °C (until constant weight), pulverized and homogenized. A subsample (~ 140 g) of the powdered sediment was then cast in wax and stored for at least one month before being measured on top a low-level extended energy-range HPGe gamma-ray spectrometer (e.g. De Corte et al., 2006). The specific activities were converted to dose rates using conversion factors calculated from the nuclear data tabulated by Adamiec and Aitken (1998).

A beta attenuation factor of 0.90 (± 5 % relative uncertainty) was adopted to correct the external beta dose rates for the effects of attenuation and etching (Mejdahl, 1979). Correction for the effect of moisture was performed as outlined in Aitken (1985). The water content in fully saturated undisturbed sediment samples was determined in the laboratory and we assumed that the time-averaged water content was half of that (± 15 % relative uncertainty). On average, this corresponds to the moisture content at the time of sampling. An internal dose rate in quartz grains of 0.013 ± 0.003 Gy ka^{-1} was adopted (Vandenberghe, et al., 2008). The contribution of cosmic rays was calculated following Prescott and Hutton (1994) and a 15 % relative uncertainty was associated with the values.

3.3.3 Anthracological analysis and radiocarbon dating

The bulk sediment samples collected from the central part of each charcoal rich layer were wet sieved in the laboratory on a 0.5 mm mesh. The residues were dried and a minimum of 100 charcoal fragments was randomly selected from each kiln and studied using a reflected light microscope (50-500x magnification) and darkfield illumination. Identifications are based on wood anatomical features described in Schoch et al. (2004)

and a reference collection of charred modern wood species held at the Royal Belgian Institute of Natural Sciences.

From the identified charcoal fragments, samples with the lowest potential age at the time of charring (i.e. *twigs*) were selected for radiocarbon dating, to avoid a potential old wood-effect. These samples were combusted to CO_2 and transformed into graphite, after which the radiocarbon concentrations were measured in a MICADAS AMS-machine at the Royal Institute for Cultural Heritage, Brussels (Belgium) (Boudin et al., 2015). Results were calibrated with OxCal 4.4 (Bronk-Ramsey, 2009) using the IntCal20 calibration curve (Reimer et al., 2020).

Table 3.2: SAR measurement sequence and conditions. *: if i = 0, D_i is the natural dose or the dose administered in the dose recovery test; if i > 0, D_i is a regenerative dose administered in the laboratory. The ratio L_x/T_x is the sensitivity corrected signal.

No.	Treatment	Measurement condition	Observed
1	Dose (D_i^*)		
2	Preheat	at 200 °C for 10 s	TL
3	Blue stimulation	at 125 °C for 40 s	L_x (OSL)
4	Test dose (D_t)	~ 2 Gy	
5	Cut heat	to 160 °C	TL
6	Blue stimulation	at 125 °C for 40 s	T_x (OSL)
7	Blue stimulation	at 280 °C for 40 s	
8	Return to 1		

3.4 Experiments and results

3.4.1 OSL dating

3.4.1.1 Luminescence characteristics

Figure 3.3a shows a natural and regenerated OSL decay curve for an aliquot of sample GLL-194350, which was collected from the dark, charcoal-rich layer in feature HS19-M3. The signals are clearly distinguishable from the background level and decay rapidly with stimulation time. The decay matches that observed for calibration quartz (Figure 3.3a, inset), as one would expect for a signal that is dominated by the fast

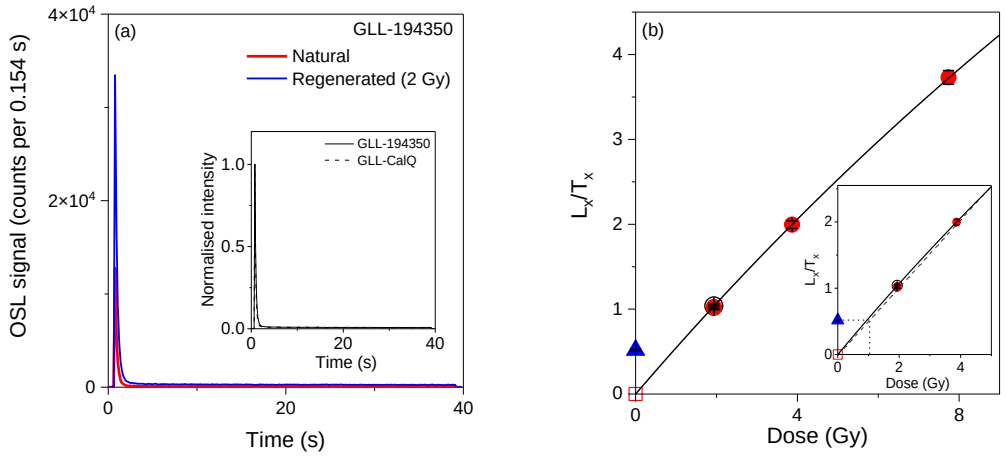

Figure 3.3: (a) OSL decay curves for an aliquot of sample GLL-194350. The natural and regenerated signals are shown as the red and blue lines, respectively. The inset compares the regenerated OSL decay curve from the sample with that from calibration quartz (GLL-CalQ). (b) SAR growth curve for an aliquot of the same sample. Recycling and recuperation points are represented by the open circle and square, respectively. The black solid line represents a single saturating exponential function fitted to the regenerated data. The natural signal (solid triangle) intersects with the linear region of the dose response curve (dashed line; inset).

component. The dose response curve is shown in Figure 3.3b and can be well represented by a single saturating exponential function (solid black line).

Up to regenerative doses of a few Gy, the growth of the signal does not significantly deviate from linearity (Figure 3.3b, inset). The dose response passes through the origin (indicating that recuperation is negligible; open square) and the measurements are reproducible (indicating that sensitivity changes are accurately corrected for; the solid and open circles overlying each other). The aforementioned example is representative for the behavior of the samples collected from the dark, charcoal rich layers ("D" in Table 3.1). This is further illustrated in Figure 3.4, which summarizes the values for recuperation, and recycling and OSL IR depletion ratios for all aliquots (n = 336) that were measured for determining the burial dose in this type of material (see §3.4.1.3). On average, recuperation amounts to 0.3 ± 0.1 % of the sensitivity corrected (L_x/T_x) natural signal (Table 3.2) and, within uncertainty, none of the individual values exceeds 5%, which was suggested by Murray and Wintle (2000) as a criterion for acceptance (Figure 3.4a). For the recycling ratio, Murray and Wintle (2000) suggested a range of acceptability in between 0.90 and 1.10. About ~ 90 % of the aliquots (n = 304; not considering individual uncertainties) yield a ratio within this range and the overall average recycling ratio (± 1 standard error) is 1.024 ± 0.003 with a relative standard deviation (RSD) of 6% (Figure 3.4b). Equally, most of the OSL IR depletion ratios fall

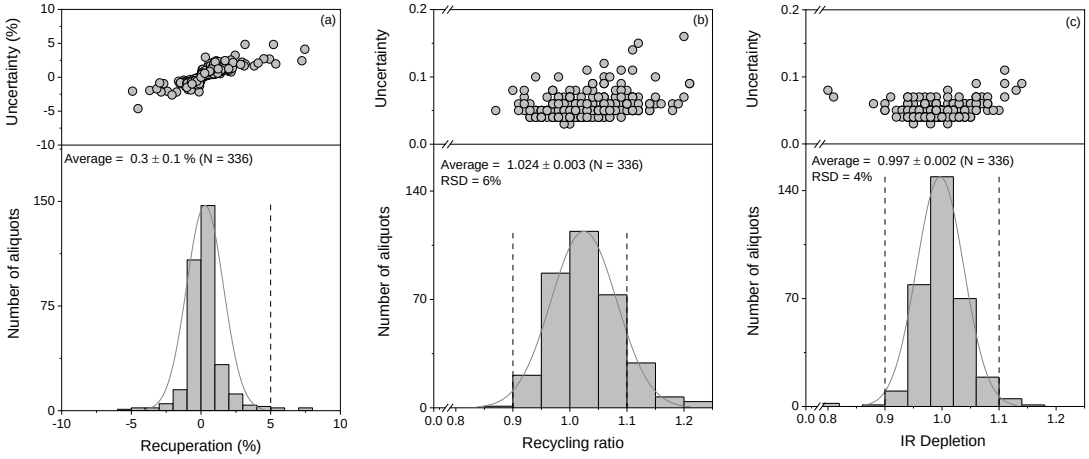

Figure 3.4: Summary of recuperation (a; expressed as percentage of the natural OSL signal), recycling (b) and OSL IR depletion (c) data for all samples collected from dark, charcoal rich ("D") layers. The vertical dashed lines (eye guides) mark a value of recuperation of 5% (a), and bracket the 0.9-1.1 interval for recycling and OSL IR depletion ratio (b, c).

within the 0.90 - 1.10 interval (n = 328, or ~ 98 % aliquots; Figure 3.4c), with an overall average (± 1 standard error) of 0.997 ± 0.002; all values are compatible with no sensitivity to stimulation with IR, indicating that there is no feldspar contamination (Duller, 2003).

Similar observations were made for samples collected in the layers with a mottled/mixed or lighter color ("D+L" and "L", respectively, in Table 3.1; see Figure 3.5).

3.4.1.2 Procedural tests

To identify the optimum measurement parameters for equivalent dose (D_e) determination, we first examined the dependence of D_e on preheat temperature for three samples (one sample for each pit) collected from dark layers ("D": GLL-194347, -53 and -58) and one sample from a dark-lighter layer ("D+L": GLL-194355).

For each sample, groups of three large (8 mm diameter) aliquots were measured at each of seven different preheat temperatures in the range of 160 °C to 280 °C. Figure 3.6 summarises the results for samples GLL-194347 and -55. For both samples, the D_e is independent of preheat temperature up to 260 °C; over the entire temperature range investigated, recycling ratios fall well within the 0.90-1.10 interval and average recuperation remains below 5 % of the corrected natural OSL signal. Similar observations were made for samples GLL-194353 and -58.

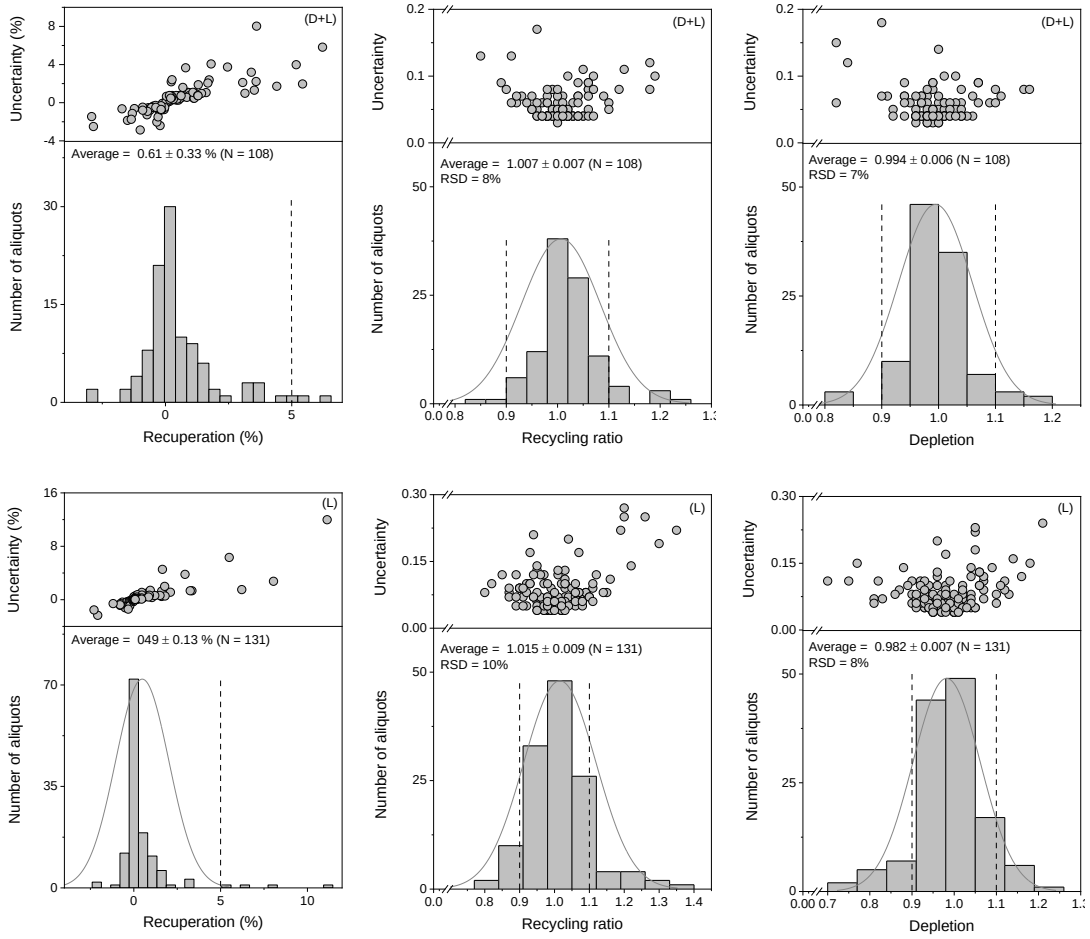

Figure 3.5: Summary of recuperation (expressed as percentage of the natural OSL signal), recycling and OSL IR depletion data for all samples collected from the from "D+L" and "L" layers. The vertical dashed lines (eye guides) mark either a value of recuperation of 5%, or bracket the 0.9-1.1 interval for recycling and OSL IR depletion ratio.

We then examined if a known laboratory dose can be measured using the same procedure as one would use for determining the natural dose. Such a dose recovery test allows identifying adverse effects of signal components and inaccurate correction for sensitivity change, and optimisation of measurement parameters (e.g. Murray and Wintle, 2003).

Natural aliquots of samples GLL-194347, -53, -58 and -55 were bleached two times for 250 s using the blue diodes at room temperature, with a 10,000 s pause at room temperature in between. They were then given a laboratory dose close to the estimated D_e and measured as outlined in the above for a range of preheat temperatures. The measured doses show no significant variation with preheat temperature up to 260 °C (Figure 3.7, for samples -47 and -55, with average measured to given dose ratios of 1.020 ± 0.004 (n = 18) and 0.973 ± 0.016 (n = 18), respectively).

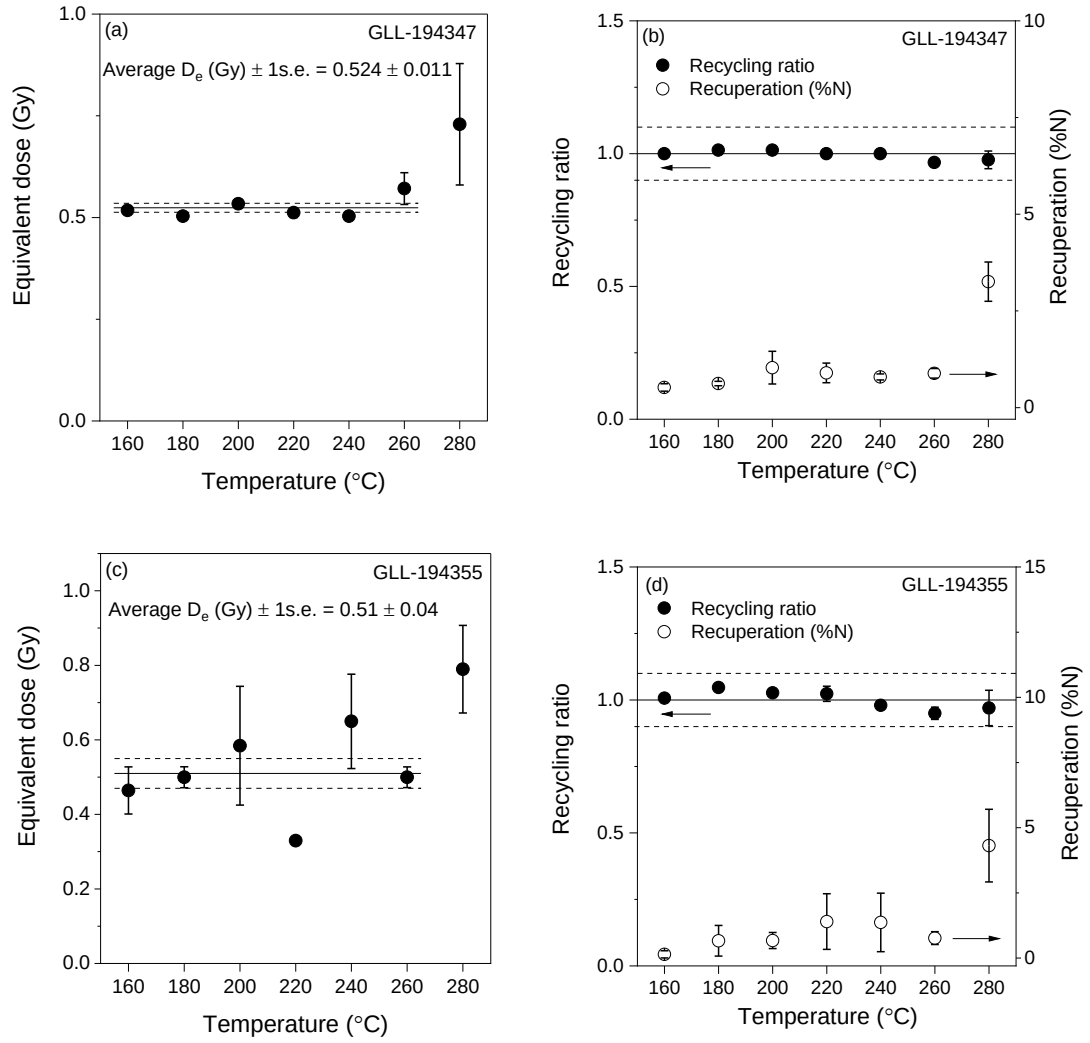

Figure 3.6: Dependence of equivalent dose (D_e) on preheat temperature for samples GLL-194347 (a) and -55 (c). Each datapoint represents the average (± 1 standard error; 1 s.e.) of 3 measurements. The dashed and dotted lines indicate the average ± 1 s.e. over the 160 – 260 °C temperature interval. Figs (b) and (d) show the corresponding recycling and recuperation data; the solid and dashed lines (eyeguides) bracket a value for the recycling ratio of 1.0 ± 0.1.

The dose recovery test was also performed using three large aliquots of each sample, but this time using only preheat temperatures of 180 °C and 200 °C. The results are summarised in Figure 3.8. Within analytical uncertainty (1 standard error), the measured to given dose ratios do not differ by more than 5 % from unity. On average, there is no significant difference in the ratio's obtained using the two preheats (10 s at 180 °C: 0.977 ± 0.010, 0.984 ± 0.011 and 0.962 ± 0.015 for "D", "L" and "D+L" samples, respectively; 10 s at 200 °C: 0.987 ± 0.013, 1.004 ± 0.006 and 1.004 ± 0.009 for "D", "L" and "D+L" samples, respectively). The results from the whole of procedural tests suggests that the laboratory measurement procedure is suitable for D_e-determination. We selected a preheat of 10 s at 200 °C for further analysis.

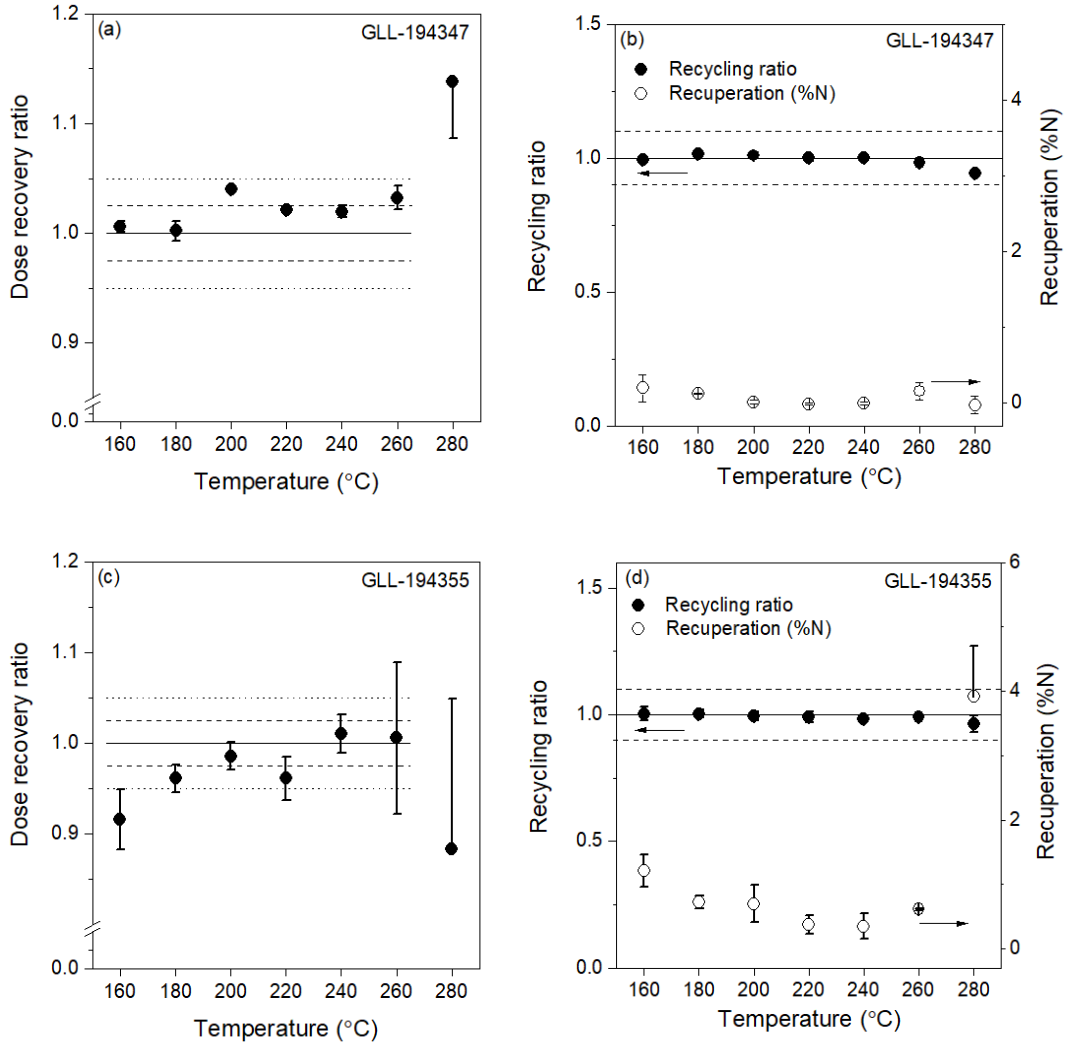

Figure 3.7: Dependence of dose recovery ratio on preheat temperature for samples GLL-194347 (a) and -55 (c). Each datapoint represents the average (± 1 standard error; 1 s.e.) of 3 measurements. The dashed and dotted lines are eyeguides and bracket a 2.5% and 5% deviation of the ratio from unity (solid line). (b,d) Corresponding data for recycling and recuperation.

3.4.1.3 Equivalent doses

For all samples collected from the dark layers ("D" in Table 3.1), 48 replicate measurements of equivalent dose (D_e) were made using small (2 mm diameter) aliquots. In between 12 and 48 small aliquots were measured for the other samples ("D+L" and "L"), as we considered them not (necessarily) directly relevant to the timing of the event of interest (charcoal production) but included them in the analyses for assessing reliability (cf. Karimi-Moayed et al., 2020). Occasionally (less than 9% of measurements), an aliquot emitted a net natural test dose signal less than three times the standard deviation (SD) of the background signal, and was excluded.

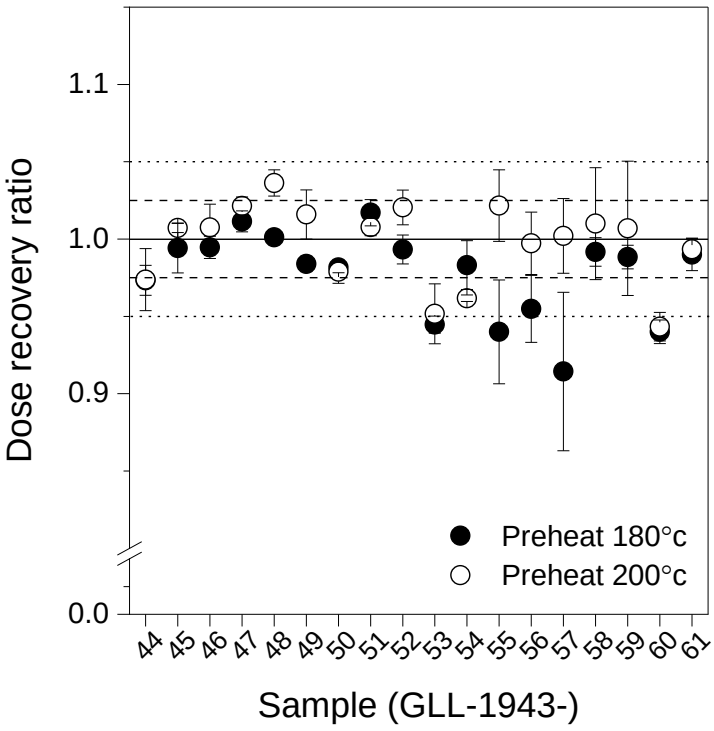

Figure 3.8: Summary of dose recovery data for all samples, obtained using preheat temperatures of 180 °C and 200 °C. The dashed and dotted lines (eyeguides) bracket a 2.5% and 5% deviation of the ratio from unity (solid line).

Following Karimi-Moayed et al. (2020), we then applied a simple criterion in which values that differed by more than 3 SD's from the average were iteratively rejected. Figure 3.9a, b and c summarise the results for three samples collected from dark charcoal-rich layers (GLL-194350, -53 and -58; one "D" sample for each site) represented as histograms. A graph of D_e versus uncertainty is shown above each histogram to visualize the precision by which each individual value was measured. For each sample, the dataset mainly consists of values that appear to belong to a single dose population and some aliquots that yielded significantly higher D_e's. The selected D_e distributions in samples from dark, charcoal-rich layers are characterized by a relative standard deviation (RSD) between 11-37 % and the mean (± 1 standard error) was used in the calculations (Table 3.1; see §3.4.1.5).

Figure 3.9d, e and f show the results for three samples from underlying lighter layers (GLL-194352 -54 and -59; i.e., one "L" sample for each site). In general, the D_e's for this type of material are spread over a wider range. Processing the data in the same manner yields distributions with RSD's ranging from 19 to 95 %. Although a smaller

number of D_e's were obtained for most of these samples, at least some of the distributions do not appear to reflect a single dose population.

This is illustrated most clearly by the results for samples GLL-194354 and -59 (Figure 3.9e and f, respectively). The D_e distributions for the other samples are presented in Figure 3.10.

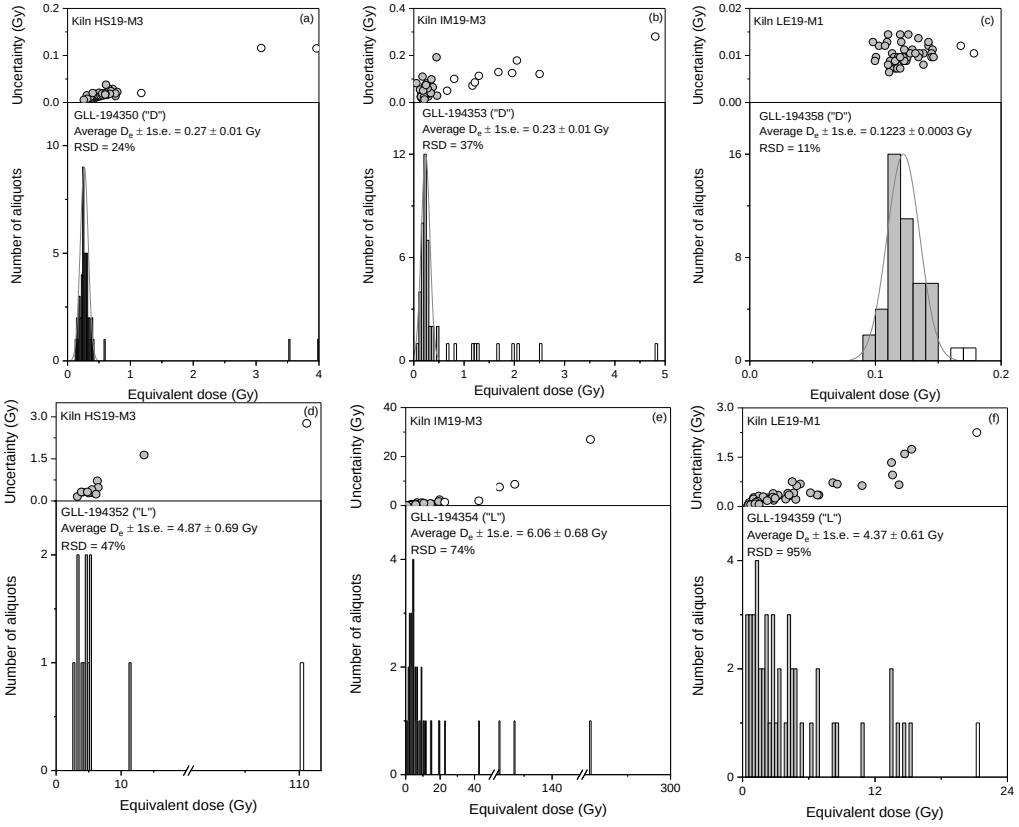

Figure 3.9: Distribution of equivalent dose in small (2 mm) aliquots of samples GLL-194350 (a), -53 (b) and -58 (c), which were collected from dark-charcoal rich ("D") layers, and of samples GLL-194352 (d), -54 (e) and -59 (f), which were collected from the corresponding underlying lighter ("L") layers. A plot of D_e versus uncertainty is shown above each histogram; the median from this distribution was used for binning the data. The open symbols refer to aliquots that were rejected for D_e calculation (see text for details).

3.4.1.4 Thermal transfer and measurement of low D_e's

The D_e's obtained for the samples collected from the dark layers range from 117 - 610 mGy (Table 3.1). They were derived from distributions as outlined in the above (see §3.4.1.3 and Figures 3.9 & 3.10), for which it is interesting to note that all aliquots that emitted a detectable net natural test dose signal also yielded a finite, non-zero dose-value. We therefore examined what the minimum dose is that one might ideally be able to measure under the given experimental conditions, especially as thermal transfer and

low signal intensity have been identified as two potential difficulties specific to the measurement of such low doses (e.g. Madsen and Murray, 2009). Two sets of experiments were performed, similar to those reported by Thomsen et al. (2007).

A first series of experiments used three samples collected from the uppermost dark layers (GLL-194344, -53 and -58). For each sample, two sets of fresh 48 small aliquots (2 mm diameter) were prepared. One set was bleached two times for 250 s with the blue diodes at room temperature, with a 10,000 s pause at room temperature in between (i.e. identical to the bleaching treatment used in the dose recovery test; §3.4.1.2), and measured using the SAR protocol employing a preheat of 10 s at 200 °C and a cut heat to 160 °C (i.e same as for D_e-determination). In this case, however, the response to only one regenerative dose of ~2 Gy was measured (as in this region the signal grows linearly with dose; Figure 3.3b), followed by a measurement of recuperation, recycling and OSL IR depletion ratio. The second set of aliquots was reset by heating to 500 °C, cooled to room temperature, and subsequently measured in the same manner. The results for both series of experiments are shown in Figure 3.11.

The measured average doses after resetting by light range from 0.5 ± 0.3 mGy to 8 ± 2 mGy, while values in between -0.5 ± 0.4 mGy to 0.6 ± 0.7 mGy were obtained in case of resetting by heat. Comparing the natural doses for these samples (520 ± 20 mGy, 230 ± 10 mGy and 122 ± 0.3 mGy for samples -44, -53 and -58, respectively; see §3.4.1.1 and Table 3.1) with the residual doses after resetting by light (8 ± 2 mGy, 3 ± 1 mGy and 0.5 ± 0.3 mGy) could hint at a relation. The values obtained after thermal resetting (0.6 ± 0.7 mGy, 0.1 ± 3 mGy and -0.5 ± 0.4 mGy) may reflect a similar dependence, although they do not differ significantly, and are also not significantly different from zero. Regardless of the mode of resetting, it is clear that, in general, any residual dose would not exceed about ~2% of the natural dose.

A second series of experiments was performed in the same way but this time a known laboratory beta dose was administered following resetting and prior to measurement (0.32 Gy, 0.16 Gy and 0.08 Gy for samples -44, -53 and -58, respectively). The data were processed as outlined in the above (§3.4.3.1) and the results are summarised in Figure 3.12. The given doses can be recovered reasonably well with overall average dose recovery ratios of 1.06 ± 0.01 (n = 138) and 1.01 ± 0.01 (n = 135), in case of optical and thermal resetting, respectively. This confirms the findings of the first series

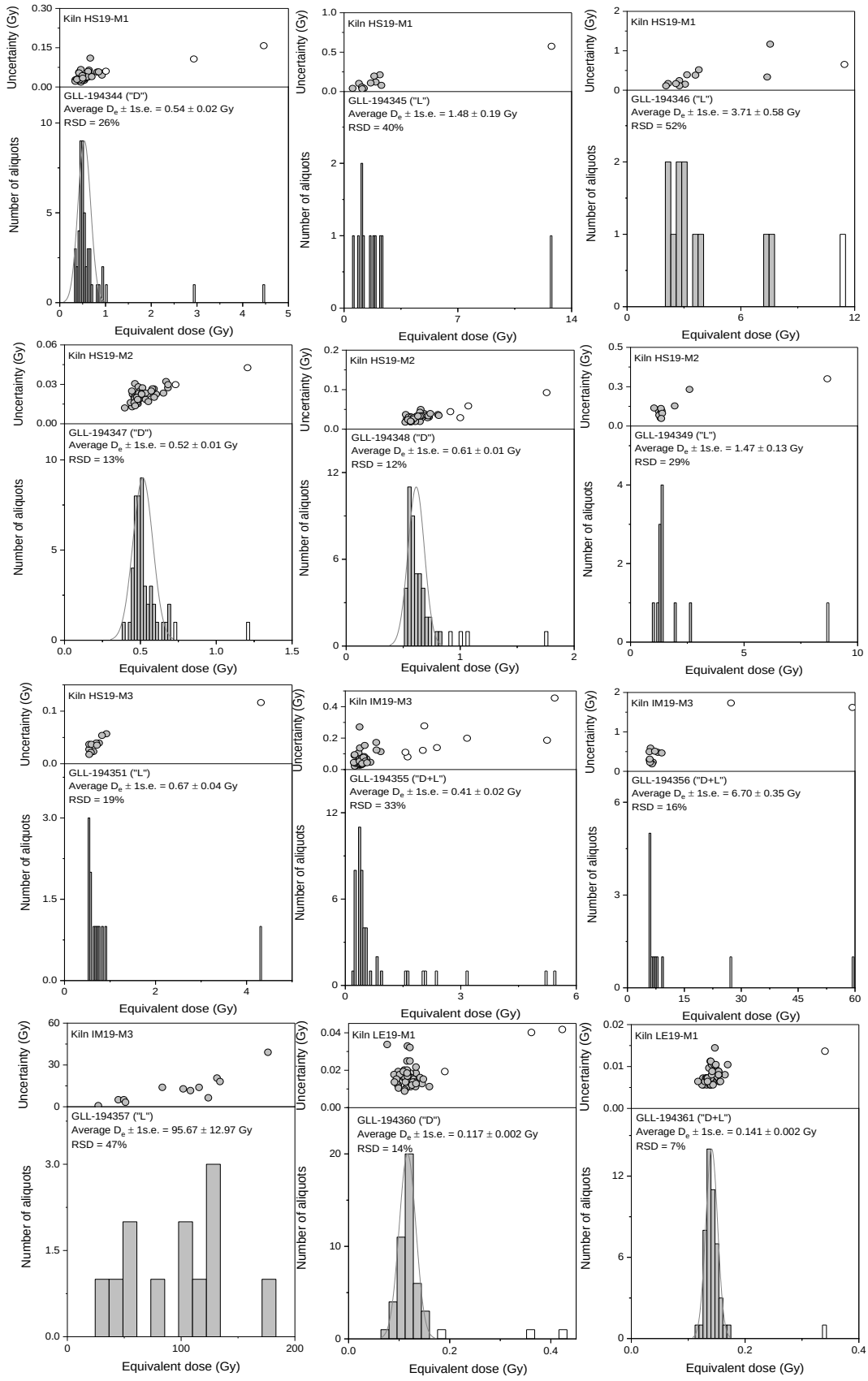

Figure 3.10: Distribution of equivalent dose in small (2 mm diameter) aliquots of all samples not included in Figure 3.9.

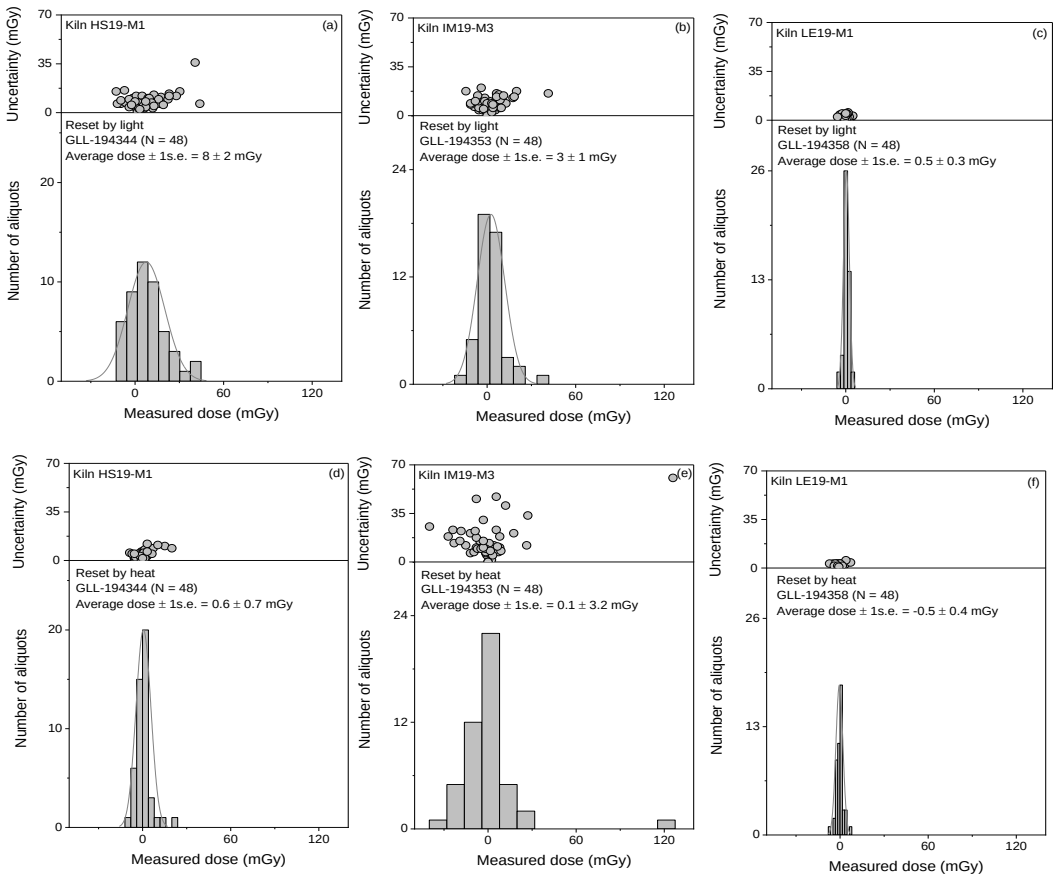

Figure 3.11: Distributions of measured dose in small aliquots (2 mm diameter) of samples GLL-194344, -53 and -58 following optical (a,b,c) and thermal (d,e,f) resetting. See text for details.

of experiments. The slight but systematic overestimation of the given dose in case of optical resetting by about 6 % may be caused by some (minor) incomplete removal of charge of optically sensitive traps, thermal transfer and/or sensitivity change which is not (entirely) corrected for by the measurement procedure.

The whole set of results demonstrates that the small and finite natural equivalent doses in our "D"-samples (§3.4.3.1; Table 3.1) are not an artefact of the measurement procedure or due to (significant) unwanted transfer processes.

3.4.1.5 OSL ages

Table 3.1 summarizes all analytical data and the calculated OSL ages. The uncertainties on the OSL ages were calculated following the procedure as outlined by Aitken (1985), with contributions from sources of systematic uncertainty as given in §3.3.3 (see also Vandenberghe, 2004; Vandenberghe et al., 2004). For samples from the "D" layers, which are of main interest, the total uncertainties range from ~ 7% to ~ 18%; they are dominated by the uncertainties that we associated with our estimates of past water

content and/or cosmic radiation (see §3.5.2.2). For the other samples ("D+L" & "L"), the total uncertainties are similar (in between ~ 7% to ~ 18%) but generally with the combined random uncertainty as the main contributor, which essentially reflects the observed spread in D_e (e.g. Figures 3.9d, e ,f) .

The OSL ages for the samples collected from the dark layers range from 0.16 ± 0.03 ka to 0.46 ± 0.04 ka (1 σ uncertainty). With the exception of sample GLL-194353, which was collected from kiln IM19-M3 and a rather complex stratigraphy, all the ages are consistent with the stratigraphic position of the samples. The OSL dates refer, at least in principle, to the time that has elapsed between the zeroing event in the past and the time of sampling (2019). To facilitate comparison with ^{14}C-dating (see §3.5.1), the OSL ages were recalculated to ages CE and expressed within 95.4% probability (2σ; Table 3.1, last column).

3.4.2 Anthracological analysis and radiocarbon dating

In the frame of this study, one radiocarbon date for each of the studied kilns was obtained (Table 3.3). The ^{14}C dates for the three kilns in Hoog Soeren Forest (HS19M1, -M2 and -M3) range from ~ 1490 to ~ 1660 cal CE. The two other kilns, LE19-M1 and IM19-M3 postdate 1650 CE, with wide age probability distributions from ~ 1680 and ~ 1940 cal CE.

The charcoal assemblages of all investigated kilns are dominated by a single *taxon* and show a very low taxonomic diversity (Table 3.4). The three charcoal kilns in Hoog Soeren (HS19) are dominated by beech (*Fagus sylvatica*; 97.2% - 100%), with only some small additional amounts of oak (*Quercus* sp.) (2.8%) in one of the kilns. The kilns at Imbosch and Leuvenum are both dominated by Scots pine (*Pinus sylvestris*) with additionally a very minor amount of common heather (*Calluna vulgaris*) in kiln IM19-M3.

3.5 Discussion

3.5.1 Comparison between OSL and ^{14}C ages, and historical sources

Figure 3.13 compares the OSL ages obtained for the samples collected from the uppermost dark layers with both the ^{14}C ages for the same horizons and the available information derived from historical sources (see §3.2). The OSL and the ^{14}C ages are consistent with the historical information for all charcoal kilns, although the latter is

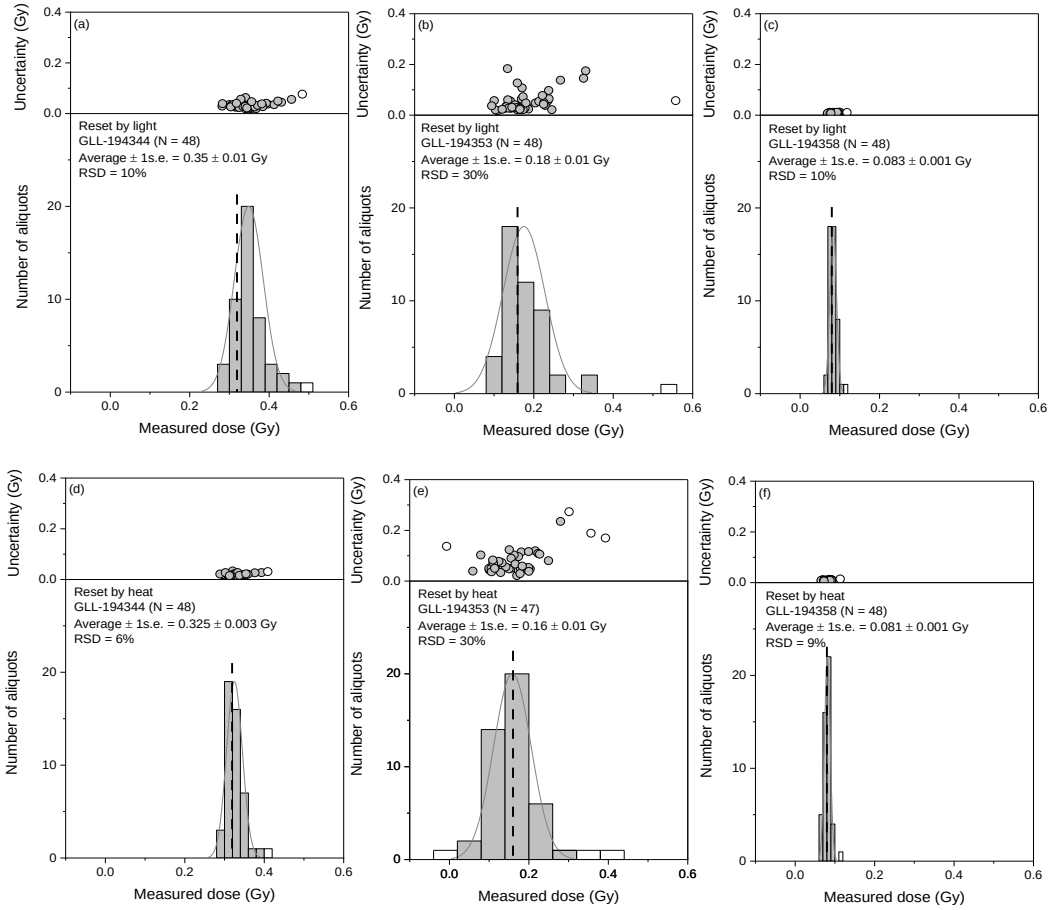

Figure 3.12: Results from dose recovery tests using small aliquots (2 mm diameter) of samples GLL-194344, -53 and -58, in which a known laboratory dose was administered following either optical (a-c) or thermal (d-f) resetting, and subsequently measured using the SAR protocol. The dashed lines indicate the given laboratory dose (0.32, 0.16 and 0.08 Gy for samples -44, -53 and -58, respectively). The open symbols refer to aliquots that were rejected from the analysis (see text for details).

particularly poorly constrained for Hoog Soeren (HS). For four out of five kilns (LE19-M1, IM19-M3 and HS19-M1&2), the OSL and ^{14}C-ages are entirely consistent.

For kiln HS19-M3, the OSL age is significantly younger than the ^{14}C age. In addition, the OSL age for this kiln is considerably younger than those for the two other kilns (HS19-M1&M2), while the ^{14}C-dates rather point at a similar age for all three of them. Wintle and Murray (2006) reiterated that, when comparing ^{14}C and OSL dating, one should note that the two methods use different materials (organic material and minerals, respectively) for dating events that were not necessarily synchronous (the end of carbon exchange versus the last exposure to heat and/or light). This is further discussed in §3.5.2. The 2 sigma total uncertainties on the OSL ages cover an age range of ~ 30 - 90 years, while the ^{14}C-age probability distributions extend over some 140 - 260 years. If one assumes that systematic sources of uncertainty (σ_{sys} in Table 3.1) are equally shared

between the OSL samples, only the random uncertainties (σ_r in Table 3.1) can be considered when comparing the OSL ages amongst each other (see also Karimi-Moayed et al., 2020). This would imply a time-resolution of 5-40 years at the 2σ level. This illustrates the potential of OSL dating as a complementary tool to ^{14}C for numerical age determination, as well as for establishing relative age relationships on centennial to even decadal timescales.

Table 3.3: Summary of results from ^{14}C-dating.

Feature	Sample ID	Sample	Lab code	uncal BP (±1σ)	cal CE (± 2σ)
HS19-M1	*Fagus sylvatica (beech)*	*twig*	RICH-29861	288 ± 23	1514 (62.0%) 1591
					1620 (33.5%) 1658
HS19-M2	*Fagus sylvatica (beech)*	*twig*	RICH-29862	317 ± 23	1494 (75.2%) 1602
					1610 (20.2%) 1644
HS19-M3	*Fagus sylvatica (beech)*	*twig*	RICH-29863	328 ± 22	1490 (95.4%) 1639
IM19-M3	*Calluna vulgaris (common heather)*	*twip*	RICH-29864	121 ± 24	1682 (25.2%) 1738
					1754 (1.1%) 1761
					1801 (69.2%) 1938
LE19-M1	*Pinus sylvestris (Scots pine)*	*twig*	RICH-29865	123 ± 23	1682 (25.0%) 1738
					1754 (1.3%) 1762
					1801 (69.1%) 1938

3.5.2 Potential difficulties with ^{14}C and OSL dating

3.5.2.1 ^{14}C-dating

Charcoal is generally considered a preferred material for ^{14}C dating and, if derived from short-lived samples, would not be expected to result in significant age overestimation due to the old-wood effect (e.g. Wagner, 1998). An old-wood effect essentially reflects the duration over which plants grow and may result in ages that predate the time of charring by a few 100 years (Waterbolk, 1971; Warner, 1990). In addition, there might be a time-lag between the death of the plant and its use for charcoal production. However, in case of short-lived samples, such an offset can be excluded. For ^{14}C dating, we used twigs with less than 10 growth rings (§3.3.3; Table 3.3). It would thus seem reasonable to expect that any age difference between the event that is actually dated (no more carbon exchange) and the event that is targeted (charcoal production) is minimal. Therefore, we can exclude an old wood effect for the ^{14}C dates obtained for the kilns. This holds even more given the time-resolution of the ^{14}C-dates of these kilns. This is

illustrated most clearly for features LE19-M1 and IM19-M3, for which the calibrated ^{14}C ages essentially cover the entire last few centuries.

Additional information on the age of the kilns comes from the combining of their charcoal assemblages with the historical information. Charcoal assemblages of all studied kilns are dominated by a single taxon and show a very low taxonomic diversity (Table 3.4). The charcoal assemblage in kiln IM19-M3 at Imbosch is dominated by pine (Pinus sylvestris). The earliest evidence for pine plantation in the vicinity of the relic feature dates back to 1764 CE (^{14}C age for kiln IM19-M3 is 1682-1938 CE). For ^{14}C dating, however, charred common heather was used. At Leuvenum forest (kiln LE19-M1) the charcoal assemblage is again dominated by pine, which is documented from ca. 1850 CE onwards (^{14}C age for kiln LE19-M1 is 1682-1938 CE). Other species were only introduced from the 1930's CE onwards. The absence of common heather (except for 1 single fragment) in the charcoal assemblages is also an argument that these kilns all postdate the conversion of heathland to forest.

In short, the combined evidence suggests that the ^{14}C-dates do not suffer from significant inaccuracy and are solely limited in terms of precision.

Table 3.4: Results from anthracological analysis (in %).

Site	HS19			IM19	LE19
Kiln	M1	M2	M3	M3	M1
Calluna vulgaris (common heather)	-	-	-	0.9	-
Fagus sylvatica (beech)	100	97.2	100	-	-
Pinus sylvestris (Scots pine)	-	-	-	99.1	100
Quercus sp. (oak)	-	2.8	-	-	-
Total (n)	107	108	115	112	115
Bark indet (n)	4	7	1	-	-

3.5.2.2 OSL-dating

Karimi-Moayed et al. (2020) previously outlined the potential pitfalls associated with OSL dating of relic charcoal kilns. We considered turbation processes to be of particular concern here, as several studies have shown that near-surficial sandy deposits are particularly prone to bio- and pedoturbation (e.g. Bateman et al., 2003; 2007b). Such processes can lead to age over- or underestimation. While our scale of analysis (2 mm diameter aliquots, and hence multigrain) may be too large for being conclusive to this respect, it does allow identifying samples which are clearly not composed of material

of the same D_e. This is most clearly illustrated by results for underlying 'L"-layers (e.g. Figure 3.9e), illustrating our rationale for incorporating these in our investigations. With respect to the small-aliquot D_e-distributions for the "D"-layers, some variability can be observed. All of them are dominated by a single dose population, however, and there is no evidence for one pit being more, or less, prone to turbation processes following the event of interest (charcoal burning). When compared to independent age information (see §3.5.1 and Figure 3.13), there is no evidence for systematic age over- or underestimation.

Of the five investigated kilns, only the OSL age for kiln HS19-M3 (sample GLL-194350) is significantly younger compared to the ^{14}C age. One possible explanation is that the dose rate for this particular sample was overestimated, e.g. owing to inaccurate determination of specific radionuclide activities and/or radioactive disequilibria, improper allowance for the effect of water and/or organic matter, and/or erroneous calculation of the contribution from cosmic rays.

An inaccuracy in radionuclide quantification owing to error in calibration of the gamma-ray spectrometer would systematically affect all results, while a random error in e.g. the preparation of this particular sample would be reflected in significantly different radionuclide activities. The dataset presented in Figure 3.13 and Table 3.1 does not point at such types of error. In some samples (and including sample GLL-194350), however, radioactive disequilibria and particularly increased levels of ^{210}Pb, are observed. We calculated the dose rates from the present-day radionuclide contents implying that, if element mobility (^{210}Pb enrichment) occurred quite recently, the corresponding dose rates are overestimated. Calculating the dose rate assuming equilibrium with an activity equal to that of the parent (^{234}Th) would increase the age of sample GLL-194350 by about 50 years, which is far from sufficient to account for the difference with the ^{14}C-age.

With respect to water content and cosmic radiation, our estimates are based on best possible knowledge and we adopted an uncertainty with these values that covers all likely scenarios (cf. §3.3.2) at the 2σ confidence interval. We adopted a value of half the water content at saturation, approximately corresponding to the moisture content at the time of sampling, and associated a relative uncertainty of 15 % (1σ) with these values. Our estimates of past moisture content vary significantly between the different sites ("F*W" in Table 3.1). If this variable was not properly accounted for, one would

thus expect a systematic effect and/or a random spread in OSL age results. The time-averaged moisture content for kiln HS19-M3 (~ 23 %) is slightly higher compared to that for other two kilns at Hoog Soeren (~ 14 - 16 %). Assuming the upper limit for the effect of water (full saturation) would increase the age for sample GLL-194350 by about 30 years. Even in combination with a lower ^{210}Pb activity (see higher), this does not allow for the apparent age underestimation. Moreover, there are no objective arguments that would corroborate the assumption of full saturation for this particular sample. The contribution of cosmic rays was calculated following Prescott and Hutton (1994) and a 15 % relative uncertainty (1σ) was associated with the values. For the samples collected from the "D"-layers, the calculated cosmic dose rate was ~ 0.25 (± 0.04) Gy/ka, amounting to ~ 17 – 38 % of the total dose rate. This is, at present, our best estimate of this component and its significance is reflected by its contribution to the total systematic uncertainty. Neglecting the contribution from cosmic rays (which would imply the highly unlikely scenario of burial below tens of meters of sediment) would increase the age for sample GLL-194350 by some 40 years.

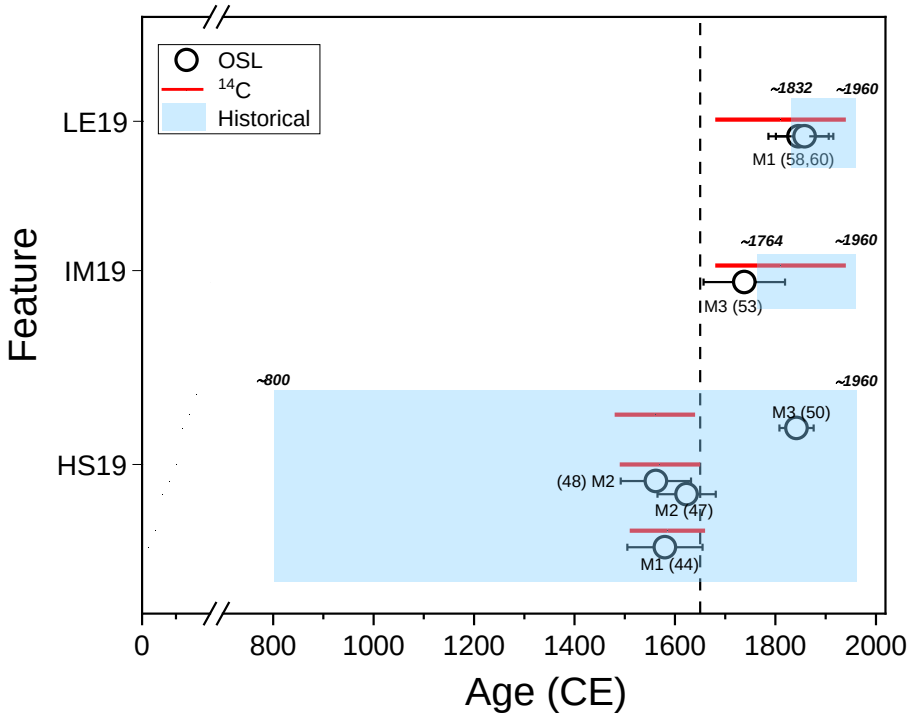

Figure 3.13: Comparison between OSL ages, calibrated ^{14}C-ages and historical evidence. The OSL ages (± 2σ total uncertainties) are represented by the open circles. The calibrated ^{14}C age ranges (95.4% probability) are indicated by the red solid lines. The blue highlighted frame the age information drawn from historical sources. All ages are expressed as ages Common Era (CE).

The content of organic matter in our samples was not determined and its effect should thus be considered as unknown. Organic matter reduces the dose rate in addition to that by water (Lian et al., 1995). If indeed significant, one would thus expect a more or less systematic underestimation of our OSL dates, which is not supported through the comparison with independent ^{14}C age information. An organic content of e.g. 15% (which is the highest value we obtained in preliminary experiments on samples of relic charcoal kilns in N Belgium) would increase the age for sample GLL-194350 by about 20 years. This gives an idea about the magnitude of the effect.

In short, the combined evidence does not suggest that the OSL ages suffer from significant and systematic inaccuracy, while being more precise than ^{14}C. The discrepancy in age results observed for kiln HS19-M3 (sample GLL-194350) remains to be understood. If indeed real, this difference could point at repeated charcoal burning at this spot with the ^{14}C and OSL dates referring to an older and a younger phase, respectively. This would then illustrate the added value of using both methods in conjunction. Interestingly, only one dark charcoal-rich layer was macroscopically recognized in the field.

3.6 Conclusions

Our study focused on the potential of OSL dating of heated sediments associated with relic charcoal kilns in a sandy substrate. For four out of five of the investigated features, there is a good agreement between the OSL dates and independent age information (historical sources and ^{14}C-dating).

There is no evidence for significant or systematic age over- or underestimation. We therefore conclude that OSL dating is a feasible alternative and complementary chronometric tool to ^{14}C-dating, which has been widely adopted in this type of research. As such, our study not only confirms the potential of the method shown by Karimi-Moayed et al. (2020) for kilns in silty subsurfaces, but extends it to comparable archives that are preserved in sandy depositional environments. Of particular importance is that, especially for post-1650 CE features, the OSL dates can be significantly more precise than ^{14}C ages and hold potential for distinguishing between features and charcoal production phases at decadal or multi-annual timescales. Such an unprecedented time-resolution would open a whole new chapter in a range of research related to past charcoal production and our understanding of historical woodland exploitation.

Chapter 4: A combined OSL and ^{14}C dating study of charcoal production in the sandy environment of Zoersel forest (N Belgium)

Nasrin Karimi Moayed, Dimitri Vandenberghe, Jan-Pieter Buylaert, Koen Deforce, Ann-Eline Debeer, Paulina Biernacka, Philippe De Smedt, Wim De Clercq, Johan De Grave,

This chapter is slightly modified from the published version in the journal Quaternary Geochronology. The modifications concern formatting, inclusion of the supplementary material in the main text, and minor suggestions made by the examination commission.

Author contributions

Nasrin Karimi Moayed: Field investigation, Sampling, Sample processing, Data analysis, Methodology, Data curation, Writing.
Dimitri Vandenberghe: Field investigation, Sampling, Methodology, Writing, review and editing.
Jan-Pieter Buylaert: Single-grain measurements.
Koen Deforce: Field investigation, Sampling, Methodology, Writing, review and editing. *Ann-Eline Debeer:* Sample processing.
Paulina Biernacka: Sampling.
Phillipe De Smedt: Field investigation.
Wim De Clercq: Supervision, Funding acquisition.
Johan De Grave: Supervision, Field investigation, Sampling, Writing, review and editing, Funding acquisition.

Abstract

We investigate the potential of quartz-based OSL-dating for application to heated sandy sediments that are closely associated with the remains of charcoal production (charcoal kilns). This is particularly relevant for post-1650 CE features, where ^{14}C-dating lacks precision. We first document the general OSL characteristics using large aliquots of sand-sized quartz. Results from procedural tests indicate that the laboratory measurement procedure should allow reliable equivalent dose estimation. The scale of analysis is then reduced to smaller aliquots for all samples, each composed of 100-200 grains, as well as to single grains for eight heated samples. For one sample, both the small and single-grain ages are consistent with the ^{14}C-ages obtained for charcoal fragments in the same sedimentary unit. Also for three other samples, single-grains yield ages consistent with ^{14}C-dating; all other OSL-ages are older although, for three of these samples, single grains and small aliquots yield results that are not significantly

different. We discuss potential sources of inaccuracy for the OSL-dates, such as dose rate determination and homogeneous incomplete resetting. The latter is the most difficult to assess and requires additional empirical data.

Keywords: Charcoal kilns, OSL dating, ^{14}C dating, small aliquots, single grain, Zoersel forest

4.1 Introduction

Before the large-scale exploitation of fossil coal in the nineteenth and twentieth century CE, charcoal production was an important activity in central and north-western Europe, leaving numerous remains of charcoal production features (kilns) in historically forested areas (Nelle, 2003; Ludemann, 2010; Deforce et al., 2021a; Carrari et al., 2017; Paradis-Grenouillet and Dufraisse, 2018; Schneider et al., 2020). Many of these kilns are still visible in the topography and are increasingly detected and mapped using remote-sensing based approaches (Deforce, 2021a; Oliveira et al., 2021; Risbøl et al, 2013). Charcoal production had a considerable influence on woodland composition and soils characteristics, and the subsequent evolution of the surficial landscape (e.g. Deforce et al., 2021b; Hirsch et al., 2017, 2018). The remains of charcoal kilns are used for the study of the distribution, age and composition of formerly wooded areas (Foard, 2001; Groenewoudt and Spek, 2016), and give information about changes in related iron production activities (Deforce et al., 2021a). In addition, the relics are increasingly used to study the stability of biochar and its relevance for carbon sequestration (e.g. Hardy et al., 2017a; Mastrolonardo et al., 2018), soil properties (e. g. Hardy et al., 2016, 2017b; Hirsch et al., 2017, 2018), and woodland regeneration and biomass production (Carrari et al., 2016a, 2016b; Buras et al., 2020).

All the aforementioned studies require robust age information for these charcoal production sites. This is commonly obtained through ^{14}C-dating of charcoal, which is abundant in the kiln remains. However, the usefulness of this approach is limited to features pre-dating c. 1650 CE (Deforce et al. 2021a). Wiggles and a plateau in the ^{14}C-calibration curve for the past c. 350 years caused by variations in solar activity and emissions from the burning of fossil fuel, make precise dating using ^{14}C for this period impossible (Stuiver, 1961; Tans et al., 1979). In exceptional cases where sufficiently large charcoal fragments could be recovered, from specific species and containing a

large number of tree rings, dendrochronology has been used to date the kilns (e.g. Raab et al., 2015; Fouédjeu et al., 2021).

It is well known that heating to sufficiently high temperatures resets luminescence signals. This has been exploited in a number of studies for dating heated materials in archaeological contexts such as ceramics, bricks and hearth stones (e.g. Aitken, 1985; Bailiff, 2007; Rhodes et al., 2010; Armitage and King, 2013), or to unravel the thermal history of quartz grains (e.g. Moska et al., 2010). Karimi-Moayed et al. (2020) recently adopted the same underlying principle and demonstrated that optically stimulated luminescence (OSL) dating of sediments that were heated during past charcoal production can be a viable complementary or alternative method to ^{14}C-dating for the age determination of charcoal kilns. Their study focuses on kilns that were well-preserved in and on silty sediments (loess) in an area that was continuously forested since the early Holocene. In this study, we investigate the applicability of the approach for dating well-preserved charcoal kilns in sandy sub-surfaces.

4.2 Material and Methods

4.2.1 Study area and sample collection

Zoersel forest is one of the few ancient woodlands in northern Belgium (Figure 4.1a), and only one of two areas in this region where well-preserved remains of past charcoal production have been found. The forest currently covers an area of about 515 ha, and is located in a depositional area that has been designated as the “Belgian sand belt” (Beerten et al., 2017; Figure 4.1a).

Deforce et al. (2013) performed a detailed study of charcoal burning activities in Zoersel forest, which included a full inventory of the kilns (through a LiDAR-based method and field surveying) as well as charcoal analysis and radiocarbon dating of ten kilns. In the frame of this study, eleven kilns were selected from this inventory, of which six were previously investigated by Deforce et al. (2013; kilns M01, M02, M06, M11, M23 and M32).

In each kiln, a small pit of about 50 × 50 cm wide and 50-80 cm deep was manually dug. In general, the stratigraphic sequences consist of a 5-10 cm thick vegetation and litter layer overlying a dark (black/grey) layer of ~ 20-45 cm thick, which is rich in charcoal and rooted through. The underlying deposits are sands that are generally

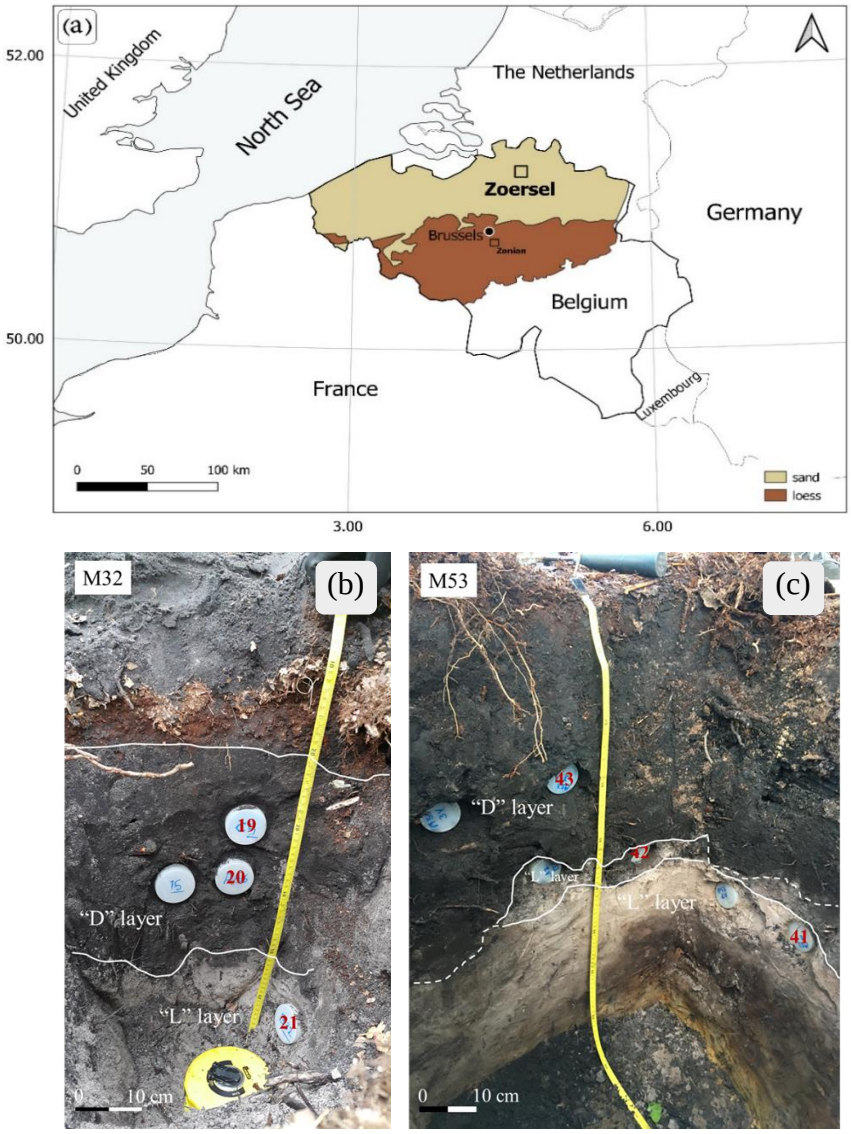

Figure 4.1: (a) Location of the study site, with the Belgian sand and loess belt are indicated as in Beerten et al. (2017). (b-c) Photographs of the exposures as sampled in features M32 and M53.

lighter in color (whitish/grey, yellow, brown), rooted through to various extents, occasionally containing some charcoal (Figs 4.1b and c).

The samples for OSL dating were collected by hammering stainless-steel tubes (5 cm diameter; 15 cm long) into the exposures. While the tubes were dug out, the surrounding sediment was collected for radionuclide analyses. In addition, undisturbed samples were taken to evaluate moisture content; these samples were collected using Kopecky rings, adjacent to the OSL samples. Thirty-two samples in total were collected. The stratigraphic position of the samples is indicated in Table 4.1, with "D" referring to the dark charcoal-rich layers and "L" referring to the samples from the underlying layers of a lighter color. A bulk sediment sample (c. 10 l) was taken from the uppermost

charcoal-rich layer in kilns M33, M49, M50, M51 and M53; these samples were collected for anthracological analysis and radiocarbon dating in addition to that by Deforce et al. (2013).

4.2.2 OSL dating

The samples were prepared following standard procedures (HCl, H_2O_2, wet and dry sieving, HF, HCl-wash, resieving) to obtain quartz grains from the 125-180 µm fraction. Luminescence measurements using large (8 mm diameter) and small (2 mm diameter) aliquots were carried out using an automated Risø TL/OSL reader equipped with blue (λ_{max} = 470 nm) and infrared (λ_{max} = 850 nm) light emitting diodes, and all signals were detected through 7.5 mm Hoya U-340 UV filter (Bøtter-Jensen et al., 2010; Lapp et al., 2015). Stimulation with the blue diodes was for 38.5 s at 125 °C and the initial 0.31 s of the decay curve minus a background evaluated from the following 0.77 s was used for the calculations. Single grains of quartz were measured using an automated Risø TL/OSL reader equipped with a single grain laser attachment (Bøtter-Jensen et al., 2003). Stimulation was for 0.8 s at 125 °C with a green (532 nm), 10 mW stabilised diode pumped solid state (DPSS) laser, and the initial 0.12 s of the decay curve minus a background evaluated from the last 0.3 s was used in the calculations. The single-aliquot regenerative-dose (SAR) protocol (Murray and Wintle, 2000, 2003) was used for determining the equivalent dose (D_e). A preheat for 10 s at 180 °C and a cut heat to 160 °C were adopted for both multiple and single-grain measurements. After the measurement of the response to the test dose (~2 Gy in all experiments), a high-temperature cleanout was performed by stimulating with the blue diodes for 38.5 s (multiple grains) or 36.8 s (single-grains) at 280 °C to minimize recuperation (Murray and Wintle, 2003). All sequences included a measurement of recuperation, recycling ratio and OSL IR depletion ratio (Duller, 2003). Dose estimates (for both multiple and single-grain measurements) were accepted if the uncertainty on the natural test dose response was less than 15%, the recycling ratio was consistent with unity within 2 sigma uncertainty, and the OSL IR depletion ratio larger than 0.9. For the small-aliquot and single-grain measurements, we added an uncertainty of 1.5% and 9%, respectively, on top of the error based on counting statistics alone (see e.g. Thomsen et al., 2005, 2007). The sediment collected for dose rate determination was dried at 110 °C (until constant weight), pulverized and homogenized. A subsample (~ 140 g) of the powdered

No	Feature	Horizon	GLL-code	Depth (cm)	^{234}Th (Bq kg^{-1})	^{226}Ra (Bq kg^{-1})	^{210}Pb (Bq kg^{-1})	^{232}Th (Bq kg^{-1})	^{40}K (Bq kg^{-1})	W	F*W (F=0.5)	W_n	Total dose rate (Gy ka^{-1})	D_e (Gy)	Age (ka) (± 1σ)	σ_r (%)	σ_{sys} (%)	σ_{tot} (%)	Age CE (± 2σ)
1	M01	D	194301	23	5.0 ± 1.0	6.5 ± 0.5	6.0 ± 1.0	5.2 ± 0.2	68 ± 2	0.42	0.21 ± 0.03	0.22	0.60 ± 0.01	0.49 ± 0.03 (46)	0.82 ± 0.09	6.84	8.47	10.89	1197 ± 179
														0.40 ± 0.01 (100)	**0.66 ± 0.06**	**4.27**	**8.47**	**9.49**	**1355 ± 126**
2	M01	D	194302	29									0.59 ± 0.01	0.44 ± 0.02 (43)	0.74 ± 0.07	4.83	8.42	9.71	1276 ± 144
														0.36 ± 0.01 (108)	**0.62 ± 0.06**	**4.54**	**8.42**	**9.57**	**1399 ± 119**
3	M02	D	194304-X14	25	6.0 ± 1.0	7.4 ± 0.3	5.0 ± 1.0	5.8 ± 0.3	94 ± 2	0.56	0.28 ± 0.04	0.17	0.65 ± 0.01	0.51 ± 0.03 (51)	0.77 ± 0.08	5.74	9.19	10.84	1247 ± 167
4	M02	D	194305	30									0.64 ± 0.01	0.56 ± 0.02 (45)	0.87 ± 0.09	4.92	9.19	10.42	1150 ± 181
5	M02	L	194306-X13	50									0.62 ± 0.01	8.74 ± 0.16 (52)	14.14 ± 1.35	2.72	9.17	9.56	-12126 ± 2706
6	M06	D	194308	25	5.4 ± 1.2	7.0 ± 0.3	8.0 ± 1.0	5.4 ± 0.2	91 ± 2	0.72	0.36 ± 0.05	0.3	0.64 ± 0.01	0.35 ± 0.01 (48)	0.56 ± 0.06	4.04	10.35	11.11	1458 ± 125
														0.35 ± 0.02 (52)	**0.54 ± 0.06**	**5.57**	**10.35**	**11.75**	**1475 ± 128**
7	M06	D	194309	33									0.63 ± 0.01	0.94 ± 0.08 (45)	1.50 ± 0.21	9	10.36	13.72	523 ± 411
														0.40 ± 0.02 (34)	**0.63 ± 0.08**	**6.3**	**10.36**	**12.13**	**1390 ± 152**
8	M06	L	194310	43									0.62 ± 0.01	1.58 ± 0.11 (54)	2.62 ± 0.34	7.66	10.38	12.9	-606 ± 677
9	M11	D	194312	26	6.0 ± 1.0	7.0 ± 0.3	7.0 ± 1.0	5.8 ± 0.2	93 ± 2	0.57	0.28 ± 0.04	0.21	0.66 ± 0.01	0.37 ± 0.01 (46)	0.54 ± 0.05	2.14	9.27	9.51	1482 ± 102
10	M11	D	194313-X13	35									0.65 ± 0.01	0.74 ± 0.05 (42)	1.14 ± 0.13	6.62	9.26	11.39	883 ± 259
11	M11	L	194314	48									0.64 ± 0.01	2.01 ± 0.14 (48)	3.14 ± 0.37	7.34	9.26	11.82	-1126 ± 743
12	M23	D	194316	24	8.0 ± 1.0	8.5 ± 0.3	8.4 ± 1.2	6.5 ± 0.2	68 ± 2	0.62	0.31 ± 0.05	0.28	0.63 ± 0.01	2.01 ± 0.21 (48)	3.20 ± 0.46	10.85	9.59	14.48	-1177± 926
														0.25 ± 0.03 (17)	**0.40 ± 0.07**	**14.09**	**9.59**	**17.05**	**1622 ± 135**
13	M23	D	194317	36									0.62 ± 0.01	0.57 ± 0.04 (43)	0.92 ± 0.12	8.07	9.59	12.53	1098 ± 231
														0.30 ± 0.02 (23)	**0.49 ± 0.06**	**6.04**	**9.59**	**11.33**	**1530 ± 111**
14	M32	D	194319	22	8.0 ± 1.0	8.2 ± 0.4	9.0 ± 1.0	6.8 ± 0.1	67 ± 2	0.52	0.26 ± 0.04	0.22	0.66 ± 0.01	0.87 ± 0.04 (48)	1.32 ± 0.14	5.16	8.9	10.29	701 ± 271
15	M32	D	194320	31									0.65 ± 0.01	0.37 ± 0.01 (43)	0.55 ± 0.05	3.15	8.88	9.42	1470 ± 103
16	M32	L	194321	50									0.63 ± 0.01	6.64 ± 0.13 (48)	10.59 ± 0.98	2.78	8.85	9.27	-8568 ± 1964
17	M33	D	194323	30	8.0 ± 1.0	8.7 ± 0.2	6.72 ± 0.94	7.3 ± 0.1	72 ± 1	0.47	0.23 ± 0.03	0.18	0.64 ± 0.01	0.51 ± 0.02 (44)	0.79 ± 0.07	3.92	8.52	9.38	1228 ± 148
														0.48 ± 0.03 (42)	**0.74 ± 0.08**	**5.6**	**8.52**	**10.2**	**1277 ± 151**
18	M33	D	194324	36									0.64 ± 0.01	1.10 ± 0.06 (45)	1.73 ± 0.18	5.78	8.5	10.28	288 ± 356
														0.49 ± 0.04 (37)	**0.77 ± 0.09**	**7.72**	**8.5**	**11.48**	**1245 ± 178**
19	M33	L	194325-X13	55									0.62 ± 0.01	5.07 ± 0.12 (45)	8.18 ± 0.73	3.03	8.46	8.98	-6156 ± 1469
20	M49	D	194327	33	8.2 ± 1.4	8.8 ± 0.5	7.90 ± 1.08	6.9 ± 0.2	78 ± 2	0.37	0.19 ± 0.03	0.16	0.68 ± 0.02	0.55 ± 0.03 (45)	0.81 ± 0.08	6.29	7.83	10.04	1209 ± 163
21	M49	D	194328	49									0.66 ± 0.02	0.83 ± 0.06 (47)	1.25 ± 0.14	7.62	7.77	10.88	767 ± 272
22	M49	L	194329	71									0.65 ± 0.02	10.66 ± 0.23 (48)	16.52 ± 1.39	3.27	7.72	8.39	-14499 ± 2770
23	M50	D	194334	27	8.0 ± 1.0	9.3 ± 0.3	10.0 ± 0.7	7.1 ± 0.1	80 ± 1	0.76	0.38 ± 0.06	0.45	0.65 ± 0.01	0.66 ± 0.05 (47)	1.02 ± 0.13	7.35	10.68	12.97	1000 ± 264
24	M50	D	194333	45	11 ± 1.0	9.6 ± 0.4	9.1 ± 0.8	7.2 ± 0.1	82 ± 1	0.53	0.27 ± 0.04	0.29	0.70 ± 0.01	1.00 ± 0.05 (47)	1.43 ± 0.15	4.93	8.97	10.23	593 ± 291
25	M50	L	194332	53	8.0 ± 1.0	10.5 ± 0.6	6.5 ± 1.2	7.2 ± 0.2	89 ± 2	0.24	0.12 ± 0.02	0.13	0.72 ± 0.02	3.18 ± 0.06 (48)	4.41 ± 0.34	3.18	7.01	7.7	-2391 ± 680
26	M50	L	194331-X15	71	6.0 ± 1.0	7.7 ± 0.2	7.7 ± 0.7	5.7 ± 0.2	113 ± 1	0.23	0.12 ± 0.02	0.14	0.78 ± 0.01	11.78 ± 0.25 (47)	15.10 ± 1.12	2.57	6.93	7.39	-13080 ± 2231
27	M51	D	194337	38	9.0 ± 1.0	8.4 ± 0.4	7.5 ± 1.2	6.7 ± 0.2	76 ± 1	0.57	0.28 ± 0.04	0.35	0.62 ± 0.02	0.66 ± 0.04 (45)	1.06 ± 0.12	6.77	9.23	11.45	963 ± 242
28	M51	L	194336	47	8.0 ± 1.0	9.3 ± 0.7	7.4 ± 0.7	7.2 ± 0.1	63 ± 1	0.25	0.12 ± 0.02	0.11	0.66 ± 0.01	1.29 ± 0.04 (47)	1.94 ± 0.16	3.7	7.17	8.07	79 ± 313
29	M51	L	194335-X15	67	5.0 ± 1.0	5.5 ± 0.2	6.2 ± 1.1	4.3 ± 0.2	91 ± 2	0.25	0.12 ± 0.02	0.11	0.66 ± 0.02	11.13 ± 0.22 (47)	16.58 ± 1.31	3.06	7.28	7.89	-14566 ± 2618
30	M53	D	194343	29	6.2 ± 0.6	7.6 ± 0.7	6.8 ± 0.5	5.6 ± 0.1	71 ± 1	0.57	0.28 ± 0.04	0.33	0.59 ± 0.01	0.64 ± 0.05 (47)	1.09 ± 0.13	7.13	9.22	11.66	934 ± 253
31	M53	L	194342	46	8.9 ± 0.5	8.1 ± 0.2	8.0 ± 1.0	6.7 ± 0.1	55 ± 1	0.36	0.18 ± 0.03	0.14	0.64 ± 0.01	2.79 ± 0.09 (45)	4.38 ± 0.38	3.49	7.95	8.68	-2359 ± 760
32	M53	L	194341	50	7.0 ± 1.0	6.6 ± 0.3	6.0 ± 1.0	5.7 ± 0.3	77 ± 1	0.19	0.09 ± 0.01	0.07	0.64 ± 0.02	2.55 ± 0.05 (46)	3.99 ± 0.30	3.15	6.84	7.53	-1967 ± 600

Table 4.1: Specific radionuclide activities used for dose rate evaluation, estimates of past moisture content (F*W; F denotes the fraction of saturation corresponding to the assumed average water content during burial period and W represents the saturation content; Aitken, 1985), calculated dose rates, equivalent doses, optical ages and random (σ_r), systematic (σ_s) and total uncertainties (σ_{tot}). The total dose rate includes the contribution from internal radioactivity and cosmic radiation. The number of accepted aliquots/grains for De-determination is given in italics between parentheses in subscript. The uncertainties mentioned with the dosimetry and D_e data are random; except for the CE ages. All uncertainties represent 1 sigma, except for the CE ages. The results from single-grain measurements are shown in bold. See Appendix C2 for "X"-denotations.

sediment was then cast in wax and stored for at least one month before being measured using a low-level extended energy-range HPGe gamma-ray spectrometer (e.g. De Corte et al., 2006). Annual doses were calculated from the present-day radionuclide activities using the conversion factors of Adamiec and Aitken (1998). Based on Mejdahl (1979) and Aitken (1985), a factor of 0.9 (± 5% relative uncertainty) was adopted to correct the external beta dose rate for the effects of attenuation and etching. Correction for the effect of moisture was performed as outlined in Aitken (1985). The water content in fully saturated undisturbed sediment samples was determined in the laboratory, and we assumed that the time-averaged water content was half of that (± 15 % relative uncertainty); on average, this corresponds to the moisture content at the time of sampling. An internal dose rate in quartz grains of 0.013 ± 0.003 Gy ka^{-1} was adopted (Vandenberghe et al., 2008). The contribution of cosmic rays was calculated following Prescott and Hutton (1994) and a 15 % relative uncertainty was associated with the values.

4.2.3 Radiocarbon dating

The bulk sediment samples were wet-sieved in the lab using a 0.5 mm mesh. Residues were dried, from which charcoal fragments with the lowest potential age at the time of charring were then selected, i.e. twigs or taxa with a low maximal expected age to avoid a potential old wood-effect.

For radiocarbon dating, the charcoal samples were combusted to CO_2 and transformed into graphite, after which the radiocarbon concentrations were measured in a MICADAS AMS-machine at the Royal Institute for Cultural Heritage, Brussels (Belgium) (Boudin et al., 2015). Results were calibrated with OxCal 4.4 (Bronk-Ramsey, 2009) using the IntCal20 calibration curve (Reimer et al., 2020).

4.3 Experiments and results

4.3.1 OSL dating

4.3.1.1 General luminescence characteristics (8 mm aliquots)

A representative decay curve obtained for one of the samples collected from the charcoal-rich layers ("D"-layer; GLL-194312) is shown in Figure 4.2a. The signals are bright and decay rapidly with stimulation time, indicating that they are dominated by the fast component (e.g. Jain et al., 2003). Figure 4.2b shows a representative dose-response curve, which can be well represented by a single saturating exponential function (solid black line). Figure 4.2b also illustrates the good behavior of the samples in the SAR protocol, with the dose response curve passing through the origin (indicating that recuperation is negligible; open square) and the ability to re-measure the response to a regenerative dose (indicating that sensitivity changes occurring throughout the measurement cycles are accurately corrected for; the solid and open circle overlying each other).

We assessed the overall suitability of the SAR measurement procedure using a dose recovery test (e.g. Murray and Wintle, 2003). For each sample, two or three natural aliquots were bleached two times for 250 s using the blue diodes at room temperature,

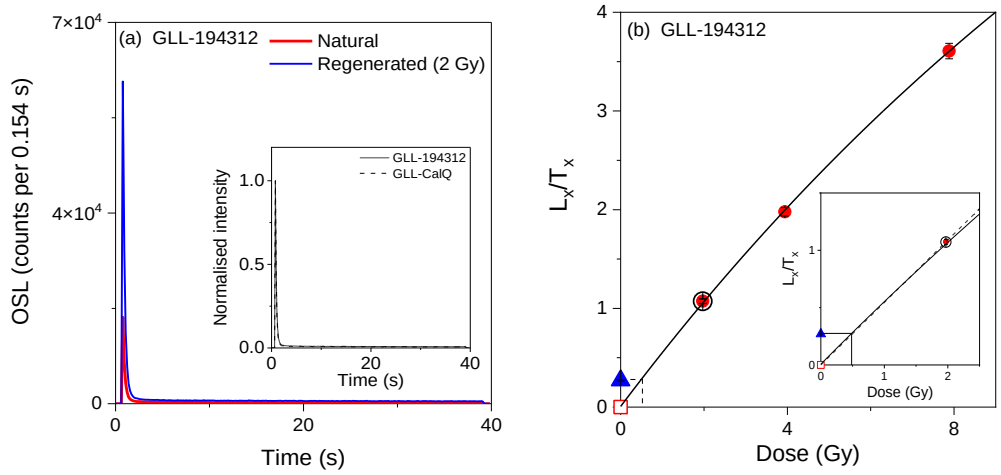

Figure 4.2: (a) OSL decay curves for an aliquot of sample GLL-194312. The natural and regenerated signals are shown as red and blue lines, respectively. The inset compares the regenerated OSL decay curve from the sample with that from calibration quartz (GLL-CalQ; signals normalized to the intensity observed in the first 0.154 s of stimulation). (b) SAR growth curve for an aliquot of the same sample. Recycling and recuperation points are represented by the open circle and square, respectively. The black solid line represents a single saturating exponential function fitted to the regenerated data. The inset illustrates a negligible difference between a single saturating exponential (solid black line) and a linear (dash-dotted line) fit to regenerated dose-responses below 2 Gy.

with a 10,000 s pause at room temperature in between. They were then given a laboratory dose close to the estimated D_e and measured with the SAR protocol as outlined above. The results are summarized in Figure 4.3. Individual ratios of measured to given dose do not deviate by more than 5% from unity, and the overall average ratio (± 1 standard error) is 0.975 ± 0.004 (n = 83). While this value is inconsistent with unity, the discrepancy is small and unlikely to be of significance in the context of the dates (and associated uncertainties) to be produced in this study. Similar observations were made for samples from the underlying "L"-layers (see Figure 4.4; overall ratio of measured to given dose ± 1 standard error = 0.999 ± 0.004; n = 30). These samples are not (necessarily) directly relevant to the timing of the event of interest (charcoal production) but were included in the analyses to aid in assessing the reliability of the results for the overlying "D"-layers (cf. Karimi-Moayed et al., 2020).

4.3.1.2 Distributions of D_e in small (2 mm diameter) aliquots

The inset to Figure 4.2b illustrates that, for samples collected from the "D"-layers, the natural OSL signal intersects with the linear region of the dose-response curve. Therefore, and following Karimi-Moayed et al (2020), we shortened our SAR sequence for D_e determination to include measurements of the sensitivity-corrected natural signal and one regenerative dose point in this linear region (chosen here as 2.0 Gy). The shortened sequence was followed by measurements of recuperation, recycling and OSL IR depletion ratio. For samples from the "L" layers, the response to additional regenerative doses was measured. For each sample, in between 48 and 54 replicate measurements of equivalent dose were made. Figures 4.5a-h show the D_e distribution in small aliquots for eight samples collected from "D" layers as histograms. A graph of D_e versus uncertainty is shown above each histogram, which is a simple tool for visualizing the precision by which each individual value was measured. The full dataset for "D" samples is shown in Figure 4.6. In general, the distributions exhibit some degree of asymmetry towards higher dose values, with relative standard deviations (RSD's) ranging from ~ 33% to ~ 139%. Following Karimi-Moayed et al. (2020), we applied a simple criterion in which values that differed by more than 3 SD's from the average were iteratively rejected, after which the mean (± 1 standard error) was used in further calculations (Table 4.1). For some samples, the 3 SD criterion appears to isolate equivalent doses that reflect a single event (e.g. GLL-194301; Figure 4.5a), while for

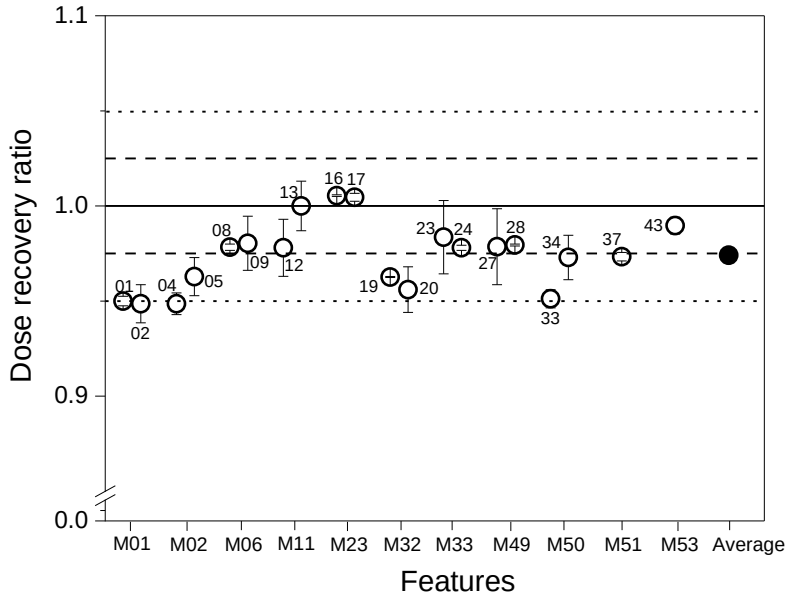

Figure 4.3: Summary of dose recovery data for the samples collected from the "D"-layers. The dashed and dotted lines are eye-guides, bracketing a 2.5% and 5% deviation of the ratio from unity (solid line).

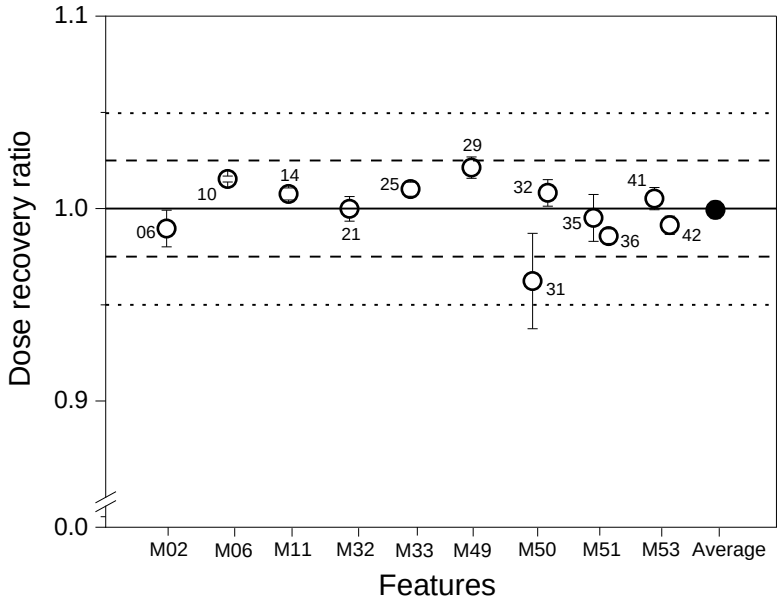

Figure 4.4: Same as in Figure.4.3., for all "L" samples.

others (e.g. GLL-194309; Figure 4.5d) it includes values that are spread over a large dose range. The resulting D_e distributions, for all samples collected from "D" layers, are characterized by a relative standard deviation between 14-73% (Figures. 4.5a-h and 4.6).

The D_e-distributions for the samples collected from the underlying "L"-layers are shown in Figure 4.6. Processing the data for the "L" samples as outlined in the above,

yields distributions with RSD's ranging from 13 to 50%; the mean equivalent doses (± 1 standard error) are summarized in Table 4.1. For some samples, the resulting distributions do not appear incompatible with single dose populations; for others, the distributions are more asymmetric.

4.3.1.3 Distributions of D_e in single grains

Single grain measurements were made for eight samples collected from the "D"-layers (kiln M01 (GLL-194301 and -02), kiln M06 (GLL-194308 and -09), kiln M23 (GLL-194316 and -17) and kiln M33 (GLL-194323 and -24)). For each sample, about 500-1200 grains were measured and analyzed as outlined in §4.2.2. Figure 4.5a´-h´ show the single-grain data for all eight samples.

For all eight investigated samples, the majority of the results appears to belong to single dose populations, with some grains yielding significantly higher D_e-values. We applied the same 3 SD-criterion as used for the small aliquots, resulting in distributions with RSD in the range of 34-57%, of which the averages (± 1 standard error) were used for age calculation (Table 4.1).

4.3.1.4 Comparison between small-aliquot and single-grain characteristics

Figure 4.7 shows the cumulative light sum of signal intensity from the single grains in the investigated samples, as well as that for calibration quartz as measured in this study. The data are plotted as the proportion of the total light sum that originates from the specified percentage of the brightest grains (cf. Duller et al., 2000). In line with earlier findings (e.g. Duller et al., 2000), none of the samples exhibits a homogenous or even distribution of light (represented by the dashed diagonal line in Figure 4.7) and, in comparison to calibration quartz, significantly less grains in the samples contribute to the total light sum. For samples GLL-194301, -02, -08, -23 and -24 over 80% of the signal originates from 7-10% of the grains; for samples -09 and -16 the corresponding percentage is 2-3% of the grains, while for sample -17 the light output is dominated by only ~ 1% of the grains.

Our small aliquots are thought to consist of 100-200 grains of 125-180 µm. Based on Figure 4.7, one implication is that the small-aliquot measurements for sample -17, and potentially also samples -09 and -16 are likely to approximate those of single grains. For the other samples, any variability will be averaged out to a larger extent. This seems to be reflected in the spread observed for the small-aliquot distributions (Figure 4.5),

with RSDs of around 51-73% and 23-44% for the less and more homogenously bright samples, respectively. Comparison of signal brightness (Figure 4.7) and the whole of D_e distributions (Figure 4.6), however, may also reveal a relationship with the degree of heating experienced by the samples. The preparation of the calibration quartz involved annealing to high temperatures for an extended period of time (e.g. to 700 °C for one hour; Hansen et al., 2015). Single grains of calibration quartz (CalQ) yield the most even distribution of signal brightness (e.g. Duller et al., 2000; Hansen et al., 2015), suggesting that heating also homogenizes signal brightness. Transposing this to the findings for our samples, and adding the assumption that the sandy sediments were originally deposited in the study region with a similar sensitivity, potentially allows ranking them to the post-depositional heating regime they experienced. The implication would be that samples -01, -02, -08, -23 and -24 experienced a more stringent heating regime. Admittedly, this hypothesis remains to be explored (see e.g. Moska et al., 2010).

4.3.1.5 OSL ages

Table 4.1 summarizes all analytical data and the calculated OSL ages. The single grain results are given in bold in Table 4.1. The uncertainties on the OSL ages were calculated following the procedure as outlined in Aitken (1985), with contributions from sources of systematic uncertainty as given by Vandenberghe (2004) and Vandenberghe et al. (2004). For all samples collected from "D" layers, which are of main interest, the total uncertainties associated with the small-aliquot ages and single-grain ages range from ~ 9% to ~ 15% and ~ 9% to ~ 17%, respectively.

Systematic uncertainty ranges from ~ 8% to ~ 11% for both single-aliquot and single-grain measurements. In general, these systematic sources are the main contributor in total uncertainty and mainly reflect uncertainty associated with our estimates of cosmic radiation and water content.

The small-aliquot OSL ages for samples collected from "D" layers range between 0.56 ± 0.06 ka and 3.20 ± 0.46 ka. For most features, and where multiple samples were collected, these results are consistent with the stratigraphic position of the samples; the samples collected from kilns M23 and M32 show a significant age reversal (e.g. when considering 3 sigma random uncertainties). The ages obtained using single grains (bold values in Table 4.1) range between 0.40 ± 0.07 and 0.77 ± 0.09 ka and are all internally consistent. For the nine features where also the underlying, lighter ("L") layers were

sampled, the small-aliquot ages are older compared to those for the overlying "D"-layers. To facilitate comparison with ^{14}C-dating (see further), the OSL ages were recalculated to ages CE and expressed within 95.4% probability (2 sigma; Table 4.1).

4.3.2 Radiocarbon dating

The results from ^{14}C-dating are summarized in Table 4.2. The oldest feature is M32, with an age in between ~ 1320 and 1420 CE. For most kilns (M02, M23, M33, M50, M51 and M53), the ^{14}C-ages point at charcoal burning during the 16th century CE. The youngest features are M01, M06 and M11; they exhibit the widest age probability distributions and appear to post-date 1650 CE.

4.4 Discussion

4.4.1 Comparison between OSL and ^{14}C ages

Figure 4.8 compares all available age results (small-aliquot OSL, single-grain OSL, ^{14}C) for the samples collected from "D" layers for the investigated kilns (see also Tables 1 and 2). The ages obtained using small-aliquots are generally older than the ^{14}C-ages, except for samples GLL-194308 (kiln M06) and -20 (kiln M32). Interestingly, kiln M32 is where the two OSL ages (samples -19 and -20) are internally inconsistent (see §4.3). The latter was in fact already hinted at by a comparison of their small-aliquot D_e-distributions (Figure 4.6), suggesting that the one observed for sample -20 is more likely to refer to a single event (regardless of whether it is also yields an accurate age). The same rationale (paraphrased to "tight" symmetric D_e-distributions) may thus explain the overestimating small-aliquot results obtained, e.g., for features M06 (sample -09), M23 (samples -16 and -17), and M33 (sample -24), however, it cannot account for the apparent and significant age overestimate that is observed for kilns M01 (samples -01 and -02) and M33 (sample -23) (see Figure 4.5 and 4.6).

The single-grain ages are significantly younger compared to those obtained using small aliquots. This is most clearly illustrated for samples GLL-194309 (kiln M06), and -16 and -17 (kiln M23), and -24 (kiln M33). For features M06 and M23, the single-grain OSL ages are also consistent with the ^{14}C ages. For features M01 and M33, however, they apparently overestimate the ^{14}C-age as well, while being only slightly (and perhaps not significantly) different from the OSL results obtained using small-aliquots for three out of four samples (i.e. samples -01, -02, and -23).

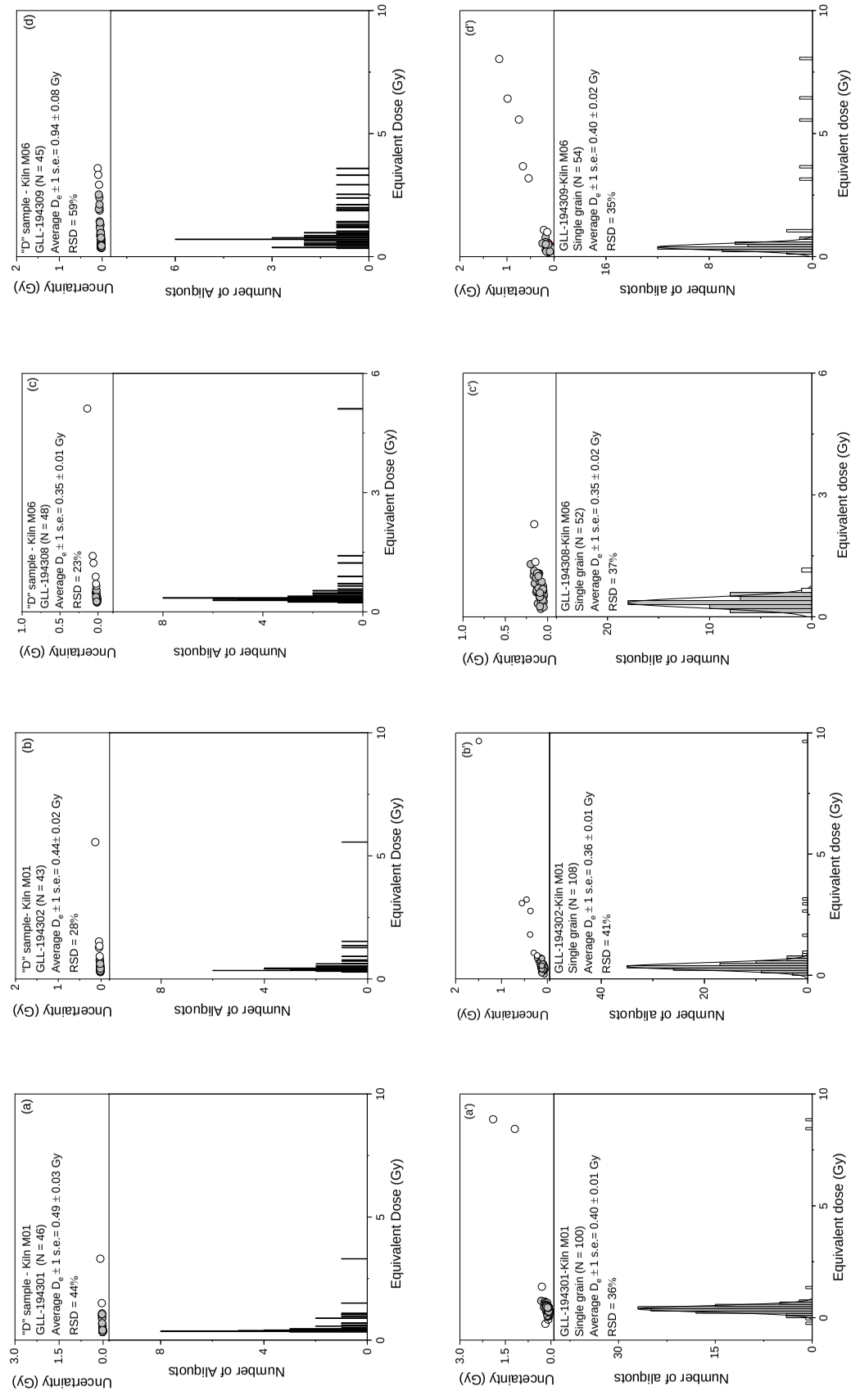
(a)
"D" sample - Kiln M01
GLL-194301 (N = 46)
Average $D_e \pm 1$ s.e.= 0.49 ± 0.03 Gy
RSD = 44%
(a')
GLL-194301-Kiln M01
Single grain (N = 100)
Average $D_e \pm 1$ s.e.= 0.40 ± 0.01 Gy
RSD = 36%
(b)
"D" sample- Kiln M01
GLL-194302 (N = 43)
Average $D_e \pm 1$ s.e.= 0.44± 0.02 Gy
RSD = 28%
(b')
GLL-194302-Kiln M01
Single grain (N = 108)
Average $D_e \pm 1$ s.e.= 0.36 ± 0.01 Gy
RSD = 41%
(c)
"D" sample - Kiln M06
GLL-194308 (N = 48)
Average $D_e \pm 1$ s.e.= 0.35 ± 0.01 Gy
RSD = 23%
(c')
GLL-194308-Kiln M06
Single grain (N = 52)
Average $D_e \pm 1$ s.e.= 0.35 ± 0.02 Gy
RSD = 37%
(d)
"D" sample - Kiln M06
GLL-194309 (N = 45)
Average $D_e \pm 1$ s.e.= 0.94 ± 0.08 Gy
RSD = 59%
(d')
GLL-194309-Kiln M06
Single grain (N = 54)
Average $D_e \pm 1$ s.e.= 0.40 ± 0.02 Gy
RSD = 35%
Uncertainty (Gy)
Number of Aliquots
Number of aliquots
Equivalent Dose (Gy)
Equivalent dose (Gy)

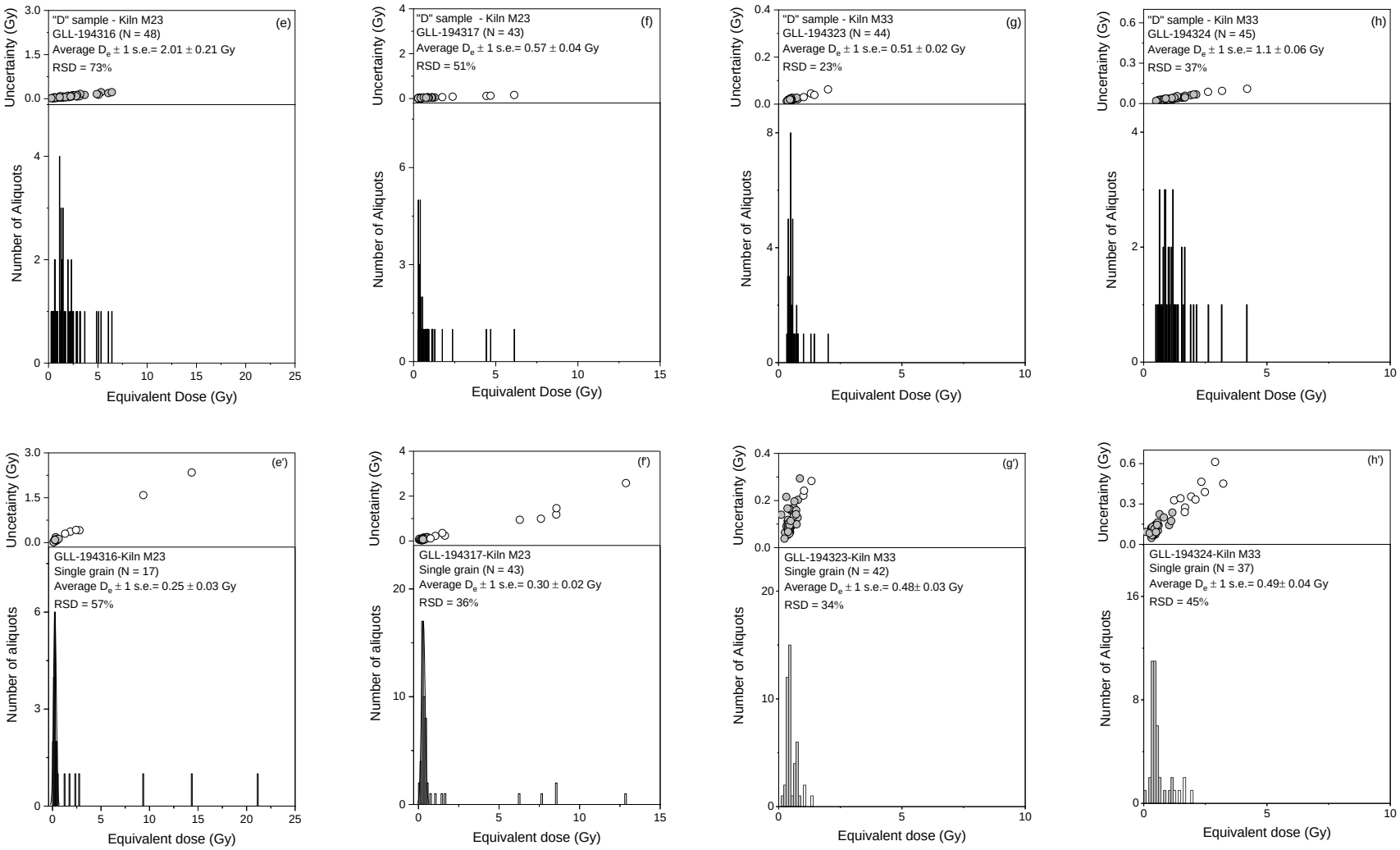

Figure 4.5: Equivalent dose distributions in small aliquots (a-h) and single grains (a´-h´) for samples GLL-194301, -02, -08, -09, -16, -17, -23 and -24. Averages and RSD's were calculated as outlined the in text.

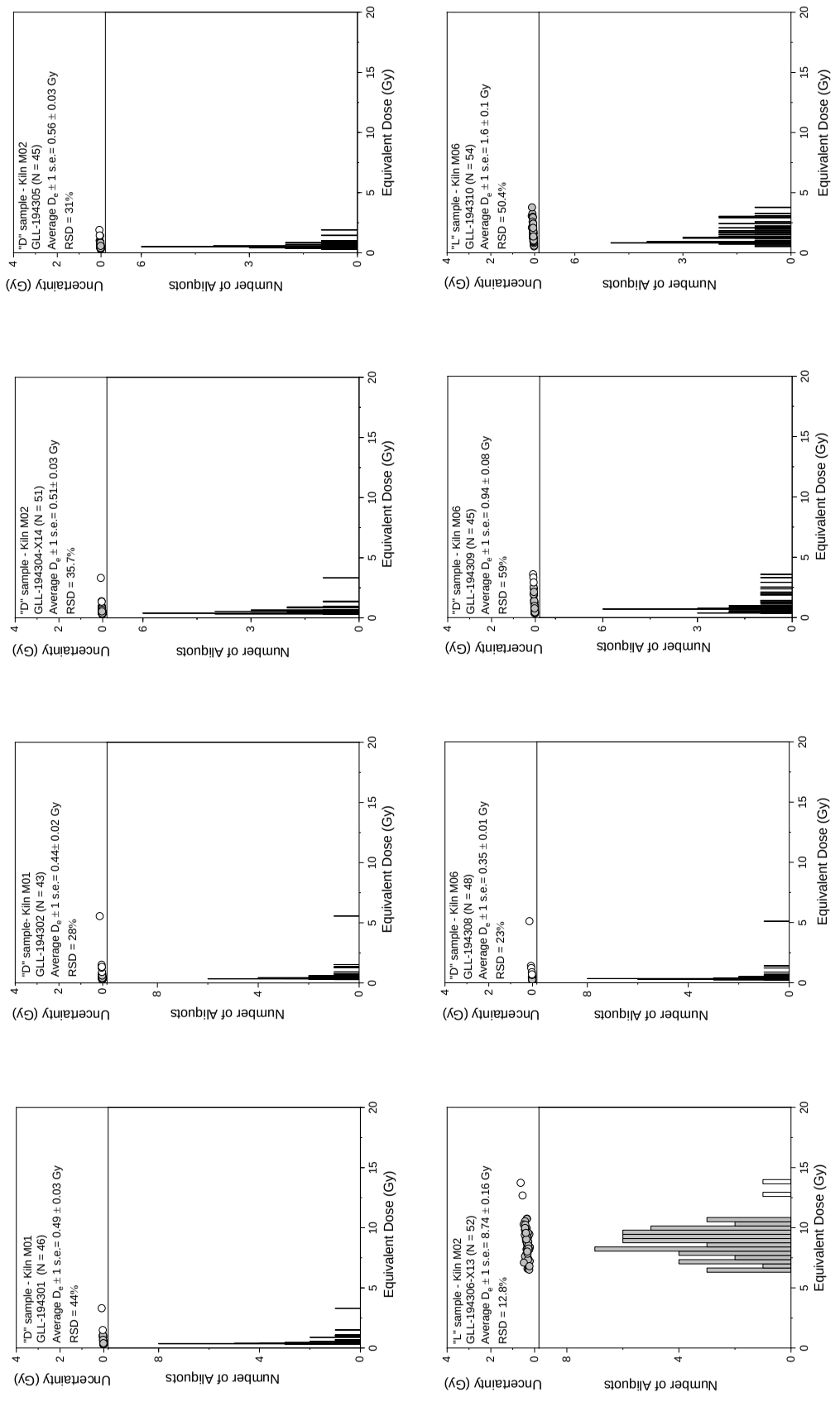
"D" sample - Kiln M01
GLL-194301 (N = 46)
Average $D_e \pm 1$ s.e.= 0.49 ± 0.03 Gy
RSD = 44%
"D" sample- Kiln M01
GLL-194302 (N = 43)
Average $D_e \pm 1$ s.e.= 0.44± 0.02 Gy
RSD = 28%
"D" sample - Kiln M02
GLL-194304-X14 (N = 51)
Average $D_e \pm 1$ s.e.= 0.51± 0.03 Gy
RSD = 35.7%
"D" sample - Kiln M02
GLL-194305 (N = 45)
Average $D_e \pm 1$ s.e.= 0.56 ± 0.03 Gy
RSD = 31%
"L" sample - Kiln M02
GLL-194306-X13 (N = 52)
Average $D_e \pm 1$ s.e.= 8.74 ± 0.16 Gy
RSD = 12.8%
"D" sample - Kiln M06
GLL-194308 (N = 48)
Average $D_e \pm 1$ s.e.= 0.35 ± 0.01 Gy
RSD = 23%
"D" sample - Kiln M06
GLL-194309 (N = 45)
Average $D_e \pm 1$ s.e.= 0.94 ± 0.08 Gy
RSD = 59%
"L" sample - Kiln M06
GLL-194310 (N = 54)
Average $D_e \pm 1$ s.e.= 1.6 ± 0.1 Gy
RSD = 50.4%
Uncertainty (Gy)
Number of Aliquots
Equivalent Dose (Gy)

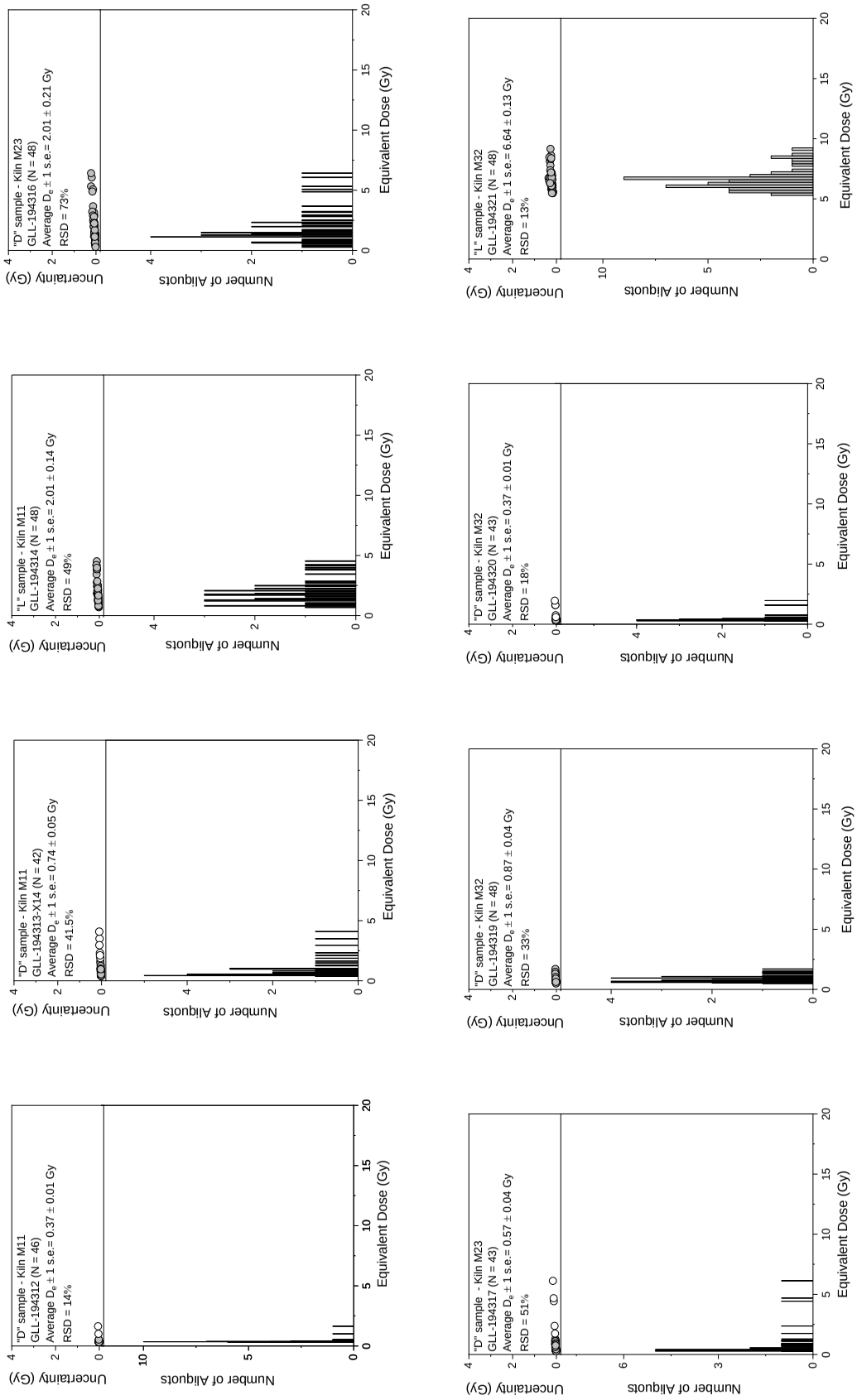
"D" sample - Kiln M11
GLL-194312 (N = 46)
Average D_e ± 1 s.e.= 0.37 ± 0.01 Gy
RSD = 14%
"D" sample - Kiln M11
GLL-194313-X14 (N = 42)
Average D_e ± 1 s.e.= 0.74 ± 0.05 Gy
RSD = 41.5%
"L" sample - Kiln M11
GLL-194314 (N = 48)
Average D_e ± 1 s.e.= 2.01 ± 0.14 Gy
RSD = 49%
"D" sample - Kiln M23
GLL-194316 (N = 48)
Average D_e ± 1 s.e.= 2.01 ± 0.21 Gy
RSD = 73%
"D" sample - Kiln M23
GLL-194317 (N = 43)
Average D_e ± 1 s.e.= 0.57 ± 0.04 Gy
RSD = 51%
"D" sample - Kiln M32
GLL-194319 (N = 48)
Average D_e ± 1 s.e.= 0.87 ± 0.04 Gy
RSD = 33%
"D" sample - Kiln M32
GLL-194320 (N = 43)
Average D_e ± 1 s.e.= 0.37 ± 0.01 Gy
RSD = 18%
"L" sample - Kiln M32
GLL-194321 (N = 48)
Average D_e ± 1 s.e.= 6.64 ± 0.13 Gy
RSD = 13%
Uncertainty (Gy)
Number of Aliquots
Equivalent Dose (Gy)

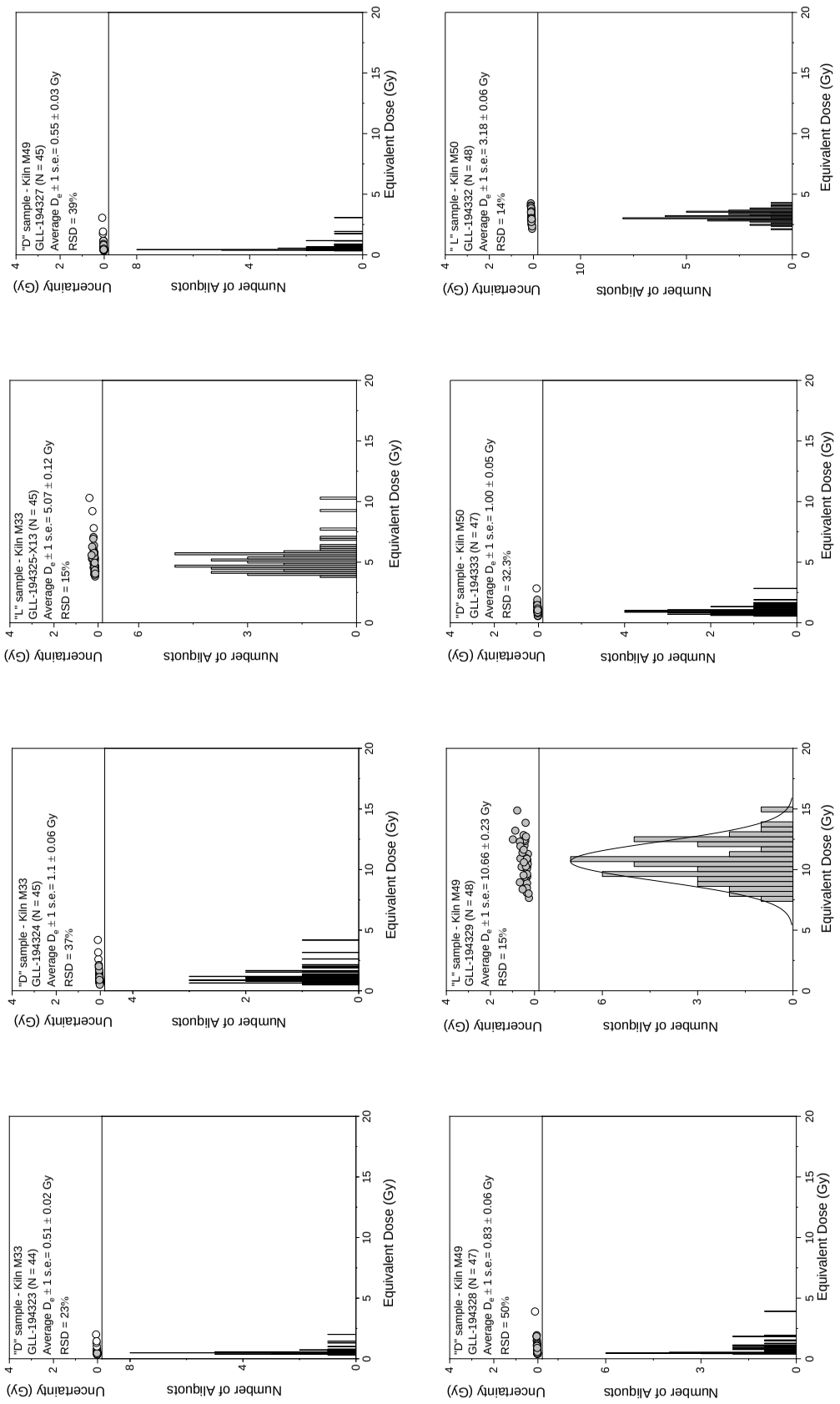
"D" sample - Kiln M33
GLL-194323 (N = 44)
Average $D_e \pm 1$ s.e.= 0.51 ± 0.02 Gy
RSD = 23%
"D" sample - Kiln M33
GLL-194324 (N = 45)
Average $D_e \pm 1$ s.e.= 1.1 ± 0.06 Gy
RSD = 37%
"L" sample - Kiln M33
GLL-194325-X13 (N = 45)
Average $D_e \pm 1$ s.e.= 5.07 ± 0.12 Gy
RSD = 15%
"D" sample - Kiln M49
GLL-194327 (N = 45)
Average $D_e \pm 1$ s.e.= 0.55 ± 0.03 Gy
RSD = 39%
"D" sample - Kiln M49
GLL-194328 (N = 47)
Average $D_e \pm 1$ s.e.= 0.83 ± 0.06 Gy
RSD = 50%
"L" sample - Kiln M49
GLL-194329 (N = 48)
Average $D_e \pm 1$ s.e.= 10.66 ± 0.23 Gy
RSD = 15%
"D" sample - Kiln M50
GLL-194333 (N = 47)
Average $D_e \pm 1$ s.e.= 1.00 ± 0.05 Gy
RSD = 32.3%
"L" sample - Kiln M50
GLL-194332 (N = 48)
Average $D_e \pm 1$ s.e.= 3.18 ± 0.06 Gy
RSD = 14%
Uncertainty (Gy)
Number of Aliquots
Equivalent Dose (Gy)

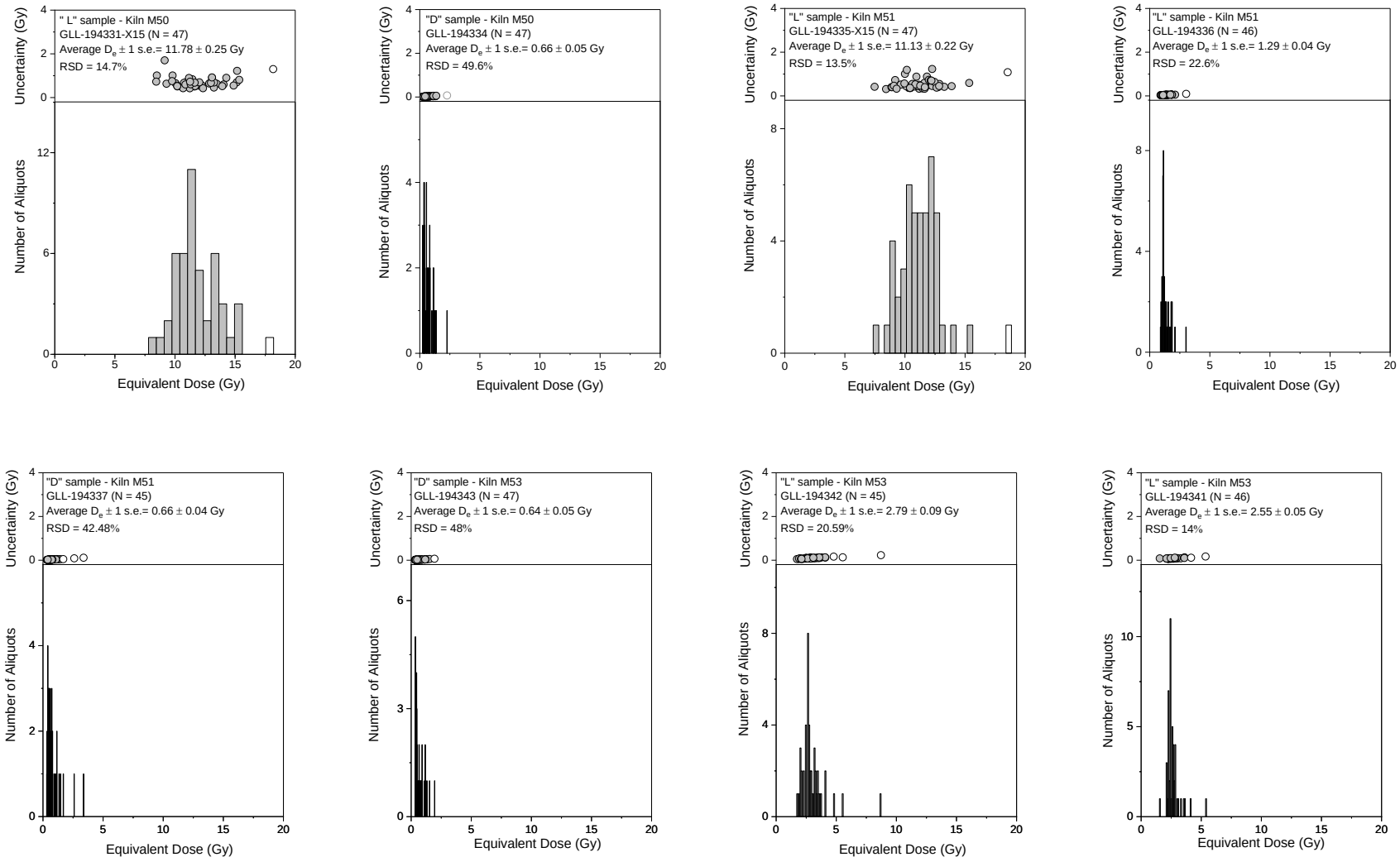

Figure 4.6: Distribution of equivalent doses in small aliquots for samples ("D" and "L"). This includes part of the data presented in Figure 4. for the sake of comparison.

Table 4.2: Summary of ^{14}C dates with 95.4% probability intervals.

Feature	Lab code	Sample type	Sample ID	Uncal BP (± 1σ)	Cal CE (± 2σ)
M01	Beta 264260	charcoal (*twig*)	*Alnus sp.*	210 ± 40	1529 – 1540 (0.6%)
					1634 – 1696 (28.9%)
					1725 – 1814 (46.4%)
					1835 – 1878 (3.1%)
					1916 – 1954 (16.4%)
M02	RICH-29084	charcoal (*twig*)	*Alnus sp.*	328 ± 24	1500 – 1600 (66.0%)
					1610 – 1660 (29.4%)
M06	Beta 264261	charcoal (*twig*)	*Alnus sp.*	250 ± 40	1513 –1601 (24.2%)
					1616 – 1684 (41.5%)
					1735 – 1805 (23.3%)
					1933 – 1955 (6.4%)
M11	Beta 264262	charcoal (*twig*)	*Alnus sp.*	160 ± 40	1663 – 1710 (17.0%)
					1717 – 1891 (61.3%)
					1910 – 1953 (17.1%)
M23	Beta 264263	charcoal (*twig*)	*Alnus sp.*	380 ± 40	1441 – 1530 (55.3%)
					1540 – 1635 (40.1%)
M32	RICH-29079	charcoal (*twig*)	*Quercus sp.*	626 ± 24	1315 –1360 (59.3%)
					1380 – 1415 (36.1%)
M33	Beta 264264	charcoal (*twig*)	*Alnus sp.*	340 ± 40	1462 – 1642 (95.4%)
M49	RICH-29083	charcoal (*twig*)	*Alnus sp.*	576 ± 24	1320 – 1340 (3.2%)
					1390 – 1440 (92.2%)
M50	RICH-29080	charcoal (*twig*)	*Alnus sp.*	344± 23	1500 – 1600 (74.8%)
					1610 – 1650 (20.6%)
M51	RICH-29081	charcoal (*twig*)	*Alnus sp.*	359± 24	1480 – 1650 (95.4%)
M53	RICH-29082	charcoal (*twig*)	*Alnus sp.*	351± 23	1490 – 1650 (95.4%)

At this stage of our investigations, the particular observations made for features M01 and M33 remain to be understood (or, vice versa, those for M06 and M23). It can only be acknowledged that OSL and ^{14}C use different materials and date different events. Also, in case of OSL-dating, heating is a homogenous process, although subject to vertical and lateral gradients, and/or may not necessarily fully reset the OSL signal (Karimi-Moayed et al., 2020; see below).

4.4.2 Resetting and mixing

The prerequisite for OSL dating is that the clock in a sample was adequately reset prior to or at the event of interest (i.e. removal of the relevant trapped charge through either heat, light or a combination of both), and that the sample remained in a closed system

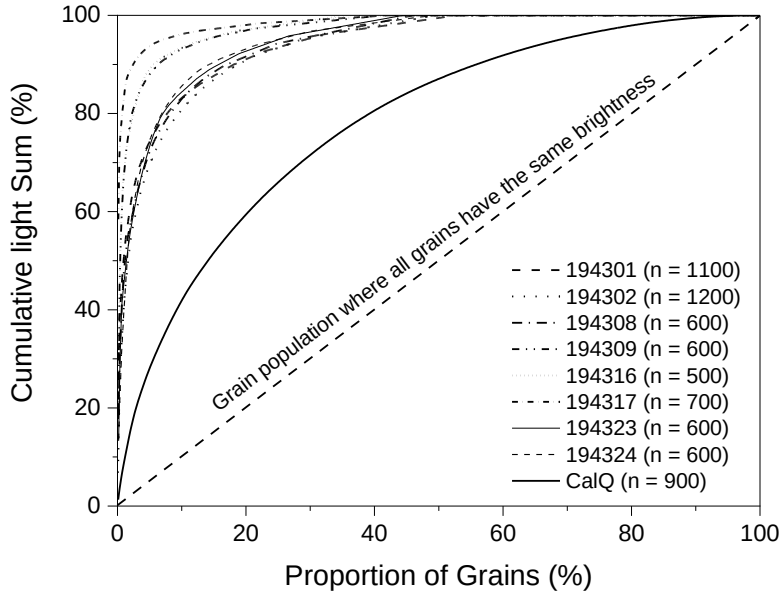

Figure 4.7: Distribution of signal intensity from single grains of eight samples collected from the "D"-layers (M01, M06, M23 and M33) in comparison to that of the calibration quartz used in the single-grain analyses.

afterwards (for the clock to accurately record time since the event of interest).

In this work, heating is presumed to be the main resetting agent. In contrast to light exposure during sediment transport, heating is a homogeneous process, but the heat is transferred as a function of vertical and lateral distance from its source (e.g. Aldeias et al., 2016). Based on Hirsch et al. (2018), temperatures within a charcoal hearth during the charring process range from 350 °C to 600 °C. For the sandy soil underlying the kiln, an approximately 2 cm thick contact zone was affected by temperatures of ~ 400 °C and the combustion of soil organic matter (which occurs at temperatures >220 °C) reached depths of ~5 cm. The quartz OSL signal used for dating is derived from the same temperature region as the thermoluminescence (TL) peak located at 325 °C (e.g., Spooner, 1994). Heating to 400 °C and prolonged heating to lower temperatures (e.g. ~220 °C) thus resets this signal. For sampling, we targeted the central part of the kilns, which is likely to have experienced the highest temperatures. However, it is not always possible to sample those regions that are expected to have locally reached the highest temperatures when working in small profile pits. The implication of such thermal gradients is that sediments can be homogeneously incompletely reset, and progressively so with increasing distance. Our dataset (increase

of OSL ages as a function of depth; Table 4.1) may very well reflect such a process of progressive homogeneous incomplete resetting for most of the kilns.

Bio/pedoturbation is a concern, however, and may have a significant effect on luminescence ages (Bateman et al., 2003, 2007b; Vandenberghe et al., 2009). On top of the remains of the charcoal kilns is a litter layer from which an initial soil develops, and the deposits are often rooted through, especially by trees. Near surficial sandy deposits are particularly prone to bio/pedoturbation (e.g., Bateman et al., 2003, 2007b).

Post-depositional mixing processes can have a significant effect in luminescence dating and, depending on their nature, result in ages that are too old or too young. To this respect, it is worth noting that all our individual D_e estimates, whether in small aliquot or single grains, are finite, non-zero values (Figures 4.5 and 4.6) and that none of the OSL-ages underestimates the ^{14}C-dates (Figure 4.8). On the other hand, in most of the samples (if not all) at least some small aliquots/single grains yield significantly higher D_e-values. This could effectively point at post-depositional mixing, and/or reflect the scale of our sampling (5 cm diameter; §4.2.1) in combination with intrinsic luminescence characteristics.

4.4.3 Dosimetric aspects

In this study, the past water contents were estimated using the samples that were collected specifically for this purpose. We adopted a value of half the water content at saturation, approximately corresponding to the moisture content at the time of sampling, and associated a relative uncertainty of 15% (1 sigma) with this value to allow for possible variations over longer times. The assumption that the discrepancy between the OSL ages and ^{14}C dates would solely be related to moisture content, implies that it must have been significantly lower throughout the burial period. Adapting an unrealistically low value of 0% decreases the OSL ages by ~ 13-22 %, which does not resolve the discrepancy. Given that, over the period to be dated, climatological conditions have been stable in the study region, we consider it unlikely that our estimates of past water content are a major source of inaccuracy.

The samples of main interest come from organic-rich layers. Organic material absorbs part of the radiation energy; the effect is a reduction of the dose rate in addition to that of moisture (e.g. Lian et al., 1995). The content of organic matter in our samples remains to be determined. If significant, however, the effect would be an increase in the OSL ages and, hence, also increase the discrepancy with the ^{14}C results. An

additional potential complication associated with the presence of organic matter concerns its distribution in relation to the mineral component that is used for OSL dating. If both would occur in fine layers, the effective beta dose rate experienced by the quartz grains might differ from the one we calculated using the radionuclide activities in the bulk material. Any such layering was not macroscopically visible during sampling. Also, comparison of radionuclide activities in samples collected from the "D" and "L"-layers (where possible; see Table 4.2), does not suggest that they are significantly higher in the original sandy sub-surface. Nevertheless, the potential effects of organic matter remain to be further investigated. The contribution of cosmic rays was calculated following Prescott and Hutton (1994) and a 15 % relative uncertainty (1 sigma) was associated with the values.

For the samples collected from the "D"-layers, the calculated cosmic dose rate was ~ 0.25 (± 0.04) Gy/ka, amounting to ~ 33–42 % of the total dose rate. This is, at present, our best estimate of this component and its significance is reflected by its contribution to the total systematic uncertainty.

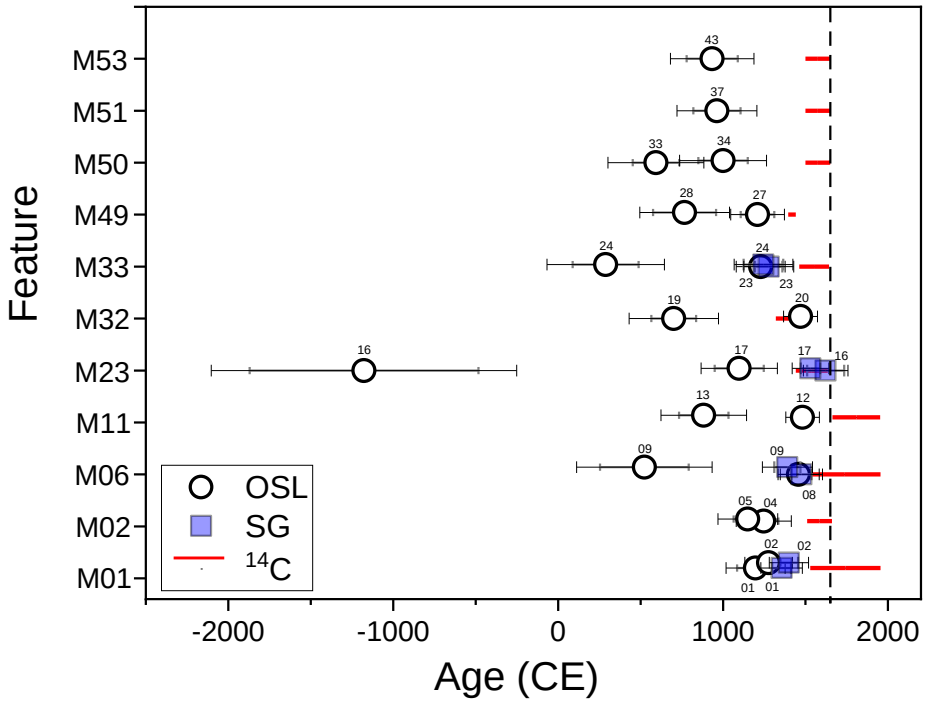

Figure 4.8: Comparison between OSL and calibrated ^{14}C-ages. The OSL data are represented by open circles (small aliquots) and blue squares (single grains); the associated random and total uncertainties are given by the black and grey error bars, respectively. The calibrated ^{14}C ages are represented as age ranges by the thick red lines. All OSL and ^{14}C-ages are expressed as ages Common Era (CE) and cover 95.4% probability. The vertical dashed line indicates 1650 CE.

4.5 Conclusions

We investigated the applicability of quartz-based OSL-dating to heated sediments associated with past charcoal production in a forested area on a sandy sub-surface. A mainstream (commonly adopted) methodology applied to small aliquots, each composed of a limited number of sand-sized grains, yields ages that are significantly older than ^{14}C-ages for charcoal extracted from the kiln remains. OSL ages were also obtained using single grains for four of the investigated features, which are either consistent or overestimate the ^{14}C-dates.

For two out of eight samples (GLL-194308, -23) that have so far been investigated using both small aliquots and single grains, the OSL results are not significantly different. In addition, the distributions of equivalent dose – especially when measured using single grains – suggest that a significant population reflects a single event. Variations in time-averaged water content and/or the effect of organic matter, which could lead to an underestimation of the dose rate, are not likely to account for the degree of discrepancy between the OSL and ^{14}C-dates.

Based on distributions of single-grain signal brightness, in combination with those of D_e, we hypothesize that information can be gained as to the relative stringency of heating experienced in the past. Homogeneous but incomplete resetting by heat could explain why (most of) the OSL-results differ from the ^{14}C-dates for associated charcoal fragments. Additional experimental evidence is needed, however, to corroborate this.

PART II: Cooking hearths

Background

In the run-up to the development of a new business park "Doorn Noord" in Ninove (E Flanders, Belgium), preliminary archaeological investigations were carried out. These consisted of historical studies, geophysical prospection, trial trenching, and field prospection (metal detection), and revealed the presence of a military camp at this location. This provided the impetus for a large scaled in-depth archaeological excavation that ran over a period of two years (20/08/2018 – 24/07/2020).

A detailed description of the results from the excavation is given by Verbrugge (2020). In short, the oldest finds are two burial mounds with an estimated diameter of more than 30 m, a complex construction history, and dating from the Final Neolithic (~ 2500 – 2000 BCE). This makes the burial mounds amongst the oldest and largest that have been found in Flanders so far. Scattered across the excavated area are various pits and traces of postholes, tentatively attributed to the Metal Ages; their function and potential relation to the burial mounds remains to be established. In Roman times (2nd century CE), a Roman settlement was established at the site, as testified by remains of houses, ditches, roads, pits, cemeteries, and various types of artefacts (e.g. tegulae, pieces of terra sigillata, fibulae). One of the most striking elements is the large number of slags (several ten thousands) that was recovered, indicating that iron production was an important activity in this settlement. Finally, a large number of finds evidences two to three early-Modern and Modern military encampments at Ninove "Doorn Noord", such as underground shelters, relic (cooking) hearths, and various types of personal belongings (pipes, plates, bottles, buttons, belt buckles, musket balls etc.). Based on direct and indirect historical information, as well as some scarce diagnostic finds, these traces reflect the passage (and temporary residence) of large armies possibly in 1692 CE and/or 1693CE, 1745 CE, and/or 1831-1838 CE.

Each of the aforementioned archaeological finds posed chronometric research questions. Especially the traces of the early-Modern and Modern military encampments are challenging. The two/three camps are located on the same site, making it extremely difficult to allocate a particular trace to a distinct phase of military presence. In addition, distinguishing between traces belonging to 1692/1693 CE and 1745 CE has been largely (and tentatively) based on differences in the morphology of the dug-out shelters/pits, which is variable; the remains are also preserved to different extents

(Verbrugge, 2020). It is thus highly desirable to obtain direct numerical and sufficiently precise age information for these features. ^{14}C-dating is not expected to help resolving this issue (see Chapter 1), leaving OSL and archaeomagnetic dating as potential alternatives. This potential is investigated in the next chapter, and follows the same rationale as for the relic charcoal kilns (Chapters 2-4).

Chapter 5: Dating early-Modern and Modern hearths on a decadal to multi-annual timescale using OSL signals from heated sedimentary quartz

Nasrin Karimi Moayed, Dimitri Vandenberghe, Arne Verbrugge, Ech-Chakrouni Souad, Wim De Clercq, Johan De Grave

This chapter is a slightly modified version of the manuscript submitted to Journal of Archaeological Science. The modifications concern formatting, inclusion of the supplementary material in the main text, and minor suggestions made by the examination commission.

Author contributions

Nasrin Karimi Moayed: Field investigation, Sampling, Sample processing, Data analysis, Methodology, Data curation, Writing.
Dimitri Vandenberghe: Field investigation, Sampling, Methodology, Writing, review and editing.
Arne Verbrugge: Field investigation, Sampling, Writing, review and editing.
Ech-Chakrouni Souad: Field investigation, Sampling, Writing, review and editing.
Wim De Clercq: Supervision, Funding acquisition.
Johan De Grave: Supervision, Field investigation, Writing, review and editing, Funding acquisition.

Abstract

Archaeological excavations at “Doorn Noord” (Ninove, East Flanders, Belgium) revealed a complex of traces of human activity and occupation, spanning several millennia. The youngest finds consist of a vast number of surficial hearths and hearth pits, that are interpreted as the remnants of military camps. Based on direct and indirect historical information, as well as a few diagnostic finds, these traces were originally assigned to possible phases of encampment in 1692 CE, 1693 CE, 1745 CE and/or 1831-1838 CE. Although widely used in archaeological research, it is well-known that radiocarbon (^{14}C) dating lacks precision for post-1650 CE features and therefore does not allow allocating a particular trace to a distinct phase of military presence.

In this study, we report on the potential of optically stimulated luminescence (OSL) signals of quartz for directly dating the heated sedimentary remains of the hearths. We consider it a test of both accuracy and precision given the availability of independent age information (historical sources and archaeomagnetic dating). Six samples from three features yielded indistinguishable optical ages, with an average age of 1748 ± 39

CE (95% probability). This OSL date coincides with historical and archaeological evidence for the presence of a large army in this area in 1745 CE. As sources of systematic uncertainty are (largely) shared, it is possible to distinguish between comparable features with a relative time-resolution of ~2%. For hearths from the last few centuries (post-1650 CE), this implies that accurate and precise numerical and relative chronologies can be established on decadal and multi-annual timescales with 95% confidence.

Keywords: OSL dating; hearth; accuracy; precision; Modern era.

5.1 Introduction

Archaeological excavations at "Doorn Noord" (Ninove, East Flanders, Belgium) revealed a complex of traces of human activity and occupation, spanning over several millennia. The oldest traces are burial mounds and features dating from the Final Neolithic/Metal Ages, followed by the remains of a Roman settlement. The youngest structures encountered consist in the remnants of three military camps, dating from three possible distinct phases within the early-Modern (15^{th} – 18^{th} CE) and Modern (18^{th} – present) period: 1692/1693 CE, the middle of the 18^{th} century CE, and the start of the 19^{th} century CE. Amongst the most remarkable traces are the vast amount of hearth pits, from which it was deduced that the site was also used for several military encampments. Subsequent excavations over an area of 9 hectares (Figure 5.1b, light orange area) of the project area of 23 hectares (Figure 5.1b, red line) revealed approximately 500 features, essentially consisting of hearth pits as well as underground shelters with well-preserved fireplaces or hearths (Figure 5.2), together with finds such as shards of cooking pots, smoker's pipes, and food waste. As different "types" of pits could be recognized during the excavation, the hypothesis emerged that this could point to successive and distinct postphases of encampment.

Chronologically diagnostic finds (coins, ceramics, stamped pipes, etc.) are scarce but point at several possible distinct phases, as also suggested by historical sources: 1692 CE, 1693 CE, 1745 CE and 1831-1838 CE. While it is not uncommon to find remains of successive military camps at one particular locality, the large scale of the excavations at "Doorn Noord" is at least regionally unique and may provide specific insights into the history of the armed conflicts in the former Southern Netherlands. However, both

the (few) finds associated with the hearths and the historical records provide indirect dating evidence, implying that the vast majority of traces cannot be allocated to a specific period of encampment. This lack of precise and direct time information hampers interpreting a potentially highly detailed record of confrontations in the Low Lands during the 17th to 19th century CE.

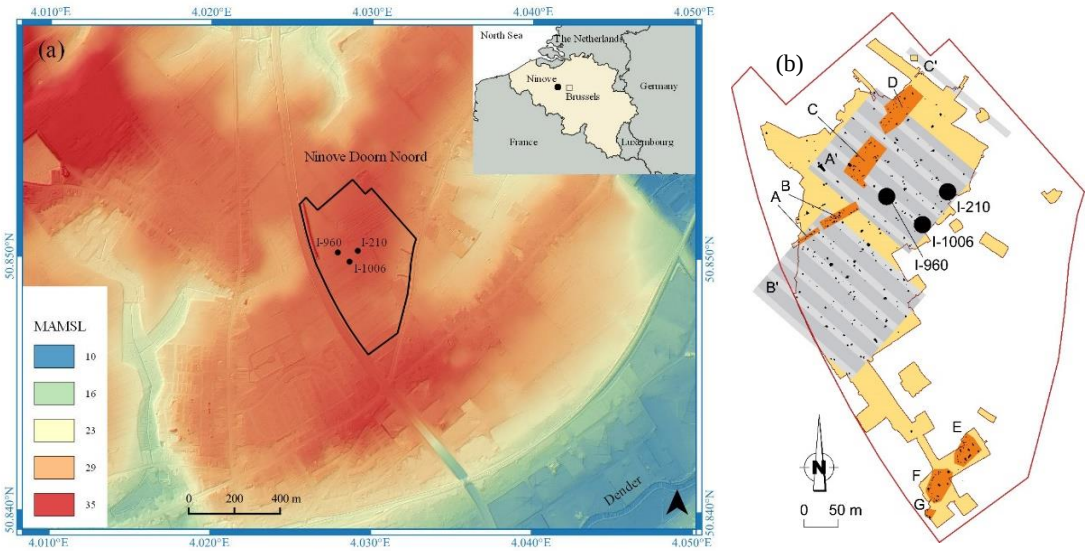

Figure 5.1: (a) Digital elevation map showing the project area in "Doorn Noord" in Ninove (black line). The investigated features (I-210, I-960, and I-1006) are indicated by the solid black circles. MAMSL: Metres Above Mean Sea Level. The inset shows the location of Ninove in Belgium. (b) The red line deliniates the project area (~ 23 ha); the excavated area (ca. 9 ha) is shaded in light orange. Based on post-excavation reconstruction, the concentrations of traces from the encampment in 1692-1693 CE are indicated by the dark orange blocks (A-G); those from the encampment in 1745 CE by the grey blocks (A'-C').

Radiocarbon (^{14}C) dating is commonly used to resolve chronological questions in archaeological research; however, its effectiveness in determining the age of features post-1650 CE is notably imprecise (Stuiver, 1961; Tans et al., 1979; Karimi-Moayed et al., 2020; Deforce et al., 2021). It was therefore not considered in the archaeological study of the military camps at Ninove "Doorn Noord", requiring that alternative chronometric tools are put to use. Archaeomagnetic dating is one such potentially powerful tool, in particular for fired materials, and it can be more precise for those periods where ^{14}C-dating is problematic (e.g. Linford, 2006; Batt et al., 2017). The approach requires a calibration curve, which is regionally specific and is constructed through archaeomagnetic analysis of known age features. Hence, it would seem desirable to complement – where possible – archaeomagnetic dating by other

Figure 5.2: (a, b) Illustrative photographs showing some of the largest structures that were excavated at Ninove "Doorn Noord". These are interpreted as dug-out shelters with remains of postholes, stairs, benches, hearth structures, and chimneys.

independent methods. Given the specific possibilities and limitations of each technique, a multi-dating approach is advantageous.

In this paper, we apply quartz-based optically stimulated luminescence (OSL) dating to three fireplaces/hearths that were found at "Doorn Noord", of which two were also dated archaeomagnetically. The application of OSL dating to anthropogenically heated materials is not new (e.g. Feathers, 2003; Bailiff, 2007; Duller, 2008a; Rhodes et al., 2010; Armitage and King, 2013; Yu et al., 2016; Sun et al., 2012, 2018; Wang et al., 2022a, b) and follows from the find that the quartz OSL signal can also be reset by heating (Wintle and Murray, 1997). Most of these studies, however, concerned well consolidated heated features such as ceramics, bricks, tiles or burnt rocks. Of interest here are heated sediments that make up the walls and/or base of early-Modern and Modern hearth pits and alcoves that were dug into the loamy subsurface (Figures. 5.2 and 5.3). These structures are well-preserved, although their texture is generally more friable compared to brick. In general, the present paper seeks to deliver a contribution to OSL dating research of heated archaeological materials, which is less extensive compared to that of unheated sediments (e.g. Madsen et al., 2009; Murray et al., 2021), and rarely concerns the last few centuries. Given that some age information is available through the archaeological finds, historical documents and archaeomagnetic dating, one could also consider our study a test of accuracy and precision. If successful, the results could contribute to an improved understanding of Modern features as preserved at Ninove "Doorn Noord", but also highlight the feasibility of applying OSL as dating tool in relatively recent historical contexts.

5.2 Material and methods

5.2.1 Study area and setting

The site "Doorn Noord" in the city of Ninove (East-Flanders, Belgium; Figure 5.1a) and extends over an elevated plateau alongside the Dender Valley (Figure 5.1b). It is situated in the Belgian loess belt (Gullentops et al., 2001; Louis, 1962). The Quaternary cover in the area has been described as consisting of windblown sediments that were deposited during the Weichselian (or perhaps the Early-Holocene) and/or slope deposits (Figure 5.3; Gullentops et al., 2001).

The archaeological research at "Doorn Noord" preceded construction works for a large business park and related roadworks. In the period 2018-2021, an area of 9 hectares was excavated. Apart from Final Neolithic burial mounds and the remains of a small Roman settlement, the finds consist of 406 of surficial hearths and hearth pits, as well as pits with hearth niches, and spread over an area of over 6.8 hectares (Figure 5.1b). Related to these hearths and pits are finds such as ceramics, coins, pipes, glass, flints, spindle whorls, buckles, buttons, glass and musket balls. As the excavation proceeded, and finds were processed and results combined with information gathered from historical cartographic sources, it became clear that these are the traces of at least three, Modern military encampments. The largest structures are interpreted as dug-out shelters, as supported by remains of postholes, stairs, benches, different types of hearth-structures, and chimneys (Figure 5.2). The hearth remains in three of these larger structures were selected in the frame of this OSL dating study (Figures 5.4a-c; features I-210, I-1006, and I-960); two of these features (I-210 and I-960) were also dated using archaeomagnetism.

Further visual photos of the sampling and collected samples from the studied structures can be found in Appendix C3.

5.2.2 Independent age information

5.2.2.1 Archaeomagnetic dating

Four hearth-structures were archaeomagnetically dated, of which two (features I-210 and I-960) are directly relevant to this study. Details on the sampling, instrumentation and magnetic measurements are beyond the scope of this paper. The archaeomagnetic dates are based on present knowledge of the secular variation of the field direction during the last three millennia in Western Europe.

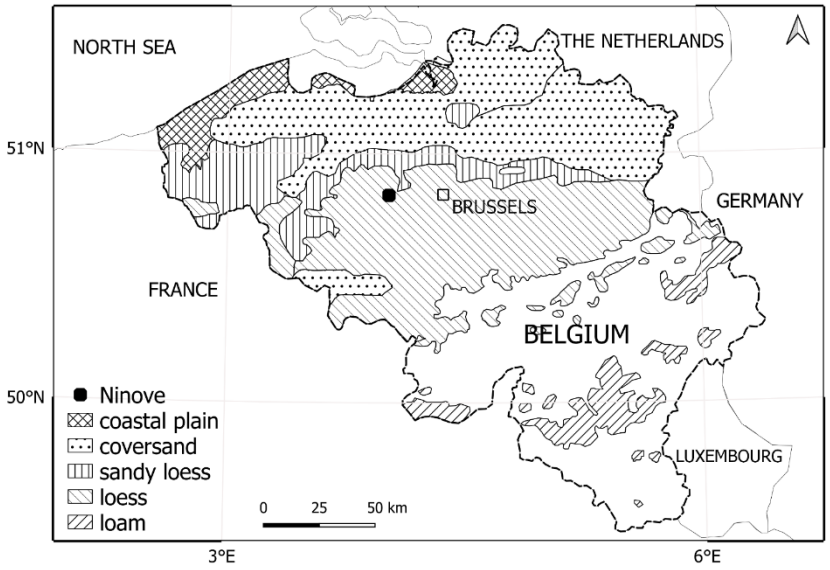

Figure 5.3: Schematic map showing the main Quaternary sedimentation areas in Belgium. from https://ncs.naturalsciences.be/quaternary/introduction-figs). The location of the study area (Ninove) is indicated by the black solid circle.

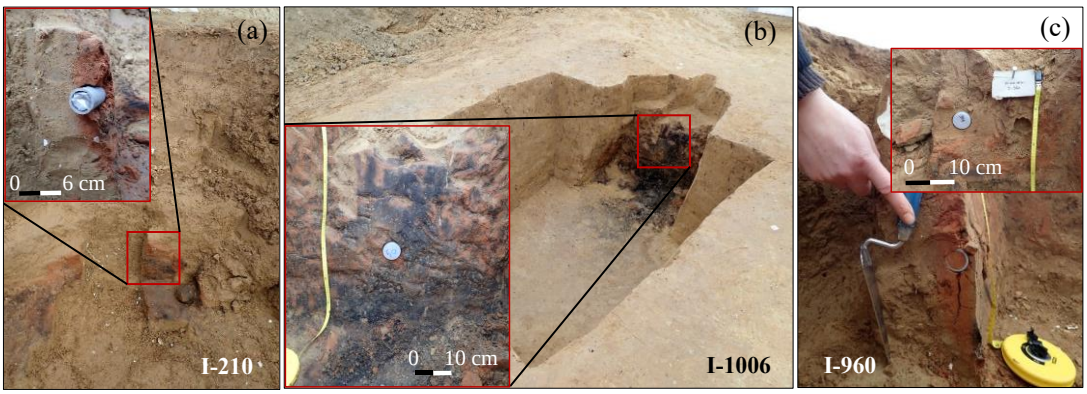

Figure 5.4: Photographs illustrate the sampling of features I-210 (a), I-1006 (b) and I-960 (c).

As the sampling site is located relatively close (~ 300 km) to the reference site Paris, the directional results were compared with the master secular variation curves of declination and inclination for France (Gallet et al., 2002). The declination and inclination reference curves were obtained using Bayesian hierarchical statistics (Lanos, 2004; Lanos et al., 2005). Following Noël and Batt (1990), probability densities of possible ages were then obtained at the 95% confidence level using the software Rendate (Lanos, 2004; Lanos et al., 2005). Due to the recurrence of the magnetic field, this resulted in multiple time-intervals, with different probabilities. For feature I-960, the archaeomagnetic age ranges are [-324, 77] CE (88.8% probability) and [460, 590] CE (6.2% probability). The age ranges obtained for feature I-210 are [1661, 1825] CE

(67.9% probability) and [-325,-134] CE (27.2% probability). Only the date of [1661-1825] CE is consistent with an early-Modern and Modern firing event.

5.2.2.2 Historical information

Several historical sources document the presence of multiple military camps at Ninove. Based on the finds and the historical evidence, the oldest two camps date from the time of the Nine Years' War (1688-1697), between the French army of Louis XIV and the forces of an international coalition led by the king of England William III (Wauters and Verbrugge, 2022; Verbrugge et al., 2022). Apart from numerous newspaper articles, diaries and marching orders, a number of cartographic images were found that show military camps at or near the excavated site "Doorn Noord" in 1692 and 1693 CE.

Local archives and newspapers, as well as a range of military documents and diaries, mention the presence of a French army at Ninove in 1745 CE. This presence and military activity can be associated with the War of the Austrian Succession (1740-1748 CE), in which France, Prussia, and Spain (amongst others) fought against the Austrian empress Maria Theresa and her allies. Although originally fought on Central and Eastern European battlefields, the battleground extended towards the Southern Netherlands from early 1744 CE onwards. Between 8 September and 15 October 1745, the French army settled in Ninove. The 1745-French campaign is well documented, and several written sources locate the camp at Ninove at or near the excavated area.

At the beginning of the excavation and the time of sampling, it was thought that a more recent phase of military encampment dating from 1831-1838 CE, might have been preserved as well. This was tentatively deduced from the find of a single copper coin, depicting Leopold I (the first King of Belgium, reigning from 1831 to 1865 CE) and a partially preserved date ("18?8", with "?" referring to the illegible digit). Post-excavation analysis, however, revealed that only the phases 1692 CE, 1693 CE and 1745 CE are present at Ninove.

5.2.3 OSL-dating

The remains of three hearths/ovens were selected for OSL dating (features I-210, I-960 and I-1006; Figures 5.4a-c). We targeted sediments with clear signs of heating, as for instance suggested by the reddish brick-like colour that is typical for burnt loess; the parent material is yellowish-grey in colour. Eight heated sediment samples in total were taken for luminescence analyses (Table 5.1) using either stainless steel (5 cm diameter;

5 cm long) or opaque PVC tubes (3 cm diameter; 15 cm long). In addition, one sample was taken from sediments that were located close to, but not visibly affected by, heating (feature I-960; inset to Figure 5.4c; sample GLL-192809 in Table 5.1). The sediment immediately surrounding each OSL-tube was collected for radionuclide analysis. Two samples were collected for determining the water content at saturation; the average of these two samples was used in the calculations.

While we aimed at sampling only the sediments that were most likely sufficiently heated, it could not be excluded that some of the sampling tubes penetrated parent material. In addition, any thermal gradient could result in homogeneous incomplete resetting. For most of the samples, we therefore extracted the inner material of the tubes in intervals of approximately 1 cm. Quartz grains from the 63-250 µm fraction were then isolated following widely adopted procedures (HCl, H_2O_2, sieving, HF; Murray et al., 2021). For luminescence measurements, quartz grains were spread out on the inner 2 mm (small aliquots) of stainless-steel discs with a thickness of 0.5 mm and a diameter of 9.7 mm, using silicon spray as adhesive. The measurements were carried out using an automated Risø TL/OSL reader equipped with blue (λ_{max} = 470 nm) and infrared (λ_{max} = 850 nm) light emitting diodes. The optically stimulated luminescence signals were detected through 7.5 mm of Hoya U-340 UV filter; irradiations were performed using a calibrated $^{90}Sr/^{90}Y$ beta-source mounted on the reader. Details on the facilities can be found in Bøtter-Jensen et al. (2003, 2010) and Lapp et al. (2015). The luminescence characteristics and equivalent doses (D_e) were determined using the single-aliquot regenerative-dose (SAR) protocol (Murray and Wintle, 2000; 2003). Unless stated otherwise, a preheat at 180 °C for 10 s and a cut heat to 160 °C were adopted. Optical stimulation was for 38.5 s at 125 °C. All the measurements used the first 0.31 s of the decay curve minus a background derived from the following 0.77 s. Each measurement of the response to the test dose (2 Gy) was followed by a stimulation for 38.5 s with the blue diodes at 280 °C to minimize recuperation (Murray and Wintle, 2003). For each aliquot, the sensitivity to stimulation with infrared light was measured (OSL IR depletion ratio; Duller, 2003), to check for the presence of feldspar. The sensitivity to infrared stimulation was defined as significant if this ratio deviated more than 10% from unity; no aliquots had to be rejected on this basis. Where applicable, the luminescence analyses focused on the samples from those intervals which, following an initial screening, showed the lowest estimates of D_e and were therefore anticipated

to have been sufficiently heated during the last firing event. The sediment collected for dose rate determination was dried at 110 °C (until constant weight), pulverized and homogenized. A subsample (~ 140 g) of the powdered sediment was then cast in wax (De Corte et al., 2006) and stored for at least one month before being measured on top a low-level extended energy-range HPGe gamma-ray spectrometer. The specific activities were converted to dose rates using conversion factors calculated from the nuclear data tabulated by Adamiec and Aitken (1998). A beta attenuation factor of 0.90 (± 5 % relative uncertainty) was adopted to correct the external beta dose rates for the effects of attenuation and etching (Mejdahl, 1979). Correction for the effect of moisture was performed as outlined in Aitken (1985). The subsurface of the study area has been described as consisting of dry loess (Louis, 1962). For the heated sediment samples, we therefore assumed that the time-averaged moisture content during burial equals half the value at saturation; a relative uncertainty of ± 30 % (1 sigma) was associated with this estimate. For the sample collected from the unheated sediments (GLL-192809), we followed Aitken (1985) and assumed an average water content corresponding to 80 % of saturation. An internal dose rate in quartz grains of 0.013 ± 0.003 Gy ka^{-1} was adopted (Vandenberghe et al., 2008). The contribution of cosmic rays was calculated following Prescott and Hutton (1994), and a 15% relative uncertainty was associated with the values.

5.3 Results

5.3.1 Luminescence characteristics and procedural tests

Figure 5.5a shows the natural and regenerated OSL decay curve for an aliquot of sample GLL-192807. The signals are clearly distinguishable from the background level and decay rapidly with stimulation time. The decay matches that observed for calibration quartz (Figure 5.5a, inset), as expected for a signal dominated by the fast component. The growth of the OSL signal as a function of dose can be well approximated by a single saturating exponential function (solid black line in Figure 5.5b). The dose response passes through the origin, indicating that recuperation is negligible (open square). It is possible to reproduce a regenerated dose point implying that sensitivity changes are accurately corrected for (the solid and open circles at overlying each other, i.e. a recycling ratio consistent with unity).

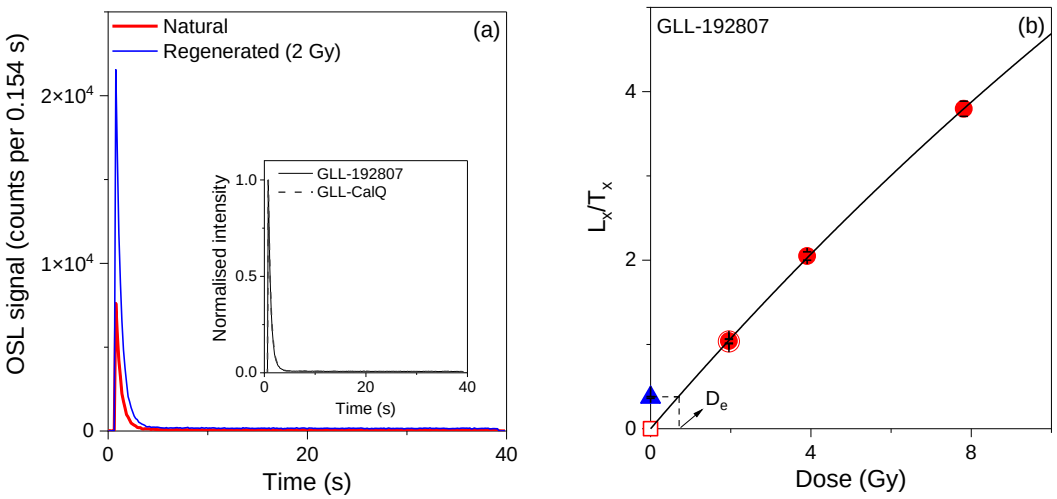

Figure 5.5: (a) OSL decay curves for a single aliquot of quartz grains extracted from sample GLL-192807. The natural and regenerated signals are shown as the red and blue lines, respectively. The inset compares the regenerated OSL decay curve from the sample with that from calibration quartz (GLL-CalQ). (b) SAR growth curve for a single aliquot of the same sample. Recycling and recuperation points are represented by the red open circle and square, respectively. The solid line is the fit of the data to a single saturating exponential function. The equivalent dose (D_e) is obtained by interpolating the natural sensitivity-corrected OSL signal (open triangle) on the SAR dose response curve.

To identify the optimum measurement parameters for D_e determination, we examined the dependence of measured dose on preheat temperature using sample GLL-192807. In a first test, groups of three natural aliquots were measured at each of seven different preheat temperatures in the range of 160 °C to 280 °C. There is no dependence of D_e on preheat temperature up to 260 °C (Figure 5.6a); across this interval, recycling ratios are consistent with unity and recuperation is less than 1% of the sensitivity-corrected natural OSL signal (Figure 5.6b).

In a second test, natural aliquots were first exposed twice to the blue diodes for 250 s at room temperature, with a 10,000 s pause in between. The aliquots were then given a dose close to the expected natural dose, and measured at each of seven different preheat temperatures in the range of 160 °C to 280 °C. The results are shown in Figure 5.6c. Across the 160 – 240 °C temperature interval, the measured doses are consistent with the known given dose; the recycling ratios are consistent with unity as well, and recuperation remains below 1% of the corrected natural OSL signal (Figure 5.6d). This second test is known as a dose recovery test and is the most complete test for assessing the performance of a particular SAR procedure for a sample (e.g. Murray et al., 2021).

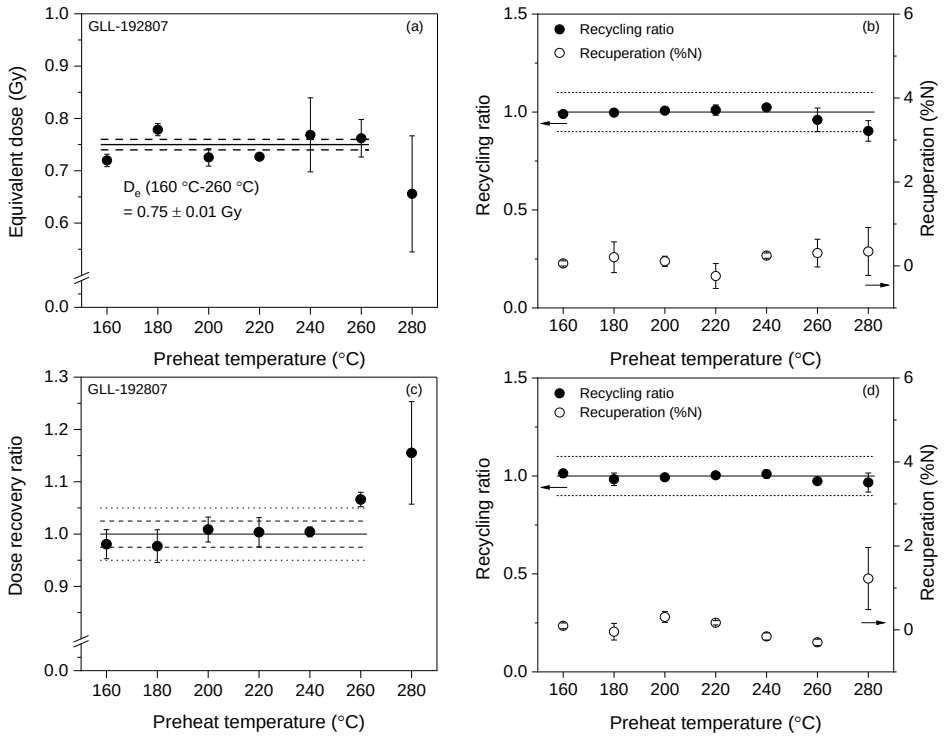

Figure 5.6: (a) Dependence of equivalent dose (D_e) on preheat temperature for sample GLL-192807. The dashed and dotted lines indicate the average ± 1 standard error over the 160 - 260 °C temperature interval. (b) Corresponding recycling and recuperation data; the solid and dashed lines (eye guides) bracket a value for the recycling ratio of 1.0 ± 0.1. (c) Dependence of dose recovery ratio on preheat temperature for sample GLL-192807. Each data point represents the average (± 1 standard error) of 5 measurements. The dashed and dotted lines are eye guides and bracket a 2.5% and 5% deviation of the ratio from unity (solid line). (d) Corresponding recycling and recuperation data; the solid and dashed lines (eye guides) bracket a value for the recycling ratio of 1.0 ± 0.1.

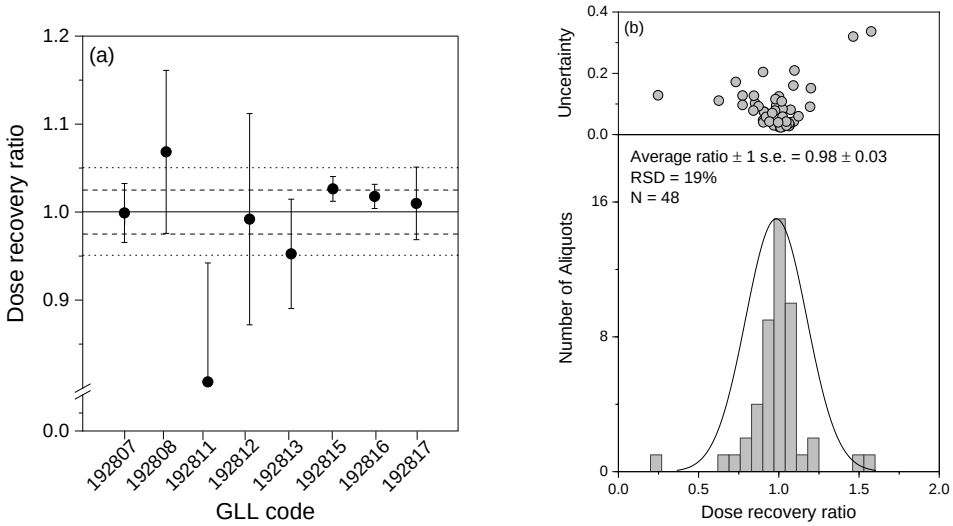

Figure 5.7: (a) Average dose recovery ratios (± 1 standard error) obtained for each sample using a preheat of 10 s at 180 °C and a cut heat to 160 °C. The dashed and dotted lines (eye guides) bracket a 2.5% and 5% deviation of the ratio from unity (solid line). (b) Summary of dose recovery data for all samples and aliquots, represented as a histogram.

The dose recovery test was repeated, this time using 6 natural aliquots for each of the eight heated sediment samples, and a preheat of 10 s at 180 °C only. The results are summarised in Figure 5.7.

For all samples except GLL-192811, and within 1 standard error, the measured dose does not differ from the known given dose by more than 2.5 % (Figure 5.7a). The discrepant result for sample -11, with an unweighted average dose recovery ratio (± 1 standard error) of 0.81 ± 0.14, is not understood. It results essentially from a very poor and significantly less precise dose recovery value (~50 % relative uncertainty) for one out of the six aliquots measured. Rejecting this aliquot from the analyses yields an average dose recovery ratio for this sample of 0.92 ± 0.09. Apart from poor precision, however, there is no other argument (e.g. on the basis of recycling or OSL IR depletion ratio, or recuperation) for rejecting this aliquot. The overall dose recovery ratio (± 1 standard error; n = 48) is 0.98 ± 0.03 (Figure 5.7b). Taking this as an average descriptor (Murray et al., 2021) suggests that the chosen experimental SAR parameters can accurately measure a known laboratory dose.

5.3.2 Equivalent dose determination

The equivalent dose in all samples was determined using the SAR protocol, as outlined in the above and using a preheat of 10 s at 180 °C. In between 48 and 52 small aliquots were measured for each burnt sample.

An aliquot that emitted a net natural test dose signal ("T_n") higher than three times the standard deviation of the background signal was included in the analyses. The results are shown as histograms in Figure 5.8 for two samples of each heated feature and in Figure 5.9 for the rest samples in this study.

Except for samples GLL-192808-X13 (feature I-960; Figure 5.8b) and -15 (feature I-1006; Figure 5.9c) the datasets mainly consist of values that appear to belong to a single dose population and a few aliquots that yielded significantly higher D_e's. For all measured aliquots, the recycling ratios are close to one and the recuperation is negligible. D_e values that differed by more than three standard deviations from the mean were iteratively rejected and the unweighted mean (± 1 standard error) of the resulting distribution was used in the calculations (Table 5.1). The unburnt sample GLL-192809 yielded a significantly higher D_e (~ 40 Gy) as would be expected for parent material that was not or only partially heated (Table 5.1; Figure 5.9a).

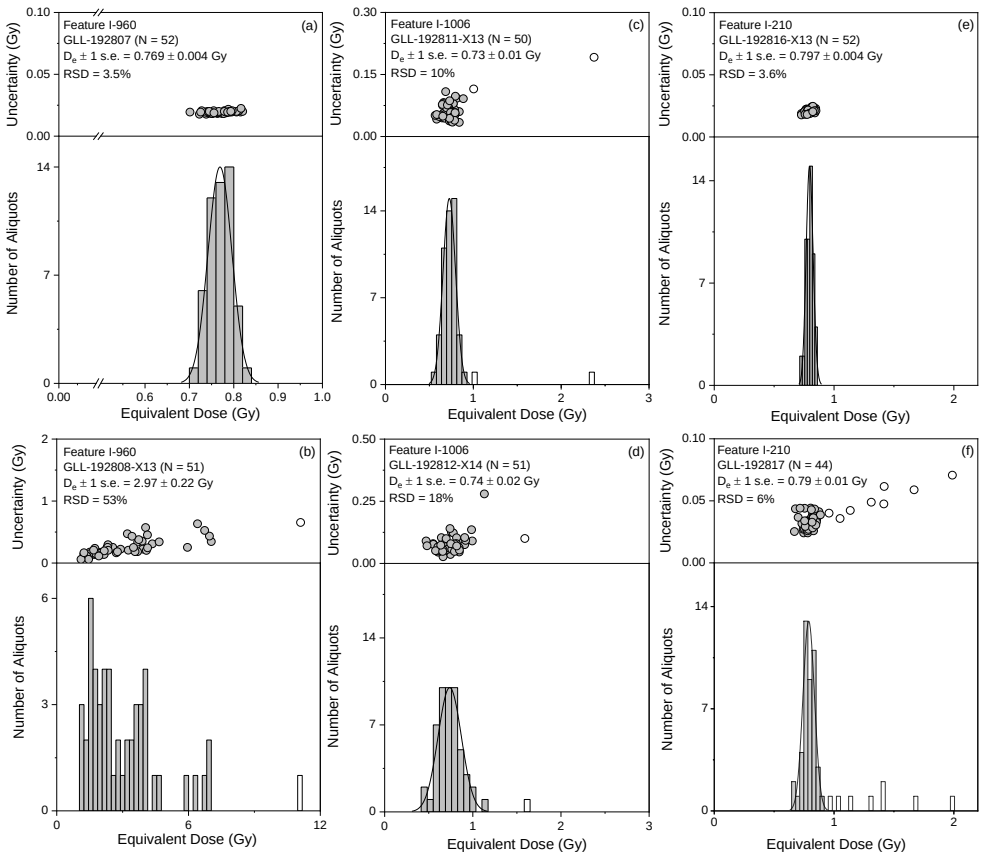

Figure 5.8: Distribution of equivalent dose in small (2 mm diameter) aliquots of two samples from each of the three investigated features. (a-b): I-960, samples GLL-192807 & -08; (c-d) I-1006, samples GLL-192811 &-12; (e-f) I-210: samples GLL-192816 & -17.

5.3.3 OSL ages

Table 5.1 summarises the analytical data, the calculated dose rates and optical ages. Uncertainties on the OSL ages were calculated following the error assessment system formalised by Aitken (1985). Additional information on the different sources of systematic uncertainty and their quantification can be found in Vandenberghe et al., 2004. The total uncertainty on the optical ages for the burnt samples ranges in between ~ 7 - 11 %; systematic sources of uncertainty are the main contributor. Excluding sample GLL-192808-X13 (owing to the large spread in D_e with an RSD of 53% after excluding the outliers; Figure 5.8b), the relative total random uncertainties remain below 5 %, and can be as low as ~1 - 3 %. If ones assumes that the uncertainties resulting from systematic effects are largely shared between the samples – an assumption that might hold to a certain extent for the different samples from the three heated features at this locality – the random uncertainties are relevant for intercomparison of the optical ages.

Sample GLL-192815 yields an optical age of 0.35 ± 0.02 ka (1 sigma random uncertainty), with a somewhat higher and more asymmetric spread in D_e (RSD = 30%) compared to the other three samples for the same feature (I-1006; see Figures 5.8c-d and Figures 5.9b-c); the latter yield a younger and internally consistent set of ages in between 0.260 ± 0.005 ka and 0.267 ± 0.008 ka (1 sigma random uncertainty; Table 5.1). The two samples taken from feature I-210 yield ages (± 1 sigma random uncertainty) of 0.264 ± 0.004 ka and 0.291 ± 0.004 ka. These ages are not consistent within 2 sigma. Based on our analysis of the D_e-distributions (Figures 5.8e-f) there is no particular reason why the average D_e in one of these samples would be less, or more, reliable than the other. An optical age of 0.279 ± 0.003 ka was obtained for sample GLL-192807 (feature I-960; for the reason outlined in the above, sample -08-X13 is excluded). Based on the distributions of D_e in samples GLL-192808 and -15, we interpret the ages for these two samples as most likely not accurately reflecting the last heating event.

Taking everything together and considering that the random uncertainty represents a minimum for the limit on precision, we consider six samples (GLL-192807, -11, -12, -13, -16 and -17), and hence the three investigated features, to be coeval. Their average age (± 1 sigma total uncertainty; calculated following Aitken, 1985) is 0.271 ± 0.020 ka, or 1748 ± 20 CE.

Sample GLL-192809 (parent material), which was taken from sediments that were not visibly affected by heating, yields an optical age of 15.3 ± 1.1 ka.

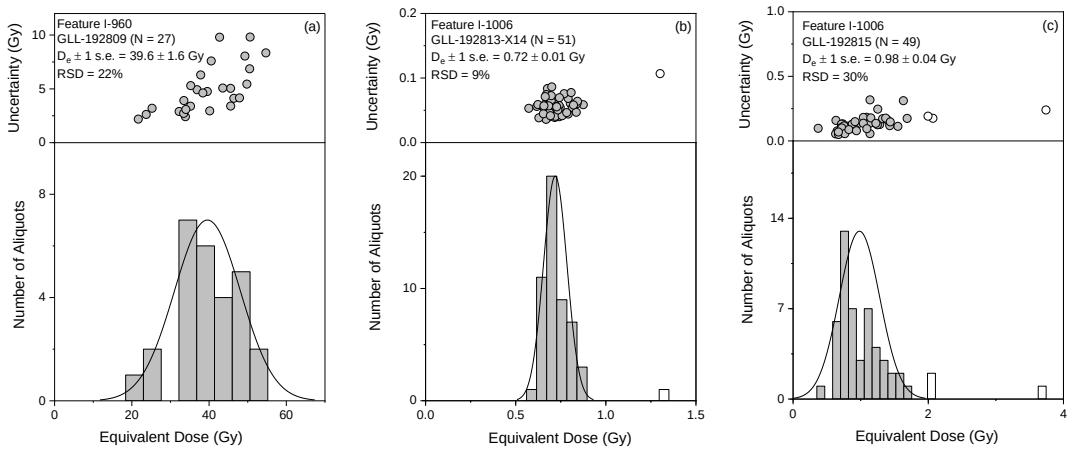

Figure 5.9: Distribution of equivalent dose in small (2 mm diameter) aliquots of samples GLL-192809 (a), -13 (b) and -15 (c).

Table 5.1: Radionuclide activities used for dose-rate evaluation, estimates of time-averaged moisture content (F*W, with the F the fraction of saturation corresponding to the time-averaged moisture content, and W the saturation content as measured in the laboratory), calculated dose rates, equivalent doses (D_e), calculated OSL ages, and random (σ_r), systematic (σ_s) and total uncertainties (σ_{tot}). The OSL ages (± 2 sigma total uncertainties) are expressed as ages Common Era (CE) in the last column.

Feature	*GLL-code*	*Material*	*^{234}Th (Bq kg^{-1})*	*^{226}Ra (Bq kg^{-1})*	*^{210}Pb (Bq kg^{-1})*	*^{232}Th (Bq kg^{-1})*	*^{40}K (Bq kg^{-1})*	*F*W*	*Total dose rate (Gy ka^{-1})*	*D_e (Gy)*	*OSL Age (ka) 1σ*	*σ_r (%)*	*σ_s (%)*	*σ_{tot} (%)*	*OSL Age (CE) 2σ*
I960	192807	Burnt	35 ± 3	42 ± 1	39 ± 2	42 ± 0.5	484 ± 2	0.14 ± 0.04	2.76 ± 0.03	0.769 ± 0.004$_{(52)}$	0.28 ± 0.02	1.06	7.23	7.31	1740 ± 41
	192808-X13	Burnt	32 ± 3	42 ± 1	34 ± 5	42 ± 0.4	495 ± 4	0.14 ± 0.04	2.71 ± 0.07	2.97 ± 0.22$_{(51)}$	1.1 ± 0.1	7.79	7.24	10.63	925 ± 233
	192809	Unburnt	30 ± 4	42 ± 1	37 ± 3	42 ± 0.5	512 ± 4	0.22 ± 0.02	2.59 ± 0.04	39.6 ± 1.6$_{(27)}$	15.3 ± 1.1	4.44	5.92	7.4	-13253 ± 2261
I1006	192811-X13	Burnt	30 ± 2	43 ± 1	33 ± 2	44 ± 0.4	502 ± 5	0.14 ± 0.04	2.75 ± 0.03	0.73 ± 0.01$_{(50)}$	0.26 ± 0.02	1.75	7.23	7.44	1754 ± 39
	192812-X14	Burnt	30 ± 2	43 ± 1	33 ± 2	44 ± 0.4	502 ± 5	0.14 ± 0.04	2.75 ± 0.03	0.73 ± 0.02$_{(51)}$	0.27 ± 0.02	2.86	7.23	7.78	1752 ± 42
	192813-X14	Burnt	30 ± 2	45 ± 1	35 ± 3	45 ± 0.6	490 ± 4	0.14 ± 0.04	2.76 ± 0.04	0.72 ± 0.01$_{(51)}$	0.26 ± 0.02	1.97	7.23	7.49	1759 ± 39
	192815	Burnt	30 ± 2	45 ± 1	35 ± 3	45 ± 0.6	490 ± 4	0.14 ± 0.04	2.76 ± 0.04	0.98 ± 0.04$_{(46)}$	0.35 ± 0.03	4.61	7.23	8.57	1664 ± 61
I210	192816-X13	Burnt	39 ± 2	41 ± 1	55 ± 3	41 ± 0.4	501 ± 4	0.14 ± 0.04	3.02 ± 0.04	0.797 ± 0.004$_{(48)}$	0.26 ± 0.02	1.47	7.25	7.39	1755 ± 39
	192817	Burnt	30 ± 4	40 ± 1	41 ± 2	39 ± 0.6	477 ± 4	0.14 ± 0.04	2.71 ± 0.03	0.79 ± 0.01$_{(40)}$	0.29 ± 0.02	1.5	7.22	7.37	1728 ± 43

5.4 Discussion

Figure 5.10 compares the archaeomagnetic and historical age information (§5.2.2) with the eight OSL ages obtained for the heated sediment samples from the investigated features (§5.3.3). Archaeomagnetic and OSL data are compared within 95% probability (2 sigma). Unless stated otherwise, the uncertainties on the OSL ages refer to the 2 sigma total uncertainties (i.e. derived from the combined random and systematic sources of uncertainty).

For feature I-960, the archaeomagnetic age as well as the OSL age for sample GLL-192808 significantly overestimate any possible date for military encampment during the early-Modern and Modern periods. OSL-sample -08 was not expected to yield an accurate age, based on the observed scatter in equivalent doses (Figure 5.8b). The OSL age of 1740 ± 41 CE for sample -07 matches historical evidence for encampment in the middle 18th century (1745 CE). An archaeomagnetic date is also available for feature I-1006; the age interval of [1661, 1825] CE (67.9 % probability) is consistent with the OSL-ages for samples -11, -12 and -13. The average OSL age for these three samples is 1755 ± 39 CE and would allocate this feature to the 1745 CE encampment. Sample -15 yields an older date of 1664 ± 61 CE, which is not inconsistent with historical evidence (1692-1693 CE or 1745 CE). In comparison to the other samples, however, the D_e's are spread over a larger range. While this spread could be sample intrinsic, the age result is not internally consistent with the three other OSL-dates for this same feature. Two OSL ages were obtained for feature I-210, which would allocate the hearth to either 1692-1693 CE, or 1745 CE. The OSL ages are not entirely internally consistent, and our experimental data do not allow identifying why one date should be preferred over the other (§5.3.3). The average OSL age dates this feature to 1742 ± 41 CE.

None of the OSL age results for the three investigated features provides evidence for them to be linked to a military encampment during 1831-1838 CE, which matches the insights grained from post-excavational analyses (§5.2.2.2). In the following discussion, we exclude the OSL-results obtained for samples GLL-192808 and -15, for the reasons outlined above (i.e. scattered dose distributions).

Within two sigma total uncertainties, all dates are clearly centred around 1745 CE (Figure 5.10), suggesting that the samples and hearths are coeval. Averaging the results

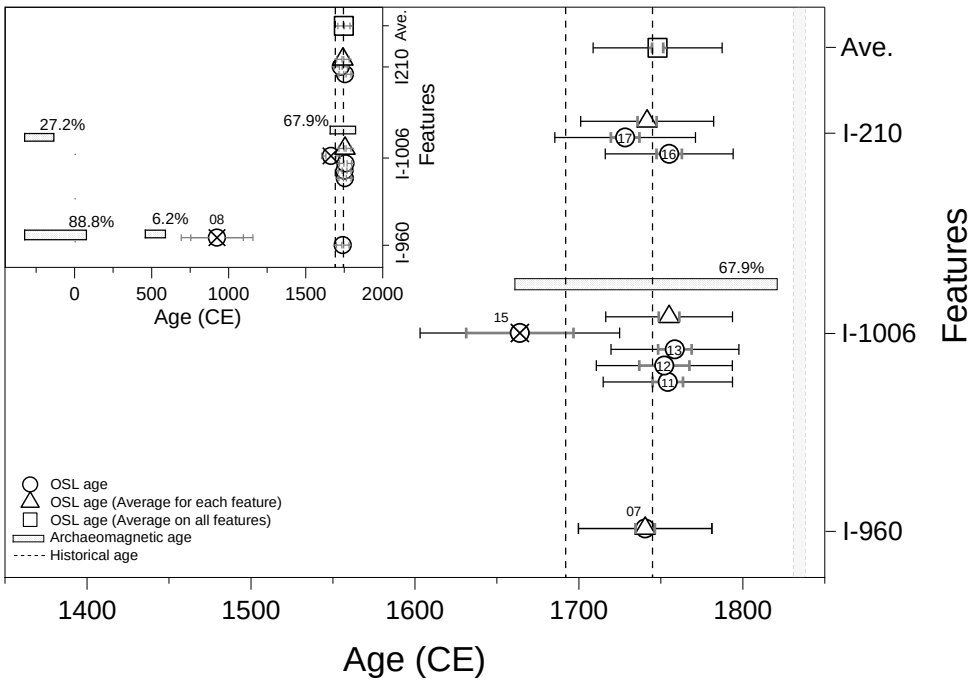

Figure 5.10: Comparison between OSL ages, archaeomagnetic age probability distributions, and historical age information. The uncertainties on the OSL and archaeomagnetic ages cover 95.4 % probability (2 sigma). Open circles represent the OSL age obtained for each sample, with the two that are crossed out referring to those that were not considered in the discussion (see sections 5.3.3 and 5.4 for details). The open triangles indicate the average OSL age for each sample; the open square the overall average OSL age. The random and total uncertainties on the OSL ages are indicated by the grey and black error bars, respectively. The archaeomagnetic age probabilities are indicated by the horizontal bars. The vertical dashed lines represent the possible phases of military encampment as derived from historical sources (1692-1693 CE and 1745 CE).

for these six samples yields a date of 1748 ± 39 CE. The uncertainty essentially arises from systematic effects, such as that associated with our estimate of past water content. Increasing the time-averaged water content with 1%, increases the optical age by about 1%. Given that no factual information is available on past water content, we adopted half of the value at saturation with an uncertainty that covers all plausible scenarios within 3 sigma (i.e. from almost completely dry, to almost saturated). While this is – at least in our opinion – an objective analysis of uncertainty, it does cover a wide range and might be an overestimate.

The comparison between the archaeomagnetic and OSL dates is of interest. In the present context, both aim at establishing the time when the sediment was heated to a sufficiently high temperature. They differ, however, in the physical mechanisms that are exploited for dating as well as in the temperatures involved, the way and scale of sampling, subsequent analysis and age calculation. A detailed discussion is beyond the

scope of this paper. Here, we limit ourselves here to how OSL might potentially provide information for archaeomagnetic dating. Firstly, the D_e-distributions in sample GLL-192808 (feature I-960) and possibly -15 (feature I-1006) indicated that these might be problematic in terms of resetting and/or disturbance. These effects can be expected to affect archaeomagnetic dating, even more so as larger volumes of samples are taken. While our dataset is limited, the results obtained for sample -08 (Figure 5.8b) may very well relate to the apparent significant overestimate in the archaeomagnetic age. Secondly, archaeomagnetic dating needs calibration data obtained through archaeomagnetic analysis of features with independent age control, and results in possible age-probability intervals (as is the case in ^{14}C-dating). On the other hand, OSL dating does not require calibration in this manner and therefore can contribute to improving archaeomagnetic calibration data bases.

The 1 sigma total uncertainty associated with an individual OSL age is ~ 7-8 % (Table 5.1) and is relevant when comparing the dates with other chronological information. For comparison between the OSL ages amongst each other and given that they were obtained for (very) similar features at the same site/location, the random uncertainties are relevant. These are in the range of 1 – 3 %. As noted for feature I-210 (samples GLL-192816 and -17) and assuming that both ages are accurate and refer to the same event, however, the observed variability can be higher (~5 %). If the dataset is extended to multiple coeval samples from different features – here taken to be samples GLL-192807, -11, -12, -13, -16 and -17, covering the three features – the observed level of precision is ~2 %, comparable to the overall expected random uncertainty of ~1 %. Within the time range under consideration here, this implies the possibility of distinguishing between features with a resolution of about 10 years, with 95 % probability.

5.5 Conclusion

An average OSL date (± 2 sigma total uncertainty; six samples) of 1748 ± 39 CE was obtained for three hearth/oven remains at Doorn-Noord, Ninove (Belgium). This OSL date matches historical and archaeological evidence for a French military camp, situated at this locality in 1745 CE, from which we conclude that the OSL date is accurate . In turn, it allows allocating these traces directly to this specific phase of encampment. The OSL dates also match one archaeomagnetic age ([1661-1825]) but

are considerably more precise. The results illustrate how OSL dating of heated features can help improve the quality of archaeomagnetic intensity calibration data bases, and aid in assessing the suitability of a sample for archaeomagnetic analysis. This is important, as also archaeomagnetic dating offers great potential for the periods where radiocarbon dating is problematic.

In addition, our study reinforces the added value of dating multiple OSL-samples from a single feature, and of doing so for multiple features. We demonstrate that this strategy may allow distinguishing, relatively, between comparable features at decadal timescales, with 95 % confidence. At least to our knowledge, this is an exceptional level of precision, which could greatly benefit archaeological studies of this type of remains from last few centuries. Apart from the apparent level of accuracy that can be achieved through OSL-dating, we highlight its possibilities for addressing chronometric issues that require high time-resolution.

Chapter 6: Discussion and conclusion

6.1 Discussion

This doctoral dissertation investigates the potential of quartz-based SAR-OSL dating for application to burnt sediments associated with relic charcoal kilns (Part I) and cooking hearths (Part II). More in particular, it seeks to explore its possible use for age determination of features that postdate 1650 CE, a time-range over which the precision of ^{14}C-dating is extremely limited.

The application of luminescence dating to heated sediments is not new in itself. In fact, the origins of the method lie in the dating of heated materials and objects such as pottery, bricks, tiles, kilns and burnt stones (TL-dating; see e.g., Aitken, 1985; Wagner, 1998). As summarized in the introduction (§1.1), however, few studies seem to have explored the potential advantages offered by subsequent and significant methodological advances, which make use of luminescence signals that are stimulated by light. In addition, and at least to our knowledge, the approach has never before been tested for dating relic charcoal kilns and cooking hearths, only in a few studies for directly dating hearths in general (Rhodes et al., 2009, 2010; Armitage and King, 2013; Yu et al., 2016; Sun et al., 2012, 2018), and rarely for tackling chronometric issues that pertain to heated materials that date from modern to contemporary times and/or require a decadal time-resolution. One notable exception with respect to the later, concerns the work by Bailiff (2007) on bricks from buildings in England with well-known ages. That study used OSL signals from quartz extracted from bricks, in combination with the SAR protocol, resulting in a set of luminescence ages that differ on average by 5 ± 10 years from the independent ages, and opens new possibilities for studying the re-use of bricks in such structures.

This study seeks to take advantage of these insights and potential possibilities. The features studied here, however, are different from bricks/brick-built structures, and therefore pose different challenges. This section aims at bringing all results together and discusses them in terms of (§6.1.1) accuracy, (§6.1.2) precision, (§6.1.3) possibilities and limitations, and (§6.1.4) suggestions for future research.

6.1.1 Accuracy

Figure 6.1 compares the independent age information with the OSL dates obtained for all charcoal kilns and cooking hearths investigated in this work. Based on this comparison, there is no evidence for systematic over- or underestimation of the OSL ages obtained for the kilns in Sonian Forest and the Veluwe. This suggests that OSL dating can yield accurate age information for this type of features. Similarly, an average OSL-date of 1748 ± 59 CE was obtained for the cooking hearths at Ninove; subsequent archaeological research showed that these can be assigned to 1745 CE (Figure 6.1).

For the relic charcoal kilns in Zoersel Forest, however, the OSL-dates generally overestimate independent age control (^{14}C). At least in part, the overestimation might be due to incomplete thermal resetting. In TL-dating, this can be detected through the "plateau test"; there is no equivalent of such a test in OSL-dating. Here, incomplete thermal resetting is inferred for those samples for which small-aliquots and single grains yield consistent ages, although they apparently overestimate the time of last charcoal burning. For six of the eight samples (75% of the samples) that were investigated, however, the single-grain ages are significantly younger than the ages obtained using small, multiple-grain aliquots. These samples can be interpreted as consisting of grains with different burial doses, which can be caused by mixing/disturbance of the sediments following the charcoal burning and/or the fact that the sampling tubes penetrated sediments that experienced different resetting regimes.

With respect to the former, it is interesting to note that all grains and aliquots that exhibited a detectable net OSL-response to a regenerative dose also yielded a finite, non-zero dose value, and this for all investigated samples regardless of the study area and lithology of the substrate underlying the relic charcoal kilns (loamy in Sonian Forest, sandy in Zoersel Forest and the Veluwe). The non-zero dose values are not an artefact of the measurement procedure (see §3.4.1.4; Figure 3.12). Apart from the age obtained for kiln HS19-M3, none of the OSL-ages underestimates the ^{14}C-dates. This suggests that any turbation processes - if still active - do not involve downwards/vertical transport of surficial material (which is assumed to be of zero-, or at least significantly-younger, age).

As to the latter (scale of sampling), heat is transferred both vertically and laterally, resulting in a thermal gradient as a function of distance from the heat source.

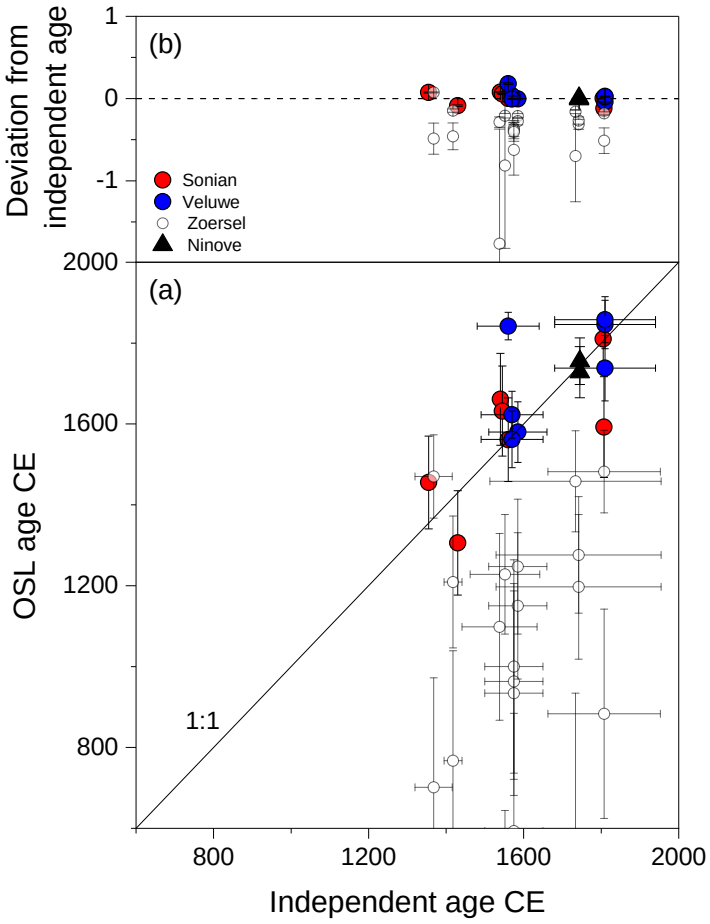

Figure 6.1: (a) Comparison of OSL ages with independent age control (^{14}C for Sonian Forest, Zoersel Forest and the Veluwe; historical information for Ninove) for all features investigated in this study. (b) The deviation from independent age control, expressed as the ratio of OSL age (minus independent age) to independent age.

Quantitative information is scarce but indicates that such gradients can be significant at cm-scale (Aldeias et al., 2016; Lu et al., 2016; Hirsch et al., 2018).

It is well-known from laboratory measurements at elevated temperature ("isothermal decay") that the fast component of the quartz-OSL signal can also be reset by prolonged exposure to lower temperatures. Murray and Wintle (1999; their Figures 4 and 5), e.g., have shown that – depending on the thermal history experienced by the grains – heating to 220 °C for ~ 6-18 hours can deplete the OSL-signal to a level indistinguishable from the background. Heating for 1 hour at 250 °C or 1 min at 300 °C generally eliminates 99.9% of the OSL signal (see Murray et al., 2021, and references therein). Following Hirsch et al. (2018), a temperature of ~550 °C is typically maintained in charcoal hearths for at least several days, resulting in a temperature of > 220 °C at a depth (in sandy substrates) of around 5 cm. This is of the same order of magnitude of the vertical

segment covered by the sampling cylinders (5 cm diameter), but significantly shorter than their length (15 cm long).

The combined dataset, i.e. the distributions of equivalent dose – and by extension age – in samples that were collected in well-defined stratigraphical panes from both the dark charcoal rich layers and the underlying sediments, and/or in samples that were analysed in lateral segments (see §5.4.1), do not allow excluding any of the aforementioned causes. Once again, it should be noted that 75% of all samples/sites investigated in this work yielded good agreement with independent age control, with no evidence for systematic age over- or underestimation. The only exception are the dates obtained for the kilns in Zoersel forest. While not understood at present, three alternative causes for this apparent age discrepancy are: (i) inaccurate assessment of the parameters used in OSL age calculation or underestimation of their associated uncertainty, (ii) vice versa, inaccurate independent age information or underestimation of the associated uncertainty and/or (iii) all ages are accurate, but refer to different events.

(i) Quantities and uncertainties in the OSL age calculation

To obtain a luminescence age, a range of quantities must be experimentally determined or estimated. Here, we assume that our analyses yield accurate results, i.e. calibration of instrumental facilities, determinations of equivalent dose (excluding potential inaccuracies introduced by the effects discussed in the above) and specific radionuclide activities, burial depth and water content at saturation, are all accurate. All reported analytical data and calculated ages are accompanied by detailed analyses of random and systematic sources of uncertainty, which follows the procedure outlined by Aitken and Alldred (1972) and Aitken (1976; 1985), and as implemented by e.g. Vandenberghe (2004). Within the frame of this work, one quantity (time-averaged moisture content) that is required for age calculation was derived from best estimates, while another (organic content) was not explicitly investigated.

Uncertainty on time-averaged moisture content is a source of error that is difficult to avoid. We adopted a relative uncertainty with the estimates of water content that covers all plausible scenarios within 2 to 3 sigma. Inaccurate estimation of the numerical value of one or more time-averaged water contents, should thus be covered through the

uncertainty associated with these values. The water content at saturation ("W"; Aitken, 1985), which was measured in the laboratory, sets an upper limit to the effect on the age, while a content of 2-3% was considered as the lower limit. The effect of water content on an OSL age (obtained using sand-sized quartz) is illustrated in Figure 6.2; in general, a change in water content by 1% corresponds to change in OSL age of about 1%. A lower value for the water content leads to an increase in the dose rate and hence a decrease in the OSL age, and vice versa. Water content is a site-specific variable, while the saturation level (or porosity) can also vary locally and significantly (Aitken, 1985; this study - Tables 2.1, 3.1 and 4.1). The combined dataset (Figure 6.2) shows no systematic and/or random deviations in OSL age results that would point at past water contents being a significant source of inaccuracy.

The effect of organic matter on the dose rate is comparable to that of water, but the absorption coefficients are different (e.g. Lian et al., 1995). The effect is illustrated in Figure 6.3. Changes in organic matter of 1% result in age differences of less than 1% (~0.7%) in OSL dating. Preliminary results (see § 3.5.2.2) indicate an organic content of up to 15% in samples collected from dark charcoal-rich layers, which would increase the age by about 11%.

Neglecting organic content would thus lead to age underestimation. It should be noted that, apart from the effect on calculated dose rate, compositional differences between a sample and the calibrants used in laboratory-based gamma-ray spectrometry can lead to significant inaccuracies in radionuclide quantification as well (De Corte et al., 2004). The potential effects of organic matter (or sample composition in general) remain to be investigated although, as indicated in the above, would appear marginal. In short, there is no evidence that would suggest that deviations from independent age control are the result from underestimation of these sources of uncertainty.

(ii) Inaccuracy of independent age information or associated uncertainty

As outlined in (i), i.e. for OSL-dating with respect to inaccuracies in numerical values and associated uncertainties, the same holds for independent age control. Addressing methodological issues associated with ^{14}C-dating, archaeomagnetic dating and/or historical age information is beyond the scope of this dissertation. Nevertheless,

charcoal is a commonly used and preferred material in ^{14}C-dating, and is generally thought to yield reliable results for pre-1650 CE features.

As clarified in § 2.2.4, 3.3.3 and 4.2.3, short-lived samples such as charred twigs, the outer growth rings from the stem, or charcoal from taxa with a relatively short maximum potential age were selected to avoid an old-wood effect. At present, there is no evidence that would point at inaccurate ^{14}C-dates; they are essentially limited by precision, as illustrated by the wide age probability distributions for features that post-date 1650 CE (Figures 2.10, 3.14 and 4.8; Tables 2.2, 3.3 and 4.2).

Some potential difficulties and inaccuracies associated with archaeomagnetic dating are outlined in § 5.5. Based on our finds, and at least for the hearths as preserved at Ninove, OSL is more likely to provide information that can help improving archaeomagnetic dating methodologies than vice versa.

The historical/written sources relevant to this work, where available, provide one or multiple possible age ranges (e.g. §3.2 and §5.3.2, Figures 3.14 and 5.10). They include maps and cartographic depictions, governmental correspondence, economic, cultural and military reports, charters, judicial and legal documents, financial records, newspaper articles, diaries and letters. Assuming that these accounts are objective to some degree, their main limitation is probably related to their circumstantial nature.

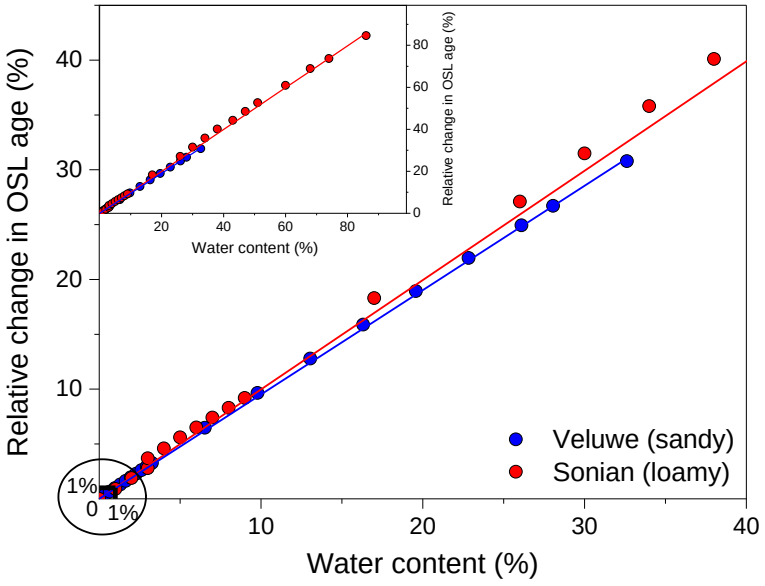

Figure 6.2: Effect of water content on an OSL age for a sample from a relatively low (sample GLL-194348**;** W = 0.33) and high (sample GLL-184301**;** W = 0.86) dose rate environment. The solid lines represent a linear fit to the data. The inset shows the same data up to the saturation level.

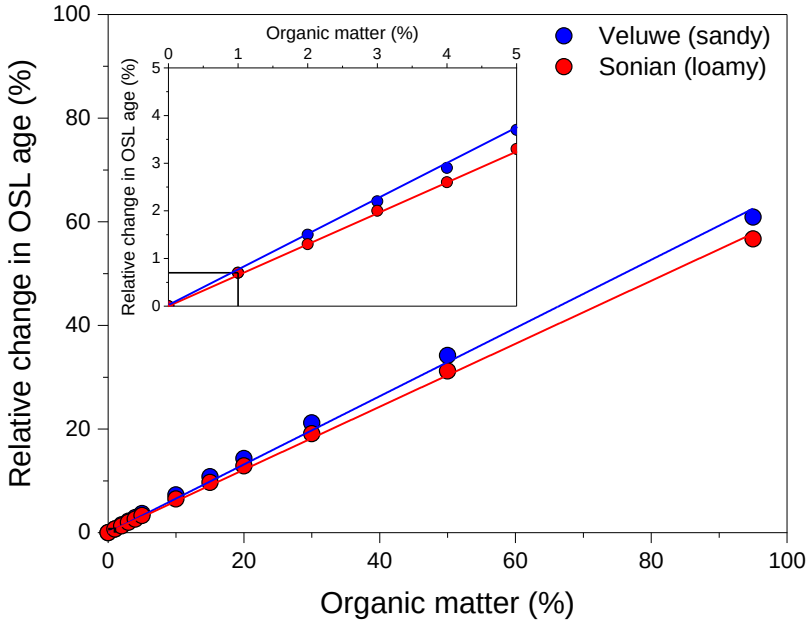

Figure 6.3: Simulated effect of organic matter on an OSL age for a sample from a relatively low (sandy) and high (loamy) dose rate environment (samples GLL-194350 and GLL-184301, respectively). The solid lines represent a linear fit to the data. The inset shows the effect over 5% of organic matter.

(iii) The event dated

Wintle and Murray (2006) reiterated that, in comparisons between luminescence and other dating methods (such as ^{14}C and archaeomagnetism), one should note that the different techniques may use different materials (e.g. organic material and minerals) to date events that were not necessarily synchronous (e.g. end of carbon exchange and shielding from heat (and/or light)). The methods differ in the physical mechanisms that are exploited for dating, the way and scale of sampling, subsequent analysis and age calculation. In all cases, it is assumed that the material that is used for dating can be confidently associated with the event of interest, i.e. the last firing event. The different clocks have different inherent limitations and possibilities, and so results obtained from a multi-method approach can be mutually informative (see e.g. Chapter 5 as to how OSL might potentially inform archaeomagnetic dating) as well as informative on particular production and preservation processes of the investigated relic features. To this respect, it should be noted that, at least for the features and sites investigated here, there is no macroscopic evidence for repeated use. Repeated use of a site for charcoal production, e.g., is likely to result in multiple layers of charcoal. This has been observed

in mountainous areas where charcoal production is done on artificial terraces (e.g. Knapp et al., 2015); these require larger constructional effort and are therefore preferentially re-used.

6.1.2 Precision

The total uncertainty on the OSL ages is typically in the range of 7-18%. It is composed of contributions from random and systematic sources of uncertainty (Aitken, 1985; Aitken and Alldred, 1972). A detailed uncertainty budget for two representative samples is summarized in Figure 6.4.

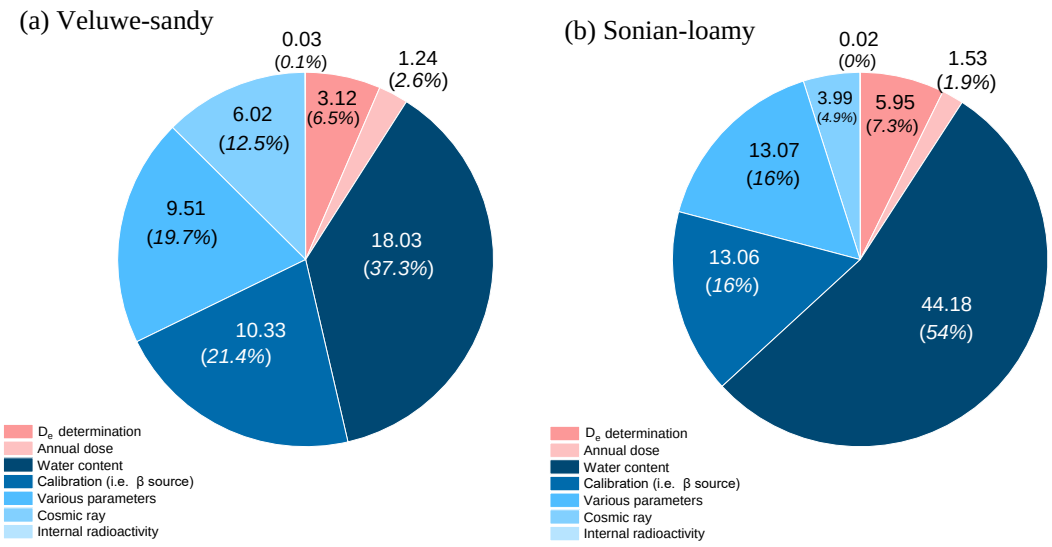

Figure 6.4: Uncertainty budget for a sample from a relatively low (sandy) and high (loamy) dose rate environment (samples GLL-194348 and GLL-184301, respectively). The values in *Italic* and between brackets indicate the relative contribution of each source of uncertainty to the total uncertainty. Random and systematic sources of uncertainty are indicted by shades of pink and blue, respectively.

Systematic sources of uncertainty are the main contributor to the total uncertainty, of which the most important are water content and cosmic radiation. The effect of water content on OSL age has been discussed and is illustrated in Figure 6.2. In most OSL-dating studies, the contribution of cosmic rays to the total dose rate (and hence the uncertainty) is usually small. Its relative importance increases, however, with decreasing burial depth and/or concentrations of naturally occurring radionuclides in the sedimentary environment (Figure 6.5).

As such, the cosmic dose rates were especially important for the near-surficial (<30 cm depths) samples collected from the dark charcoal rich layers in Zoersel Forest and

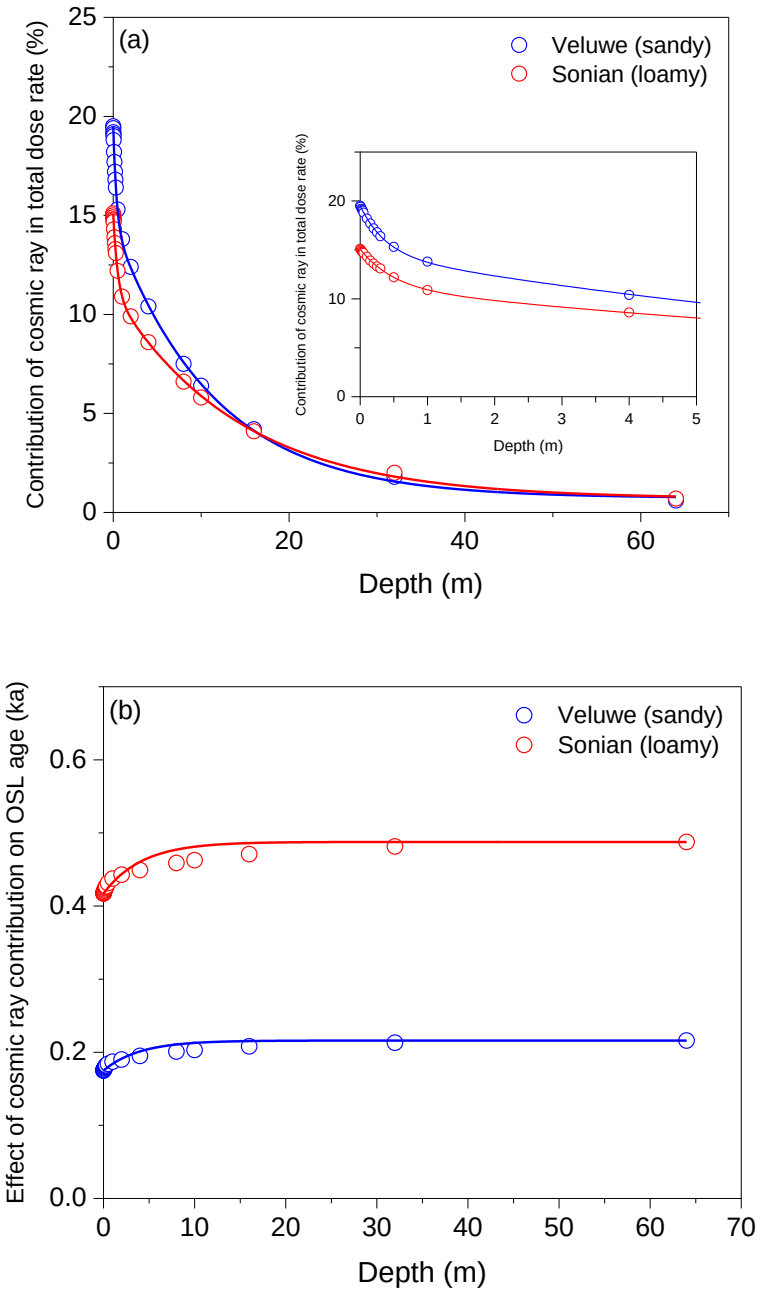

Figure 6.5: (a) Relative contribution of cosmic radiation to the total dose rate as a function of depth for a sample from a relatively low (sandy) and high (loamy) dose rate environment (samples GLL-194350 and GLL-184301, respectively). The inset shows the relative contribution in the upper 150 cm of sediment. (b) Simulation of the change in the OSL age (ka) that was obtained for these samples (open circles) for varying scenarios of burial depth (and hence decreasing cosmic ray dose).

the Veluwe, with fractional contributions to the total dose rate in the range of 17-42% (see §3.5.2.2 and §4.4.3). Random sources of uncertainty are those related to the measurements (i.e. determination of D_e and specific radionuclide activities). They are in the range of 1-11%, and in between 1-8% if only those samples are considered for which the analysis of the D_e-distributions did not hint at external sources of scatter (e.g.

owing to mixing). Given that all analytical data were obtained using the same methodology and instrumental facilities, it is reasonable to assume that at least some sources of systematic uncertainty are shared between samples. While this is straightforward with respect to beta-source calibration (D_e-determination), it is more complex with respect to other parameters (given the fractional importance of each component, which is variable). Nevertheless, to a first approximation and at least for samples collected from the same locality, one could assume that uncertainties associated with the calibration of the gamma-ray spectrometer, conversion and attenuation factors, and internal and cosmic dose rate are also (largely) shared. If one extends this to include uncertainties on time-averaged water content, one ends up with random sources of uncertainty only.

To compare OSL with independent age information (such as ^{14}C-dates), it is important to take into account the total uncertainties. In this study, the total uncertainties associated with the OSL and radiocarbon (^{14}C) ages are generally comparable for most pre-1650 CE features, but for post-1650 CE features, OSL dating can provide better precision with an average reduction in uncertainty of ~ 50%. This is exemplified by feature M4 in Sonian, which demonstrates an OSL age estimate of 1810 ± 57 years and a radiocarbon age estimate of 1807 ± 113 years, highlighting the increased precision offered by OSL dating. When comparing luminescence ages, systematic sources of uncertainty are (largely) shared by the features, so that they can be left out. By using random uncertainties as the minimum precision limit, it is possible to distinguish between features and phases with a significantly higher time resolution. As illustrated in Chapter 5 (Ninove), this precision can be as good as 1-3%, i.e. a decadal or multi-annual timescale for features from the last few centuries.

6.1.3 Possibilities and limitations

The heated features investigated here are less well-defined compared to, e.g., bricks or pieces of pottery. Unless fully excavated, for example, their dimensions are unknown, with potential implications as to sampling and the degree of resetting. Also, they represent systems that are not as closed, in that they are much more prone to all forms of disturbance at (sub)microscopic scales following the event that is targeted. In short, the heated sediments associated with relic kilns and hearths pose additional challenges compared to the heated features more commonly investigated using luminescence dating. Finally, unlike in luminescence dating of unheated sediments (to derive

sediment deposition chronologies), homogeneous but incomplete thermal resetting cannot be detected by examining the distributions of D_e.

In general, this work used facilities and procedures that are widely adopted in the OSL-dating of sand-sized sedimentary quartz (with the most likely exception of that of single-grains, as relatively few labs have access to the required instrumental facilities). The same sampling tubes were used for all case studies. Materials and layers that were most likely affected by past heating (e.g. the dark layers rich in charcoal, and/or brick-colored sediments) were targeted for sampling. In case of doubt, the inner material of sampling tubes was processed in increments (e.g. Chapter 5). The procedures for sample preparation and the subsequent range of analytical measurements can be considered standard as well. Testing such a more or less-standardized approach was considered important, given that OSL-dating is complex and costly (although the latter can be subject to debate).

Based on the results obtained in this work, standard procedures do not seem to compromise accuracy and precision. Accuracy is limited by the usual factors (resetting, mixing/disturbance etc.). The discrepancy between the OSL and ^{14}C ages for the kilns at Zoersel Forest is not understood at present, although it should be noted that apparently accurate ages were obtained for at least three of the investigated kilns. Small-aliquot OSL-dating of multiple samples collected in well-defined stratigraphic panes, however, aids in assessing reliability. This is feasible as the linear part of the dose response curve can be exploited for generating large amounts of data (see § 2.4.2.5). Single-grain measurements were performed for a limited number of samples only. Nevertheless, for six out of the eight investigated samples, the difference between the ages obtained using small-aliquots and single-grains is significant, while for the other half it is small to insignificant. This dataset is too limited to be conclusive as to whether or not analysis of single grains should be performed more routinely for this type of features.

At the very least, the combined dataset shows that accurate OSL ages can be obtained. For pre-1650 CE features, the precision is comparable to that of ^{14}C-dating and the two methods can be considered as complementary. If charcoal is present, it is probably more likely that the community of "users" will prefer ^{14}C-dating over OSL, as the former is well-embedded and probably better known. The implicit assumption here, however, is that one has indeed some prior knowledge on this pre-1650 CE age of the features of

interest. It is especially for post-1650 features that OSL dating offers significant advantages as the results are considerably more precise.

As discussed in previous subsections, numerical ages for post-1650CE features can be obtained with a precision of 8 – 10 % (1 sigma total relative uncertainty), i.e. with a time resolution of some tens of years. For some studies, however, it is also of great interest to assess whether comparable features (and the activity they represent) date from a single phase, or from multiple successive phases. In such cases, relative age relationships are relevant and the data obtained in this work show that these can be accomplished to within a few % (i.e. $\leq$ 10 years, for post-1650 features; 1 sigma). It can be noted that the same holds for pre-1650 CE features, which can be considered as an argument in favor of a combined ^{14}C-OSL dating strategy for older relics as well.

6.1.4 Suggestions for future research

All in all, the results obtained in this work are considered as highly encouraging; the ones obtained for the kilns in Zoersel Forest, however, come with caveat emptor. As the proof is in the pudding, a very first and general suggestion for future research would be to apply the methodologies used in this work, to more of such features, from more sites. This should be feasible, especially for relic charcoal hearths, as for these ^{14}C-dating is, or has been, commonly performed. The following concerns more specific and methodological suggestions.

(i) The added value of single-grain analysis remains to be established. This is important given that this type of analysis requires dedicated equipment and instrument time, and is laborious. The single-grain analyses performed in this work confirms earlier finds in that most of the luminescence emitted and detected, originates with only a small portion of the grains (see §4.3.1.4; Figure 4.). One could consider reducing the size of the aliquot even further to, e.g., 1 mm diameter. Such aliquots would theoretically comprise some 10 sand-sized (125-180 µm) grains, of which subsequent analyses would approach that of single grains even more effectively and be less labour-intensive.

(ii) Following on the above, it would be of great interest to investigate whether the distribution of signal brightness can inform about the stringency of heating (resetting) experienced by the grains (§4.3.1.4; see also Adamiec, 2005; Moska and Murray, 2006; Lai et al., 2008; Zhang et al., 2022). Similarly, the range of variation in sensitivity occurring throughout a SAR measurement cycle could be informative (e.g. Murray and Wintle, 2000). If successful, this could provide an instrumental, stand-alone means for differentiating between sufficiently heated, partially heated and unheated materials (Appendix C2 provides a summary of our initial observations regarding brightness and sensitivity changes in this study).

(iii) In this work, a strategy for sampling the charcoal kilns was adopted that consisted of collecting multiple samples from well-defined horizontal and vertical panes, and from the top, base, and bottom of each layer. This is generally considered good field practice. Sampling tubes were used with a diameter of 5 cm, and a length of 15 cm. Given that a detailed excavation of each and every kiln of interest is virtually impossible for a range of practical reasons, and given the complexity of (usually unknown) vertical and horizontal thermal gradients, future sampling campaigns could consider using tubes with smaller dimensions. To optimize ideal sampling strategies for this type of features, it would be extremely useful to investigate “modern” analogues, such as for instance features resulting from actual/recent charcoal burning. Accompanied by monitoring temperatures and thermal gradients, and subsequent excavations and sampling (also for micromorphological analyses and assessment of soil physicochemical parameters; see further), such investigations would be highly informative on heat transfer and resetting mechanisms.

(iv) When studying such modern analogues and very young features, and hence dealing with very small to zero doses, it is suggested that care is taken to optimize signal to noise ratios, limits of detection are determined, and data are analyzed and interpreted accordingly.

(v) Some dosimetric issues might benefit from improvement, e.g. with respect to the potential effect of organic matter; others might be more difficult to tackle. To this respect, it could be of interest to investigate the potential of subtraction techniques (Aitken, 1985; Feathers, 2002; Li et al., 2008), which essentially aim at eliminating external dose rate contributions (and hence the associated uncertainties). Given the increased levels of precision that can be attained with the SAR protocol and the significant advances made in the dating of K-feldspar (e.g. Buylaert et al., 2012), this could be a track worthwhile pursuing.

(vi) The samples for which the largest discrepancy between their OSL and ^{14}C-age has been observed, are characterized by relatively low radionuclide concentrations. While this is merely an observation, future research could target other features in similar low dose rate environments (i.e. quartz-rich sandy substrates) to assess whether this apparent relation is coincidental, or not.

(vii) While our study focused on very fine and fine sand-sized quartz, other grain-size fractions (e.g. silt) and/or minerals (e.g. K-feldspar, plagioclase feldspar, zircon, undifferentiated polymineral fractions) may qualify as well. Sand-sized K-feldspar is attractive owing to its brightness and large internal radioactivity, implying greater precision and a reduced dependence on the external dose rate (and hence on e.g. moisture and organic content). It would then need to be investigated, however, to what extent these potential advantages are offset by anomalous fading, thermal transfer, incomplete resetting and intricacies in evaluating the dose rate. Similarly, zircon and apatite are of interest owing to their bright luminescence and high internal activity (much higher than for K-feldspar). Studies that seek to revisit these minerals using state-of-the-art luminescence techniques and methodologies would need to consider, amongst others, anomalous fading, dose-rate evaluation and practical complexities (e.g. mineral separation in dark room conditions). As mentioned higher (v), the potential of subtraction techniques, which involve the analyses of multiple grain-size and/or mineral fractions, remains to be explored as well.

(viii) In situations where it is of interest to establish relative age relationships between comparable features at a single site, the minimum precision limit is governed by random uncertainties only (as systematic sources of uncertainty are (largely) shared). It is then desirable to minimize these random uncertainties, which can - at least in principle - be accomplished by increasing the number of measurements of D_e (hence reducing the standard uncertainty on the mean D_e). Future luminescence studies on post-1650 CE features are encouraged to exploit the linear part of the dose-response curve to generate such sufficiently large datasets without the need for additional instrument time. This also implies that the rate-limiting steps in obtaining OSL-ages over this time/dose range would relate to sample-preparation and dose rate determination. Therefore, the time saved in measurement primarily applies to the absence of radiation exposure for an extended period. For instance, utilizing this approach with a finger calculator can reduce a two-day measurement to just six hours.

(ix) Recent studies (e.g., Fouédjeu et al., 2021) have demonstrated the potential of dendrochronological analysis of charcoal fragments. At least in principle, this approach can date post-1650 CE features with an annual time resolution. Future chronometric studies of charcoal kilns would thus benefit from this approach, both in terms of methodological development and application. In practice, however, it may not always be possible to include dendrochronology in precisely dating the old phases due to the absence of charcoal fragments

(x) Furthermore, the study by Fouédjeu et al. (2021, amongst others), also highlights the potential of an integrated and interdisciplinary approach that combines archaeological, micromorphological, soil science and dendrochronological analyses to better-assess the chronology, architecture and operational modes of post-1650 CE charcoal production. In addition, micromorphological- and microstratigraphic analyses could provide deeper insights into the processes of bio- and pedoturbation and their effects on the preservation and dating of the relict charcoal kilns.

(xi) This study focused on heated sediments associated with relic hearths and kilns, with an emphasis on those used to produce charcoal. At some locations charcoal production can be related to pre-industrial iron production (e.g. Deforce e al., 2021a). From that perspective, the work presented here could be extended to burnt sediment associated with roasting places (Ghyselbrecht, 2018; see Appendix C).

Finally, there is still considerable interest in, and demand for, accurate and precise dates for bricks and tiles (essentially consisting of burnt sediment). Pivotal work by Bailiff (2007) already showed that luminescence dating is highly suited for addressing such type of chronometric questions. The finds presented in this work indirectly corroborate this and might perhaps contribute to incentives towards revisiting luminescence dating of bricks and tiles. If so, such research could seek to incorporate recent insights and developments in surface exposure and burial dating using luminescence techniques (Sohbati et al., 2012, 2015; Souza et al., 2019). This is a potentially highly exciting new avenue of luminescence research.

6.2 Conclusions

This study aimed at investigating the potential of quartz-based SAR-OSL dating for application to burnt sediments associated with either charcoal burning, or domestic activities (cooking and/or heating).

Accuracy is evaluated by comparing the OSL-dates with independent age information (essentially ^{14}C-dates) for features that pre-date 1650 CE. It is concluded that OSL dating can yield accurate ages. The precision is comparable to that of ^{14}C, implying that the chronometric methods are complementary.

^{14}C-dating for post-1650 CE features appears accurate, but lacks precision. For features dating from the last few centuries, OSL-dating can be as accurate as ^{14}C-dating, but is significantly more precise. In general, it is concluded that – for this period of time – OSL-dating offers an unprecedented temporal resolution: this for establishing numerical chronologies (i.e. a date in years CE) and even more so for establishing relative or “floating” chronologies; at least in principle, the latter holds for pre-1650 CE features. Apart from a range of potential applications, another implication is that

OSL-dating may be able to provide information for other chronometric techniques, such as archaeomagnetic dating, in terms of sampling strategies and sample selection, as well as calibration curves. Additional strengths of OSL-dating are that it is less material specific (as it uses minerals that are common in the sedimentary environment) and does not require calibration.

Appendix A

A.1 Luminescence measurement facilities

All measurements in this study were made with either a Risø TL/OSL-DA-12 or TL/OSL-DA-15 reader (Figure A.1.1). Both systems allow fully automated measurement sequences to be run for quartz, feldspar or polymineral samples. The notations "DA-12" and "DA-15" refer to the original models, which were refurbished and upgraded throughout the years, making them essentially comparable to the current model "DA-20".

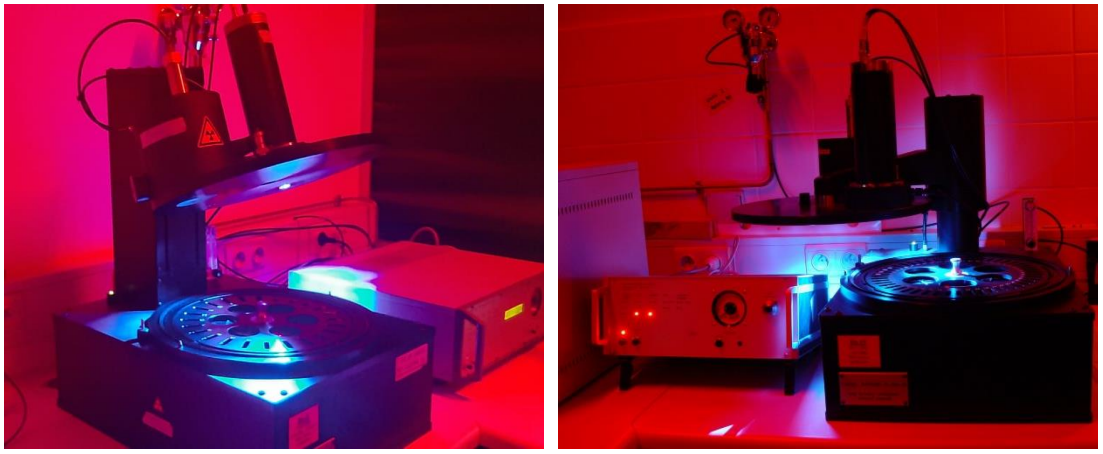

Figure A.1.1: Illustrative picture of the DA-12 (left) and DA-15 (right) reader in the Ghent Luminescence Laboratory.

The basic features of both readers are the same, as depicted in Figs. A.1.2. Essentially, the reader consists of a light-tight sample chamber that houses a turntable in which the aliquots can be placed. The turntable positions the aliquots above a lift mechanism, which raises the samples into the measurement position. The lift mechanism contains a heating element which allows reproducible heating (e.g. for preheating, measuring OSL at an elevated temperature, or recording thermoluminescence). The luminescence signals emitted by the samples are optically filtered and detected using a photomultiplier tube (PMT). In this study, all signals were detected through 7.5 mm of Hoya U-340 filter.

Each reader is equipped with an irradiation unit housing a 40mCi $^{90}Sr/^{90}Y$ beta source. During the measurement sequence, the aliquots are sequentially moved between the measurement/heating position and the irradiation position (Figure A.1.2B). When

irradiation takes place, the active side of the source faces downward towards the aliquot positioned precisely beneath the irradiation unit.

The source is mounted in a rotating stainless-steel wheel that is activated pneumatically; it takes 0.11 seconds for the source to rotate 180° (e.g. from the closed to open position; https://www.fysik.dtu.dk/english/research/radphys/research/radiation%20instruments/tl_osl_reader/manuals; Guide to "The Risø TL/OSL Reader"). This time offset is constant for all irradiations and is negligible for long radiations. It can become significant, however, when equivalent dose determination involves the use of very short irradiation times (e.g. < 2 s). It can be compensated for by subtracting the offset from the programmed irradiation time, or avoided by either exploiting the linear part of the dose response curve or through the use of dose reduction kits (both involving longer irradiation times). Both beta sources were calibrated using in-house developed calibration quartz (GLL Cal-Q). The source strengths are 0.0551 ± 0.0003 Gy/s and 0.0761 ± 0.0003 Gy/s for the DA-12 and DA-15, respectively; these values apply to the reference date of 19/09/2022, and 90-125 μm quartz grains mounted on the inner 8 mm of stainless-steel discs (diameter = 9.7 mm, thickness = 0.5 mm).

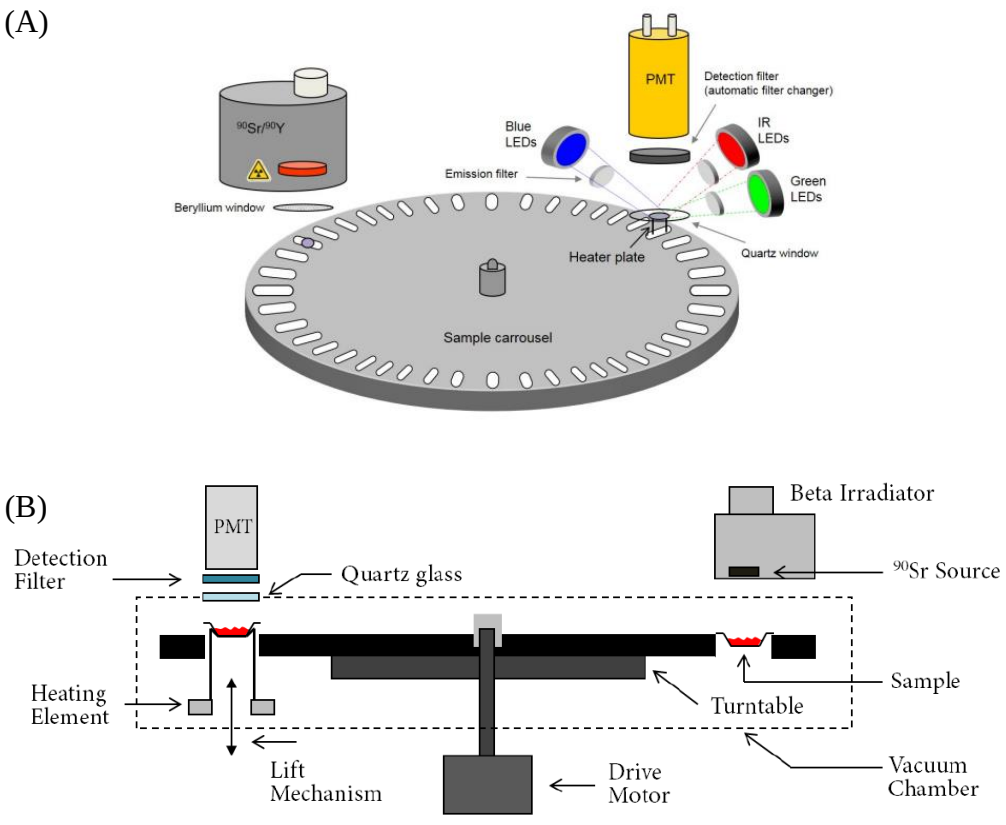

Figure A.1.2: (A,B) Schematic drawing of the Risø TL/OSL reader (fyzik.dtu.dk).

The main difference between the DA-12 and DA-15 systems concerns the specifications of the optical stimulation and light detection systems. The DA-12 is equipped with a bialkali EMI 9235QA PM tube. The optical stimulation unit consists of an array of 21 IR LEDs emitting at 875 nm and 28 blue LEDs emitting at 470 nm (Bøtter-Jensen et al., 2003), delivering a power (at 100%) of approximately 120 mW/cm^2 and 35 mW/cm^2 at the sample position, respectively (Sørensen, priv. comm., 2023). The DA-15 is equipped with the automated Detection and Stimulation Head ("DASH"). The PMT is an Electron Tube PDM 9107-CP-TTL. The optical stimulation unit contains two blue LEDs (470 nm, $84mW/cm^2$), two green LEDs (525 nm, $44mW/cm^2$) and three infrared LEDs (850 nm, $160mW/cm^2$) (Lapp et al., 2015; Sørensen, priv. comm., 2023). Although no use was made of it in this work, the DASH is also equipped with an automated detection filter changer.

For more information on the luminescence measurement facilities, we refer to Bøtter-Jensen et al. (2010) as well as https://www.fysik.dtu.dk/english/research/radphys/research/radiation-instruments/tl_osl_reader.

A.2 Low-background gamma ray spectrometry

The gamma-ray spectrometric analyses were performed using a Canberra (now Mirion Technologies) extended-energy range high-purity p-type coaxial Ge detector (XtRa HPGe), in a low-background lead castle. The data were acquired using a Canberra DSA-2000 Digital Spectrum Analyzer and Genie^{TM} 2000 software. The gamma-ray spectrometric setup is nick-named "Bertha" and, apart from the MCA, has not changed over the past 25 years (Fig. A.2.1).

All measurements were carried out on dried (at 110°C, until constant weight), pulverized and homogenized material, which was cast in wax to prevent radon loss and to ensure a reproducible counting geometry (Murray et al., 1987; De Corte et al., 2006). The resulting "wax pucks" have a cylindrical geometry (diameter ~ 6.4 cm) and, depending on the amount of material available, can have a height of ~ 1 cm, 2 cm or 4 cm. When preparing the pucks, it was aimed at maintaining a sediment/wax weight ratio of 70/30. Following preparation, the samples were stored for at least 1 month before being measured on top of the detector.

The system was calibrated for the aforementioned geometries in a relative way using the radiometric reference materials RGK-1, RGU-1 and RGTh-1 issued by the IAEA,

Vienna (IAEA, 1987). These standards were measured at regular intervals to verify calibration and instrument stability. The in-house produced secondary standard "Volkegem loess" (De Corte et al., 2007) was measured as well.

All spectra were processed using Hypermet-PC (Fazekas et al., 1997). Corrections for different detection efficiencies between samples and calibrants were made using SOLCOI (KAYZERO version 5A / SOLCOI 2006). For the samples from silty or loamy (Sonian Forest & Ninove – Chapters 2 & 5) and sandy substrates (Veluwe & Zoersel – Chapters 3 & 4) the elemental compositions of "Volkgem loess" and "Ossendrecht sand" (Hossain, 2003; his Table 5.1) were used in the calculations. The following daughter nuclides (and photo-peaks) of the ^{238}U decay series were considered: ^{234}Th (E_γ = 63.3 keV), ^{214}Pb (E_γ = 295.0 keV and 351.9 keV), ^{214}Bi ($E\gamma$ = 609.3keV and 1764.5 keV) and ^{210}Pb (E_γ = 46.5 keV); ^{226}Ra was also considered using the "method of choice" suggested by De Corte et al. (2005). For the Th decay series these were: ^{228}Ac (E_γ = 338.3 keV, 911.2 keV and 969.0 keV), ^{212}Pb ($E\gamma$ = 238.6 keV) and ^{208}Tl ($E\gamma$ = 583.2 keV and 2614.5 keV). The K concentration was obtained using the ^{40}K gamma line at 1460.8 keV. The unweighted average of the results obtained using the photo-peaks of ^{226}Ra, ^{214}Pb and ^{214}Bi (± 1 standard error, adopting the largest of observed and expected uncertainties) was used to calculate the specific activity of (and hence the contribution to the dose rate by) ^{226}Ra; for ^{232}Th, the same was done using all daughters and peaks. It can be noted that the gamma-spectrometry system is calibrated for concentrations as expressed in mg/kg (IAEA, 1987); conversion to specific activities (Bg/kg) uses the data tabulated by Adamiec and Aitken (1998).

Figure A.2.1: Illustrative photograph of Bertha in the Ghent Luminescence Laboratory.

Appendix B

B.1 Kiln types

The earliest indications of charcoal production can be traced back to the late Iron Age (800 BC-57 BC) or the early Roman period (57 BC-402 AD; Hirsch et al., 2017; Deforce et al., 2018, 2020). Prior to approximately 1200-1300 CE, charcoal production predominantly occurred in small pits known as pit kilns (see Figure B.1.1,2).

Figure B.1.1: Making charcoal in a pit kiln (Bert, 2007).

Pit kilns were partly dug into the ground (Bert, 2007) and generally exhibit shallow rectangular outlines, with straight vertical sides, a flat bottom of the sediment and sides of the pit (Deforce et al., 2021). During the Early Middle Ages, a transition occurred towards circular pit kilns, which became predominant during the High Middle Ages (Deforce et al., 2018; Figure B.1.2). In both rectangular and circular pit kilns, the firing process began with the creation of an open fire in a shallow pit. Once the fire was well-established, it was covered with leaves and/or earth to limit the oxygen supply. The carbonization process of the burning wood typically took in between 7 hours to 3 days to complete, after which the charcoal was retrieved from the pit (Deforce et al., 2021). Within the relics of these pits, a layer of charcoal of variable thickness is commonly observed. These kilns are also characterized by the absence of animal and human bone, ceramics, and other artifacts. The size of the pit kilns decreased gradually from the Roman period until around 1200-1300 CE, coinciding with a substantial increase in the usage of mound kilns which allow producing larger volumes of charcoal (Deforce et al., 2021). Pit kilns are no longer visibly recognizable in the contemporary landscape

and are typically only encountered by chance during archaeological prospection, trial trenches and excavations (Nelle, 2003; Groenewoudt, 2007; Deforce et al., 2018; Figure B.1.2). Consequently, our understanding of these older charcoal production kilns remains limited in terms of their historical context, evolution, and performance.

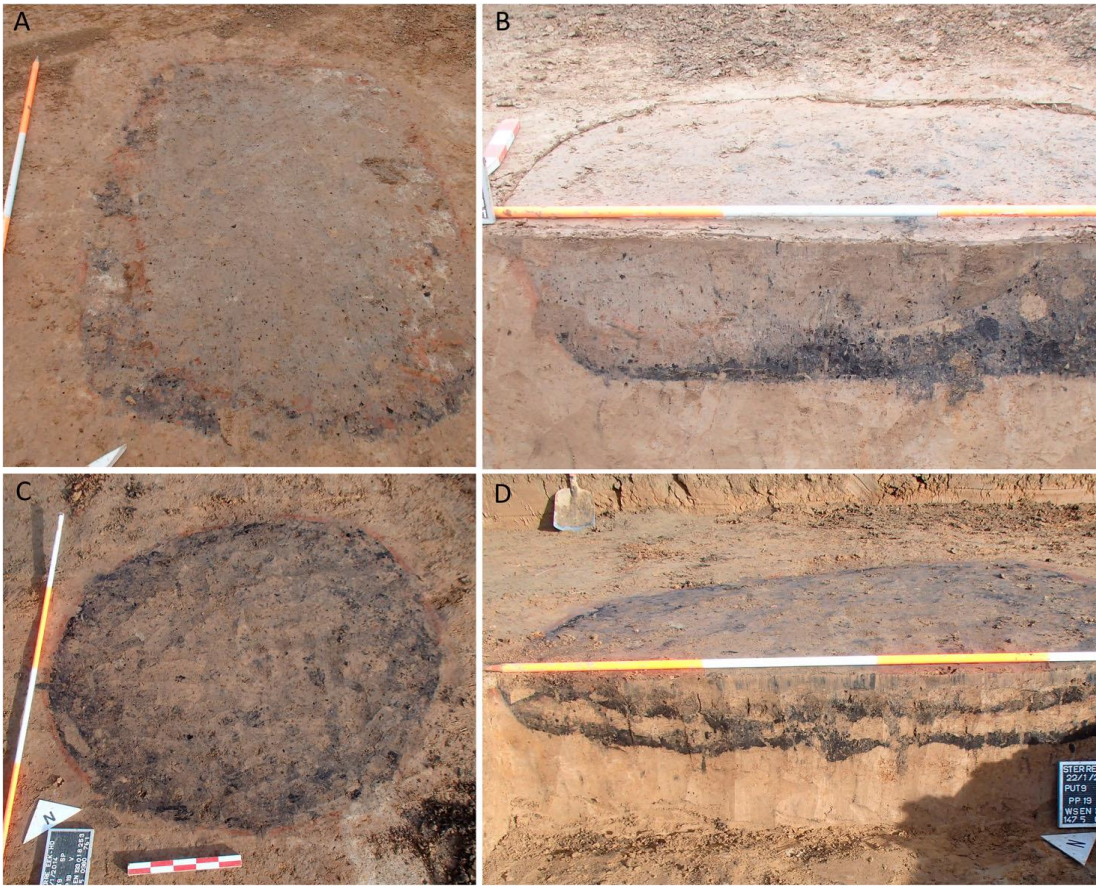

Figure B.1.2: Rectangular (A, B) and circular pit kilns (C, D); from Deforce et al. (2018).

From approximately 1200-1300 CE onwards, as mentioned, pit kilns were replaced by above-ground mound-shaped kilns for charcoal production (Figure B.1.3; Deforce et al., 2021). The construction process involved leveling the ground and clearing it of vegetation, debris, and any remnants of previous charcoal production (in the case kilns were reused). They were built by stacking wood in a dome or elongated shape, reminiscent of a large beehive (Figures B.1.3, B.2.1, in which a central chamber was created to serve as the focal point for the firing process. Also in this case, the wood was covered by e.g. soil and leaves to limit and control the oxygen supply. Sealable ventilation shafts and a central chimney were often part of the construction. Once the

firing process was completed, the kiln was allowed to cool down, and the charcoal was harvested.

Given that the mound-shaped kilns are situated above-ground, their remnants can form visible elevations in the landscape, which can be detected and mapped using e.g. LiDAR technology, modern geophysical techniques and/or field surveys. As a result, our current knowledge of past charcoal production is largely derived from these relics, and hence a period starting from around 1300 CE.

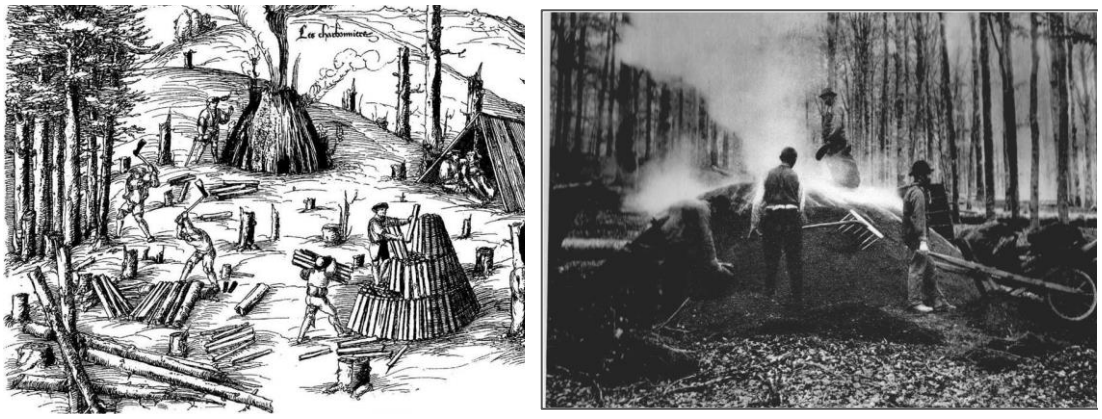

Figure B.1.3: (Left) Charcoal burning in 16th century in France (Bert, 2007, Ludemann, 2010). (Right) Charcoal production in a mound kiln in the forest near Anlier, southern Belgium (Deforce et al., 2020).

B.2 On mound-kiln structure and temperature regimes

Figs B.2.1a,b generally illustrate the mound kiln structure and operation. The duration of the charcoal burning process depends on the dimensions and size of the kiln, as well as the control of the air flow system that traps and regulates the heat inside the kiln. According to Hirsch et al. (2018), the pyrolysis process for charcoal production could take up to 20 days, varying based on the size of the charcoal hearth. Temperatures inside the hearth typically range from 350 to 600°C during the charring process. Localized areas near the chimney, on the other hand, can reach temperatures of up to 750°C. Although the temperature within a charcoal hearth fluctuates during operation, a temperature of around 550°C is consistently maintained for several days, depending on the size of the hearth (Hirsch et al., 2018).

In case of sandy soils, Hirsch et al. (2018) showed that the visible effects on soil mineralogy were primarily confined to the uppermost 2 cm, where temperatures of approximately 400°C were observed during the process of pyrolysis. These temperature conditions lasted several days. Soil organic matter combustion, which typically occurs

at temperatures above 220°C, penetrated to depths of about 5 cm. It is important to note that the heating source within the kiln was centrally located (Figure B.2.1a,b), and the temperature gradually decreased with depth within the stratigraphic layers. A set of controlled experiments by Aldeias et al (2016) showed that, for temperatures typically operated in a charcoal kiln, sediments as much as 10 cm directly below the heat source routinely reach temperatures of 200 °C after 6 hours. Their results also indicate that, in fires of longer durations, and given that temperatures below surface continue to rise long after the heat source is extinguished, higher temperatures can be reached at these depths.

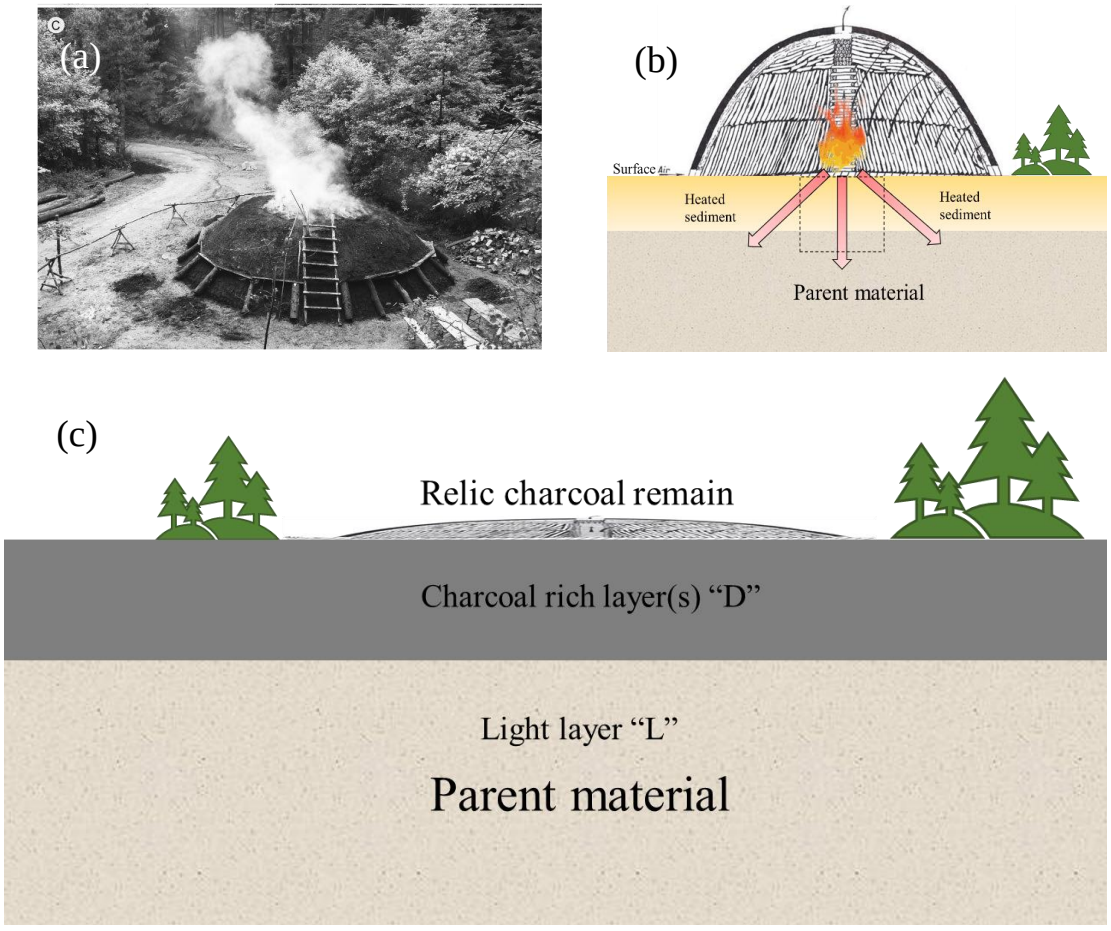

Figure B.2.1: (a) A mound charcoal kiln just after the start of the charring process (Ludemann, 2015). (b) Mound-shaped charcoal furnace combustion schematic. Logs were stacked on the ground to form a dome-shaped furnace. Airflow channels were considered for combustion and quality coal. To uniformly heat the kiln, the heat source was often placed in the middle. Heat propagation in all directions into the earth and kiln bottom layers decreases with depth, as shown by the arrows. The thermal source heated sedimentary materials nearby. (c) Depicts how relic charcoal mound kilns look in the field today. There are one or more layers with charcoal fragments, giving these layers a typical dark aspect. The charcoal-rich layers are most likely to have been highly exposed to heat. Going deeper in the stratigraphy would reduce the amount of heat and might have been insufficient for the luminescence signal to be reset.

B.3 Selection of kilns for sampling and sampling strategy

B.3.1 Site selection

The research question underlying this dissertation is essentially an experimentally driven one: can we use OSL to obtain meaningful age information for these features (*potential*)? The kilns investigated in this study were therefore primarily selected on (i) prior knowledge (more or less) as to their preservation at a location and (ii) the availability of independent age information, or the possibility to obtain this information within the timeframe of this work. In addition, we considered that heat might be transferred differently in loamy (Sonian Forest) and sandy (Zoersel Forest and the Veluwe) substrates. It should be noted that the features and sites studied here are of interest to the general public as well (i.e. from the perspective of heritage, and natural reserves for example).

B.3.2 (Ideal) sampling strategy

Following the above (section B.2), the ideal sampling strategy would target those materials that experienced the most stringent heat regime in the past. Essentially, one would thus prefer to take samples as close to the former main heat source (chimney) as possible, while making sure that the samples collected do indeed contain a sufficient amount of datable material (in this case quartz grains from the sediment). This is an ideal strategy, requiring that each kiln is excavated to some degree of detail. This may not be possible in practice for a variety of reasons, e.g. because excavations are extremely time consuming and expensive, and/or should be as minimally invasive as possible. In addition, such strategies may not aid in detailed diachronic research of charcoal production, which requires that large datasets can be obtained within a reasonable period of time.

This dissertation adopted a pragmatic approach, which also connects with its experimentally driven approach (see higher). We initially intended to target sediment samples immediately underlying the dark charcoal rich horizons. The rationale was that – given that the charcoal is there, which required some temperature for production – these sediments must have experienced some degree of resetting as well. At the same time, we were interested in seeing whether a sufficient amount of quartz could be extracted from these dark charcoal-rich layers as well. And – by extension – how the

whole process (including preparation, operation and harvesting of the kilns) could have affected e.g. underlying layers.

Based on the finds presented in this work, samples collected from the dark charcoal-rich horizons are more likely to yield meaningful OSL ages. Nevertheless, it is recommended that multiple samples (2, ideally 3) are taken in well-defined stratigraphic panes to check for consistency. Sampling should also include the parent material, preferably as far to the heat source as possible. It is acknowledged that, in this dissertation, OSL sensitivity was underexplored to indicate resetting mechanisms; such samples and investigations would aid in forwarding future research. We have used OSL-sampling tubes with a diameter of 5 cm. Other dimensions are possible and are at first instance governed by the thickness of the layer that preserves the event of interest, the spatial resolution at which one seeks to sample, and the lithological/mineralogical composition (e.g. a sufficient amount of quartz from the very fine to fine sandy-sized fraction). Given that the relic charcoal kilns are all located close to the surface, any visible effects of pedo-/bioturbation should be noted. We also recommend that, from each lithological unit, separate samples are collected for radionuclide analyses and porosity measurements. Especially the latter does not seem to be commonly adopted in the luminescence dating community, although it is a well-established technique in soil sciences.

The aforementioned findings are based on current knowledge, and further research (see Section 6.1.4) is expected to expand our understanding by investigating OSL sensitivity resetting mechanisms, exploring alternative sampling dimensions, documenting visible effects of pedo-/bioturbation, and including radionuclide analyses and porosity measurements from separate lithological samples.

B.3.3 Reuse or multiple use of kiln sites and potential disturbances

A Charcoal kilns in mountainous and hilly areas are often reused mainly due to the topography that limits the availability of flat areas, prompting the reuse of existing kiln sites. The practice of mixing charcoal leftovers and earth/soil from previous charcoal burning sessions rather than using freshly excavated soil to cover the kilns is known to be widely adopted. In these cases, the terrace where the kiln is situated, is typically cleared before each reuse, and the removed soil is recycled to cover the new wood pile. Consequently, each carbonization process generates a mixture of old and new

sediments and charcoals (Fouedjeu et al., 2021), which is likely to adversely influence OSL and radiocarbon ages.

The reuse of charcoal kilns in low-relief areas, such as Belgium and the Netherlands, is considered extremely rare based on previous research and our sampling observation, it is not entirely impossible. However it has been documented that the charcoal burners in these areas moved kiln sites as the tree line retreated during wood harvesting.

Mixing of sediments and fragments of old charcoal with newly produced charcoal would, as mentioned constitute a potential problem in reused kilns. Also, even during charcoal harvesting after one firing event, the possibility of disturbance between the upper (heated) and lower (less heated or unheated) sediment layers must be considered. To gain a comprehensive understanding of these processes, complementary studies such as archaeological investigations and micromorphology, which focus on soil characteristics, are recommended (Fouedjeu et al., 2021).

Appendix C – supplementary data

C.1 Roasting places – Sonian Forest

Initial work on the potential of OSL dating for application to charcoal kilns in the Sonian Forest was reported by Ghyselbrecht (2018). That study, however, also included an investigation of heated sediments associated with roasting places. These results are briefly summarized here.

Primitive metallurgical activity in the Sonian Forest is believed to have started around 800 BCE (Pierron,1905). The extraction of iron from iron-rich sandstone in the Brussels Formation began during the period of Roman occupation (Mees, 1989). Metallurgical furnaces were used to heat the sandstone, extracting the iron. Roasting places, i.e. heating the raw ore in open air, were employed to improve the ore's properties and concentrate the iron by removing water and organic materials. This roasting process also increased the ore's porosity and thereby enhanced its reducibility (Joosten, 2004).

Ghyselbrecht (2018) collected OSL samples from two metallurgical furnaces (R1 and R2; Figure C.1.1). From furnace R1, a sample was also collected from the underlying parent material that, on the basis of color, did not seem to be affected by heating. The samples were processed following exactly the same procedures, methods and equipment as outlined in this dissertation. For both features, radiocarbon ages were available as well.

The analytical data and OSL ages are summarized in Table C.1.1. Note that the dose rates were recalculated, adopting the same assumption for the time-averaged moisture content as used in Chapter 2. The results from ^{14}C-dating are summarized in Table C.1.2. Figure C.1.2 compares the ^{14}C-ages and the OSL ages obtained for the roasting places (red bars and open square; for the sake of completion, the data for the charcoal kilns are included as well (blue bars and open circles; see Fig. 2.10). The calibrated ^{14}C ages and the OSL-ages are expressed on the same age scale (Age CE) and cover 95.4% probability.

The OSL age obtained for furnace R2 underestimates the radiocarbon dates using remains of a Fagus sylvatica twig and overestimates the radiocarbon dates with Salix populus. The OSL age for furnace R1 underestimates the ^{14}C age.

Although the dataset is limited, the results hint at some difficulties with the independent age determination and/or the OSL-dating. At least from the perspective of OSL-dating,

this is somewhat surprising as the sediments that were sampled and dated, were clearly affected by heating, as indicated by the pronounced orange/reddish color (as in the case for the ovens/hearths in Ninove; see Chapter 5).

Figure C.1.1: Pictures illustrating the sampling of metallurgical furnaces R1 and R2. "M" samples collected for evaluation of the moisture content.

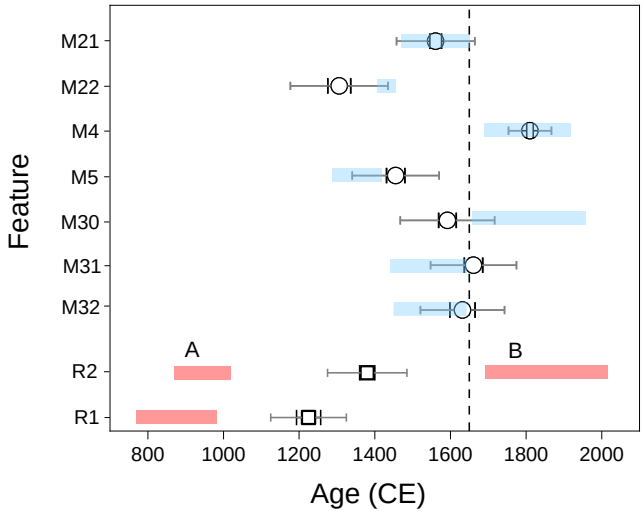

Figure C.1.2: Comparison between OSL and calibrated ^{14}C-ages for roasting places. The OSL data are represented by open squares; the associated random and total uncertainties are given by the black and grey error bars, respectively. The calibrated ^{14}C ages for the roasting places are represented as age ranges by the red highlighted boxes; the blue highlighted boxed refer to those obtained for the charcoal kilns; see §2.3.2, Fig 2.10. R2 (A) was radiocarbon dated using remains of a *Fagus sylvatica* twig, R2 (B) with *Salix populus*. All ages are expressed as ages Common Era (CE) and cover 95.45 % probability.

Table C.1.1: Specific radionuclide activities used for dose rate evaluation, estimates of past moisture content (F*W; F denotes the fraction of saturation corresponding to the assumed average water content during burial period and W represents the saturation content; Aitken, 1985), calculated dose rates, equivalent doses, optical ages and random (σ_r), systematic (σ_s) and total uncertainties (σ_{tot}). The total dose rate includes the contribution from internal radioactivity and cosmic radiation. The number of accepted aliquots/grains for D_e-determination is given in italics between parentheses in subscript. The uncertainties mentioned with the dosimetry and D_e data are random; except for the CE ages. The OSL ages (± 2 sigma total uncertainties) are expressed as ages Common Era (CE) in the last column.

Feature	*Layer*	*GLL-code*	*Depth*	*^{234}Th*	*^{226}Ra*	*^{210}Pb*	*^{232}Th*	*^{40}K*	*F*W*	*Total dose rate*	*D_e*	*Age*	*σ_r*	*σ_{sys}*	*σ_{tot}*	*Age CE*
			cm	*(Bq kg^{-1})*	*(Bq kg^{-1})*	*(Bq kg^{-1})*	*(Bq kg^{-1})*	*(Bq kg^{-1})*	*(%)*	*(Gy ka^{-1})*	*(Gy)*	*(ka)*	*(%)*	*(%)*	*(%)*	*(±2σ)*
R1	Burnt	160801	20	41 ± 3	37.2 ± 0.7	28 ± 2	36.9 ± 0.4	462 ± 5	13 ± 2	2.61 ± 0.03	2.06 ± 0.03 $_{(69)}$	0.79 ± 0.05	2.05	5.95	6.29	1225 ± 100
	Unburnt	160802	40	41 ± 3	37.2 ± 0.7	28 ± 2	36.9 ± 0.4	462 ± 5	13 ± 2	2.61 ± 0.03	24 ± 2 $_{(24)}$	9.20 ± 1.07	9.96	5.95	11.6	-7186 ± 2135
R2	Burnt	160804	20	30 ± 1	33.2 ± 0.3	33 ± 1	31.2 ± 0.3	384 ± 4	39 ± 6	1.91 ± 0.02	1.22 ± 0.02 $_{(68)}$	0.64 ± 0.05	1.61	8.12	8.28	1380 ± 105

Table C.1.2: ^{14}C data within 95% probability.

Sampling site	Sample code	Sample ID	Lab code	Uncal BP	Cal AD (2σ)
R1	16/ZO/R1-1	*Carpinus betulus*	RICH-23696	1136 ± 26	770-990
	16/ZO/R1-2	*Fagus sylvatica*	RICH-23693	1124 ± 26	778-990
R2	16/ZO/R2-1	*Fagus sylvatica*	RICH-24501	1114 ± 28	870-1020
	16/ZO/R2-2	*Salix/populus*	RICH-24497	203 ± 27	1690-2016

C.2 The effect of heating on luminescence characteristics

Quite a number of studies have shown that heating increases the luminescence sensitivity of quartz and that this increase is a function of both time and temperature (e.g. Bøtter-Jensen et al., 1995; Wintle and Murray, 2000; Jain et al., 2003; Moska and Murray, 2006; 2010).

In her study of the roasting places in Sonian Forest, Ghyselbrecht (2018; see Appendix C.1) observed that burnt samples generally displayed a higher sensitivity than the unburnt ones. When subjected to a test dose of 6.10 Gy, the burnt sample GLL-160801, e.g., exhibited a response that was 5 to 7 times higher compared to that of the unburnt sample GLL-160802 (Fig. C.2.1a). Ghyselbrecht (2018) also observed that the quartz extracted from burnt material exhibited a significantly higher degree of sensitivity change throughout a SAR measurement sequence (Fig. C.2.1b).

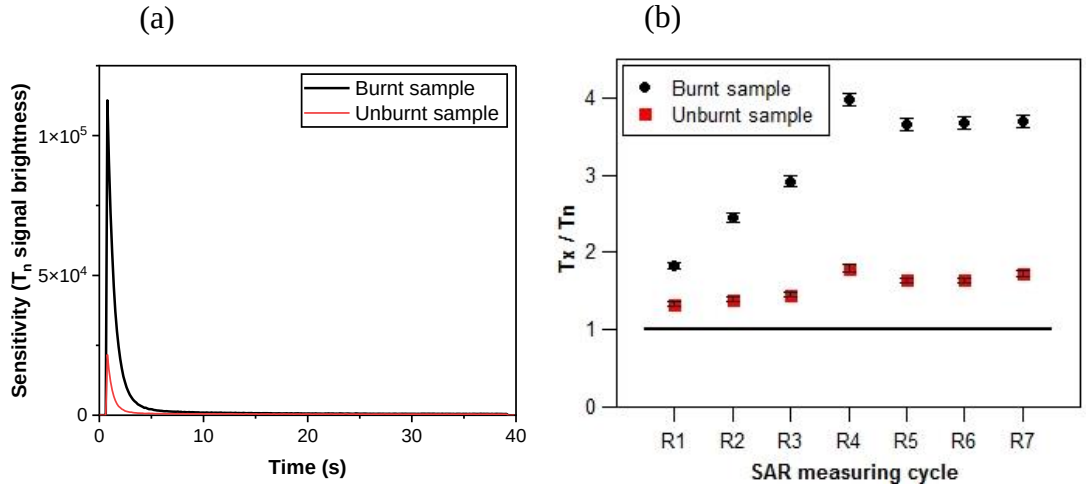

Figure C.2.1: (a) Comparison of T_n signal brightness for an aliquot of heated quartz (GLL-160801; represented by black curve) and unheated quartz (GLL-160802; represented by red curve). (b) Comparison of sensitivity changes occurring throughout identical SAR measurement sequences for an aliquot of heated quartz (GLL-160801; represented by black circles) and unheated quartz (GLL-160802; represented by red squares). The change is expressed as the ratio between the test dose signals for regenerative responses (T_x) and the test dose signal observed after measuring the natural OSL signal (T_n). The black line (eye guide) represents a ratio of unity.

This behavior was not further investigated in the frame of this dissertation. For the sake of illustration, however, Figs. C.2.2 and C.2.3 show the test dose signal brightness and variation in sensitivity change throughout a SAR sequence for samples collected from the "D" and "L"-layers in the relic charcoal kilns M31 and M32 (see Chapter 2 for details), respectively. Upon exposure to a test dose of 2 Gy, the heated sample in kiln

M31 displayed a response that was 4 to 7 times greater than the unheated samples (Fig. C.2.2). Conversely, there was no notable increase in sensitivity observed between the heated sample in kiln M32 and the deepest unheated sample, GLL184315 (Fig. C.2.2). However, a substantial increase of up to 5 times was observed when compared to the other unheated sample, GLL184313.

Surprisingly, one of the unheated samples in kiln M31 displayed a higher rate of sensitivity change, contrary to what was expected (i.e. GLL-184305). This anomaly was attributed to the peculiar behavior of one of the three measurement aliquots. Overall, the samples, including the aforementioned anomaly, exhibited similar degrees and variabilities in sensitivity change, making them indistinguishable from each other based on this criterion (see Fig. C.2.3).

For most of the samples collected at Ninove Doorn-Noord (Chapter 5), the inner material of the sampling tubes was extracted in intervals of about 1 cm. These are denoted as “X11” to “X13” or “X14”, with the former referring to the deepest part into the profile and the latter to the material closest to exposed surface (see §C3.2). For each of these intervals, a rough estimate of the ED was obtained at the initial stage of the investigations (“screening”), in order to select those in which the OSL clock was more likely to have been reset in the past. The results are summarized in Table C.2.1. In some of the samples (GLL-192808 and -13), a clear increase in ED with depth into the tubes can be observed. This may point at different degrees of resetting (e.g. thermal gradient) and/or simply reflect the sampling tubes penetrating into and thus sampling the original parent material.

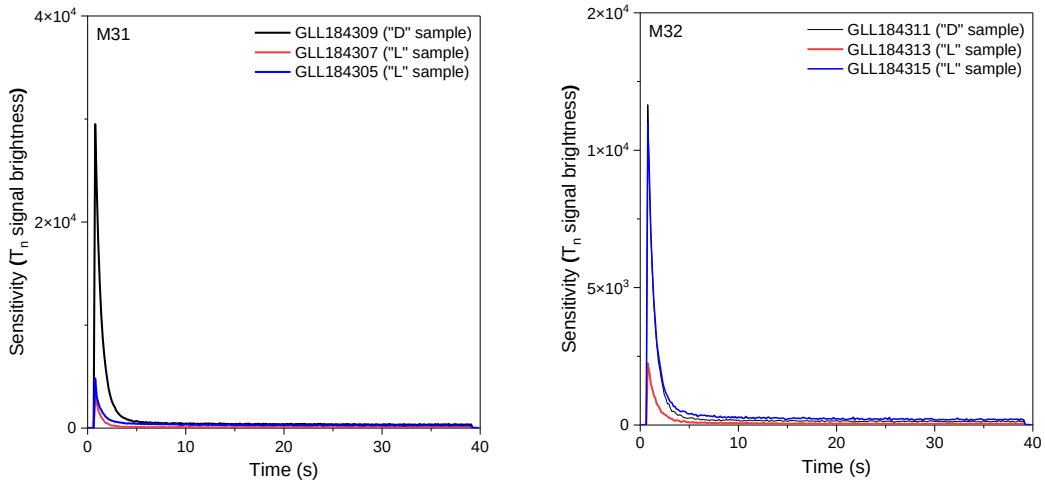

Figure C.2.2: Comparing net natural test dose signal brightness, this illustration showcases the sensitivity variations between heated and unheated samples in kilns M31 and M32.

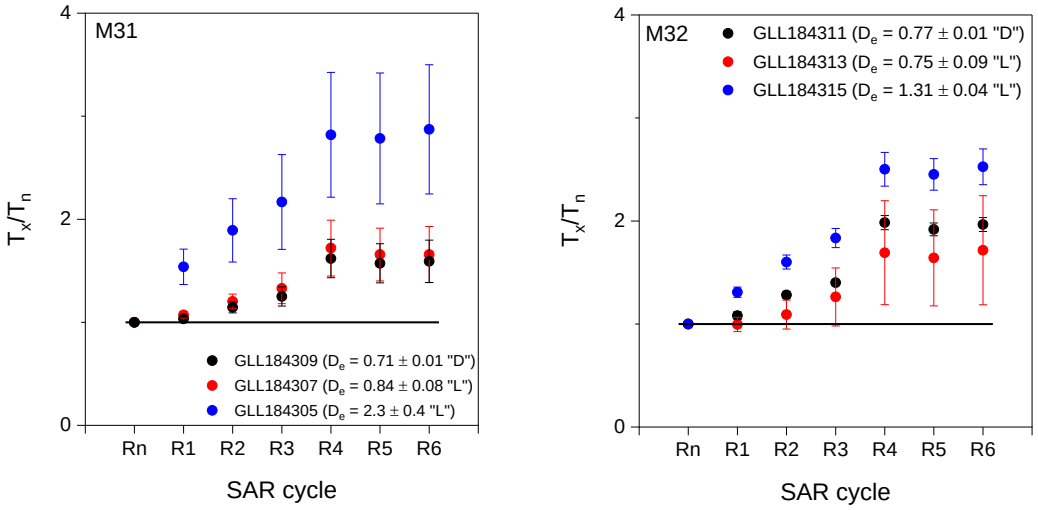

Figure C.2.3: Comparison of sensitivity changes occurring in identical SAR measurement sequences for "D" and "L" samples from relic charcoal kilns M31 and M32 (See Chapter 2). Each data points represents the average (± 1 standard error) of three aliquots. The black lines (eye guides) represent a T_x/T_n ratio equal to unity.

At the Ninove site, an opportunity arose to collect a sample from the parent material (unburnt sediment) for the purpose of comparing the brightness and signal sensitivity between heated and unheated materials. To investigate this characteristic in heat-exposed samples obtained from this site, a comparison was carried out by examining the brightness in T_n signals. We assessed the sensitivity of burnt and unburnt sub-samples. Our findings revealed that sub-sample GLL-192816-X13, representing the interval likely exposed to higher heating, consistently demonstrated higher sensitivity compared to the unheated interval (Fig. C.2.4a). Specifically, when exposed to a test dose of 2 Gy, the heated sub-sample GLL-192816-X13 exhibited a response that was 3 times greater than the unheated sub-samples. However, this observation did not hold true for the remaining samples (-08, -11, -12 and -13), as they exhibited similar levels of sensitivity and making them virtually indiscernible from one another. (e.g., Fig. C.2.4b).

Figure C.2.5 displays the sensitivity changes observed in identical SAR measurement sequences for the average of 2 or 3 aliquots from each subsample of samples GLL-192808 (Fig. C.2.5 a) and -13 (Fig. C.2.5 b). Sub-sample 192808-X13, located closest to the exposed surface, exhibits a gradual increase in sensitivity, while for the other two sub-samples, the sensitivity either decreases or remains constant. Also for the fractions extracted from sample GLL-192813, the sensitivity throughout the SAR-measurement

Table C.2.1: Equivalent doses (D_e's; ± 1 standard error) for the different intervals extracted from the inner material of the samples collected in Ninove (see Chapter 5). The subscripts indicate the number of aliquots used for calculating the D_e.

Subsample code	D_e (Gy)
192808-X11	27.80 ± 1.22 $_{(3)}$
192808-X12	17.94 ± 5.17 $_{(3)}$
192808-X13	2.97 ± 0.22 $_{(51)}$
192811-X11	0.67 ± 0.10 $_{(3)}$
192811-X12	0.76 ± 0.13 $_{(3)}$
192811-X13	0.73 ± 0.01 $_{(50)}$
192812-X11	0.65 ± 0.05 $_{(3)}$
192812-X12	0.67 ± 0.02 $_{(3)}$
192812-X13	0.69 ± 0.04 $_{(3)}$
192812-X14	0.73 ± 0.02 $_{(51)}$
192813-X11	11.30 ± 2.67 $_{(3)}$
192813-X12	1.39 ± 0.31 $_{(3)}$
192813-X13	0.67 ± 0.02 $_{(3)}$
192813-X14	0.72 ± 0.01 $_{(51)}$
192816-X11	0.78 ± 0.00 $_{(3)}$
192816-X12	0.83 ± 0.01 $_{(3)}$
192816-X13	0.797 ± 0.004 $_{(48)}$

sequences remains constant, excluding perhaps for the deepest slice for which the sensitivity may (slightly) decrease. For the three other samples (GLL192811, -12, and -16), no variation in ED as a function of depth into the sampling tubes/profile was observed (Table C.2.1). The equivalent dose, obtained in the same size and quantity (Table C.2.1), yields a consistent outcome, with no significant increase in sensitivity for sample -11, and up to the 3 times for samples -12 and -16 (Figure C.2.6). Although the characteristic change for samples 12 and 16 pertains to the deeper sub-samples, the uniformity of the equivalent dose suggests that all materials, from the surface to the depths, were likely subjected to uniform and homogeneous heating.

To explore the sensitivity characteristics further, a comparison was carried out by analyzing the variations in test dose signals at different regeneration doses for all the measured aliquots in equivalent dose measurements for burnt material (GLL-192807

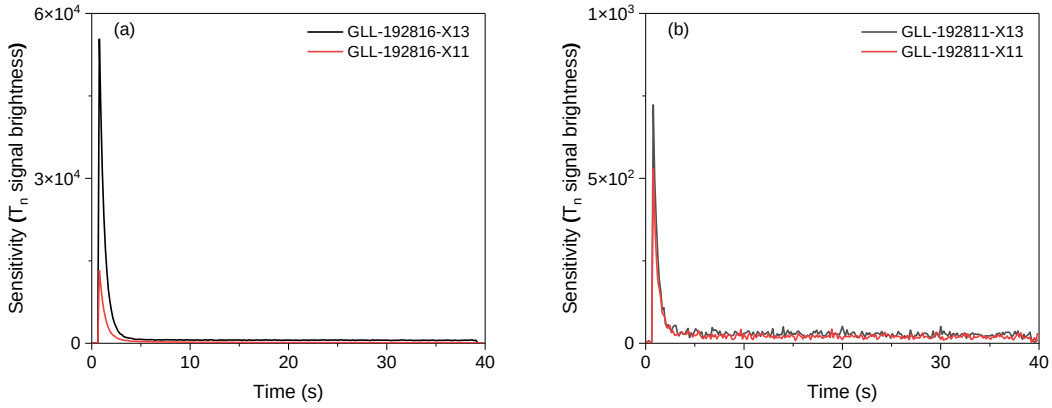

Figure C.2.4: This illustration demonstrates the differences in sensitivity between samples with varying degrees of heating, as observed through natural test dose signal brightness. In panel (a), the heated subsample GLL-192816-X13 exhibits higher sensitivity. In panel (b), sample GLL-192811 is identified as a candidate where sensitivity cannot be distinguished.

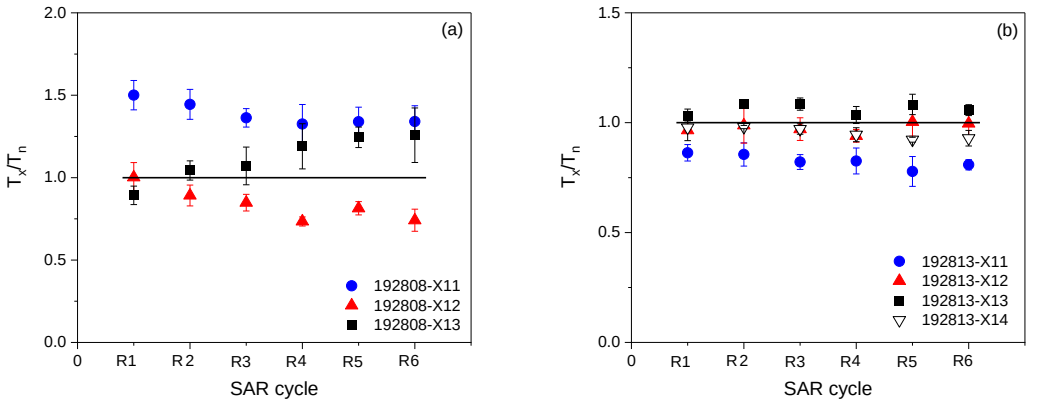

Figure C.2.5: Comparison of sensitivity changes in identical SAR measurement sequences of different subsamples from samples GLL-192808 and -13; each point is the average of 2 or 3 aliquots (details in the text and Chapter 5).

and -08) as well as unburnt material (GLL-192809) found in feature I960 (refer to Chapter 5; Table 5.1). All the measurements were carefully controlled for sample 08, and out of the 53 measurements conducted, 52 cases (98% of the measurements) exhibited the same behavior, indicating no significant change or extreme gradient. In the case of the unheated sample, mild downward sensitivity changes were observed, albeit to a lesser degree. Figure C.2.7 visually illustrates the observed sensitivity changes in identical SAR measurement sequences for the average of 2-3 aliquots for the three samples collected from feature I-960. Samples GLL-192807 and -08 (X13)

were collected from heated sediments associated with the hearth, while sample -09 was collected from (unheated) parent material. Contrary to our initial expectations, no significant difference was found between the heated and unheated sediments. However, there was a subtle upward trend observed in the sensitivity of the heated sample (192808-X13), and a slight downward trend in the results of the unheated sample.

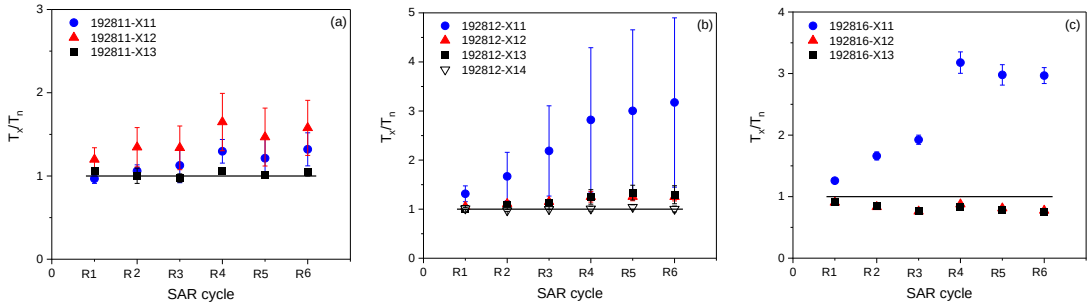

Figure C.2.6: Same as in Fig. C.2.5 for samples GLL-192811, -12 and -16; each point is the average of 2 or 3 aliquots.

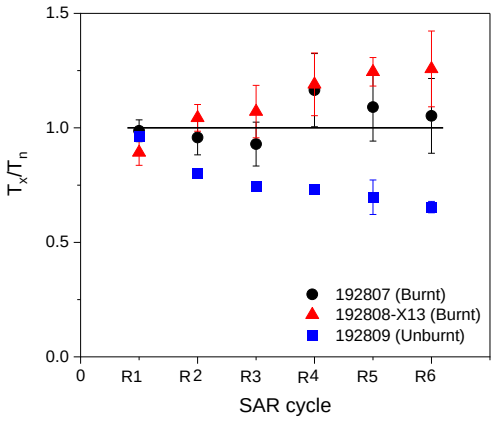

Figure C.2.7: Comparison of sensitivity changes occurring throughout identical SAR measurement sequences for the burnt and unburnt samples taken from I960 feature in Ninove (see Chapter 5).

C.3 Visual compilation of sampling in the Ninove Site

This section offers additional visual documentation of the sampling process and schematics associated with the X-slices in Ninove. The provided pictures provide further insight into the sampling methodology and serve to enhance the understanding of the X-slice analysis.

C.3.1 Feature I960

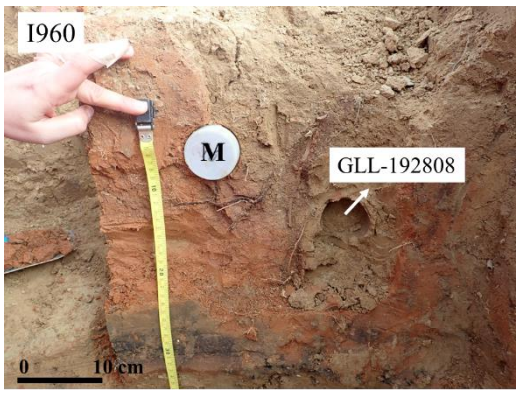

C.3.2 Feature I1006

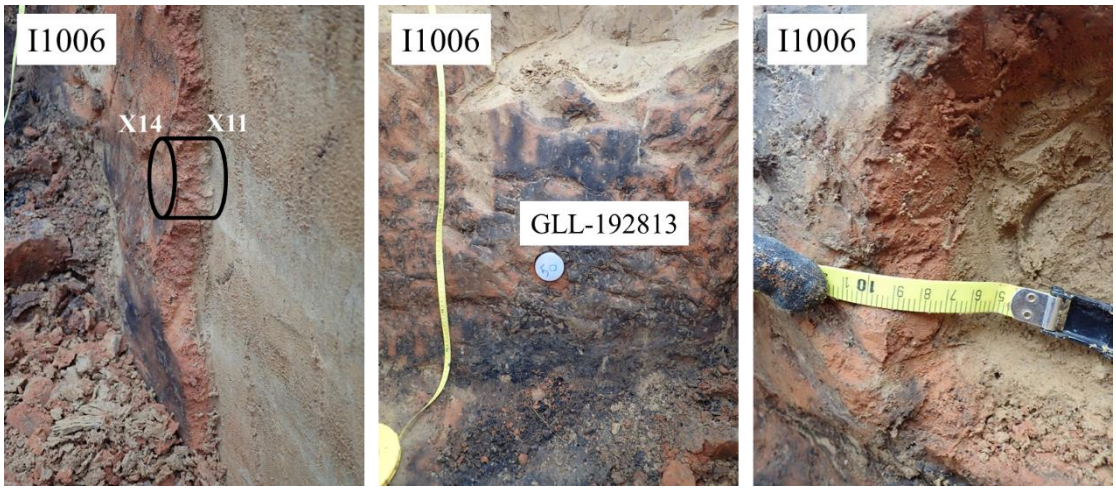

The schematic below illustrates the sampling method and the position of each sub-sample for samples GLL-192811 and GLL-192813 in relation to heated and unheated materials. In Table C.2.1, the equivalent dose values for sample GLL-192811 indicate that all the sub-samples were obtained from well-heated materials, distinct from the burnt sediments. However, for sample GLL-192813, the sub-samples located in the deeper part of the tube (X11 and X12) contained substances that were not thoroughly heated, resulting in non-reset signals. Consequently, the equivalent dose for these sub-samples is significantly higher, as shown in Table C.2.1.

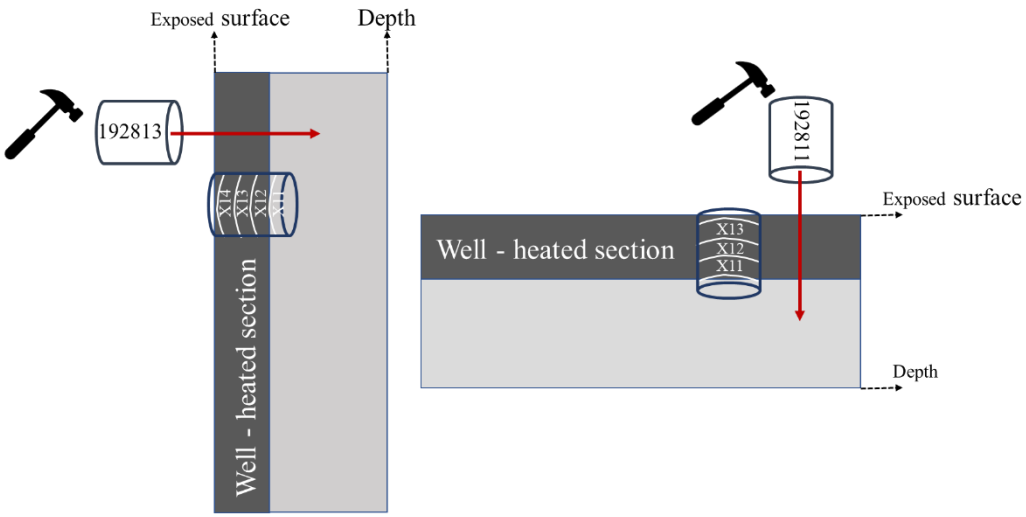

C.3.3 Feature I210

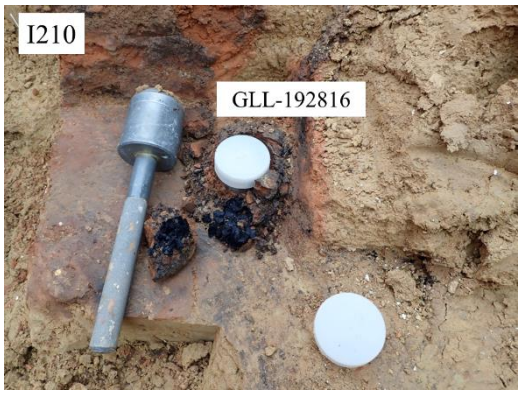

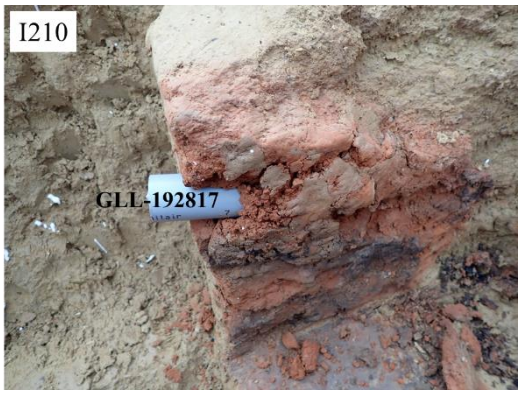

References

Adamiec, G. (2005). Properties of the 360 and TL emissions of the '110°C peak' in fired quartz. Radiation Measurements 39(1):105-110. https://doi.org/10.1016/j.radmeas.2004.03.006.

Adamiec, G., Aitken, M.J. (1998). Dose-rate conversion factors: update. Ancient TL, 16, 37-50.

Aitken M.J. (1976): Thermoluminescent age evaluation and assessment of error limits: revised system. Archaeometry 18: 233-238.

Aitken M.J. and Alldred J.C. (1972). The assessment of error limits in thermoluminescent dating. Archaeometry, 14, 257-267. https://doi.org/10.1111/j.1475-4754.1972.tb00068.x.

Aitken, M.J. (1985). Thermoluminescence Dating. Academic Press, London, 359p., ISBN: 0-12-046380-6.

Aitken, M.J. (1990). Science-based dating in archaeology. Longman, pp. 274.

Aitken, M.J. (1998). An introduction to optical dating. The Dating of Quaternary Sediments by the Use of Photon-Stimulated Luminescence. Oxford University Press, Oxford, 267p., ISBN: 0-19-854092-2.

Aitken, M.J., Moorey, P.R.S., Ucko, P.J. (1972). The authenticity of vessels and figurines in the Hacilar style. Archaeometry, 13, 89-141.

Aitken, M.J., Tite, M.S., and Reid, J. (1964). Thermoluminescence dating of ancient ceramics. Nature, 202: 1032-1033.

Aldeias, V., Dibble, H., Sandgathe, D., Goldberg, P., McPherron, Shannon, J.P. (2016). How heat alters underlying deposits and implications for archaeological fire features: A controlled experiment. Archaeological Science, 67, 64-79. https://doi.org/10.1016/j.jas.2016.01.016.

Armitage, S.J., and King, G.E. (2013). Optically stimulated luminescence dating of hearths from the Fazzan Basin, Libya: a tool for determining the timing and pattern of Holocene occupation of the Sahara. Quaternary Geochronology, 15, 88-97. https://doi.org/10.1016/j.quageo.2012.10.002.

Armitage, S.J., King, G.E. (2013). Optically stimulated luminescence dating of hearths from the Fazzan Basin, Libya: A tool for determining the timing and pattern of Holocene occupation of the Sahara. Quaternary Geochronology 15, 88-97.

Bailiff, I. K. (2007). Methodological developments in the luminescence dating of brick from English late-medieval and post-medieval buildings. Archaeometry, 49, 827-851. https://doi.org/10.1111/j.1475-4754.2007.00338.x.

Bateman, M. D. (2019). Handbook of Luminescence Dating. Springer.

Bateman, M.D., Buckland, P.C., Chase, B., Frederick, C.D., Gaunt, G.D. (2007a). The Late-Devensian proglacial Lake Humber: new evidence from littoral deposits at Ferrybridge, Yorkshire, England. Boreas, 37, 195-210. https://doi.org/10.1111/j.1502-3885.2007.00013.x.

Bateman, M.D., Boulter, C.H., Carr, A.S., Frederick, C.D., Duan, P., Wilder, M. (2007b). Detecting post-depositional sediment disturbance in sandy deposits using optical luminescence. Quaternary Geochronology, 2, 57-64. https://doi.org/10.1016/j.quageo.2006.05.004.

Bateman, M.D., Frederick, C.D., Jaiswal, M.K., Singhvi, A.K. (2003). Investigations into the potential effects of pedoturbation on luminescence dating. Quaternary Science Reviews 22, 1169-1176. https://doi.org/10.1016/S0277-3791(03)00019-2.

Batt, C.M., Brown, M.C., Clelland, S.J., Korte, M., Linford, P., Outram, Z. (2017). Advances in archaeomagnetic dating in Britain: New data, new approaches and a new calibration curve. Journal of Archaeological Science, 85, 66-82. http://dx.doi.org/10.1016/j.jas.2017.07.002.

Bayliss, A. (2009). Rolling Out Revolution: Using Radiocarbon Dating in Archaeology. Radiocarbon, 51(1), 123-147. https://doi.org/10.1017/S0033822200033750.

Beerten K., Heyvaert V., M.A., Vandenberghe D.A.G., Van Nieuwland J., Bogemans F. (2017). Revising the Gent Formation: a new lithostratigraphy for Quaternary wind-dominated sand deposits in Belgium. Geologica Belgica, 20, 95-102. https://doi.org/10.20341/gb.2017.006.

Benea, V., Vandenberghe, D., Timar, A., Van Den Haute, P., Cosma, C., Gligor, M., And Florescu, C. (2007). Luminescence Dating Of Neolithic Ceramics From Lumea Nouă, Romania. Geochronometria, 28, 9-16. https://doi.org/10.2478/v10003-007-0027-9.

Boosten, M., Van Benthem, M., De Bruin, B., Jansen, P. (2010). Excursie Hoog Soerense Bos: Symposium 'Dansende bomen en oude bossen – Cultuurhistorie en bosbeheer op de Veluwe'.

Bösken, J.J., And Schmidt, CH. (2020). Direct and indirect luminescence dating of tephra: A review. Journal Of Quaternary Science, 35, 39-53. https://doi.org/10.1002/jqs.3160.

Bøtter-Jensen, L., McKeever, S.W.S., Wintle, A.G. (2003a). Optically stimulated luminescence dosimetry. Elsevier Science, 374p., ISBN: 0-444-50684-5.

Bøtter-Jensen, L., Andersen, C.E., Duller, G.A.T., Murray, A.S. (2003b). Developments in radiation, stimulation and observation facilities in luminescence measurements. Radiation Measurements, 37, 535-541. https://doi.org/10.1016/S1350-4487(03)00020-9.

Bøtter-Jensen, L., Thomsen, K. J., and Jain, M. (2010). Review of optically stimulated luminescence (OSL) instrumental developments for retrospective dosimetry. Radiation Measurements, 45, 253-257. https://doi.org/10.1016/j.radmeas.2009.11.030.

Boudin, M., Van Strydonck, M., Van Den Brande, T., Synal, H.A., and Wacker, L. (2015). RICH - A new AMS facility at the Royal Institute for Cultural Heritage, Brussels, Belgium. Nuclear Instruments and Methods in Physics Research, Section B: Beam Interactions with Materials and Atoms, 361, 120-123. https://doi.org/10.1016/j.nimb.2015.04.006.

Bronk-Ramsey, C. (2009). Bayesian analysis of radiocarbon dates. Radiocarbon, 51(1), 337-360. https://doi.org/10.1017/S0033822200033865.

Bronk-Ramsey, C. (2010). OxCal Program v4.1.5. Radiocarbon Accelerator Unit, University of Oxford.

Buis, J. (1985). Historia Forestis: Nederlandse bosgeschiedenis. H&S Uitgevers: Utrecht.

Buras, A., Hirsch, F., Schneider, A., Scharnweber, T., van der Maaten, E., Cruz-García, R., Raab T., and Wilmking, M. (2020). Reduced above-ground growth and wood density but increased wood chemical concentrations of Scots pine on relict charcoal hearths. Science of The Total Environment, 717, 137189. https://doi.org/10.1016/j.scitotenv.2020.137189.

Buylaert, J.P., Jain, M., Murray, A.S., Thomsen, K.J., Thiel, Ch., Sohbati., R. (2012). A robust feldspar luminescence dating method for Middle and Late Pleistocene sediments. Boreas. https://doi.org/10.1111/j.1502-3885.2012.00248.x.

Buylaert, J.P., Murray, A.S., Huot, S., Vriend, M.G.A., Vandenberghe, D., De Corte, F., and Van den haute, P. (2006). A comparison of quartz OSL and isothermal TL measurements on Chinese loess. Radiation Protection Dosimetry, 119, 474-478. https://doi.org/10.1093/rpd/nci518.

Carrari, E., Ampoorter, E., Bottalico, F., Chirici, G., Coppi, A., Travaglini, D., Verheyen, K. and Selvi, F. (2017). The old charcoal kiln sites in Central Italian forest landscapes. Quaternary International, 458, 214-223. https://doi.org/10.1016/j.quaint.2016.10.027.

Carrari, E., Ampoorter, E., Verheyen, K., Coppi, A., Selvi, F. (2016a). Former charcoal kiln sites in Mediterranean forest areas: a hostile microhabitat for the recolonization by woody species. iForest - Biogeosciences and Forestry, 10, 136-144 . https://doi.org/10.3832/ifor1701-009.

Carrari, E., Ampoorter, E., Verheyen, K., Coppi, A., Selvi, F. (2016b). Former charcoal kiln platforms as microhabitats affecting understorey vegetation in Mediterranean forests. Applied Vegetation Science 19, 486-497. https://doi.org/10.1111/avsc.12238.

Chamberlain, E.L., Wallinga J., Reimann T., Goodbred Jr., S.L., Steckler, M.S, Shen, Z., Sincavage, R. (2017). Luminescence dating of delta sediments: Novel approaches explored for the Ganges-Brahmaputra-Meghna Delta. Quaternary Geochronology 41, 97-111. https://doi.org/10.1016/j.quageo.2017.06.006.

Cresswell, A.J., Carter, J., Sanderson, D.C.W. (2018). Dose rate conversion parameters: Assessment of nuclear data. Radiation Measurements, 120, 195-201. https://doi.org/10.1016/j.radmeas.2018.02.007.

Cunningham, A. C., Murray, A.S., Armitage, S., Autzen, M. (2018). High-precision natural dose rate estimates through beta counting. Radiation Measurement, 120, 209-214. https://doi.org/10.1016/j.radmeas.2018.04.008.

Cunningham, A.C., Wallinga, J. (2010). Selection of integration time intervals for quartz OSL decay curves. Quaternary Geochronology, 5, 657-666. https://doi.org/10.1016/j.quageo.2010.08.004.

De Corte, F., Vandenberghe, D., De Wispelaere, A., Buylaert, J.P., Van den haute, P. (2006). Radon loss from encapsulated sediments in Ge gamma-ray spectrometry for the annual radiation dose determination in luminescence dating. Czech Journal of Physics, 56, D183-D194. https://doi.org/10.1007/s10582-006-0504-9.

De Corte, F., Vandenberghe, D., Hossain, S.M., De Wispelaere, A., and Van Den Haute, P. (2004). The effect of different sample-calibrant composition in gamma-ray spectrometry for the assessment of the radiation dose rate in the luminescence dating of sediments. Journal of Radioanalytical and Nuclear Chemistry, 262, 261-267. https://doi.org/10.1023/B:JRNC.0000040884.16458.de.

De Corte, F., Umans, H., Vandenberghe, D., De Wispelaere, A., Van den haute P. (2005). Direct gamma-spectrometric measurement of the ^{226}Ra 186.2 keV line for detecting ^{238}U/^{226}Ra disequilibrium in determining the environmental dose rate for the luminescence dating of sediments. Applied Radiation and Isotopes, 63, 589-598. https://doi.org/10.1016/j.apradiso.2005.05.008.

De Corte, F., Vandenberghe, D., Hossain, S. M., De Wispelaere, A., Buylaert, J. -P., & Van den Haute, P. (2007). Preparation and characterization of loess sediment for use as a reference material in the annual radiation dose determination for luminescence dating. Journal of Radioanalytical and Nuclear Chemistry, 272, 311-319. https://doi.org/10.1007/s10967-007-0522-5.

De Rijk, J.H. (2011). De geschiedenis van de Hoog Soerense malebossen en het probleem van gemeenschappelijk bosbezit. Jaarboek voor Ecologische Geschiedenis 2011. Themanummer: Bossen in de Lage Landen. 115-138.

De Vos, B. (2005). Bodemcompactie en de invloed op de natuurlijke verjonging van Beuk in het Zoniënwoud. Januari 2005. IBW.Bb R 2005.004. In opdracht van het Fonds Generale Maatschappij van België voor het Zoniënwoud onder auspiciën van de Koning Boudewijnstichting. Instituut voor Bosbouw en Wildbeheer, Geraardsbergen.

Deforce, K. (2021). Casestudy Maredsous-Biert (B.). Vlekken in akkerland ten zuiden van Maredsous. Remote sensing in de Nederlandse archeologie (landbodems), Amersfoort, 62-65.

Deforce, K., Bastiaens, J., Cromb´e, P., Deschepper, E., Haneca, K., Laloo, P., Van Calster, H., Verbrugghe, G., De Clercq, W. (2020). Dark Ages woodland recovery and the expansion of beech. A study of land use changes and related woodland dynamics during the Roman to Medieval transition period in northern Belgium. Netherlands Journal of Geosciences , 99 , 2020 , e12. https://doi.org/10.1017/njg.2020.11.

Deforce, K., Boeren, I., Adriaenssens, S., Bastiaens, J., De Keersmaeker, L., Haneca, K., Tys, D., Vandekerkhove, K. (2013). Selective woodland exploitation for charcoal production. A detailed analysis of charcoal kiln remains (ca. 1300-1900 AD) from Zoersel (northern Belgium). Journal of Archaeological Science 40, 681-689. https://doi.org/10.1016/j.jas.2012.07.009.

Deforce, K., Groenewoudt, B., and Haneca, K. (2021a). 2500 years of charcoal production in the Low Countries: The chronology and typology of charcoal kilns and their relation with early iron production. Quaternary International, 593-594, 295-305. https://doi.org/10.1016/j.quaint.2020.10.020.

Deforce, K., Vanmontfort, B. and Vandekerkhove K. (2021b). Early and High Medieval (c. 650 AD - 1250 AD) charcoal production and its impact on woodland composition in the Northwest-European lowland: a study of charcoal pit kilns from Sterrebeek (Central Belgium). Environmental Archaeology 26, 168-178. https://doi.org/10.1080/14614103.2018.1538087.

Derese, C., Vandenberghe, D., Eggermont, N., Bastiaens, J., Annaert, R., and Van den haute, P. (2010). A medieval settlement caught in the sand: Optical dating of sand-drifting at Pulle (N Belgium). Quaternary Geochronology, 5, 336-341. https://doi.org/10.1016/j.quageo.2009.01.003.

Drailly, C., Deforce, K. (2019). Two Late Iron Age charcoal kilns from the Arlon forest (Arlon, province of Luxemburg, Belgium). Lunula (Brussel). Archaeologia protohistorica, 27, 129-132. http://hdl.handle.net/1854/LU-8604128.

Dulias, R. (2018). Drift sand fields as a result of past and current deforestation in the Silesian-Cracow Upland, Poland. Land Degradation and Development, 29, 1530-1539. https://doi.org/10.1002/ldr.2888.

Duller G.A.T. (2011). What date is it? Should there be an agreed datum for luminescence ages? Ancient TL, 29, 1-3.

Duller G.A.T., Botter-Jensen L., Murray A.S. (2000). Optical dating of single sand-sized grains of quartz: sources of variability. Radiation Measurements, 32, 453-457. https://doi.org/10.1016/S1350-4487(00)00055-X.

Duller, G.A.T. (2003). Distinguishing quartz and feldspar in single grain luminescence measurements. Radiation Measurements, 37, 161-165. https://doi.org/10.1016/S1350-4487(02)00170-1.

Duller, G.A.T. (2004). Luminescence dating of Quaternary sediments: Recent advances. Quaternary Science, 19(2), 183–192. https://doi.org/10.1002/jqs.809.

Duller, G. A. T. (2008a). Single-grain optical dating of Quaternary sediments: why aliquot size matters in luminescence dating. Boreas, 37(4), 589-612. https://doi.org/10.1111/j.1502-3885.2008.00051.x.

Duller, G.A.T. (2008b). Luminescence Dating: guidelines on using luminescence dating in archaeology. Journal of Quaternary Science, 24, 644-645. https://doi.org/10.1002/jqs.1328.

Durcan, J.A. (2018). Assessing the reproducibility of quartz OSL lifetime determinations derived using isothermal decay. Radiation Measurements, 120, 234-240. https://doi.org/10.1016/J.radmeas.2018.06.020.

Durcan, J.A., King, G.E., Duller, G.A.T. (2015). DRAC: Dose Rate and Age Calculator for trapped charge dating. Quaternary Geochronology, 28, 54-61. https://doi.org/10.1016/j.quageo.2015.03.012.

Duvivier, C. (1861). La Forêt Charbonnière (Carbonaria Silva). Revue d'histoire et d'archéologie 2, 1-26.

Fazekas B., Molnár G. Belgya T., Dabolczi L. and Simonits A. (1997). Introducing HYPERMET-PC for automatic analysis of complex gamma-ray spectra. Journal of Radioanalytical and Nuclear Chemistry. 215, 271-277. https://doi.org/10.1007/BF02034477.

Feathers, J.K. (2002). Luminescence Dating in Less Than Ideal Conditions: Case Studies from Klasies River Main Site and Duinefontein, South Africa. Journal of Archaeological Science, 29, 177-194. https://doi.org/10.1006/jasc.2001.0685.

Feathers, J.K. (2003). Use of luminescence dating in archaeology. Measurement Science and Technology, 14, 1493-1509. https://doi.org/10.1088/0957-0233/14/9/302.

Foard, G. (2001). Medieval woodland, agriculture and industry in rockingham forest, northamptonshire. Medieval Archaeology, 45, 41-95. https://doi.org/10.1179/med.2001.45.1.41.

Foster, D., Swanson, F., Aber, J., Burke, I., Brokaw, N., Tilman, D., Knapp, A. (2003). The importance of land-use legacies to ecology and conservation. BioScience 53, 77-88. https://doi.org/10.1641/0006-3568(2003)053[0077:TIOLUL]2.0.CO;2.

Fouédjeu, L., Saulnier, L., Lejay, M., Dušátko, M., Labbas, V., Jump, A., Burri, S., Buscaino, S., Py, V. (2021). High resolution reconstruction of modern charcoal production kilns: An integrated approach combining dendrochronology, micromorphology and anthracology in the French Pyrenees. Quaternary International 593–594, 306-319. https://doi.org/10.1016/j.quaint.2020.11.033.

Galbraith, R.F. (1988). Graphical Display of Estimates Having Differing Standard Errors. Technometrics, 30, 271-281. https://doi.org/10.2307/1270081.

Gale, R. (2003). Wood-based Industrial Fuels and Their Environmental Impact in Lowland Britain. In The Environmental Archaeology of Industry. Symposia of the Association for Environmental Archaeology 20, edited by P. Murphy and P. E. J.Wiltshire, 30-47.Oxford:Oxford Books.

Gallet Y., Genevey A. & Le Goff, M. (2002). Three millennia of directional variations of the Earth's magnetic field in Western Europe as revealed by archaeological artefacts. Physics of the Earth and Planetary Interiors, 131, 81-89. https://doi.org/10.1016/S0031-9201(02)00030-4.

Gautier, A. (2001). Luminescence dating of archaeometallurgical slag: use of the SAR technique for determination of the burial dose. Quat. Sci. Rev. 20, 973-980. https://doi.org/10.1016/S0277-3791(00)00010-X.

Gavin., D.G. (2001). Estimation Of Inbuilt Age In Radiocarbon Ages Of Soil Charcoal For Fire History Studies. RADIOCARBON, 43, 1, 27–44. https://doi.org/10.1017/S003382220003160X.

Gebhardt, A. (2007). Impact of charcoal production activities on soil profiles: the micromorphological point of view. ArcheoSciences, 31, 127-136. https://doi.org/10.4000/archeosciences.833.

Ghyselbrecht, E. (2018). OSL Dating Of Natural And Cultural Heritage: Case Studies On Sonian Forest (B) And Stonehenge (UK). MSc thesis, Universiteit Gent.

Groenewoudt, B. J. (2007). Charcoal Burning and Landscape Dynamics in the Early Medieval Netherlands. In Arts and Crafts in Medieval Rural Environment, Ruralia VI, edited by J. Klápště, and P. Sommer, 327-337. Turnhout: Brepols. http://doi.org/10.1484/M.RURALIA-EB.3.1150.

Groenewoudt, B., and Spek, T. (2016). Woodland dynamics as a result of settlement relocation on Pleistocene sandy soils in The Netherlands (200 BC–AD 1400). Rural Landscapes: Society, Environment, History 3, 1-17. http://doi.org/10.16993/rl.20.

Guérin, G., Mercier, N., Adamiec, G. (2011). Dose-rate conversion factors: update. Ancient TL, 29, No 1.

Guidorzi, L., Fantino, F., Durisi, E., Ferrero, M., Re, A., Vigorelli, L., Visca, L., Gulmini, M., Dughera, G., Giraudo, G., Angelici, D., Panero, E., Giudice, A.L. (2021). Age determination and authentication of ceramics: advancements in the thermoluminescence dating laboratory in Torino (Italy). IMEKO International Measurement Confederation in Acta Imeko, 10, 32-39. https://doi.org/10.21014/acta_imeko.v10i1.813.

Gullentops, F., Bogemans, F., De Moor, G., Paulissen, E., Pissart, A. (2001). Quaternary lithostratigraphic units (Belgium), in: Bultynck, P., Dejonghe, L. (Eds.), Guide to a revised lithostratigraphic scale of Belgium. Geologica Belgica 4/1-2, Bruxelles, 153-164.

Hansen, V., Murray, A.S., Buylaert, J.-P., Yeo, E.-Y., Thomsen, K.J. (2015). A new irradiated quartz for beta source calibration. Radiation Measurement, 81, 123-127. https://doi.org/10.1016/j.radmeas.2015.02.017.

Hardy, B., and Dufey, J. E. (2012). Estimation des besoins en charbon de bois et en superficie forestière pour la sidérurgie wallonne préindustrielle (1750-1830). Deuxième partie: les besoins en superficie forestière. Revue forestière française. https://doi.org/10.4267/2042/48747.

Hardy, B., Cornelis, J.T., Houben, D., Lambert, R., and Dufey, J.E. (2016). The effect of pre-industrial charcoal kilns on chemical properties of forest soil of Wallonia, Belgium. European journal of soil science, 67, 206-216. https://doi.org/10.1111/ejss.12324.

Hardy, B., Cornelis, J.T., Houben, D., Leifeld, J., Lambert, R., and Dufey, J.E. (2017a). Evaluation of the long-term effect of biochar on properties of temperate agricultural soil at pre-industrial charcoal kiln sites in Wallonia, Belgium. European Journal of Soil Science, 68, 80-89. https://doi.org/10.1111/ejss.12395.

Hardy, B., Leifeld, J., Knicker, H., Dufey, J.E., Deforce, K., and Cornélis, J.T. (2017b). Long term change in chemical properties of preindustrial charcoal particles aged in forest and agricultural temperate soil. Organic Geochemistry, 107, 33-45. https://doi.org/10.1016/j.orggeochem.2017.02.008.

Hart, J.L., Van De Gevel, S.L., Mann, D.F., and Clatterbuck, W.K. (2008). Legacy of charcoaling in a western highland rim forest in Tennessee. American Midland Naturalist, 159, 238-250. https://doi.org/10.1674/0003-0031(2008)159[238:LOCIAW]2.0.CO;2.

Hirsch, F., Raab, T., Ouimet, W., Dethier, D., Schneider, A., and Raab, A. (2017). Soils on historic charcoal hearths: Terminology and chemical properties. Soil Science Society of America Journal, 81(6), 1427-1435. https://doi.org/10.2136/sssaj2017.02.0067.

Hirsch, F., Schneider, A., Bauriegel, A., Raab, A., and Raab, T. (2018). Formation, classification, and properties of soils at two relict charcoal hearth sites in Brandenburg, Germany. Frontiers in Environmental Science, 6, Article 94. https://doi.org/10.3389/fenvs.2018.00094.

Hong, D.G., Yi, S. B., Galloway, R. B., Tsuboi, T., Hashimoto, T. (2000). Optical dating of archaeological samples using a single aliquot of quartz by blue light. Journal of Radioanalytical and Nuclear Chemistry, 247, 179-184. https://doi.org/10.1023/A:1006704207173.

Hossain S.M. (2003). A critical comparison and evaluation of methods for the annual radiation dose determination in the luminescence dating of sediments. Ph.D. thesis, Ghent University.

IAEA reference material (1987). Preparation and Certification of IAEA Gamma Spectrometry Reference. Materials RGU-1, RGTh-1 and RGK-1, Report IAEA/RL/148, Vienna, Austria.

Jain, M., Murray, A.S., and Bøtter-Jensen, L. (2003). Characterisation of blue-light stimulated luminescence components in different quartz samples: Implications for dose measurement. Radiation Measurement 37, 441-449. https://doi.org/10.1016/S1350-4487(03)00052-0.

Jain, M., Murray, A.S., Denby, P.M., Tsukamoto, S., Gibling, M.R., and Scotia, N. (2005). Revisiting TL : Dose measurement beyond the OSL range using SAR. Ancient TL, 23, 9-24.

Joosten, I. (2004). Technology of early historical iron production in The Netherlands. Thesis Free University Amsterdam, Geoarchaeological and Bioarchaeological Studies.

Karimi-Moayed, N., Vandenberghe, D. A. G., Deforce, K., Bastiaens, J., Ghyselbrecht, E., Debeer, A. E., De Smedt, P., De Clercq, W., De Grave, J. (2020). Bypassing the Suess-effect: Age determination of charcoal kiln remains using OSL dating. Journal of Archaeological Science, 120, 105176. https://doi.org/10.1016/j.jas.2020.105176.

KAYZERO/SOLCOI software for using the k0-standardization method, V. 5A. Ghent University and DSM Research, 2003.

Khamsiri, S., Venunan, P., Khaokheiw, C., Silapanth, P., Banron, S., Pailoplee, S. (2022a). Late iron-smelting production of Angkor Highland, metallurgical site at Buriram Province, northeastern Thailand: A view from luminescence dating. Archaeological Research in Asia, 31, 100395. https://doi.org/10.1016/j.ara.2022.100395.

Khamsiri, S., Venunan, P., Khaokheiw, C., Silapanth, P., Banron, S., Pailoplee, S. (2022b). Luminescence dating of archaeometallurgical slag from Buriram Province, northeastern Thailand. ScienceAsia, 48, 788-796. https://doi.org/10.2306/scienceasia1513-1874.2022.114.

Kim, J., Wright, D.K., Hwang, J., Kim, J., Oh, Y. (2019). The old wood effect revisited: a comparison of radiocarbon dates of wood charcoal and short-lived taxa from Korea. Archaeological and Anthropological Sciences, 11:3435–3448. https://doi.org/10.1007/s12520-018-0766-8.

Kirchmeier, H., Kovarovics. A. (2016). Nomination Dossier "Primeval Beech Forests of the Carpathians and Other Regions of Europe" as extension to the existing Natural World Heritage site "Primeval Beech Forests of the Carpathians and the Ancient Beech Forests of Germany" (1133bis). Klagenfurt.

Knapp, H., Nelle, O., and Kirleis, W. (2015). Charcoal usage in medieval and modern times in the Harz Mountains Area, Central Germany: wood selection and fast overexploitation of the woodlands. Quaternary International, 366, 51-69. https://doi.org/10.1016/j.quaint.2015.01.053.

Koops, R. (2021). De Leuvenumse Woudtempel: Een boshistorisch onderzoek naar het gebruik en de ontginning van het Leuvenumse Bos van 1692 tot heden. Master thesis. Rijksuniversiteit Groningen, 13, 52-59.

Koster, E. A. (2009). The "European Aeolian Sand Belt": Geoconservation of Drift Sand Landscapes. Geoheritage, 1, 93-110.

Lambers, K., Verschoof-van der Vaart, W.B., Bourgeois, Q.P. (2019). Integrating remote sensing, machine learning, and citizen science in Dutch archaeological prospection. Remote Sens. 2019, 11(7), 794. https://doi.org/10.3390/rs11070794.

Lamothe M, (2004). Optical dating of pottery, burnt stones, and sediments from selected Quebec archaeological sites. Canadian Journal of Earth Sciences, 41, 659-667. https://doi.org/10.1139/e04-032.

Langohr, R. (2009). Het Zoniënwoud, uniek voor aardwetenschappen en archeologie. In: De Vrienden van het Zoniënwoud, Het Zoniënwoud. Een nieuwe visie op een patrimonium met toekomst, pp. 181-196. Éditions Mardaga, Wavre – Uitgeverij Groeninghe, Kortrijk.

Lanos, Ph. (2004). Bayesian inference of calibration curves: application to archaeomagnetism, in Tools for Constructing Chronologies: Crossing Disciplinary Boundaries. Lecture Notes in Statistics, 177, 43-82.

Lanos, Ph., Le Goff, M., Kovacheva, M. and Schnepp, E. (2005). Hierarchical modeling of archaeomagnetic data and curve estimation by moving average technique. Geophysical Journal International, 160, 440-476. https://doi.org/10.1111/j.1365-246X.2005.02490.x.

Lapp, T., Kook, M., Murray, A. S., Thomsen, K. J., Buylaert, J. P., and Jain, M. (2015). A new luminescence Detection and Stimulation Head for the Risø TL/OSL reader. Radiation Measurements, 81, 178-184. https://doi.org/10.1016/j.radmeas.2015.02.001.

Lepoivre, A., Septembre, G. (1941). Le charbon de bois : traité pratique de carbonisation. Chiron, Paris, France.

Leung, P.L., Tang, Q., Li, M., Zhang, C. (2005). The preliminary application of OSL in comparison with TL for authentication of ancient Chinese bricks. Radiation Measurement, 40, 1-4. https://doi.org/10.1016/j.radmeas.2004.05.012.

Li, B., Li, S-H., and Wintle, A.G. (2008). Overcoming Environmental Dose Rate Changes In Luminescence Dating Of Waterlain Deposits. Geochronometria, 30, 33-40. https://doi.org/10.2478/V10003-008-0003-Z.

Li, B., Roberts, R.G., Brumm, A., Guo, Y.J., Hakim, B., Ramli, M., Aubert, M., Gr¨un, R., Zhao, J.X., E. Saptomo, W. (2016). IRSL dating of fast-fading sanidine feldspars from Sulawesi, Indonesia. Ancient TL, 34, No. 2.

Lian O.B., Richards R.G. (2006). Dating the Quaternary: progress in luminescence dating of sediments. Quaternary Science Reviews 25, 2449-2468. https://doi.org/10.1016/j.quascirev.2005.11.013.

Lian, O.B., Hu, J., Huntley, D.J., Hicook, S.R. (1995). Optical dating studies of Quaternary organic-rich sediments from southwestern British Columbia and northwestern Washington State. Canadian Journal of Earth Sciences, 32, 1194-1207. https://doi.org/10.1139/e95-098.

Liang, P., Forman, S.L. (2019). LDAC: An Excel-based program for luminescence equivalent dose and burial age calculations. Ancient TL, 37, No. 2.

Linford, P. (2006). Archaeomagnetic Dating: Guidelines on Producing and Interpreting Archaeomagnetic Dates. English Heritage, Swindon. http://dourbes.meteo.be/aarch.net/linford.pdf.

Liritzis I., Galloway, R.B., Theocrats, T.S. (1994). Thermoluminescence dating of ceramics revisited: optical stimulated luminescence of quartz single aliquot with green light-emitting diodes. Journal of Radioanalytical and Nuclear Chemistry 188, Letters, 189-198.

Liritzis I., Galloway R.B. and Hong D.G. (1997). Single aliquot dating of ceramics by green light stimulation of luminescence from quartz. Nuclear Instruments and methods in Physics Research B 132, 457-467. https://doi.org/10.1016/S0168-583X(97)00456-4.

Liritzis, I., Jin, Z., Fan, A., Sideris, A., and Drivaliari, A. (2016). Late helladic and later reuse phases of kastrouli settlement (Greece): Preliminary dating results. https://doi.org/ 10.5281/zenodo.163775.

Louis, A. (1962). Verklarende tekst bij het kaartblad Ninove 86 E. in Bodemkaart van België, LWONL.
Louis, A. (1969). Bijdrage tot de kennis van de bodemgesteldheid tussen Dender en Zenne. Unpublished PhD-thesis, Rijksuniversiteit Gent.

Ludemann, T. (2003). Large-scale reconstruction of ancient forest vegetation by anthracology - a contribution from the Black Forest. Phytocoenologia 33 (4), 645–666. 10.1127/0340-269X/2003/0033-0645.

Ludemann, T. (2010). Past fuel wood exploitation and natural forest vegetation in the Black Forest, the Vosges and neighbouring regions in western Central Europe. Palaeogeography, Palaeoclimatology, Palaeoecology, 291, 154-165. https://doi.org/10.1016/j.palaeo.2009.09.013.

Madsen, A.T., Murray, A.S. (2009). Optically stimulated luminescence dating of young sediments: A review. Geomorphology, 109, 3-16. https://doi.org/10.1016/j.geomorph.2008.08.020.

Martin, L., Fang, F., Mercier N., Incerti, S., Grün, R., Lefrais, Y. (2018). 2D modelling: A Monte Carlo approach for assessing heterogeneous beta dose rate in luminescence and ESR dating: Paper I, theory and verification. Quaternary Geochronology, 48, 25-37. https://doi.org/10.1016/j.quageo.2018.07.004.

Mastrolonardo, G., Francioso, O., and Certini, G. (2018). Relic charcoal hearth soils: A neglected carbon reservoir. Case study at Marsiliana forest, Central Italy. Geoderma, 315, 88-95. https://doi.org/10.1016/j.geoderma.2017.11.036.

McKeever, S. W. S. (1985). Thermoluminescence of Solids. Cambridge University Press.
Mees, F. (1989). Base maps and soil survey of undistrubed iron industry sites in the Zonien Forest (Loess Belt, Belgium). MSc dissertation. Universiteit Gent. p. 117.

Mejdahl V. and Bøtter-Jensen L. (1994). Luminescence dating of archaeological materials using a new technique based on single aliquot measurements. Quaternary Geochronology (Quaternary science Reviews) 13, 551-554. https://doi.org/10.1016/0277-3791(94)90076-0.

Mejdahl V. and Bøtter-Jensen L. (1997). Experience with the SARA OSL method. Radiation Measurements 27, 291-294. https://doi.org/10.1016/S1350-4487(96)00149-7.

Mejdahl, V. (1979). Thermoluminescence dating: Beta-Dose Attenuation in Quartz Grains. Archaeometry, 21, 61-72.

Metalidis, I., Deckers, P., Vanmontfort, B., Langohr, R. (2008). Archaeologisch onderzoek op GEN Lijn 161, TR 101311 (Groenendaal, Hoeilaart). EPA Rapport 3. Eenheid Prehistorische Archeologie, Katholieke Universiteit Leuven, 55 p. https://doi.org/10.13140/RG.2.2.23603.02082.

Moska, P., and Murray, A. S. (2006). Stability of the quartz fast-component in insensitive samples. Radiation Measurements, 41(7–8), 878–885. https://doi.org/10.1016/j.radmeas.2006.06.005.

Moska, P., Murray, A.S., Bluszcza, A. (2010). Luminescence properties of single grain quartz to determine the history of a sample from the Sahara Desert. Quaternary Geochronology, 5, 96-101. https://doi.org/10.1016/j.quageo.2009.07.002.

Murray A.S. and Buylaert J.P. (2017). Francqui Workshop, Department of Geology, UGent, 5-6 October 2017.

Murray A.S. and Mejdahl V. (1999). Comparison of regenerative-dose single-aliquot and multiple-aliquot (SARA) protocols using heated quartz from archaeological sites. Quaternary Geochronology 18, 223-229. https://doi.org/10.1016/S0277-3791(98)00055-9.

Murray A.S., Olley J.M. (2002). Precision and accuracy in the optically stimulated luminescence dating of sedimentary quartz: a status review. Geochronometria, 21, 1-16.

Murray A.S., Wintle A.G. (2000). Luminescence dating of quartz using an improved single-aliquot regenerative-dose protocol. Radiation Measurements, 32, 57-73. https://doi.org/10.1016/S1350-4487(99)00253-X.

Murray, A.S, Marten, R., Johnston, A., and Martin, P. (1987). Analysis for naturally occuring radionuclides at environmental concentrations by gamma spectrometry. Radioanalytical and Nuclear Chemistry, 115, 263-288. https://doi.org/10.1007/BF02037443.

Murray, A.S., Arnold, L.J., Buylaert, J.P., Guérin, G., Qin, J., Singhvi, A.K., Smedley, R., & Thomsen, K.J. (2021). Optically stimulated luminescence dating using quartz. Nature Reviews, Methods Primers, 1, 72. https://doi.org/10.1038/s43586-021-00068-5.

Murray, A.S., Thomsen, K.J., Masuda, N., Buylaert, J.P., Jain, M. (2012). Identifying well-bleached quartz using the different bleaching rates of quartz and feldspar luminescence signals. Radiation Measurements, 47, 688-695. https://doi.org/10.1016/j.radmeas.2012.05.006.

Murray, A.S., Wintle, A.G. (1999). Isothermal decay of optically stimulated luminescence in quartz. Radiation Measurements, 30, 119-125. https://doi.org/10.1016/S1350-4487(98)00097-3.

Murray, A.S., Wintle, A.G. (2003). The single aliquot regenerative dose protocol: Potential for improvements in reliability. Radiation Measurements, 37, 377-381. https://doi.org/10.1016/S1350-4487(03)00053-2.

Nelle, O. (2003). Woodland history of the last 500 years revealed by anthracological studies of charcoal kiln sites in the Bavarian Forest, Germany. Phytocoenologia, 33, 667-682. https://doi.org/10.1127/0340-269X/2003/0033-0667.

Noël M. and Batt C. (1990): A method for correcting geographically separated remanence directions for the purpose of archaeomagnetic dating. Geophysical Journal International, 102, 753-756.

Olesen, M.W. (2019). Iron smelting during the late iron age in central jutland. In: A Stamnes, A., Risbol, O., Stenvik, L.F. (Eds.), Investigating Early Iron Production by Modern Remote Sensing Technologies, vols. 2–2019. The Royal Norwegian Society of Sciences and Letters, 17-33.

Oliveira, C., Aravecchia, S., Pradalier, C., Robin, V., Devin, S. (2021). The use of remote sensing tools for accurate charcoal kilns' inventory and distribution analysis: Comparative assessment and prospective. International Journal of Applied Earth Observation and Geoinformation. 105, 102641. https://doi.org/10.1016/j.jag.2021.102641.

Paradis-Grenouillet, S., and Dufraisse, A. (2018). Deciduous oak/chestnut: Differential shrinkage of wood during charcoalification? Preliminary experimental results and implications for wood diameter study in anthracology. Quaternary International, 463, 258-267. https://doi.org/10.1016/j.quaint.2017.06.074.

Patzlaf, R., Oliveira, R.R., Araujo, D., Scheel-Ybert, R. (2018). Historical charcoal kilns: a method to compare the surrounding vegetation with the vegetation and the anthracological data in forested slopes of Rio de Janeiro Estate, RJ. In: Sandrine Paradis-Grenouillet; Sylvain Burri; Romain Rouaud. (Org.). Charbonnage, charbonniers, charbonnières Confluence de regards autour d'un artisanat méconnu. 1ed.Limoges: Presses Universitaires de Provence, 2018, 1, 173-178.

Pierik, H. J., van Lanen, R. J., Gouw-Bouman, M. T. I. J., Groenewoudt, B. J., Wallinga, J., & Hoek, W. Z. (2018). Controls on late-Holocene drift-sand dynamics: The dominant role of human pressure in the Netherlands. Holocene, 28, 1361-1381.

Pleiner, R. (2000). Iron in Archaeology: The European Bloomery Smelters. Prague: Archeologigky Ustav Avcr.

Potter, N., Brubaker, K., and Delano. H. (2013). Lidar reveals thousands of 18th and 19th century charcoal hearths on South Mountain, South Central Pennsylvania. Presented at the Geologic Society of America 48th Annual Meeting, Bretton Woods, NH. 18-20.

Prescott, J. R., and Hutton, J. T. (1994). Cosmic ray contributions to dose rates for luminescence and ESR dating: Large depths and long-term time variations. Radiation Measurements, 23, 497-500. https://doi.org/10.1016/1350-4487(94)90086-8.

Raab, A., Takla, M., Raab, T., Nicolay, A., Schneider, A., Rösler, H., Heussner, K.-U. and Bönisch, E. (2015). Pre-industrial charcoal production in Lower Lusatia (Brandenburg, Germany): Detection and evaluation of a large charcoal-burning field by combining archaeological studies, GIS-based analyses of shaded-relief maps and dendrochronological age determination. Quaternary International, 367, 111-122. https://doi.org/10.1016/j.quaint.2014.09.041.

Raab, T., Hirsch, F., Ouimet, W., Johnson, K.M., Dethier, D., and Raab, A. (2017). Architecture of relict charcoal hearths in northwestern Connecticut, USA. Geoarchaeology, 32, 502-510. https://doi.org/10.1002/gea.21614.

Raab, T., Raab, A., Bonhage, A., Schneider, A., Hirsch, F., Birkhofer, K., Drohan, P., Wilmking, M., Kreyling, J., Malik, I., Wistuba, M., van der Maaten, E., van der Maaten-Theunissen, M. , Urich, T. (2022). Do small landforms have large effects? A review on the legacies of pre-industrial charcoal burning. Geomorphology 413 (2022) 108332. https://doi.org/10.1016/j.geomorph.2022.108332.

Reimer, P.J, Austin, W., Bard, E., Bayliss, A., Blackwell, P., Bronk Ramsey, C., Butzin, M., Cheng, H., Edwards, R., Friedrich, M., Grootes, P., Guilderson, T., Hajdas, I., Heaton, T., Hogg, A., Hughen, K., Kromer, B., Manning, S., Muscheler, R., Palmer, J., Pearson, C., van der Plicht, J., Reimer, R., Richards, D., Scott, E., Southon, J., Turney, C., Wacker, L., Adolphi, F., Büntgen, U., Capano, M., Fahrni, S., Fogtmann-Schulz, A., Friedrich, R., Köhler, P., Kudsk, S., Miyake, F., Olsen, J., Reinig, F., Sakamoto, M., Sookdeo, A., and Talamo, S. (2020). The IntCal20 Northern Hemisphere radiocarbon age calibration curve (0–55 cal kBP). Radiocarbon, 62.

Reimer, P.J., Bard, E., Bayliss, A., Beck, J.W., Blackwell, P.G., Bronk Ramsey, C., Grootes, P.M. (2013). IntCal 13 and Marine 13 radiocarbon age calibration curves 0– 50,000 Years cal BP. Radiocarbon 55, 1869-1887. https://doi.org/ 10.2458/azu_js_rc.55.16947.

Rengers, F.K., Pagonis, V., Mahan, Sh.A. (2017). Can thermoluminescence be used to determine soil heating from a wildfire? Radiation Measurements, 107, 119-127. https://doi.org/10.1016/j.radmeas.2017.09.002.

Rhodes, E.J. (2011). Optically Stimulated Luminescence Dating of Sediments over the Past 200,000 Years. Annual Review of Earth and Planetary Sciences, 39, 461-488. https://doi.org/10.1146/annurev-earth-040610-133425.

Rhodes, E.J., Fanning, P.C., Holdaway, S.J. (2010). Developments in optically stimulated luminescence age control for geoarchaeological sediments and hearths in western New South Wales, Australia. Quaternary Geochronology, 5, 348-352. https://doi.org/10.1016/j.quageo.2009.04.001.

Rhodes, E.J., Fanning, P.C., Holdaway, S.J. (2010). Developments in optically stimulated luminescence age control for geoarchaeological sediments and hearths in western New South Wales, Australia Quaternary Geochronology, 5, 348-352.

Rhodes, E.J., Fanning, P.C., Holdaway, S.J., Bolton, C.C. (2009). Archaeological surfaces in western NSW: stratigraphic contexts and preliminary OSL dating of hearths. Terra Australis, 28, 189-200.

Riedesel, S., and Autzen, M. (2020). Beta and gamma dose rate attenuation in rocks and sediment. Radiation Measurements, 133, 106295. https://doi.org/10.1016/j.radmeas.2020.106295.

Risbøl, O., Bollandsås, O.M., Nesbakken, A., Ørka, H.O., Næsset, E., Gobakken, T. (2013). Interpreting cultural remains in airborne laser scanning generated digital terrain models: effects of size and shape on detection success rates. Journal of Archaeological Science, 40, 4688-4700. https://doi.org/10.1016/j.jas.2013.07.002.

Rutkiewicz, P., Malik, I., Wistuba, M., Sady, A. (2017). Charcoal kilns as a source of data on the past iron industry (an example from the River Czarna valley, Central Poland). Environmental & Socio-economic Studies 5, 12-22. https://doi.org/10.1515/environ-2017-0012.

Schmidt-Wiegand R. (1981). Carbonaria silva. In: Reallexion der Germanischen Altertumskunde, band 4, edited by J. Hoops, 341-342. Berlin: De Gruyter.

Schneider, A., Bonhage, A., Hirsch, F., Raab, A., and Raab, T. (2022). Hot spots and hot zones of soil organic matter in forests as a legacy of historical charcoal production. Forest Ecology and Management 504, 119846. https://doi.org/10.1016/j.foreco.2021.119846.

Schneider, A., Bonhage, A., Raab, A., Hirsch, F., and Raab, T., (2020). Large-scale mapping of anthropogenic relief features—legacies of past forest use in two historical charcoal production areas in Germany. Geoarchaeology, 35, 474. https://doi.org/10.1002/gea.21782.

Schoch, W., Heller, I., Schweingruber, F.H., Kienast, F. (2004). Wood anatomy of central European Species. Online version: www.woodanatomy.

Schweingruber, F.H. (1990). Microscopic wood anatomy: Structural variability of stems and twigs in recent and subfossil woods from Central Europe. Eidgenössische Forschungsanstalt WSL, Birmensdorf.

Sohbati, R., Murray, A. S., Buylaert, J.-P., Almeida, N. A. C. & Cunha, P. P. (2012). Optically stimulated luminescence (OSL) dating of quartzite cobbles from the Tapada do Montinho archaeological site (east-central Portugal). Boreas 41, 452–562 (2012). https://doi.org/10.1111/j.1502-3885.2012.00249.x.

Sohbati, R., Murray, A. S., Porat, N., Jain, M., and Avner, U. (2015). Age of a Prehistoric 'Rodedian' Cult Site Constrained by Sediment and Rock Surface Luminescence Dating Techniques. Quaternary Geochronology 30: 90–99. https://doi.org/10.1016/j.quageo.2015.09.002.

Souza, P.E. Sohbati, R., Murray, A.S., Kroon, A., Clemmensen, L.B., Hede, M.U., Nielsen, L. (2019). Luminescence dating of buried cobble surfaces from sandy beach ridges: a case study from Denmark. Boreas 48, 841-855. https://doi.org/10.1111/bor.12402.

Spooner, N.A. (1994). On the optical dating signal from quartz. Radiation Measurements, 2-3. 593-600. https://doi.org/10.1016/1350-4487(94)90105-8.

Spooner N. A., Prescott J. R. and Hutton J. T. (1988). The effect of illumination wavelength on the bleaching of the thermoluminescence (TL) of quartz. Quaternary Science Reviews, 7, 325-329. https://doi.org/10.1016/0277-3791(88)90023-6.

Stoneham, D. (1991). Authenticity testing. In: Scientific Dating Methods, Göksu H.Y., Oberhofer M., Regula D. (eds), pp. 175-192. (Kluwer Academic Publishers).

Stuiver, M. (1961). Variations in radiocarbon concentration and sunspot activity. Geophysical Research, 66, 273-276. https://doi.org/10.1029/JZ066i001p00273.

Sun, M., Sun, Y.,Wei, H., Hou, G., Xianba, J., Xie, L., et al. (2021). Luminescence dating of relics in ancient cities provides absolute dates for understanding humanland relationships in qinghai lake basin, northeastern Tibetan plateau. Front. Earth Sci. 9, 701037. https://doi.org/10.3389/feart.2021.701037.

Sun, Y.J., Chongyi, E., Lai, Z.P., Hou, G. (2018). Luminescence dating of prehistoric hearths in Northeast Qinghai Lake and its paleoclimatic implication. Archaeological and Anthropological Sciences 10, 1525-1534.

Sun, Y.J., Lai, Z.P., Madsen, D.B., Hou, G.L. (2012). Luminescence dating of a hearth from the archaeological site of Jiangxigou in the Qinghai Lake area of the northeastern Qinghai-Tibetan plateau. Quaternary Geochronology, 12, 107–110.

Tack, G., Van Den Bemt, P., and Hermy, M. (1993). Bossen van Vlaanderen. Een historische ecologie. Davidsfonds, Leuven, Belgium; 1993-01.

Takano, M., Yawata, T., and Hahimoto, T. (2003). Luminescence dosimetry of archaeological and ceramic samples using a single- aliquot regenerative dose method. Journal of Radioanalytical and Nuclear Chemistry 255(2), 365-368. https://doi.org/10.1023/A:1022521224134.

Tans, P.P., De Jong, A.F.M., and Mook, W.G. (1979). Natural atmospheric ^{14}C variation and the Suess effect. Nature, 280, 826-828. https://doi.org/10.1038/280826a0.

Taylor, R. E. (2014). Radiocarbon dating: an archaeological perspective. Academic Press.

Taylor, R.E., & Bar-Yosef, O. (2014). Radiocarbon Dating: An Archaeological Perspective (2nd ed.). Routledge. https://doi.org/10.4324/9781315421216.

Thomas, P.J., Nagabhushanam, P., Reddy, D.V. (2008). Optically stimulated luminescence dating of heated materials using single-aliquot regenerative-dose procedure: a feasibility study using archaeological artefacts from India. Journal of Archaeological Science, 35, 781-790. https://doi.org/10.1016/j.jas.2007.06.015.

Thomsen, K. J., Murray, A. S., Bøtter-Jensen, L., and Kinahan, J. (2007). Determination of burial dose in incompletely bleached fluvial samples using single grains of quartz. Radiation Measurements, 42, 370-379. https://doi.org/10.1016/j.radmeas.2007.01.041.

Thomsen, K.J., Murray, A.S., BZtter-Jensen, L. (2005). Sources of variability in OSL dose measurements using single grains of quartz. Radiation Measurements, 39, 47-61. https://doi.org/10.1016/j.radmeas.2004.01.039.

Tsukamoto S., Duller, G., Murray, A.S., Choi, J.H. (2009). Luminescence dating in geomorphology. Geomorphology, 109, 1-78.

Van ‘t Hoff, B. (1964). De oudste kaart van Overijssel. VORG Verslagen en Medelingen. 79.

Van der Ben, D., Nijhoff, R., and Deronde, L. (1997). Het Zonienwoud: een natuurmonument en zijn geschiedenis. Lannoo.

Van der Plicht, J., Bronk Ramsey, C., Heaton, T., Scott, E., & Talamo, S. (2020). Recent Developments in Calibration for Archaeological and Environmental Samples. Radiocarbon, 62(4), 1095-1117. https://doi.org/10.1017/RDC.2020.22.

Van Ranst E. (1981). Vorming en eigenschappen van lemige bosgronden in Midden- en Hoog-België. PhD thesis, Rijksuniversiteit Gent, 215p.

Van Ranst, E., De Coninck, F., Tavernier, R., Langohr, R. (1982). Mineralogy in silty to loamy soils in Central and High Belgium in respect to autochtonous and allochtonous materials. Bulletin de la Société Belge de Géologie, 91, 27-44.

Vandekerkhove, K., Deforce, K., and Bastiaens, J. (2018). Historic-ecological position of beech in the area of the Sonian Forest and an overview of beech-forest-related biodiversity present in the forest. Rapporten van het Instituut voor Natuur-en Bosonderzoek, 28. https://doi.org/10.21436/inbor.14173748.

Vandenberghe, D. (2004). Investigation of the optically stimulated luminescence dating method for application to young geological dediments. PhD thesis, Universiteit Gent, 358p.

Vandenberghe, D., Hossain, S.M., De Corte, F., Van den haute, P. (2003). Investigations on the origin of the equivalent dose distribution in a Dutch coversand. Radiation Measurements, 37, 433-439. https://doi.org/10.1016/S1350-4487(03)00051-9.

Vandenberghe, D., Kasse, C., Hossain, S.M., De Corte, F., Van Den Haute, P., Fuchs, M., and Murray, A.S. (2004). Exploring the method of optical dating and comparison of optical and ^{14}C ages of Late Weichselian coversands in the southern Netherlands. Journal of Quaternary Science, 19, 73-86. https://doi.org/10.1002/jqs.806.

Vandenberghe, D., De Corte, F., Buylaert, J.P., Kučera, J., and Van den haute, P. (2008). On the internal radioactivity in quartz. Radiation Measurements, 43, 771-775. https://doi.org/10.1016/j.radmeas.2008.01.016.

Vandenberghe D., Jain, M., Murray, A.S. (2009a). Equivalent dose determination using a quartz isothermal TL signal. Radiation Measurements, 44, 439-444. https://doi.org/10.1016/j.radmeas.2009.03.006.

Vandenberghe, D., Vanneste, K., Verbeeck, K., Paulissen, E., Buylaert, J.P., De Corte, F., and Van den haute, P. (2009b). Late Weichselian and Holocene earthquake events along the Geleen fault in NE Belgium: OSL age constraints. Quaternary International, 199, 56-74. https://doi.org/10.1016/J.QUAINT.2007.11.017.

Vander Linden, H. (1923). La forêt charbonnière. Revue belge de philologie et d'histoire 2-2, 203-214.

Verbrugge A. (2020). Archeologisch onderzoek Ninove Doorn Noord - Archeologierapport - 2018E210. SOLVA, pp. 54.

Verbrugge, A., Wauters, E., Cherretté, B., Poulain, M., and Brion, M. (2022). Les campements militaires à Ninove (1667-1748): premiers résultats des fouilles archéologiques. The archaeology of conflicts : early modern military encampments and material culture. In BAR International Series 3093. p.99-113. http://hdl.handle.net/1854/LU-01GNAGMVY737XY9FDCB1VAAMMH.

Verschoof-Van Der Vaart, W.B., Lambers, K., Kowalczyk, W., and Bourgeois, Q.P.J. (2020). Combining deep learning and location-based ranking for large-scale archaeological prospection of LiDAR data from the Netherlands. ISPRS International Journal of Geo-Information, 9(5).

Wagner G.A. (1998). Age determination of young rocks and artifacts: physical and chemical clocks in Quaternary geology and archaeology. Springer-Verlag Berlin Heidelberg, 466p., ISBN: 3-540-63436-3.

Wallinga, J. (2002a). Optically stimulated luminescence dating of fluvial deposits: a review. Boreas, 31(4), 303-322. https://doi.org/10.1111/j.1502-3885.2002.tb01076.x.

Wallinga, J. (2002b). On The Detection Of Osl Age Overestimation Using Single-Aliquot Techniques. Geochronometria, 21, 17-26, Journal on Methods and Applications of Absolute Chronology.

Wang, C.X., Ji, X., Wu, Y., Jin, Z., Zhang, Y., Chen, M., Wang, N., Fan, A. (2022a). Quartz OSL and TL dating of pottery, burnt clay, and sediment from Beicun archaeological site, China. Quaternary Geochronology, 70, 101281. https://doi:10.1016/j.quageo.2022.101281.

Wang, C-X., Zhang, X., Zhang, Y., Wu Y., Huang, C., and Fan, A. (2022b). Luminescence dating of heated quartz extracted from burnt clay and pottery excavated from the Lingjiatan archaeological site, China. Front. Earth Sci. 10:933342. https://doi.org/10.3389/feart.2022.933342.

Warner, R. B. (1990). A proposed adjustment for the “old wood effect”. In Pact, 29, 159-172.

Waterbolk, H.T. (1971). Working with radiocarbon dates. In Proceedings of the prehistoric society, 37, 15-33. Cambridge University Press.

Wauters, E. & Verbrugge, A. (2022). Les campements militaires à Ninove (1667–1748): instruments de recherche et contexte historico-militaire. The archaeology of conflicts: early modern military encampments and material culture. In BAR International Series 3093. https://doi.org/10.30861/9781407359618.

Willis, K.J., Birks, H.J.B. (2006). What is natural? The need for a long-term perspective in biodiversity conservation. Science, 314, 1261-1265.

Wintle A.G. & Murray A.S. (1997). The relationship between quartz thermoluminescence, photo-transferred thermoluminescence and optically stimulated luminescence. Radiation Measurements 27, 611-624. https://doi.org/10.1016/S1350-4487(97)00018-8.

Wintle A.G. (2008). Luminescence dating of Quaternary sediments. Boreas 37, 469-677.

Wintle, A.G., and Murray, A.S. (2006). A review of quartz optically stimulated luminescence characteristics and their relevance in single-aliquot regeneration dating protocols. Radiation Measurements, 41, 369-391. https://doi.org/10.1016/j.radmeas.2005.11.001.

Yu, L., An, P., and Lai, Z. (2016). Different Implications Of Osl And Radiocarbon Ages In Archaeological Sites In The Qaidam Basin, Qinghai-Tibetan Plateau. GEOCHRONOMETRIA, 43 , 188–200. https://doi.org/10.1515/geochr-2015-0048.

Zander, A., Strebler, D., Classen, E., Rethemeyer, J., and Brückner, H. (2019). Roman traces in Germania magna: New thermoluminescence and pIRIR 290 data from a lime kiln at Bergisch Gladbach, Germany. Archaeometry 61, 506–518. https://doi.org/10.1111/arcm.12435.

Zhang, J., Li, S.H., Sun, J., Lü, T., Zhou, X., And Hao, Q. (2022). Quartz luminescence sensitivity variation in the Chinese loess deposits: the potential role of wildfires. Journal Of Quaternary Science, 38, 49-60. ISSN 0267-8179. https://doi.org/10.1002/jqs.3462.

Zimmerman, D.W.M., Yuhas, P., Meyers, P. (1974). Thermoluminescence authenticity measurements on core material from the Bronze Horse of the New York Metropolitan Museum of Art. Archaeometry, 16 , 19-30. https://doi.org/10.1111/j.1475-4754.1974.tb01089.x.

Zuyderwyk, J. 2020. De vroegmiddeleeuwse ijzerwinning op de Veluwe. Ingrediënten voor een nieuw verhaal. In Op zoek naar Hamaland. Jubileumboek AWN18, p. 194-215.